UNIVERSITAT POLITÈCNICA
DE CATALUNYA

Ph.D. Dissertation

Next Generation Passive Optical Networks based on Orthogonal Frequency Division Multiplexing techniques

Author:	Francisco Javier Escayola Elias
Advisor:	Maria Concepción Santos Blanco, Ph.D. Associate Professor Universitat Politècnica de Catalunya (UPC)
Co-Advisor:	Iván Nicolás Cano Valadez, Ph.D. Universitat Politècnica de Catalunya (UPC)

Optical Communications Group (GCO)
Department of Signal Theory and Communications (TSC)
Universitat Politècnica de Catalunya (UPC)

Barcelona, October 2015

The work described in this Thesis was performed in the Signal Theory and Communications department of the Universitat Politècnica de Catalunya/BarcelonaTech.

Francisco Javier Escayola Elias
Next Generation Passive Optical Networks based on OFDMA techniques
Subject headings: OFDM, Optical communications, PONs and telecomm

Printed in Barcelona, Spain

ISBN:
Reg:

Abstract

In recent decades, the industry of communications has acquired huge significance, and nowadays constitutes an essential tool for the society information. Thus, the exponential growth in demand of broadband services and the increasing amount of information to be transmitted have spurred the evolution of the access network infrastructure to effectively meet the user needs in an effective way in terms of costs of both installation and maintenance.

Passive optical networks (PON) are currently considered the most efficient and least costly alternative to deploy fiber to the home environment. In order to allow many users simultaneously coexist PONs based on time multiplexing (TDMA) have been developed. Looking ahead, however, it is expected that these techniques do not meet the requirements on access networks. In consequence, other multiple access techniques such as Wavelength Division Multiplexing Access (WDMA) or Orthogonal Frequency Division Multiplexing Access (OFDMA) are currently under study and development for use in the next generation of PONs. Particularly, in recent years OFDM has stood out among the scientific community to be considered a solution with great potential on future implementation of PONs. This is especially true due to the capacity of OFDM to work with multilevel modulations, its high tolerance to chromatic dispersion, and its high flexibility and granularity in terms of bandwidth management.

Given the above, the aim of this Thesis is to study deeply the advantages and challenges of implementing the standard OFDM as an access network solution; likewise, it offers solutions to improve its performance. In order to evaluate the main structures and strategies for OFDM-based PON, a comparative analysis of all of them is performed firstly, highlighting their sensitivity levels, maximum range and number of users.

A key aspect for network providers is the cost of operation, deployment and maintenance of networks. As a low-cost solution, this Thesis proposes a network model called Statistical-OFDMA-PON based on intensity modulation and direct detection. In addition, dynamic bandwidth management strategies are applied into this model getting an improvement in the power balance which in turn, allows to increase the maximum range and the scalability in number of users.

One of the main OFDM problems is the Peak-to-Average Power Ratio (PAPR)

which increases with the number of carriers. This thesis proposes a new algorithm based on folding the signal and transmitting auxiliary information in order to compensate the PAPR effect and thus increase the sensitivity of the optical system.

On the other hand, OFDMA requires a large number of operations in the digital domain resulting in a high computational effort, which in turn results in an increased cost. For this reason, this Thesis presents a study on the optimization of the required resolution in the Digital-to-Analog / Analog-to-Digital Converters (DAC/ADCs) maintaining the transmission quality. The optimization of the computation time may make the OFDMA-based optical network more attractive for future PONs.

Finally, another problem concerning the OFDM optical networks is their sensitivity to Phase Noise (PN). In this regard, this Thesis presents a study of the effect of the laser linewidth and its dependence on signal bandwidth. A mitigation technique based on pilot tones is implemented and the limiting values for the laser linewidth are found to be within the reach of present low-cost light sources.

Resumen

En estas últimas décadas, la industria de las comunicaciones ha adquirido gran importancia y hoy en día, constituye una herramienta imprescindible para el funcionamiento en la sociedad de la información. Así pues, el crecimiento exponencial en la demanda de servicios de banda ancha y la carga de información cada vez mayor que se necesita transmitir ha estimulado la evolución de las infraestructuras del tramo de acceso a la red para poder satisfacer las necesidades del usuario de forma efectiva en términos de costes de instalación y de mantenimiento.

Las redes ópticas pasivas (Passive Optical Networks, PON) son actualmente consideradas la alternativa más eficiente y de menor coste para desplegar fibra hasta los hogares. Con el fin de permitir que muchos usuarios coexistan simultáneamente se han desarrollado PONs basadas en multiplexación en tiempo (Time Division Multiplexing Access, TDMA). De cara al futuro, sin embargo, se prevé que estas técnicas no permitan cubrir las exigencias sobre las redes de acceso. En consecuencia, otras técnicas de acceso múltiple al medio como el acceso múltiple por división de longitud de onda (Wavelength Division Multiplexing Access, WDMA) o el acceso múltiple por división de frecuencia ortogonal (Orthogonal Frequency Division Multiplexing Access, OFDMA) se encuentran actualmente en proceso de estudio y desarrollo para su uso en la futura generación de PONs. En concreto, en los últimos años OFDM se ha destacado entre la comunidad científica al considerarse una solución con gran potencial para su futura implantación en redes de acceso pasivas. Esto es especialmente cierto debido a la capacidad que el OFDM para trabajar con modulaciones multinivel, así como su alta tolerancia a la dispersión cromática y a la gran flexibilidad y granularidad que posibilita en términos de gestión del ancho de banda.

Por todo lo anterior, el objetivo de esta Tesis es estudiar con profundidad las ventajas y los retos de aplicar el estándar OFDM como solución de red de acceso; del mismo modo, ofrece soluciones para mejorar su rendimiento. Con el objetivo de evaluar las principales estructuras basadas en OFDM-PON, en primer lugar se realiza un análisis comparativo de todas ellas destacando sus niveles de sensibilidad, máximo alcance y número de usuarios.

Un aspecto fundamental para los proveedores de red es el coste de operación, despliegue y mantenimiento de las redes. Como solución de bajo coste, esta Tesis

propone un modelo de red llamado Statistical-OFDMA-PON que se basa en modulación de intensidad y detección directa. Además, este modelo se completa con estrategias de gestión dinámica del ancho de banda de los usuarios que conforman la estructura de red propuesta consiguiendo una mejora en el balance de potencias que permite aumentar distancia y número de usuarios.

Uno de los principales problemas del OFDM es el alto nivel de la relación de potencia de pico a potencia media (Peak-to-Average Power Ratio, PAPR) creciente con el número de portadoras. Esta Tesis propone un nuevo algoritmo basado en el pliegue de la señal y la transmisión de información auxiliar para compensar el efecto del PAPR aumentando así la sensibilidad del sistema óptico.

Por otro lado, OFDMA requiere un número elevado de operaciones en el dominio digital resultando en un alto esfuerzo computacional que a su vez se traduce en un aumento del coste. Por esta razón, esta Tesis presenta un estudio sobre la optimización de la resolución requerida en los conversores analógico-digital (Digital-to-Analog/Analog-to-Digital Converters, DAC/ADCs) manteniendo la calidad de transmisión. La optimización del tiempo de cómputo requerido puede dotar de un mayor atractivo la solución de red óptica basada en OFDMA.

Finalmente, otro de los problemas que presentan las redes ópticas OFDM es su sensibilidad frente al ruido de fase (Phase Noise, PN). En este aspecto, esta Tesis presenta un estudio del efecto del ancho de línea del láser y su dependencia con el ancho de banda de la señal. Técnicas de mitigación basadas en tonos piloto han sido implementadas y se han encontrado los valores limitantes del ancho de línea dentro del alcance de los láseres de bajo coste.

Resum

En les últimes dècades, la indústria de les comunicacions ha adquirit gran importància i avui en dia, constitueix una eina imprescindible per al funcionament de la societat de la informació. Així doncs, el creixement exponencial en la demanda de serveis de banda ample i la carga d'informació cada cop major que es necessita per transmetre ha estimulat l'evolució de les infraestructures del tram d'accés a la xarxa per a poder satisfer les necessitats del usuari de forma efectiva en termes de costos d'instal · lació i de manteniment.

Les xarxes òptiques passives (Passive Optical Networks, PON) són actualment considerades la alternativa més eficient i de menor cost per a desplegar fibra fins les llars. Amb el fi de permetre que molts usuaris coexisteixin simultàniament s'han desenvolupat PONs basades en multiplexació en temps (Time Division Multiplexing Access, TDMA). De cara al futur, no obstant, es preveu que aquestes tècniques no permetin cobrir les exigències sobre les xarxes d'accés. En conseqüència, altres tècniques d'accés múltiple al medi com l'accés múltiple per divisió de longitud d'ona (Wavelength Division Multiplexing Access, WDMA) o l'accés múltiple per divisió de freqüència ortogonal (Orthogonal Frequency Division Multiplexing Access, OFDMA) es troben actualment en procés d'estudi i desenvolupament per al seu ús en la futura generació de PONs. En concret, en els últims anys OFDM s'ha destacat entre la comunitat científica al considerarse una solució amb un gran potencial per a la seva futura implantació en PONs. Això es deu especialment a la capacitat que el OFDM per a treballar amb modulacions multinivell, així com la seva tolerància a la dispersió cromàtica i a la gran flexibilitat y granularitat que possibilita en termes de gestió de l'ample de banda.

Per tot lo esmentat, l'objectiu d'aquesta Tesis es estudiar amb profunditat les avantatges i els reptes d'aplicar l'estàndard OFDM com a solució de xarxa d'accés; del mateix mode, ofereix solucions per a millorar el seu rendiment. Amb l'objectiu d'avaluar les principals estructures basades en OFDM-PON, en primer lloc es realitza un anàlisis comparatiu de totes elles destacant els seus nivells de sensibilitat, màxim abast i número d'usuaris.

Un aspecte fonamental per als proveïdors de xarxa és el cost d'operació, desplegament i manteniment de les xarxes. Com a solució de baix cost, aquesta Tesis proposa un model de xarxa anomenat Statistical-OFDMA-PON que

es basa en modulació d'intensitat i detecció directa. A més, aquest model es completa amb estratègies de gestió dinàmica de l'ample de banda dels usuaris que conformen l'estructura de la xarxa proposada aconseguint una millora en el balanç de potències que permet augmentar distancia i número d'usuaris.

Un dels principals problemes de l'OFDM es l'alt nivell de la relació de potència de pic a potència mitjana (Peak-to-Average Power Ratio, PAPR) creixent amb el número de portadores. Aquesta Tesis proposa un nou algoritme basat en el plegament de la senyal i la transmissió d'informació auxiliar per a compensar l'efecte del PAPR augmentant així, la sensibilitat del sistema òptic.

Per altre banda, OFDMA requereix un número elevat d'operacions en el domini digital resultant en un alt esforç computacional que al seu torn, es tradueix en un augment del cost. Per aquesta raó, aquesta Tesis presenta un estudi sobre l'optimització de la resolució requerida en els conversos analògic-digitals (Digital-to-Analog/Analog-to-Digital Converters, DAC/ADCs) mantenint la qualitat de transmissió. L'optimització del temps de còmput requerit pot dotar d'un major atractiu la solució de xarxa òptica basada en OFDMA.

Finalment, un altre dels problemes que presenten les xarxes òptiques OFDM es la seva sensibilitat en front el soroll de fase (Phase Noise, PN). En aquest aspecte, aquesta Tesis presenta un estudi de l'efecte de l'ample de línia de làser i la seva dependència amb l'ample de banda de la senyal. Tècniques de mitigació basades en tons pilot han estat implementades y s'han trobat els valors limitants de l'ample de línia dins de l'abast dels làsers de baix cost.

Acknowledgements

Este documento es el resultado de cuatro años de arduo trabajo en los que la perseverancia, la frustración, la paciencia, la consecución de logros, la búsqueda de la perfección, el cansancio, el inconformismo y el amor por la investigación y el conocimiento, se han combinado con la finalidad de aportar mi pequeño granito de arena a este mundo en constante desarrollo. No obstante, la culminación de esta intensa aventura no habría sido posible sin el soporte de aquellos que te rodean con su alma, te contagian su optimismo y te recuerdan quien eres cuando es menester. Así pues, es de recibo y un gran placer tener la posibilidad de agradecer su colaboración en la andadura de lo que hasta el momento representa el proyecto más importante de mi vida y el que me produce mayor satisfacción y orgullo.

En primer lugar quiero agradecer a mi directora María Concepción Santos el apoyo incondicional que me ha demostrado a lo largo de estos años. Siempre has tenido las puertas de tu tiempo abiertas para mí con una sonrisa y predisposición infinita. Hemos reído, hemos discutido y hemos aprendido juntos, además de inculcarme la búsqueda de la perfección y la voluntad para realizar un trabajo bien hecho. Siento una gran admiración hacia ti no solo por tu mente brillante sino por tu inmenso corazón.

En segundo lugar, y no menos importante, quiero agradecer a mi codirector, compañero y amigo Iván Nicolás Cano, la disponibilidad por tenderme su mano siempre que lo he necesitado, por ajustar ese engranaje que me faltaba para poder ver la luz y por esas horas en el laboratorio donde tanto me has enseñado. Has sido mi faro de Alejandría durante estos cuatro años y te admiro no solo por lo que me has enseñado a nivel científico, sino por lo que me has enseñado a nivel humano.

Agradezco a Josep Prat por abrirme las puertas del GCO y darme la oportunidad de trabajar junto a ingenieros excepcionales, así como permitir involucrarme en el proyecto europeo Accordance (FP7/2007-2013) sobre el cual se ha basado esta tesis doctoral. Te agradezco que me hayas hecho sentir en todo momento, uno más de la familia.

También quiero agradecer a esa pequeña familia formada por (en orden alfabético) Ferran Anglada, Francesc Bonada, Eric Borland, Pau Borotau, Adolfo

Lerín, Javier Martínez y Víctor Polo así como todos los compañeros con los que he tenido el placer de coincidir durante esta aventura, como José Antonio Ibarra y Ricardo Barrios, por estar a mi lado en los momentos buenos y en los no tan buenos, por todo lo que he aprendido de ellos y por permitir dejarme entrar en sus vidas.

En términos financieros, quiero también agradecer a la Agencia de Gestió d'Ajuts Universitaris i de Recerca (AGAUR) de la Generalitat de Catalunya y al proyecto EU-FP7 Accordance el poder realizar esta Tesis durante los últimos cuatro años.

A nivel personal, tengo la inmensa suerte de estar rodeado de muchísima gente que me quiere y que cree en mí. Personas sin las cuales, yo no sería yo. Personas a las que les debo gran parte de mis éxitos. Quiero dar un inmenso gracias a todas aquellas personas que han hecho de mi vida un jardín del edén. Aun así, de todas ellas, siempre habrá dos a las que les debo muchísimo, mi brazo izquierdo y mi brazo derecho, mi pierna izquierda y mi pierna derecha, singulares espejos en los que reflejarme, personas admirables que quiero y que considero mis hermanos. Gracias Eloy Conchillo y Enric Sauret.

Finalmente, quiero dedicar mi mayor logro a las tres mujeres de mi vida. A mi madre, María Elias, la persona que me lo ha dado todo sin pedir nada, una vida repleta de momentos inolvidables, una educación inmejorable, una enseñanza basada en la perseverancia y el inconformismo hacia lo ordinario. Me inculcó el deseo de llegar siempre a las estrellas. A mi abuela, Manuela Solé, con la que tuve una conexión más allá de lo tangible y de la que hoy aun lloro su pérdida. Y por último a mi pareja, mi compañera de vida, mi gran amiga, mi cómplice, mi todo, Zoraida Mateo. Te agradezco que seas mi confesora, te agradezco cada consejo que me das, te agradezco cada sonrisa, cada beso y cada abrazo que me regalas, te agradezco el apoyo ilimitado que me demuestras, te agradezco los ánimos y la fuerza que me insuflas en los momentos más bajos, en definitiva gracias por acompañarme en esta vida y creer en mí hasta cuando yo mismo no creo.

Contents

Acronyms

ACCORDANCE	A converged Copper-Optical-Radio OFDMA-based access Network with high Capacity and Flexibility
ACO-OFDM	Asymmetrically clipped OFDM
ADC	Analog-to-Digital Converter
AM	Amplitude Modulation
AM-OFDM	adaptive modulation OFDM
AMOOFDM	Adaptively Modulated optical OFDM
AO-OFDM	All-optical OFDM
APD	Avalanche PD
AWG	Arrayed Waveguide Gratings
AWGN	Additive White Gaussian Noise
B2B	Back-to-Back
BB	Baseband
BER	Bit Error Rate
BpS	Bits per Symbol
BPSK	Binary Phase-Shift Keying
BR	Bit Rate
BT	British Telecom
BW	Bandwidth
CCDF	Complementary Cumulative Distribution Function
CD	Chromatic Dispersion
CO	Coherent
C-OFDM	conventional OFDM
CO-oOFDM	Coherent Detection-optical OFDM
CP	Cyclic Prefix
CS	Carrier Suppression

CSPR	Carrier-to-Signal Power Ratio
DAC	Digital-to-Analog Converter
DC	Direct Current
DCO-OFDM	DC-biased optical OFDM
DD	Direct Detection
DD-oOFDM	Direct Detection-optical OFDM
DFB	Distributed Feedback
DFT	Discrete Fourier Transform
DINLD	Dispersion-Induced Nonlinear Distortion
DM	Dynamic Margin
DL	Data Label
DML	Direct Modulated Laser
DMT	Discrete Multi-Tone
DS	Downstream
DSB	Double Sideband
DSL	Digital Subscriber Line
EAM	Electro-Absorption Modulator
EBA	Elastic Bandwidth Allocation
EDFA	Erbium Doped Fiber Amplifier
EO	Electro-Optical
EPON	Ethernet Passive Optical Network
ER	Extinction Ratio
EU	European Union
EVM	Error Vector Magnitude
FDM	Frequency Division Multiplexing
FEC	Forward Error Correction
FFT	Fast Fourier Transform
FPGA	Field-Programmable Gate Array
GB	Guard Band
GI	Guard Interval
GPON	Gigabit Passive Optical Network
GUI	Graphical User Interface
HS	Hermitian Symmetry
ICI	Inter-channel Interference

IDFT	Inverse Discrete Fourier Transform
IEEE	Institute of Electrical and Electronics Engineers
IFFT	inverse Fast Fourier Transform
IM	Intensity Modulation
IMD	Intermodulation Distortion
ISI	Inter-symbol Interference
LPE	Low-Pass Equivalent
LPF	Low-Pass Filter
LTE	Long Term Evolution
M2P	Multipoint-to-Point
MAC	Media Access Controller
MC	Multicarrier
MCM	Multicarrier Modulation
MI	Modulation Index
MIMO-OFDM	Multiple-Input Multiple-Output OFDM
MZM	Mach-Zehnder Modulator
NF	Noise Figure
NG-PON	Next Generation Passive Optical Network
NP	Null Point
OBI	Optical Beat Interference
OBM-OFDM	Orthogonal Band Multiplexed-OFDM
ODN	Optical Distribution Network
OFDM	Orthogonal Frequency Division Multiplexing
OFDM-PON	Orthogonal Frequency Division Multiplexing-Passive Optical Network
oIQ	Optical In-Phase/Quadrature
OLT	Optical Line Terminal
ONU	Optical Network Unit
OOB	Out-Of-Band
oOFDM	optical OFDM
P2P	Point-to-Point
PAPR	Peak-to-Average Power Ratio
PD	Photodiode
PN	Phase Noise
PON	Passive Optical Network

PTS	Partial Transmit Sequence
QAM	Quadrature Amplitude Modulation
QB	Quantization Bits
QP	Quadrature Point
QPSK	Quadrature Phase-Shift Keying
RB	Rayleigh Backscattering
RF	Radio-Frequency
RIN	Relative Intensity Noise
RN	Remote Node
R-OFDMA-PON	Remodulated-OFDMA-PON
RSOA	Reflective Semiconductor Optical Amplifier
RTO	Real-Time Oscilloscope
RX	Receiver
SARDANA	Scalable Advanced Ring-based Passive Dense Access Network Architecture
SC	Subcarrier
SCMA	Subcarrier Multiplexing Access
SCMA-PON	ubcarrier Multiplexing Access-Passive Optical Network
SL	Sign Label
SLM	Selected Mapping Technique
SL-OFDM	Sign Labeled-OFDM
SMF	Single Mode Fiber
SNR	Signal-to-Noise Ratio
SOA	Semiconductor Optical Amplifier
S-OFDMA-PON	Statistical-OFDMA-PON
SR	Sample Rate
SSB	Single Sideband
TDM	Time Division Multiplexing/Quadrature
TDMA	Time Division Multiplexing Access
TDMA-PON	Time Division Multiplexing Access-Passive Optical Network
TDM-PON	Time Division Multiplexing-Passive Optical Network
TDWDM-PON	Time Dense Wavelength Division Multiplexing-Passive Optical Network
TI	Tone Injection
TR	Tone reservation

TW	Time Window
TWDM-PON	Time-Wavelength Division Multiplexing-Passive Optical Network
TX	Transmitter
UDWDM-PON	Ultra Dense Wavelength Division Multiplexing-Passive Optical Network
UPC	Universitat Politècnica de Catalunya
US	Upstream
VOA	Variable Optical Attenuator
VPI	Virtual Photonics Interface
WDMA	Wavelength Division Multiplexing
WDMA	Wavelength Division Multiplexing Access
WDM-PON	Wavelength Division Multiplexing-Passive Optical Network
Wi-Fi	Wireless Fidelity
WiMax	Worldwide Interoperability for Microwave Access
XGPON	10Gigabit Passive Optical Network
ZP	Zero Padding

Symbols and Notations

Roman symbols

A_{LO}	Local oscillator amplitude/Laser amplitude
c	Light speed in vacuum
c_{ik}	ith information symbol at the kth SC in TX
c'_{mn}	mth information symbol at the nth SC in RX
CP_{DSB}	Double sideband cyclic prefix length
CP_{min}	Minimum cyclic prefix length
CP_{SSB}	Single sideband cyclic prefix length
D	Dispersion
E_0	Field Amplitude
E_{in}	Input field
E_{out}	Output field
f_k	Frequency at the kth SC
f_n	Frequency at the nth SC
f_{opt}	Optical emission frequency
g_k	Waveform for the kth SC
g_n	Waveform for the nth SC
$H(\omega)$	Transfer function
$i_D(t)$	Current after photodiode
$I(t)$	Current
I_{bias}	Bias current
$I_{RF}(t)$	Radio-Frequency current
I_{th}	Threshold current
L	Length
m	Modulation index

N	Number of subcarriers
$p(t)$	Rectangular baseband function
P_c	Carrier power
P_C	Complementary cumulative distribution function
P_{in}	Input power
P_{out}	Output power
$q(t')$	Squared windowing function
$r(t)$	Received signal
R	Responsivity
$\Re$	Real part
$s(t)$	Transmitted signal
S_L	Slope frequency
t	Time
t_D	Maximum channel delay/Delay spread
t_G	Time guard interval
t_k	Time delay at the kth SC
t_n	Time delay at the nth SC
T_{FDM}	FDM symbol period
T_{MC}	Multicarrier symbol period
T_{OFDM}	OFDM symbol period
T_s	Symbol period
v_g	Group velocity
$V(t)$	Electrical voltage
$V_{RF}(t)$	Radio-Frequency voltage
$x(t)$	Information signal
$Z[nT_s]$	Signal in the digital domain

Greek symbols

$\Delta\nu$	Linewidth
$\beta(\omega)$	Optical fiber propagation constant
β_0	Constant optical phase
β_1	Group delay
β_2	Group delay variation

Δf	Frequency spacing
$\Delta\tau_g$	Pulse broadening due to time delay
$\Delta\omega$	Signal bandwidth
λ	Wavelength
τ_g	Group delay
ϕ_k	Phase at the kth SC
ω	Angular frequency
ω_0	Baseband angular frequency
ω_d	Angular laser frequency detunning
ω_{ref}	Optical fiber reference angular frequency
ω_{RF}	Radio-Frequency angular frequency

List of Figures

List of Tables

Chapter 1

Introduction

In recent decades, the communications industry has experienced an exponential evolution, especially due to the increasing bandwidth (BW) demand per user. Undoubtedly, the unparalleled properties for data transmission (TX) offered by optical fiber cables have been the enabler of such a dramatic growth.

With the deployment of Time Division Multiplexing Access-based (TDMA) standards such as Gigabit Passive Optical Network (GPON) or Ethernet Passive Optical Network (EPON) for access networks taking place in the recent years, a new breed of fast home internet access has emerged, which in turn has led to increased BW demand. Now, as the new generation of optical access networks is envisioned targeting longer reach, higher bit rates (BR), higher user count, greater flexibility, more efficient resource management, cost-effectiveness, reduced energy consumption and requiring new features such as convergence with mobile networks, TDMA is starting to show its weaknesses and new modulation formats need to be sought.

Figure 1.1 (left) shows the evolution of access network capacity for both the upstream (US), user to network, and downstream (DS), network to user, directions. As seen, the forecast is that by 2020 the required capacity of networks should reach between 100Gbps and 250Gbps in DS and between 40Gbps and 250Gbps in US. With capacities of present TDMA standards around 2.5/1.25Gbps respectively for US/DS [1], there is clearly a long way to go and great research efforts are required for technology to be able to cope with demand.

Figure 1.1 (right) depicts a map with the evolution of the (Passive Optical Network) PON-standards and their multiple access protocols along these last years, taking into account the capacity per user which they are able to provide. As shown, even if the dominant multiplexing technology to date has been TDMA, a future generation of PON will need to resort to other alternatives in order to reach the aforementioned capacities.

Operators on their side are interested in extending the PONs coverage area

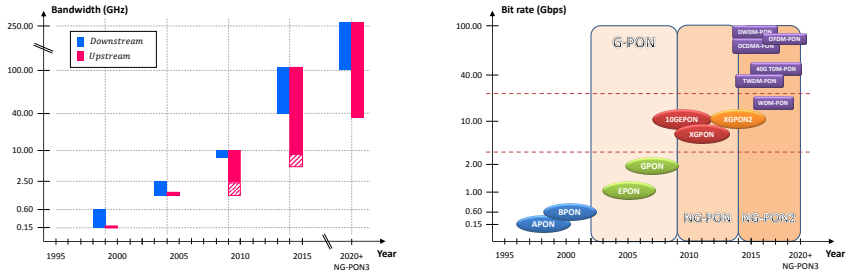

Figure 1.1: Capacity trend for PONs [2] (left) and evolution of the multiple access protocols capacity per user (20km) (right).

in order to reduce the required infrastructure. Specifically, typical network reach of current standards such as GPON and 10Gigabit-PON (XG-PON) is around 20km and 60km respectively, and it is expected that future PON developments target extensions between 80km and 100km for Next Generation-PON2 (NG-PON2) and NG-PON3 [3].

As a step towards next generation PONs, within European project ACCORDANCE (A converged Copper-Optical-Radio OFDMA-based access Network with high Capacity and Flexibility) [4] an assessment of the potential of OFDM techniques has been conducted, and specifically an experimental validation of a TX with a NG-PON2 scenario based on Orthogonal Frequency Division Multiplexing-PON (OFDM-PON) through a fiber reach higher than 100km has been performed. Partners in the project include operators such as TID and DT, providers such as Alcatel-Lucent, academic institutions such as UPC, AIT, KIT and UH, and administrators such as JCP-Connect and Euprocom OÜ. UPC contributions have focused mainly on physical layer studies where the works developed within this Thesis have played an important role.

1.1 Basic structure of PONs

In an access network, the optical fiber can be deployed basically by three different schemes: it may either use a point-to-point (P2P) topology in which each subscriber is connected to the central office by means its own optical fiber; by adding a Remote Node (RN) consisting on a concentration switch between the central office and the subscribers; or by replacing the previous active RN by a distribution switch or similar passive distribution device. The most common deployment method is the latter since it presents a good trade-off between performance, costs and complexity and they are referred as Passive Optical Networks or PON. Moreover, they show great potential for high BW information transport [5] and they can be operated economically thanks to shared usage of fiber and optical transceivers [6].

Figure 1.2 illustrates the basic topology of a PON. As it can be seen, a PON

is composed by the OLT, the ONUs, and peripheral devices that distribute the signal and are located in the RN. Furthermore, the whole network is composed of two main parts: the feeder network, from the OLT to the first RN, and the Optical Distribution Network (ODN) from the first RN to the ONU's.

Depending on the direction of the traffic, the information exchange process in a PON is referred to as either US or DS. The DS mode consists of signal broadcasting from the OLT to all ONUs. Data is encrypted and sent by the OLT to the RNs which distribute the information towards its corresponding ONU. In the US, the optical network becomes a multipoint-to-point (M2P) network between different ONUs and the OLT so signals must be combined using a multiple access protocol.

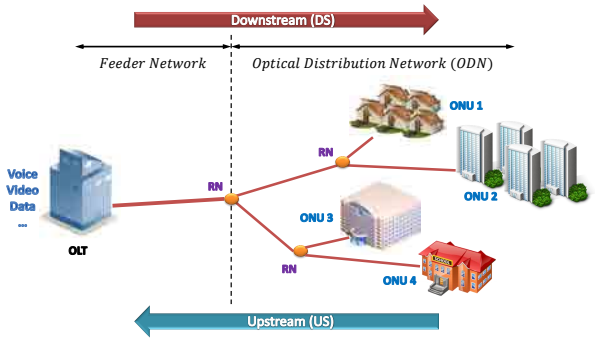

Figure 1.2: PON topology

Generally, the US is more challenging than the DS, therefore multiple access protocols will be explained with emphasis on the US in the following section.

1.2 Multiple access protocols for PONs

To satisfy the requirements of future PON systems, both US and DS traffic require efficient multiplexing techniques.

The great simplicity and technology maturity and reliability of TDMA protocols have provided a solid ground base for massive deployment of PONs and they constitute the technologies behind current standards of reference such as GPON and EPON. As evolution towards longer reach and higher capacities is considered, there is a little room for improvement when using TDMA. Also, TDMA strategies lack the required flexibility in transmission protocols and in allocation of network resources, and are not very easily scalable.

As shown in figure 1.3 (left) when TDMA protocol is used in a PON [7], the OLT dedicates a fixed length time slot to each of the ONUs, so that they can make use of the full USBW for the duration of their assigned time slot. The challenge for the OLT is to correctly range each ONU and successfully

synchronize to every data burst at the US optical link.

Due to the scalating BW demand per user, TDMA is starting to show its weaknesses and other multiple access protocols such as WDMA, Subcarrier Multiplexing Access (SCMA) whose main representative is OFDMA, have been positioned as candidates for the new generation of optical access networks. In what follows a brief review of the basic characteristics of the alternative access protocols is made.

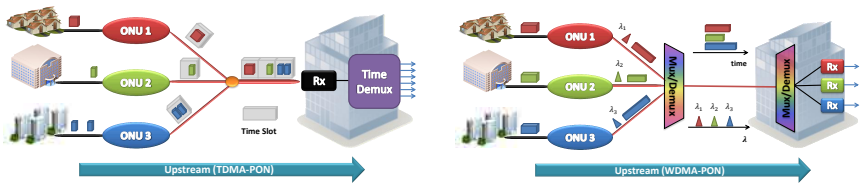

Figure 1.3: US channel scheme for a TDM-PON (left) and WDM-PON (right).

Figure 1.3 (right) shows a scheme of a WDM-PON [8, 9]. This protocol employs separate wavelength channels from the OLT to the ONUs in the DS direction. Selection of the information of each ONU can be made through wavelength demultiplexers based on Arrayed Waveguide Gratings (AWG) located at the RN or by optical filters at each ONU. In the US, each ONU modulates its information in an optical carrier of different wavelength. The use of wavelengths gives desirable properties to the network, such as scalability, security, high BW per user and protocol transparency. Furthermore, a higher power budget may be made available by the use of AWGs at the RN. By contrast, it also complicates the optics requiring wavelength control techniques and lacks granularity. As an example of hybrid PON topology, the European project SARDANA (Scalable Advanced Ring-based Passive Dense Access Network Architecture) [10, 11] presents a topology with a central WDM ring, to offer instant communication protection in case of fiber cut, plus TDM.

On its side, the architecture of SCMA-PON [12,13] consists on one dedicated electrical subcarrier for each ONU. As said, an important subclass of SCMA adding spectral efficiency is OFDMA. As figure 1.4 shows, OFDMA-PON follows the same architecture of conventional PON and uses different electrical bands for DS and US. In both, the DS and US traffics, the OFDM-PON architecture divides the total OFDM BW in N sub-bands, each containing a number of subcarriers (SC) assigned to one user.

Taking into account that OFDMA-PON is the topology analyzed and used in this Thesis, it is suitable to firstly introduce the concept of OFDM in order to better understand how it works and which are their main advantages and challenges when it is used in PONs.

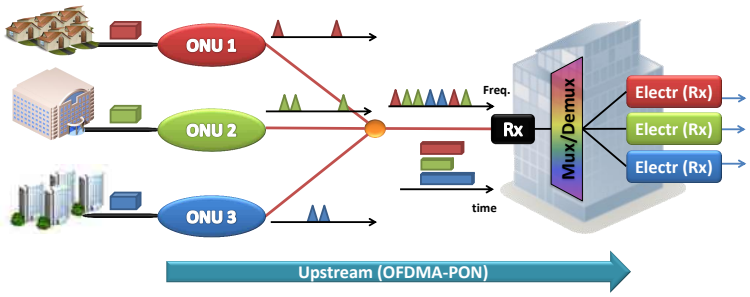

Figure 1.4: Upstream channel scheme for an OFDMA-PON.

1.3 OFDM basic principles

Basically, OFDM is a SCMA protocol which ensures a specific frequency distance between the SCs equal to the inverse of the duration of a symbol in order to fulfill the orthogonality condition. The fundamental principle remains in decomposing the high rate data stream into N lower rate streams and then TX them simultaneously over a number of SCs.

The whole data sequence of an OFDM frame is thus, the sum of many frequencies which contain part of the information. Firstly, as shown in figure 1.5, data is mapped into symbols and then converted from serial to parallel. The symbol is thus made longer so that one symbol at most is affected by Intersymbol Interference (ISI) [14] and linear channel distortions can be compensated by simple one-tap equalization.

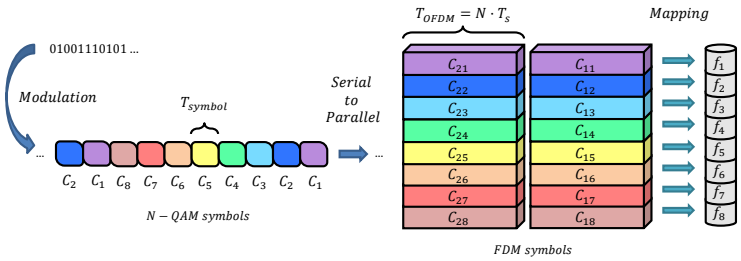

Figure 1.5: Data transmission in FDM.

The use of this technique was firstly well stablished in the current broadband wireless communications systems mainly because it is an effective solution to ISI caused by a dispersive channel and because it is robust against channel selective frequency fading. This is because when data is transmitted through a large number of SCs, only part of the information is lost in case of frequency fading whereas in single-carrier TX the whole sequence is affected.

The main features of OFDM are that they provide a protocol-transparent,

simple and robust network by taking advantage of mature electronics through keeping the processing and multiplexing of users and data in the electronic stage. Moreover, it shares the good features of WDM, such as transparency and flexibility, while adding granularity and simplicity of implementation by shifting complexity to the electronic domain. It is also possible to dynamically allocate the SCs to users which can help to optimize the access. Finally, it is a technique which may allow a convergence of wired and wireless access, as a step towards the universality of access networks.

The underlying basis of OFDM mainly applied to wireless communications have been investigated for almost 40 years, specifically since 1966 when R. Chang proposed the fundamental principles of OFDM as a way to overlap multiple channels within a limited BW without interferences by adjacent channel [9]. Afterwards, in the early 1970s, S.B. Weinstein and P.M. Elbert showed that multicarrier modulation (MCM) can be accomplished using Discrete Fourier Transform (DFT) [12]; and in the mid-eighties, the key studies of L.J. Cimini lead to the adoption of OFDM as a standard in mobile communications [13]. On the access arena, in the mid-nineties, Digital Subscriber Line (DSL) connections adopted a variation of OFDM called Discrete Multi-Tone (DMT) and finally from the late nineties onwards, this technique has been successfully adopted in many standards by the Institute of Electrical and Electronics Engineers (IEEE) committee such as Wireless Fidelity (Wi-Fi) [15], Worldwide Interoperability for Microwave Access (WiMax) [16] and Long Term Evolution (LTE) [17, 18].

In spite of those good features, it was not until the late 1990s, that OFDM emerged as an innovative technique for chromatic dispersion (CD) compensation in reconfigurable optical long-haul networks. The natural question to ask is then, why is it only recently that OFDM has started to be considered as a suitable format for optical communications?

1.4 OFDM in optical communications, why now?

The race in optical communications based on OFDM techniques did not begin until the late nineties, although OFDMA was used in the field of radiofrequency decades ago. Historically, the first optical OFDM system proposal may be traced back to Q. Pan and R.J Green publication in 1996 [19], where the performance comparison between the hybrid multichannel Amplitude Modulation/OFDM (AM/OFDM) and the conventional Amplitude Modulation/Quadrature Amplitude Modulation (AM/QAM) systems in an impulsive noise environment was presented. However, it was not until 2006 with the record-breaking optical OFDM system demonstration presented in a paper by J. Lowery and J. Armstrong [20], that a true revolution started about applying OFDM for optical fiber communications.

Indeed, the reason for such a late start of OFDM into the optical communications realm can be found in the fact that the natural characteristics of optical

communication systems differ significantly from those of standard OFDM modulation techniques.

To start with, the phenomena of light generation and detection are generally based on one-to-one conversions between electrons and photons, and therefore electrical currents of voltages correspond to optical power or intensity. Thereby, optical communication systems based on intensity (rather than amplitude) modulation and direct (square-law) detection (IM/DD) are the most popular way of sending electrical information over an optical carrier. As a consequence of the square modulus relation between electrical and optical magnitudes, there is not a direct mapping between electrical and optical spectra. Thus, conventional IM/DD optical communications systems are by nature not directly compatible with conventional OFDM systems since linear signal transformations caused by the channel translate into nonlinear distortions at the end-to-end transmission systems level. Precisely one of the reasons behind the success of OFDM techniques lies in its ability to compensate for the channel impairments, but the effectiveness of compensation is severely reduced if the channel transfer characteristic is not linear, such as in IM/DD optical communications.

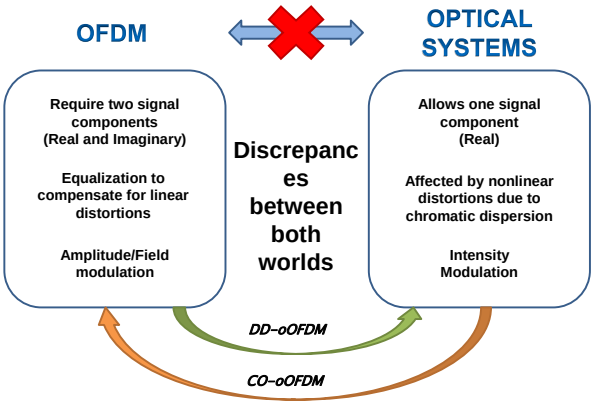

Figure 1.6: OFDM modulation in time domain (left) and in frequency domain (right).

On the other hand, in a standard OFDM signal two signal components (in-phase and in-quadrature) are TX. By contrast, in an IM/DD system the information is conveyed by the optical wave envelope only while the optical phase information is usually lost.

There are mainly two ways around the problem: it is either the optical system that changes so that it adapts to the defining characteristics of OFDM or it is OFDM systems that are adapted to the intrinsic nature of optical systems. The latter option gives rise to the broad class of optical Direct Detection optical OFDM (DD-oOFDM) systems which this Thesis mainly focuses on, while the former are known as Coherent optical OFDM (CO-oOFDM) system approaches. A review of the basic characteristics of all the different optical OFDM approaches and a classification is contained within chapter 3.

Beyond the above explained difficulties in adapting the typical characteristics of optical systems to OFDM systems, another good reason behind the lag in application of OFDM to optics is the high data rates typical of optical communications. Indeed, it is only recently that Digital Signal Processing (DSP) speeds are approaching the required performance level [21].

1.5 A little history...

As said, the first serious proposals of OFDM in optical communications targeted long-haul network applications at mid-2000. In the evolution towards reconfigurable networks the basic goal of those demonstrations was to dynamically compensate the effect of CD. Thus, the confined and narrow spectrum of OFDM and its capacity to eliminate virtually all ISI made it an ideal candidate for networks with many reconfigurable optical add and drop multiplexers [22]. Furthermore, with the explosive, multimedia-driven growth of Internet traffic, it became evident that unless fiber BW was used more efficiently, the operation spectrum range of optical amplifiers and even the fiber channel capacity itself would be exceeded [23–25]. These vital considerations first made the high-profile case for optical OFDM in the context of spectrally efficient, next-generation 100Gbps long-haul fiber communications [16, 26–28].

The revolutionary article published in 2006 by J. Lowery and J. Armstrong where a simple technique to convert an optical IM in an AM was proposed [20] showed that the properties of OFDM could advantageously be exploited and successful TX of a 10Gbps signal through a fiber length of 4000km was achieved. A year later, the world's first coherent (CO) detection experiment with line rate of 8Gbps over 1000km [29] was reported by W. Shieh. From there onwards, the TX capacity continued to grow about ten times per year, the number of groups with interest in the optical OFDMA grew exponentially and mirroring the two first key demonstrations, two major research directions appeared: the one initiated by J. Lowery and J. Armstrong basically targeting low-cost scenarios, the DD-oOFDM systems and the one started by W. Shieh and focused on achieving a high spectral efficiency and sensitivity, called CO-oOFDM systems.

Once the case for OFDM in the long-haul area was made through many successful record-breaking demonstrations showing feasibility of oOFDM systems with practical relevance, the idea of taking advantage of OFDM techniques in order to solve the congestion of optical access networks was increasingly gaining momentum. The abovementioned ACCORDANCE project consortium, composed by partners from several countries of European Union (EU), investigated a new paradigm for the access networks in that direction. Specifically, this project explored the potential of OFDMA techniques for optical access networks which could offer at the same time optical backhauling for wireless and copper-based networks.

As already told, the expected contributions of this Thesis work are in line with the objectives of ACCORDANCE and aim at establishing the principles of oOFDM TX systems, identifying benefits and challenges, and providing and analyzing solutions for improvement focusing on applications to OFDM-PONs.

In the next section the alternatives for NG-PONs are reviewed in order to provide an overview of the potential of OFDM protocols to provide the basis of a NG-PON that is up to the expectations above described. We will highlight benefits and challenges of OFDM in order to set the basis for the Thesis objectives.

1.6 Optical OFDM for access networks

The four major reasons to use OFDM as multiple access protocol in optical communication services are its ability to cope with frequency selective channels through equalization; the use of cyclic prefix (CP) to avoid both ISI and ICI, its high BW granularity and its flexibility for dynamic resource allocation.

In access, much as in long-haul, the two major trends for definition of an oOFDM system are DD-oOFDM and CO-oOFDM. However, while for long-haul networks, both options are in quite fair competition, the specifics of access networks generally make lower-cost DD-oOFDM a preferred alternative. As it will be seen the choice of a specific oOFDM flavor for access will depend on many factors such as the traffic direction (US/DS), user count and reach or power equalization, among others.

Table 1.1 shows a comparative of the most important multiple access protocols technologies in section 1.2 in optical communications, considering their main capabilities and characteristics.

The major advantages of OFDMA as a suitable technology for use in optical access networks can be found firstly in its ability to support multi-level modulation in a dynamical way, it is a protocol-independent [16] and also presents an efficient dispersion compensation allowing to achieve spectrally-efficient, high-speed and long-reach access over a legacy PON fiber plant. Furthermore, the OFDMA SCs can be used as finely-granular BW resources for highly-dynamic multi-user traffic. On the other hand, an additional advantage is that OFDMA implementations are largely DSP-based and can thus be realized in silicon to achieve cost-efficient reconfigurable volume-driven implementations. Furthermore, OFDM was extensively used in wireless communications and mobile broadband standards facilitating the current convergence with optical communications.

Moreover, this technique shows a better optical spectral efficiency and granularity than WDMA systems since it allows narrower channel spacing; however, it requires high speed data processing equipment which increases complexity, energy consumption and cost. Also, several issues regarding the users multiplexing

in the US still remain to be solved.

Capabilities	TDMA	WDMA	OFDMA
Maximum capacity	Very High	High	Low
Granularity	High	Low	High
Network management (DBA flexibility)	Low	Medium	High
Spectral efficiency	Low	Medium	High
Scalability	Low	High	Medium
Cost	Low	Very High	High
Maintenance	Simple	Difficult	Difficult
Security	Low	High	Low
Optical Budget	31dB	29-43dB	30-36dB
Dispersion limited reach	<40km	<20-60km	<100km
Split	64	80	64
Protocol independent	Low	High	Medium
Synchronization	Critical	Relaxed	Medium
System maturity	Commercial	Development	Research
Power OLT	Low	High	Medium
Power ONU	Medium	Low	High
Receiver Bandwidth	Single channel	2x Sum of channel BW (DSB)	Sum of channel BW (SSB)
Detector shared at head-end	Yes	No	Yes
Expensive components	➢ Broadband Laser ➢ Shared broadband optical receiver	➢ Dense WDM wavelength selected ➢ Stabilized DFB	➢ Broadband laser ➢ Shared broadband optical receiver ➢ Analog components (DSP, RF local oscillators)
Upgrading possibilities	➢ Higher channel speed ➢ More λ	➢ Higher channel speed ➢ More λ	➢ Higher channel speed ➢ More λ ➢ Higher level QAM (Bit Loading)

Table 1.1: Comparative NG-PON technologies of different parameters and capabilities [18, 30].

Notice that the abovementioned multiplexing technologies are not mutually exclusive, and in fact, important advantages may be derived from combined approaches. In that respect, hybrid multiple-access strategies have been proposed such as TWDM-PON (TDM/WDM-PON) [31], TDWDM-PON (TDM/DWDM-PON) [32], SCM/ WDM-PON [33] and OFDM/WDM-PON [34, 35].

To sum up, the OFDM-PON benefits comprises the granularity, the flexibility and the dynamic allocation of the SCs, it spectral efficiency against the other techniques and a suitable power budget although it is higher in WDM-PON and a high dispersion reach in comparison with TDMA and WDMA; on contrary, the maximum capacity within this kind of networks is a critical challenge as well as the cost, the maintenance, the security and the power consumption. From the point of view of the signal TX, OFDM-PON also presents several challenges. Most of them will be studied in this Thesis and different algorithms, techniques and architectures will be proposed for their relief. The most important impairments which can be found in an OFDM-PON are its higher sensitivity to Phase Noise (PN) and frequency offsets, and its higher Peak-to-Average Power Ratio (PAPR) which can distorts the signal until be impossible to detect it correctly.

Other important problem addressed is related to the heavy data processing

required by OFDM techniques which makes them costly and power inefficient. The Thesis thus, includes studies about determination of the minimum number of bits required in DAC/ADC conversions. Hence, OFDM in optical communications can be considered sufficiently novel issue to investigate in greater depth and unveil its potential for future optical networks.

1.7 Scope of the dissertation and structure

This Ph.D. Thesis is focused on exploiting the potential of OFDM standards in low-cost access optical communications.

This document is composed of nine chapters and five appendices. After this introduction, chapters from 2 to 4 comprise the relevant state-of-art and the comparison between the most relevant strategies for an OFDM-PON. Chapters 5 to 8 present the main contributions of this Thesis and finally in the last chapter, the conclusions and the future lines close the overall document.

Chapters 2 and 3 offer a deep study about the optical and the electrical domain. Chapter 2 is divided into three parts: the optical part, the electrical part and the combination of both. Firstly, the main techniques for light modulation are presented at the beginning. This parts ends with an overview of the conventional IM/DD general model and an introduction about the main linear distortion and its effects over the optical signal sent: the Dispersion-Induced Nonlinear Distortion (DINLD), the Carrier Suppression (CS) and the PN. Next, the basic principles of the OFDM modulation are discussed and analytically presented, as well as a diagram block of the electrical coder and decoder modules of an OFDM system. This part ends with a detailed analysis of the CP technique to avoid ISI and ICI. Finally, the optical and electrical parts are combined to present the oOFDM system strategies and classify them with its main characteristics.

Chapter 3 addresses the CD effect analytically since is the main limiting impairment in the Single Mode Fiber (SMF) TX systems of interest in this Thesis. Furthermore, special attention is devoted to the fiber reference frequency parameter. It is mathematically described for both, a Single Sideband (SSB) and Double Sideband (DSB) signals. In addition, the minimum CP length for both cases is also obtained from previous analysis. Next, the DINLD and the CS effects due to CD briefly described in chapter 2 are deeply analyzed in a simulation environment. This chapter ends with the study of the evolution of the electrical and optical spectra, and the corresponding constellations by simulation of a conventional IM/DD oOFDM system after compensating each of the CD effects.

Considering the OFDM standard is still young in optical communications and systems comparisons found in the literature take into account only a few of the oOFDM options, from the exhaustive list of oOFDM alternatives presented in chapter 2 we select the eight more relevant ones to be tested under the

same conditions in order to compare their performances and stablish a power budget ranking. Thus, this ranking will allow to associate the devices used with the sensitivity, as well as consider if the difference in power budget justifies the network cost. This chapter is divided into three big sections. Firstly, the characteristics and common features of overall compendium of oOFDM systems are presented and listed. Next, the eight oOFDM systems are divided into three groups depending on if it has to modify the electrical domain, the optical domain or both. This section plots the performance of each oOFDM system against the variation of the electrical BW, the modulation format or the fiber reach. The chapter ends with an overall oOFDM system comparison considering mainly the sensitivity, the DSP usage, the power budget and the number of users.

Chapters 5 and 6 correspond to the main contributions of this Ph.D. In chapter 5, two solutions for an OFDM-PON based on ACCORDANCE project are presented: the high performance Remodulated-OFDMA-PON (R-OFDMA-PON) and the cost-effective Statistical-OFDMA-PON (S-OFDMA-PON), designed in the Universitat Politècnica de Catalunya (UPC) labs. This chapter includes an analysis of the Optical Beat Interference (OBI) and PN effects caused by the detection of several decorrelated optical sources since it constitutes an important impairment in the multiplexing of users in the US. Afterwards, the design of the ONU and the OLT modules prototypes of the S-OFDMA-PON is described. Finally, this new PON architecture is experimentally analyzed by using two different approaches for the ONUs to place their information into disjoint electrical spectral bands: the digital multiplexing and the multiband multiplexing. On the one hand, EBA is applied to the first approach in order to study the power budget performance. Thus, this chapter proposes to use the extra sensitivity obtained from the ONU whose BW was reduced, to compensate the differential link losses of an existing infrastructure. This aims to reduce costs of the network deployment by reusing the infrastructure already deployed. On the other hand, with the multiband approach both the complexity and the energy requirements of the overall system are reduced since it allows to reduce the amount of data processed by each ONU. Therefore, it is experimentally analyzed and compared with the digital multiplexing approach in order to balance the difference in sensitivity with the difference in complexity.

Chapter 6 is focused in proposing techniques to mitigate the PAPR which is one of the main impairments affecting OFDM transmissions. It first presents the PAPR concept as well as the principal reduction techniques. Afterwards two novel algorithms are described: the Data Labeled-OFDM (DL-OFDM) and a particularization of it called Sign Labeled-OFDM (SL-OFDM). The former consists on folding the signal when a high PAPR is detected and adding side information about the sign and the number of folds of a specific sample to be correctly unfolded at the decoder. On contrary, the latter folds the signal when negative samples are detected and adds side information about the sign the samples. The basic difference between both algorithms is that DL-OFDM is used to mitigate the PAPR effect and SL-OFDM is used to extend the dynamic range of the optical system by eliminating the need of a carrier to detect the signal. The DL-OFDM algorithm is introduced and added in a P2P oOFDM

network based on IM and DD (ID01). Next, the M2P analysis is carried on the S-OFDMA-PON with digital multiplexing approach. The network performance obtained is finally compared with the same PON without the algorithm in both, DS and US to evaluate the improvement provided by the algorithm. The same procedure is performed with SL-OFDM in a network based on AM and DD (AD01).

Chapter 7 aims to optimize the resolution required for the Analog-to-Digital and Digital-to-Analog Converters (ADC/DAC) devices to guarantee a given performance. Notice that a reduction of the ADC/DACs complexity can directly be translated into a reduction of the network cost and energy consumption. An introduction about these devices can be firstly found and afterwards the analyses presented are divided into two sections. Firstly, the quantization is analyzed and compared in two P2P oOFDM systems based on DD: with IM and with AM. Afterwards, the IM/DD system is moved on the laboratory to be experimentally analyzed under different FFT sizes and modulation format conditions. At the end of the chapter, the performance of the S-OFDMA-PON with both digital multiplexing and multiband multiplexing approaches against the variation of the ADC resolution is simulated and compared.

Finally, chapter 8 focuses on the PN effect in scenarios with several decorrelated optical sources such as the R-OFDMA-PON described in chapter 5. In this chapter, pilot tones are used to compensate the PN effect and the relation between the modulation format, the FFT size, the BW and the laser linewidth is studied through simulations. Along this chapter two kind of BW are considered, the BW per SC and the total data BW. This differentiation is important here since results indicate that the laser linewidth tolerance directly depends on the BW per SC. Thus, firstly, the pilot tone insertion algorithm is introduced. Next, it is applied in a P2P oOFDM network based on AM and DD and the sensitivity against the laser linewidth is plotted considering different BRs, modulation formats and FFT sizes. Finally, the laser linewidth is fixed and the maximum optical fiber reach is measured for a Quadrature Phase-Shift Keying (QPSK) modulation, different FFT sizes. Notice that a laser linewidth reduction can also be translated into a cost reduction.

1.8 Research contribution

The different novelties of this Ph.D. dissertation have been disseminated through several research contributions. In particular: 2 journal papers, 9 conference papers and 1 patent of invention.

Chapter 5: 2 journal papers and 6 conference papers,

- [**J1**] Iván N. Cano, Xavier Escayola, Philipp C. Schindler, María C. Santos, Victor Polo, Juerg Leuthold, Ioannis Tomkos, and Josep Prat, "Experimental Demonstration of a Statistical OFDM-PON With Multiband

ONUs and Elastic Bandwidth Allocation [Invited]," J. Opt. Commun. Netw. 7, A73-A79 (2015).

- [**C1**] I. Cano, X. Escayola, P. Schindler, M. C. Santos, V. Polo, J. Leuthold, and J. Prat, "Experimental Demonstration of Multi-band Upstream in Statistical OFDM-PONs and Comparison with Digital Subcarrier Assignment," in Optical Fiber Communication Conference, OSA Technical Digest (online) (Optical Society of America, 2014), paper Th3G.4.
- [**C2**] I. Cano, X. Escayola, A. Peralta, V. Polo, M. C. Santos, and J. Prat, "A Study of Flexible Bandwidth Allocation in Statistical OFDM-based PON," in. Proc. of 15th ICTON, Cartagena, Spain, 2013, paper Tu.D3.1.
- [**C3**] I. Cano, A. Peralta, V. Polo, X. Escayola, M. Santos, and J. Prat, "Differential link-loss compensation through dynamic bandwidth assignment in statistical OFDMA-PON," in Optical Fiber Communication Conference/National Fiber Optic Engineers Conference 2013, OSA Technical Digest (online) (Optical Society of America, 2013), paper OTh3A.5.
- [**C4**] I. Cano, M.C. Santos, X. Escayola, V. Polo, E. Giacoumidis, C. Kachris, I. Tomkos, Member, IEEE, and J. Prat, Member, IEEE, "An OFDMA-PON with Non-Preselected Independent ONU Sources and Centralized Feedback Wavelength Control: Dimensioning and Experimental Results" in. Proc. of 14th ICTON, Coventry, UK, 2012, paper Tu.B3.3.
- [**C5**] I. Cano, A. Peralta, X. Escayola, V. Polo, M. C. Santos, and J. Prat, "Experimental assessment of an OFDMA-based statistical PON with flexible bandwidth allocation and sign-labels," in Asia Communications and Photonics Conference, OSA Technical Digest (online) (Optical Society of America, 2012), paper PAF4C.4.
- [**J2**] I. Cano, M. C. Santos, V. Polo, F. X. Escayola, and J. Prat, "Dimensioning of OFDMA PON with non-preselected independent ONUs sources and wavelength-control," Opt. Express 20, 607-613 (2012).
- [**C6**] I. Cano, M. C. Santos, X. Escayola, V. Polo, and J. Prat, "An OFDM-PON with non-preselected ONUs: dimensioning and experimental results," in Advanced Photonics Congress, OSA Technical Digest (online) (Optical Society of America, 2012), paper AW4A.4.

Chapter 6: 1 patent of invention and 1 conference paper,

- [**P1**] J. Prat, I. Cano, M. C. Santos and X. Escayola, "Método de codificación-decodificación de la amplitud de la señal mediante plegado y etiquetas de información auxiliares", Oficina Española de Patentes y Marcas Madrid, España, Patente de invención, 14 de septiembre 2012.
- [**C7**] I. N. Cano, X. Escayola, V. Polo, M. C. Santos, and J. Prat, "Sign Labeled OFDM with Intensity-Modulation Direct Detection in PON," in

European Conference and Exhibition on Optical Communication, OSA Technical Digest (online) (Optical Society of America, 2012), paper P6.04.

Chapter 7: 1 conference paper,

- [**C8**] X. Escayola, I. Cano, M. Santos, J. Prat, "OFDM-PON performance with limited quantization," in. Proc. of 15th ICTON, Cartagena, Spain, 2013, paper We.A3.2.

Chapter 8: 1 conference paper,

- [**C9**] X. Escayola, I. Cano, M. C. Santos and J. Prat, "Laser Linewidth requirements for remote heterodyne OFDM based PON scenario," in Proc. of 16th ICTON, Graz, Austria, 2014, paper Tu.A3.6.

Chapter 2

Optical OFDM systems

This chapter provides in a first part a basic overview of the characteristics of conventional IM/DD TX systems which begins with a review of the main techniques for light modulation such as the Direct Modulated Laser (DML) [36], the Mach-Zehnder Modulator (MZM) [37] and the Electro-Absorption Modulator (EAM) [38] and ends with an analysis of the main impairments that affect this kind of systems such as the DINLD [39], the CS [40] and the PN [41]. After that, the bases of OFDM [42] signal modulation are examined, the different blocks which compose the electrical coder and decoder based on OFDM are presented and an important feature such as the use of CP is analyzed. Finally, many different options of oOFDM TX systems are discussed and classified [43, 44].

2.1 Optical transmission systems

2.1.1 Direct Modulation vs. External Modulation

As it is well known, the phenomena of light generation and detection in communications are mostly based on one-to-one conversions between electrons and photons taking place in semiconductor diodes, and therefore electrical currents or voltages correspond to optical power or intensity. It is then only natural that the first optical communication systems that appeared in the 70s [45, 46] exploited the linear dependence of the optical output power of a direct-biased semiconductor laser diode with the feeding current in order to send information over an optical carrier. After some propagation length in fiber, the information signal was recovered as an electrical current at the output of a reverse-biased photodiode (PD). Due to the nature of the conversion processes, these first optical communications are known as IM/DD systems.

Once the feasibility of optical communication systems through the DML and DD photoreceivers was established, the increase in the link's data rate and

reach demand stimulated the search for best-performing alternatives. During the 80s [47], a device for the external modulation of light based on the Pockel's effect in crystals such as LiNbO3, was demonstrated giving rise to electro-optical (EO) external light modulators. Later on [48], the external modulation of light in a semiconductor through the Franz-Keldysh effect was demonstrated, opening the door to semiconductor external modulators or EAM, as they are presently known. While EO modulators feature great versatility allowing for a tight control of the characteristics of the modulation, EAMs allow for direct integration with semiconductor laser sources and are usually a cheaper and less complex option. That makes each one a preferred option in different application scenarios, so that both alternatives find widespread use as a device for the external modulation of light.

One of the advantages of an external modulation of light is that an independent optimization of the light source and the modulating device may be performed so that for example solid-state laser sources instead of semiconductor lasers may be employed with higher output powers, lower linewidths, reduced Relative Intensity Noise (RIN) and chirps, etc. In splitting up the light generation and data modulation functions, it also allows for a remote feeding of the optical carrier which enables centralized carrier PON approaches with ONU remodulation such as those in SARDANA [10, 11]. Furthermore, the independent injection of carrier source and data also allows independent control of the respective power levels.

In the following sections, the characteristics and principles of these three types of light modulation techniques: DML, MZM and EAM are analyzed in detail. Also, since in a basic mode of operation, the signal to be modulated is proportional to the intensity of the optical signal, an analysis of the mathematical principles of an IM/DD system and the main impairments that affect the quality of the received (RX) signal when propagated through fiber will be provided in a generic way.

2.1.2 Direct Modulated Laser

As said, a DML is the most natural and straight-forward way to modulate a signal over an optical carrier. The DML is based on a directly biased P-N junction where photons are generated from recombination of electron-hole pairs in a stimulated way once the population inversion has been achieved for a current above the laser's threshold [36]. A feeding current provided to the laser is thus composed of a Direct Current (DC)-bias and a superposed data signal. The bias needs to ensure operation over the threshold current in order to avoid signal clipping. In figure 2.1 (left) the relationship between the optical power and the applied bias current is depicted.

Over the transfer function, the main parameters of the DML are shown. It is possible to infer from the image that above the threshold current a linear relation exists between the power of the optical signal and the electrical current;

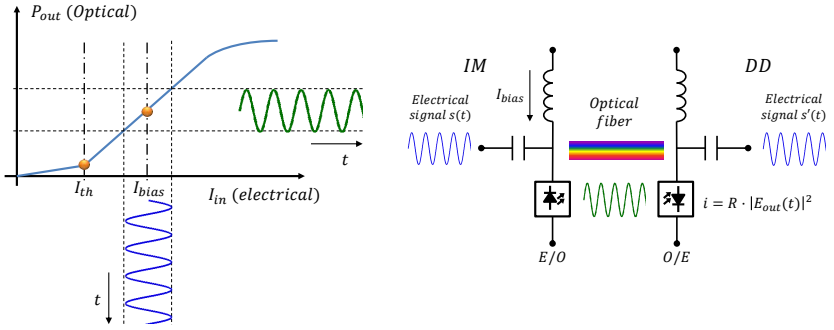

Figure 2.1: DML modulation transfer function (left) and IM/DD system based on a DML at the TX and a single PD at the RX.

such relation is defined by the slope efficiency ($S_L = \triangle P/\triangle i$). Consequently, the output power can be expressed mathematically as:

$$P_{out}(t) = S_L \cdot (I(t) - I_{th}) \tag{2.1}$$

where S_L is the slope efficiency, I_{th} is the threshold current and $I(t)$ the current of the input signal which for our purposes here it is assumed that is composed of a DC/bias current and a time-varying Radio-Frequency (RF) current, so it can be written as $I(t) = I_{bias} + I_{RF}(t)$. The bias current I_{bias} is required to keep the information signal above the threshold current I_{th} in order to avoid distortion due to clipping. This leads to:

$$P_{out}(t) = S_L \cdot (I_{bias} - I_{th}) + S_L \cdot I_{RF}(t) \tag{2.2}$$

In connection to the analysis carried out in section 2.1.5, the above is written as:

$$P_{out}(t) = P_c \cdot (1 + m \cdot x(t)) \tag{2.3}$$

where P_c is identified as the carrier power and m as the normalized IM modulation index (MI), so:

$$P_c = S_L \cdot (I_{bias} - I_{th}); \qquad m = \frac{I_{RF}}{I_{bias} - I_{th}} \tag{2.4}$$

being I_{RF} the amplitude of $I_{RF}(t)$ in (2.3):

$$I_{RF}(t) = I_{RF} \cdot x(t) \tag{2.5}$$

with $x(t)$ an information signal normalized to unity amplitude.

2.1.3 Mach-Zehnder Modulator

The Pockel's or EO effect gives rise to an optical index change proportional to an applied electrical field [37,49]. Therefore, it allows to achieve a phase modulation of an optical signal propagating along a material possessing a Pockel's response when a low-frequency electric field is applied. In order to translate that into an optical AM useful for conventional optical communications, an interferometric configuration may be used where the optical signal is split and made to travel along different paths which undergo different phase modulations. When the signals are recombined again an AM is obtained through their interference.

The most usual interferometric configuration for EO integrated modulators is the Mach-Zehnder interferometer, illustrated in figure 2.2 (right). As seen, in the most generic case two different signals which are composed by a bias voltage and a time varying information signal may be applied to each of the interferometric branches.

In order to establish the fundamental operation principles of the MZM, we will focus in the conventional push-pull mode, consisting in providing a single input voltage to the device which is applied to both interferometric branches with opposite signs. Following the notation in the figure, let $\phi(t) = \phi_U(t) = -\phi_L(t)$ be the magnitude of the phase shift in any of the interferometric branches and let V_π the parameter that quantifies the strength of the Pockel's effect by providing the voltage swing required to go from a situation of constructive to destructive interference between the two branches, that is, from zero to 180º relative phase shift. The MZM transfer curve as a function of input electrical voltage $V(t)$ in the push-pull configuration, respectively for the output power or intensity and the output field amplitude is given by

$$P_{out}(t) = 2P_{in} \cdot cos^2\left(\frac{\pi}{2V_\pi} \cdot V(t)\right) \tag{2.6}$$

$$E_{out}(t) = \frac{2E_{in}}{\sqrt{2}} \cdot cos\left(\frac{\pi}{2V_\pi} \cdot V(t)\right) \tag{2.7}$$

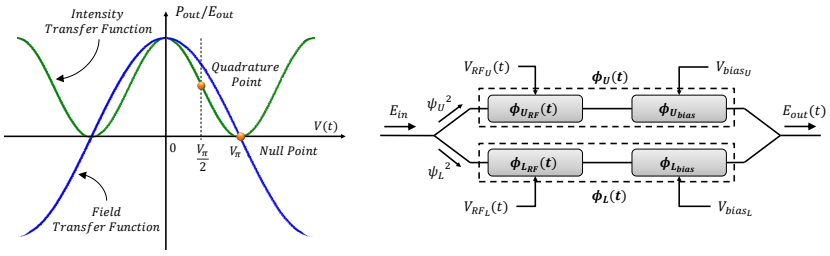

Figure 2.2: MZM response (left) and its generic scheme (right).

Figure 2.2 (left) illustrates the MZM modulation transfer function, both

from the viewpoint of output intensity (green curve) and from the viewpoint of output field amplitude (blue curve). A salient feature of a MZM modulation which clearly distinguishes it from other types of optical modulation is that it may offer different modulation characteristics depending on which voltage biasing is used. The most usual modes of operation are the Quadrature biasing Point (QP) and the Null biasing Point (NP), whose main characteristics are outlined next.

The QP is the point with maximum linearity of the intensity transfer function (green curve in figure 2.2 left) and considering the transfer function is periodic, the QP bias could be chosen to be $(2n+1)/2$ times the V_π, with n an integer, where the slope of the intensity transfer function alternates negative and positive sign. Therefore, when biased at QP, the MZM features an IM with great resemblance to that which could be obtained with a DML (figure 2.1 left).

Without loss of generality and in order to stress the resemblance with DML systems, the bias voltage is set at the positive slope point by considering for example the bias voltage at $-V_\pi/2$. Thus, considering $V(t) = V_{bias} + V_{RF}(t)$, the output power $P_{out}(t)$ from (2.6) is given by:

$$P_{out[QP]}(t) = P_{in} \cdot \left[1 + cos\left(\frac{\pi}{V_\pi} \cdot V_{RF}(t) - \frac{\pi}{2}\right)\right] \tag{2.8}$$

which using the trigonometric identity $cos(x - \pi/2) = sin(x)$ and the small signal condition $sin(x) \approx x$, ($V_{RF} \ll V_\pi$) can be finally simplified as:

$$P_{out[QP]}(t) = P_{in} \cdot \left[1 + \frac{\pi}{V_\pi} \cdot V_{RF}(t)\right] \tag{2.9}$$

$$E_{out[QP]}(t) = E_{in} \cdot \sqrt{1 + \frac{\pi}{V_\pi} \cdot V_{RF}(t)} \tag{2.10}$$

where it is seen that the carrier power (P_c) and the normalized IM modulation index (m) of the generic expression (**??**) for the DML case are

$$P_c = P_{in}; \qquad m = \frac{\pi \cdot V_{RF}}{V_\pi} \tag{2.11}$$

being V_{RF} the amplitude of $V_{RF}(t)$ in (2.9):

$$V_{RF}(t) = V_{RF} \cdot x(t) \tag{2.12}$$

With $x(t)$ an information signal normalized to unity amplitude.

On the other hand, for a bias voltage of V_π or any integer multiple of it, the device works on the point of maximum linearity of the field transfer function; this is the NP and the type of modulation is AM.

Thus, when MZM is biased at NP with $V_{bias} = V_\pi$, the output power (2.6)

is given by:

$$\begin{aligned} P_{out[NP]}(t) &= P_{in} \cdot \left[1 - cos\left(\frac{\pi}{V_\pi} \cdot V_{RF}(t)\right)\right] \\ &= 2P_{in} \cdot sin^2\left(\frac{\pi}{2V_\pi} \cdot V_{RF}(t)\right) \end{aligned} \tag{2.13}$$

which assuming the small signal condition $sin(x) \approx x$, leads to:

$$P_{out[NP]}(t) = \frac{P_{in}}{2} \cdot \left[\frac{\pi}{V_\pi} \cdot V_{RF}(t)\right]^2 \tag{2.14}$$

$$E_{out[NP]}(t) = \frac{P_{in}}{\sqrt{2}} \cdot \left[\frac{\pi}{V_\pi} \cdot V_{RF}(t)\right] \tag{2.15}$$

where, as it was anticipated, it is seen that no optical carrier is present and the field amplitude follows the modulating signal while the intensity is proportional to its squared value.

2.1.4 Electro-Absorption Modulator

The EAM, illustrated in figure 2.3 (right), is another kind of optical external modulator. It is based on the Franz-Keldysh effect in a semiconductor-based planar waveguide composed of multiple p-type and n-type layers that form multiple quantum wells [29, 38].

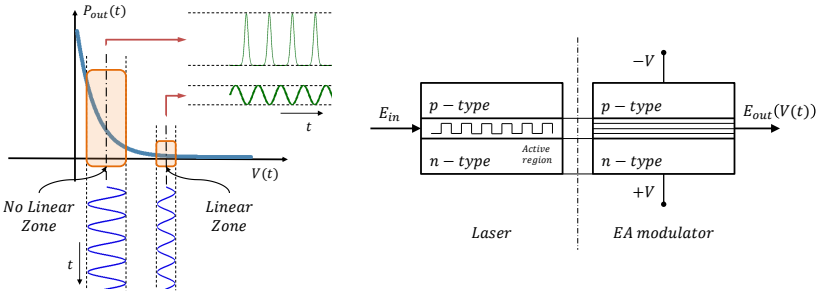

Figure 2.3: EAM transfer function (left) and its generic scheme (right) [38].

The basic effect is that the EAM section acts as a voltage-controlled detector that causes some photons of the incoming light to be lost in the form of a current towards the electrical driving circuit. The attenuation suffered by the light is thus dependent on the driving voltage that changes the responsivity of the voltage-controlled detector so that it experiences a significant change in absorption when the voltage is applied [49, 50]. It therefore becomes possible to control the amplitude of the optical signal at the output of the modulator by

using an electrical signal. A typical absorption versus applied voltage transfer function for an EAM is shown in figure 2.3 (left).

EAMs are advantageous in several applications, because contrary to EO modulators, they do not require polarization control and can be easily and cost-effectively integrated with lasers. On the downside, they are not as versatile as MZM and feature high values of chirp.

2.1.5 Effect of linear channel distortions on IM/DD systems

Due to the specific characteristics of IM/DD systems, the impact of linear distortions imposed by the channel over the RX signal quality needs a careful examination. As it is well known, the most important linear distortion in SMF TX in the 3rd window is the CD. In this section, three different effects of CD in IM/DD systems will be analyzed: the DINLD, the CS or RF amplitude fading effect, and the PN decorrelation.

2.1.5.1 IM/DD general model

The basic model of an IM/DD system consists on a TX where an information signal in the form of an electrical current or voltage is transformed into photons following a linear relation with optical power or intensity, and a RX where a PD detects the incoming signal and converts it again into an electrical current. Figure 2.4 illustrates the generic scheme of an IM/DD optical system.

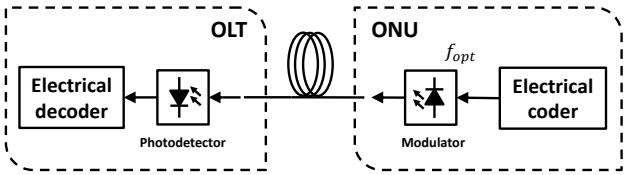

Figure 2.4: Basic scheme of a conventional IM/DD optical system.

Even when the DML can be considered the main representative example of IM modulator, as previously discussed, both an MZM in its QP and also an EAM may be employed to provide an IM of a signal into an optical carrier, in an external way.

The general expression for the low-pass equivalent (LPE) intensity modulated field is:

$$E_{out}(t) = E_{in} \cdot \sqrt{1 + m \cdot x(t)} = \sqrt{P_c} \cdot \sqrt{1 + m \cdot x(t)} \tag{2.16}$$

where E_{in} is the power at the input of the IM modulator, m is the normalized

MI (modulation depth) and $x(t)$ is the modulation signal normalized to unity amplitude. In order to give insight into the spectral content of the signal, a Taylor series expansion of the modulation field is considered:

$$E_{out}(t) \cong E_{in}\left[1 + \frac{m}{2}x(t) - \frac{m^2}{8}x^2(t) + \frac{m^3}{16}x^3(t) - \dots\right] \tag{2.17}$$

Following this, a pure tone modulation signal will give rise to an IM optical signal containing multiple sidebands at both sides of the carrier at spectral distances corresponding to the harmonics of the modulation signal, see figure 2.5. At the RX, the optical signal is DD with a PD which converts it back into an electrical signal through a square law transfer function. Mathematically, this process can be expressed as:

$$i_D(t) = R \cdot |E_{out}(t)|^2 = R \cdot (E_{out}(t) \cdot E^*_{out}(t)) \tag{2.18}$$

where R is the responsivity of the PD, and $E_{out}(t)$ and $E^*_{out}(t)$ are the optical field and its complex conjugate.

2.1.5.2 Dispersion-induced nonlinear distortion

The DD signal is obtained from the mixing of the RX optical signal with itself, whereby all the optical spectral components beat in pairs. In the ideal case where no channel distortions affect the signal, the optical spectral components would have the precise amplitudes and phases so that the sidebands beatings generating the same electrical frequency harmonic will cancel out and only the modulation signal will be present at the detector's output. See figure 2.5.

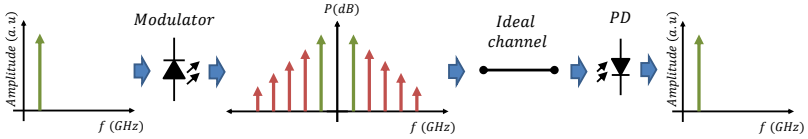

Figure 2.5: Conventional IM/DD transmission system with an ideal channel.

In contrast, when channel linear distortions such as CD alter the amplitudes and phases of the optical sidebands, no complete cancellation of harmonics generated through sidebands beatings may take place giving rise to nonlinear signal distortion on an end-to-end system level [39]. See figure 2.6.

Therefore, a conventional IM/DD optical system with a dispersive channel converts the linear distortions into nonlinear distortions due to the nonlinear square modulus transfer functions of the modulation and detection processes. As a consequence, the harmonics of the signal are not totally removed and the efficiency of conventional linear equalizers is low.

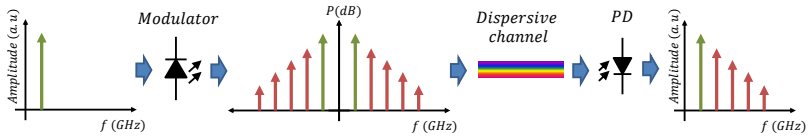

Figure 2.6: Conventional IM/DD transmission system with a dispersive fiber.

2.1.5.3 Carrier suppression

The optical modulated signal is naturally a DSB signal with two spectral bands at each side of the carrier. When a DSB signal is DD, the resulting signal comes from the beating in pairs between the frequency components of the optical signal at the input of the PD. This means that as the optical components are allocated at each side of the optical carrier and at the same distance from it, each sideband has acquired a different phase propagation delay and therefore, the beating will fall in the same electrical frequency in the detected signal, thus adding up their respective contributions. Thereby, constructive or destructive, interferences may take place depending on the respective phase acquired by each sideband through propagation as a consequence of CD, and some frequency bands may be totally lost [40].

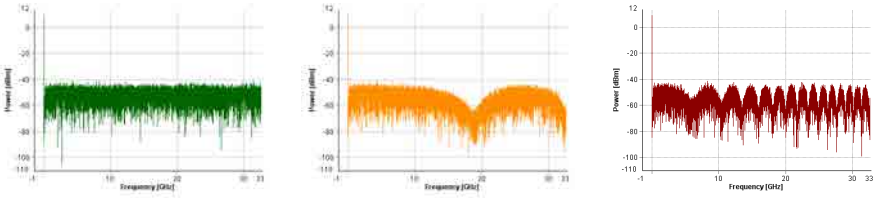

Figure 2.7: Electrical spectrum after the PD for a 80Gbps 4-QAM DSB signal with fiber lengths of 0km (left), 10 km (center) and 100 km (right).

Figure 2.7 shows the DD electrical spectrum of the same IM/DD system with different fiber lengths, specifically back-to-back (B2B), 10km and 100km. As shown, the longer the optical fiber, the higher the effect of the CD and therefore, the lower the frequency at which the first fading occurs. In chapter 3, three methods to avoid the CS are analyzed.

2.1.5.4 Phase noise

The PN in optical communications is basically generated by the effect of the laser finite BW and originates from fast random fluctuations of the laser emission wavelength. This PN is one of the main sources of degradation in auxiliary carrier detection schemes in which usually there is no coherence between the signal and the optical carrier used for detection, i.e. there are decorrelated. This

effect is mathematically analyzed in chapter 5 and pilot tones methodology to mitigate this effect is studied in chapter 8.

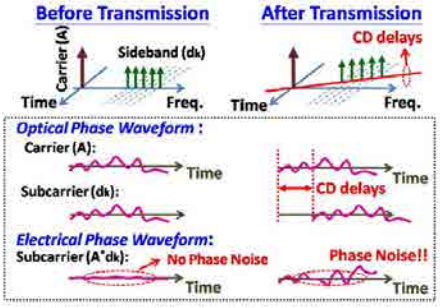

Figure 2.8: Impact of CD over phase noise generation in DD optical OFDM transmission [41].

Nevertheless, even when the optical carrier and the signal are modulated from the same laser source, and therefore they are coherent/correlated, phase shifts among SCs may appear on the detected signal due to the effect of CD. Thus, as it is illustrated in figure 2.8, in presence of CD, if a large spectral gap between the signal sideband and the optical carrier is left and/or a long distance is propagated, the optical carrier and the signal can become decorrelated and the detected signal degraded [41, 51].

2.2 Orthogonal Frequency Division Multiplexing: a review

In this section, the basic principles of OFDM [42] are reviewed starting from the more generic concept of Multicarrier (MC) systems of which OFDM is considered a particular case. The required orthogonality condition is discussed followed by a description of the analog OFDM systems which serves the purpose of allowing to understand the basic features of OFDM and MC systems in general. After that, the more practically relevant digital OFDM system based on the FFT algorithm is presented.

Finally, the different parts of the electrical coder and decoder modules of an OFDM communications system are illustrated and the concept of the CP, as a method to mitigate the effects of the CD due to the optical channel is discussed.

2.2.1 Multicarrier systems

The fundamental principle of a MCM is to decompose the rate data stream into N lower rate streams and then transmit them simultaneously over different SC signals.

Mathematically, the expression of a MC signal is given by:

$$s(t) = \sum_{i=-\infty}^{+\infty} \sum_{k=-\infty}^{N} c_{ik} \cdot g_k(t - iT_{MC}) \tag{2.19}$$

where c_{ik} is the ith information symbol at the kth SC, g_k is the waveform for the kth SC, N is the number of SCs and T_{MC} is the period of a MC frame, where $T_{MC} = N \cdot T_s$ with T_s the sample (symbol) frame. This signal is then sent through the channel and RX at the decoder. Assuming, $r(t)$ as the RX signal, the detected information symbols for the MC block are given by:

$$c'_{mn} = \int_{-\infty}^{+\infty} r(t) \cdot g_n^*(t - mT_{MC})dt \tag{2.20}$$

where c'_{mn} is the mth information symbol at the nth SC in RX and g_n is the waveform for the nth SC. Steaming from the above, assuming the channel does not cause any distortion to the signal so that $r(t) = s(t)$ and a perfect time synchronization between the TX and the RX, so that $m = i$, for each RX symbol to be correctly decoded, the SC signals must verify the following orthogonality condition:

$$\int_{-\infty}^{+\infty} g_k(t) \cdot g_n^*(t)dt \begin{cases} 0, & (k \neq n) \\ 1, & (k = n) \end{cases} \tag{2.21}$$

2.2.2 FDM systems

In the specific case of FDM, the SCs are windowed pure-tone signals, which can be written in a complex form as

$$g_k(t) = p(t) \cdot e^{j2\pi f_k t} \tag{2.22}$$

where $p(t)$ is a baseband (BB) windowing function. From (2.19) the sent signal $s(t)$ for a FDM multicarrier system is:

$$s(t) = \Re\left[\sum_{i=-\infty}^{+\infty} \left(p(t - iT_{FDM} \cdot \sum_{i=-\infty}^{+\infty} c_{ik} \cdot e^{j2\pi f_k(t - iT_{FDM})}\right)\right] \tag{2.23}$$

where the period of the FDM signal has been denoted by T_{FDM}. In the general case here presented, c_{ik} are the complex numbers representing the symbols to be TX in the specific modulation format of choice, usually a multilevel QAM, which could even be different for every SC when bit loading algorithms are used [52].

The scheme of the FDM TX is shown in the left side of figure 2.9 where the complex multipliers represent in practice phase-quadrature up and down-conversion stages respectively for the TX and RX. As shown, the symbols to be TX are arranged into packs of length N and then converted from serial to parallel in order to assign each of the N symbols in a pack to a different FDM subchannel by multiplying it by the corresponding SC signal. After the SC multiplication stage, the SC signals are added together and converted back to serial to form the FDM signal that will be sent through the channel.

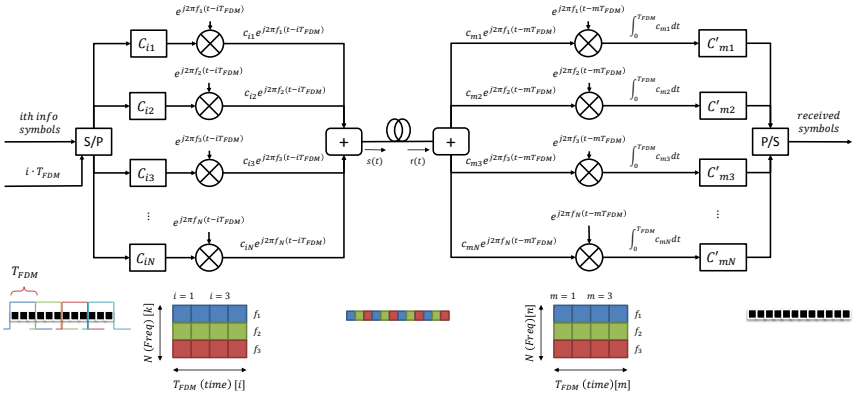

Figure 2.9: Conceptual diagram for a generic MC system.

At the RX side, the scheme of the optimum detector is shown in figure 2.9. The RX signal $r(t)$ is distributed over N channels where it gets multiplied by the complex conjugate of each SC signal in a phase-quadrature down-converter stage, and then low pass filtered (LPF) [42]. An ideal serial-to-parallel conversion is assumed so that FDM blocks in TX exactly correspond to FDM blocks in RX.

Steaming from (2.20) and assuming an ideal channel so that $r(t) = s(t)$, the decoded symbol in the nth subchannel for a generic i FDM block can be written as:

$$c'_n = \int_{-\infty}^{+\infty} \left(p^2(t') \cdot \sum_{k=1}^{N} c_{ik} \cdot e^{j2\pi(f_k - f_n)t'} \, dt \right) \tag{2.24}$$

where f_n is the frequency associated at the nth SC and where $t' = t - iT_{FDM}$. It is useful to define a squared windowing function $q(t)$ as:

$$q(t) = p^2(t) \tag{2.25}$$

With that definition, (2.24) can be written in compact form as:

$$c'_n = \sum_{k=1}^{N} \left(c_k \cdot \int_{-\infty}^{+\infty} q(t') \cdot e^{j2\pi(f_k - f_n)t'} dt \right) \tag{2.26}$$

Following from this, the condition for proper detection of the symbols in subchannel n is:

$$\int_{-\infty}^{+\infty} q(t') \cdot e^{j2\pi(f_k - f_n)t'} dt \begin{cases} 0, & (f_k \neq f_n) \\ 1, & (f_k = f_n) \end{cases} \tag{2.27}$$

Which, takes us to the orthogonality condition in (2.21) particularized to the FDM case. It is useful to picture this orthogonality condition into the frequency domain. Picking up from (2.24), and using the definition in (2.25) one may arrive to:

$$\begin{aligned} c'_n &= \sum_{k=1}^{N} c_k \cdot [P(\omega - (\omega_k - \omega_n)) * P(\omega - (\omega_k - \omega_n))] \,|_{\omega=0} \\ &= \sum_{k=1}^{N} c_k \cdot [Q(\omega - (\omega_k - \omega_n))] \,|_{\omega=0} \end{aligned} \tag{2.28}$$

with $P(\omega)$ and $Q(\omega)$ the Fourier transforms of the pulse functions $p(t)$ and $q(t)$ respectively. Reading from (2.28), the FDM symbol in the subchannel n is obtained at the RX by adding up the values obtained when particularizing at $\omega = 0$ each of the spectra obtained when shifting $Q(\omega)$ to the frequency difference between each of the N SCs and SC n. This is graphically illustrated in figure 2.10 for the subchannel $n = 2$ of a system of $N = 4$ SCs with a constant SC spacing $\triangle f$. As it can be seen, the orthogonality condition is not fulfilled in the case shown because when decoding any specific channel there's a non-zero contribution coming from other channels.

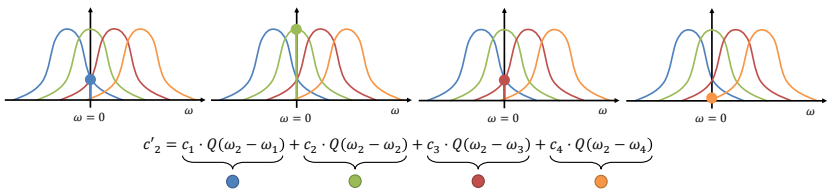

Figure 2.10: Graphical interpretation of expression (2.28).

Thus, from the orthogonality condition (2.27), it follows that for an FDM symbol to be decoded without ICI, the windowing function should be such that when convolved with itself and translated to any of the frequencies in the FDM

system, its value at the zero frequency is sufficiently small, as illustrated in figure 2.11.

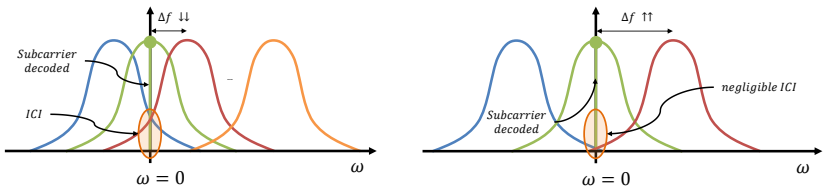

Figure 2.11: Illustration of decoding process in the frequency domain in the cases with significant and negligible ICI, respectively left and right.

This means that sufficiently broad spectral frequency guard bands are required, i.e.:

$$T_{FDM}(f_k - f_n) \gg 1 \implies \Delta f \gg \frac{1}{T_{FDM}} \tag{2.29}$$

That results in wide spectral band requirements for FDM systems. In the next section, one method to fulfill the orthogonality condition in a MC system without compromising the spectral efficiency is analyzed.

2.2.3 Analog OFDM

Building on the result of the previous section, if an ideal rectangular pulse is used such that

$$g_k(t) = p(t) \cdot e^{j2\pi f_k t} \quad \text{where} \quad p(t) = \begin{cases} 1 & (0 < t \leq T_{OFDM}) \\ 0 & (t \leq 0\, t > T_{OFDM}) \end{cases} \tag{2.30}$$

where, in this case, the period of the MC signal has been denoted T_{OFDM} in order to stress the difference with the MC systems explained above. As the square windowing function is used in this case, one has:

$$q(t) = p(t) \cdot p(t) = p^2(t) = p(t) \tag{2.31}$$

Considering again that $r(t) = s(t)$ and the decoded symbol in the n subchannel for a generic i OFDM block and assuming a rectangular pulse, expression (2.24) results in:

$$c'_n = \sum_{k=1}^{N} \left[c_k \cdot \left(\frac{1}{T_{OFDM}} \cdot \int_{-T_{OFDM}/2}^{T_{OFDM}/2} \left(p(t') \cdot e^{j2\pi(f_k - f_n)t'} \right) dt \right) \right] \tag{2.32}$$

Solving for the integral, a sinc-shaped spectrum is obtained.

$$\begin{aligned} c'_n &= \sum_{k=1}^{N} \left[c_k \cdot \frac{1}{T_{OFDM}} \left(\frac{e^{j2\pi(f_k - f_n)t'}}{j2\pi(f_k - f_n)t'} \right)_{-\frac{T_{OFDM}}{2}}^{\frac{T_{OFDM}}{2}} \right] \\ &= \sum_{k=1}^{N} \left[c_k \cdot sinc\left(\pi(f_k - f_n)T_{OFDM}\right) \right] \end{aligned} \tag{2.33}$$

As in previous cases, in order to avoid the ICI effects over the signal sent, (2.33) has to fulfill the orthogonality condition, which in this case is given by:

$$sinc(\pi(f_k - f_n)T_{OFDM}) \begin{cases} 0 & (f_k \neq f_n) \\ 1 & (f_k = f_n) \end{cases} \tag{2.34}$$

Just as before, in the FDM case, one option with this specific square pulse windowing function in order to fulfill the orthogonality condition required to correctly decode the sent symbols is to ensure a very large spectral gap between SCs. Taking the case of a constant spacing $\triangle f$ between SC, that means $\triangle f \gg 1/T_{OFDM}$. Furthermore, due to the special characteristics of the sinc spectrum, an alternative is to distribute the SCs so that they are aligned with the zero crossing points of the $q(t')$ function spectrum, i.e.

$$\Delta f = \frac{1}{T_{OFDM}} = \frac{1}{N \cdot T_s} \tag{2.35}$$

Thereby, according to the decoding process as given by expression (2.28) and applying (2.35) to fulfill the orthogonality condition, each sent symbol may be correctly decoded in spite of SC's spectra overlap. See figure 2.12.

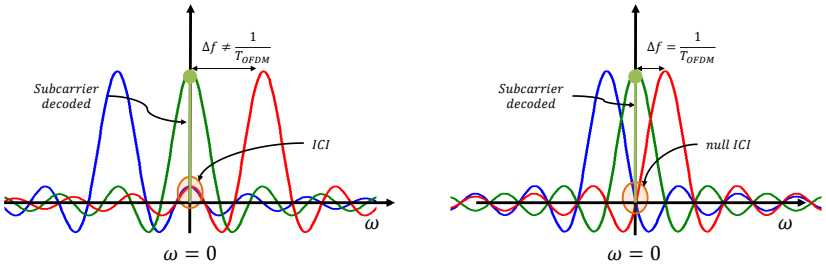

Figure 2.12: Illustration of decoding process in the frequency domain in the cases of with and without ICI, respectively left and right. The difference is the choice of the SC spacing relative to the symbol length.

2.2.4 Digital OFDM

The main drawback in analog OFDM is the requirement of an individual TX/RX pair for each sub-channel. Cost-efficient implementation of OFDM systems with a large number of SCs is accomplished in the digital domain through efficient FFT algorithms. The expression of the OFDM signal in the digital domain is obtained by sampling the data signal with a $1/T_s$ rate and then taking IFFT. The result is a digital version of (2.23) sampled at time intervals $t = nT_s$, with n an integer number.

$$z\left[nT_s\right] = \sum_{k=1}^{N} c_k \cdot e^{j2\pi\left(\frac{k-1}{NT_s}\right)nT_s} = \sum_{k=1}^{N} c_k \cdot e^{j2\pi\left(\frac{k-1}{N}\right)n} = IFFT\left\{c_k\right\} \qquad (2.36)$$

Therefore the OFDM modulation process is equivalent to applying the inverse FFT (iFFT) algorithm over the symbols to be sent and then performing DAC.

2.2.5 Coder and decoder modules

Figure 2.13 illustrates the stages of a conventional OFDM coder (left) and decoder (right). As seen, in the coder, the incoming bit sequence is firstly parallelized and modulated into complex symbols, usually applying a multilevel coding (M-QAM) which can be different for every SC if power loading and bit loading algorithms are employed [53]. A training symbol insertion stage follows, so that known OFDM symbol frames are sent before each data packet, for RX synchronization and channel estimation purposes. Then, some SCs can be set to zero for relaxing the requirements of the DAC, and others can be used to send pilot tones for frequency response estimation and offset compensation. Then, the iFFT algorithm is applied and the CP is appended, just before DAC and anti-alias filtering.

In a general case, two signals corresponding to the real and the imaginary parts of the OFDM symbol are obtained from the BB OFDM coding, which are fed to the optical modulation stage; an exception are DMT systems such as those used in xDSL protocols, which by the imposition of Hermitian Symmetry (HS) between the SCs cancel the imaginary part signal.

Between BB coder and decoder, corresponding with the dashed line boxes in figure 2.13, there is the optical part of the system: from the modulator up to the RX stage, through the optical channel. As it will be seen and analyzed throughout the Thesis, there are presently many different options to implement this part, each one with advantages and drawbacks, so that different alternatives may find application into different scenarios.

At the BB decoder module, the reverse process is carried out in order to post-process and recover the data sent. The real and imaginary parts, of the

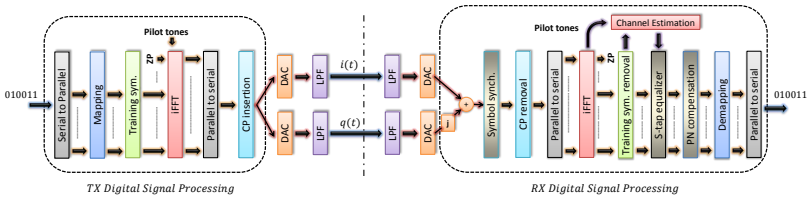

Figure 2.13: OFDM baseband coder (left) and decoder (right) block diagram.

RX BB OFDM signal provided by the optical demodulation stage at the RX are firstly LPF to avoid the alias at high frequencies and sent to a pair of ADCs in order to be digitalized. The data sequence is synchronized with the preamble added in the TX and CP extraction takes place. The sequence is then converted from serial to parallel and demodulated with a FFT algorithm.

Afterwards, zero-padded SCs and pilot tones are extracted. The training sequence symbols are removed and together with the pilot tones, are sent to the channel estimation module, whose output is used to update the equalizer coefficients and the PN compensation stage. Each SC is then demodulated according to the corresponding modulation format and finally, the restored bit sequences are serialized to recover the information sequence sent.

2.2.6 Cyclic prefix

Steaming from the properties of the digital implementation of OFDM based on FFT is a powerful technique to overcome the CD effect imposing a different delay to each SC and causing a symbol to spread in time polluting adjacent symbols in a phenomenon called ISI, see figure 2.14 (left).

In order to avoid ISI, there is a technique consisting in adding a time guard (t_G) interval between OFDM symbols in order to accommodate the polluted signal part, leaving a time interval which only contains information from the useful data symbol unharmed.

In figure 2.14 (left) three different SC channels have been plotted. Blue and green colors have been used to identify symbols corresponding to different OFDM blocks. As seen, in TX each colors remains into its corresponding block, whereas in RX the symbol has spread into the neighboring block and therefore there is a time interval where both, green and blue colors are mixed up.

By contrast in figure 2.14 (right), a guard time interval t_G greater than the maximum channel delay t_D ($t_G > t_D$), is inserted in between OFDM blocks so that it may allocate the portion of the signal that spreads out into neighboring blocks. As seen, at the RX side, there are no time intervals that contain information coming from different OFDM blocks and therefore no ISI is present.

The problem with a guard time interval that contains no signal (silent guard

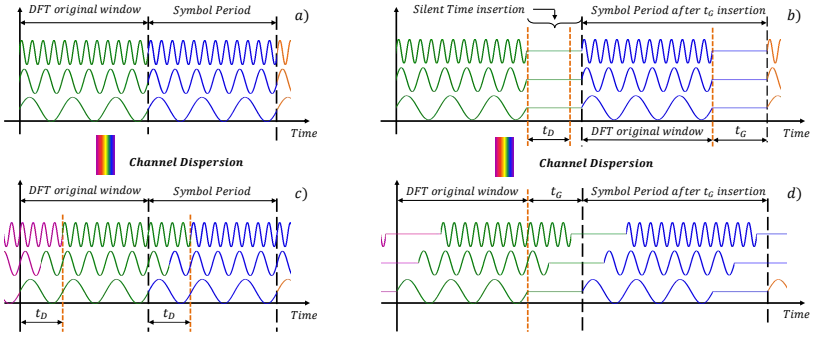

Figure 2.14: Signals before being sent a) b), and after being affected by CD c) d), and without t_G a) c) and with t_G b) d).

interval) arises when trying to decode the different subchannels in a block because the RX signal is composed by windowing functions with a different delay depending on the SC with which they have been modulated. From (2.23) particularized for the OFDM case, the expression of the signal in TX is:

$$s(t) = \Re\left[\sum_{i=-\infty}^{+\infty}\left(p\left(t - i\left(T_{OFDM} + t_G\right)\right)\right.\right. \\ \left.\left. \cdot \sum_{k=1}^{N} c_{ik} \cdot e^{j2\pi f_k\left(t - i\left(T_{OFDM} + t_G\right)\right)}\right)\right] \quad (2.37)$$

where T_{OFDM} is the period of the MC signal, t_G the silent guard time and $p(t)$ a rectangular pulse with a width of T_{OFDM}. Considering an ideal serial-to-parallel conversion as in (2.24), the expression of the decoded symbols after the signal is TX through an optical fiber and affected by the CD is given by:

$$c'_n = \sum_{k=1}^{N} c_k \cdot \int_{-\infty}^{+\infty} p(t' - t_k) \cdot p(t' - t_n) \cdot e^{j2\pi f_k (t' - t_k)} \cdot e^{j2\pi f_n (t' - t_n)} dt \quad (2.38)$$

where $t' = t - i\left(T_{OFDM} + t_G\right)$. Notice that $p\left(t' - t_n\right)$ is the windowing function in RX whose delay t_n may be adjusted so to minimize the decoding errors but in any case t_n is a fixed delay whereas t_k represents a different delay acquired by every SC due to CD.

As it can be understood graphically through figure 2.15, the multiplication of the RX signal, composed of SCs with different delays (in red) with a fixed delay RX window (in blue) results in squared windowing functions in RX, $q_k(t')$ (in magenta) whose temporal width is smaller than T_{OFDM}, and which as seen in figure 2.15 (right), do not fulfill the orthogonality condition causing ICI.

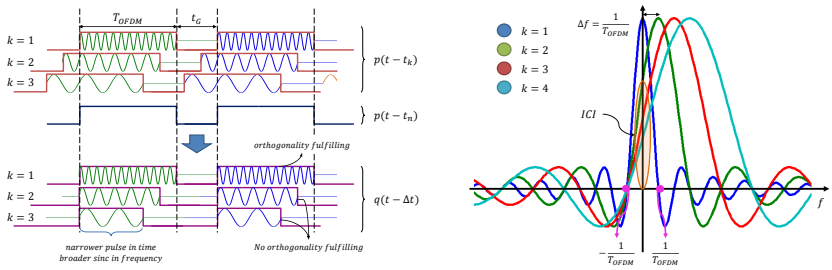

Figure 2.15: OFDM symbols before decoding and after decoding (left) and the corresponding frequency spectra of the decoded symbols (right) with a silent guard time.

The periodicity of the SC signals may be exploited in order to remove this ICI by filling the time guard interval with a cyclic extension of the corresponding SC, instead of leaving it "silent". As shown in figure 2.16 (right), this is equivalent to expanding the windowing function in TX so that it occupies the whole expanded OFDM block $p'(t)$ with $T_{OFDM} + t_G$ width. In that case, regardless of the delay considered in the RX windowing function, the squared windowing function $p'(t - t_k) \cdot p(t - t_n) = q(t)$ is a perfect rectangular pulse with exact length of T_{OFDM}, and therefore, the orthogonality is kept. The guard time guarantees no ISI while the cyclic extension of the SC into this guard time maintains the orthogonality in RX (after the CP is removed by multiplying by the windowing function in RX) and avoids ICI.

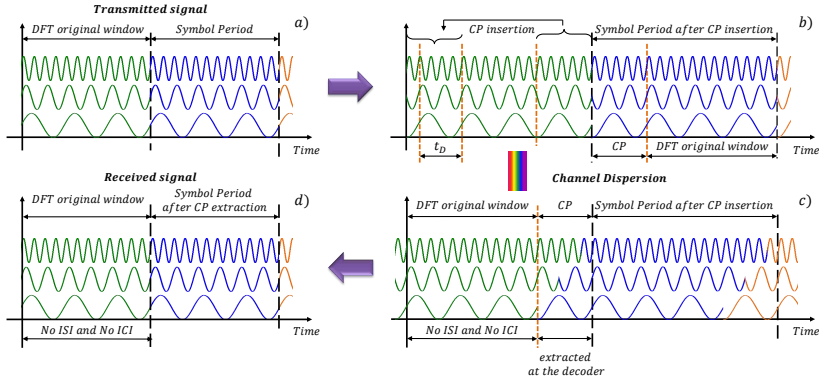

Figure 2.16: Original TX signal (a), TX signal after CP insertion (b), RX signal affected by CD (c) and RX signal after CP extraction (d).

Finally, as it follows from the expressions, depending of the delay chosen for the RX windowing signal (a choice left to synchronization), even when in any case an integer number of complete periods of the SC are always contained into an OFDM time block, at the beginning of the RX window the starting phase may be different for each SC and also different from the sent starting phase which may lead to errors in the phase of the decoded complex numbers

representing the symbols (in (2.37) it is represented by the factor $e^{-j2\pi f_k \cdot it_G}$). This is easily fixed through equalization by training sequences.

2.3 Optical OFDM systems

Now that the basic characteristics of conventional optical systems and conventional OFDM systems have been reviewed, let us see and try to understand in this section the fundamental features of the different oOFDM systems that may be defined. The classification starts from the conventional IM/DD oOFDM systems [55–57], which Lowery exploited in its revolutionary article [20], continues with AM/DD systems [43], and ends with the most complex and expensive optical systems being the AM/CO oOFDM systems [44, 58, 59].

Table 2.1, at the end of this section, contains the plausible combinations between modulation and detection techniques and its main features. As can be seen, optical systems are classified by their descriptive names, the devices and most important characteristics which are analyzed in following sections. Furthermore, they are also given an acronym which will be used along this Thesis in order to facilitate their searching and connection. The meaning of the acronym's letters is:

- **I**: Intensity modulation
- **D**: Direct Detection
- **IG**: Effective-Amplitude Modulation with Guard-Band
- **AG**: Direct-Amplitude Modulation with Guard-Band
- **A**: Direct-Amplitude Modulation
- **C**: Coherent Detection
- **R**: Remote heterodyne or auxiliary carrier

2.3.1 Intensity modulation with direct detection systems (IM/DD)

Figure 2.17 illustrates the architectures of a basic optical TX system based on IM/DD in both direct and external modulation versions.

Since only one signal component, the intensity, is to be modulated over the optical carrier, the HS is imposed among the SCs. This means that the negative and positive frequency components at the input of the iFFT are complex conjugates of each other, i.e.

$$c_{i1} = c_{i\frac{N}{2}+1} = 0 \quad \& \quad c_{ik} = c^*_{iN_{sc}-k+2} \quad \text{for} \quad k = 2, \ldots, \frac{N}{2} \tag{2.39}$$

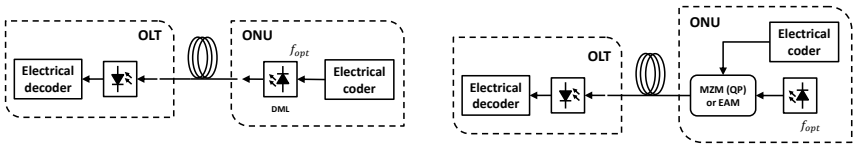

Figure 2.17: Basic scheme of a conventional IM/DD optical system with direct IM (left) and with external IM (right) (ID01).

resulting in a purely real signal such as:

$$z[nT_s] = \sum_{i=-\infty}^{\infty} \sum_{k=2}^{\frac{N}{2}+1} 2\,|c_{ik}| \cdot cos\left(2\pi \frac{(k-1)}{N}(n-1) + \phi_k\right) \tag{2.40}$$

Assuming the matrix of FDM symbols and SCs from figure 2.9, figure 2.19 (left) shows it graphically after applying the HS condition. This technique is very efficient from a component point of view since it can be achieved by modifying the inputs at the iFFT without the use of any extra devices. The downside of HS is that it halves the total data rate.

As seen in section 2.1.5.2, the signal sent through a dispersive channel in an IM/DD system cannot be effectively recovered through linear equalization due to the nonlinear distortion arising from the square law nature of the modulation/demodulation processes characteristic of IM/DD systems. Since the nonlinear distortion terms arise as a consequence of the second order nonlinearity characteristic of IM/DD systems, the IMD products appear at the difference and sum components of the signal frequencies (red subcarriers in figure 2.18). By leaving an optical frequency guard band (GB) between the optical carrier and the signal band with at least the same BW as the signal [57, 60–62], IMD may be made to fall in electrical frequency bands that are non-overlapping with the data band and filtered out at RX.

Figure 2.18 (left) illustrates the optical modulated signal obtained with a reduced spectral GB size. In contrast, in figure 2.18 (right) a wide enough spectral GB avoids the overlap between the IMD band and the data band. As seen through the graphs and as abovementioned, the minimum GB necessary so that the IMD band does not overlap the data signal band is as wide as the data band. In some applications, some overlap may be tolerated as it will be shown in section 3.2.

The addition of a GB effectively linearizes the system, at least for the active frequency band, so that removing the IMD through electrical filtering allows a significant increasing of the efficiency of linear equalizers. Two main options for GB addition may be considered labeled here as the **digital** and the **analog** options. Both are listed in the summary table 2.1 and illustrated in figure 2.19.

The digital option entails zero padding (ZP) the relevant subcarriers. As

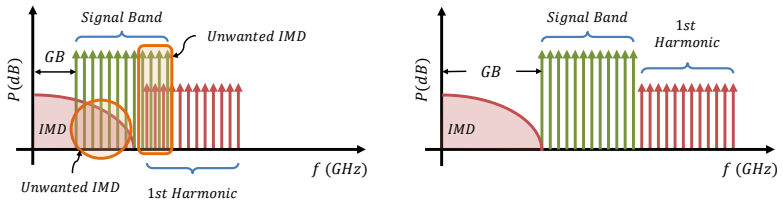

Figure 2.18: Electrical spectra in detection with a shorter GB (left); and with the minimum GB width that avoids overlapping of IMD and signal.

shown, firstly the HS is applied whereby a half of the matrix is the conjugate of the other half, and finally the symbols corresponding to the SCs within the GB and their corresponding in the conjugate part of the matrix are set to zero obtaining a data matrix such as the right one of the figure 2.19 (left). This option is cost-effective but it implies to further reduce the efficiency of the TX since more redundant data is sent.

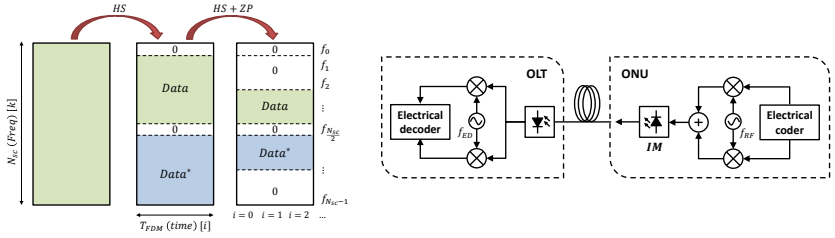

Figure 2.19: Digital (IGD01) (left) and analog (IGD02) (right) options for GB insertion.

The analog option, on its side, involves the incorporation of electrical frequency up and down converter stages respectively for the TX and RX as it is illustrated in both sides of the optical system of figure 2.19 (right). The strong point of this option is that it fully exploits the maximum data rate allowed by the digital section of the TX/RX and it even allows to drop the requirement of HS by using phase-quadrature up-conversion stages. As a downside, it requires more equipment. In any case, the addition of the analog GB implies a cost increase if the same data rate is to be maintained.

2.3.2 Amplitude modulation with direct detection systems (AM/DD)

In the previous section, the necessity of an optical GB between the optical carrier and the data signal band in order to avoid the IMD was discussed. Actually, this system provides an equivalent to an AM in an end-to-end TX system basis as it

allows the use of linear equalizers to remove the effect of CD or any other kind of linear channel distortion into the signal. In order to emphasize this aspect, this Thesis calls them **effective-AM/DD** systems. However, as seen in the optical modulation systems (section 2.1), the common way to obtain an optical modulated signal whose amplitude linearly follows an information signal is to use a MZM biased in NP. In this section this **direct-AM/DD** systems will be analyzed as well as the different RX options and their characteristics. A good thing about using a MZM in NP is that it allows to obtain an AM signal without the requirement of a GB.

On the other hand, as seen in section 2.1.3, the linear relation between the amplitude of the optical signal and the data signal in the MZM biased at NP is accompanied by the cancellation of the optical carrier. This means that in order to DD the signal sent, an auxiliary carrier has to be injected prior to detection. Owing to the square-law characteristic of the PD, the detected signal will contain the beating between the carrier and the signal and also the squared value of the information signal which will be seen as second-order IMD.

Thus, in order to avoid this IMD which contaminates the information signal, the spectral location of the optical carrier needs to be carefully selected so that the detected signal spectral components and IMD products do not overlap in frequency and the IMD may be filtered out. This method is analogous to the effective-AM transmission systems where the use of GB and an electrical filtering were used in order to correctly detect the signal sent avoiding the effects of IMD.

In order to dissociate the IMD from the data band, an auxiliary carrier is placed at a distance from the TX carrier equal to $f_{RF} = 3B/2$, with B the signal BW, so by adding an additional RF down-conversion stage in RX as seen in figure 2.20, an AM demodulation is effectively obtained.

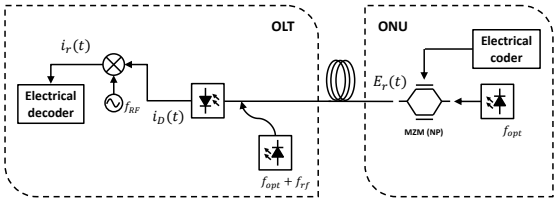

Figure 2.20: Basic scheme of a direct-AM/DD optical system with a MZM biased in NP as a modulator and a remote heterodyne RX with optical carrier addition and electrical down-conversion (ADR01). If $f_{RF} < 3B/2$, the detected signal is contaminated with IMD even in absence of linear distortions.

As a main difference between the direct-AM/DD oOFDM system in figure 2.20 and the conventional IM/DD oOFDM system covered in section 2.3.1 when no GB is present is that in the latter the signal is only corrupted with IMD when linear channel distortions come into play, while in the former, IMD is present even for the ideal channel case. Therefore for almost ideal channels one may have an IMD-free detected signal in IM/DD systems while in order to avoid

IMD a GB will always be required in direct-AM/DD systems. As advantages of direct-AM/DD system over IM/DD systems, since no carrier needs to be TX a higher power may be allocated to the data band and also the CSPR may be freely chosen. Another advantage is found in the avoidance of the OBI effect between TX carriers from different users in the US of OFDM-PONs [69]. However, notice that, due to a reduced Extinction Ratio (ER) in state-of-the-art MZM with values around 30-40 dB, a residual optical carrier is still present in practice which may affect the quality of the TX [70–72].

Even when the conceptual system differs very little if the auxiliary carrier is added at the TX or at the RX sides, in practice it becomes a very relevant difference for PONs because it means to have either passive or active RXs at the ONUs. Specifically, the insertion of the auxiliary carrier at the RX, labeled in table 2.1 as remote heterodyne/homodyne RXs, allows more power to be TX with an accompanying increase in the available power budget.

Same as in IM/DD systems, the optical auxiliary carrier insertion may take place either at the TX or at the RX, which as it was seen in the previous section, carries out some implications more of a practical rather than a conceptual nature.

Mathematically and referring to figure 2.20, the expression at the output of the MZM is $E_r(t) = I(t)$ where $I(t)$ is the real part of the OFDM coded signal. It is then seen that the HS condition will be a requirement for this system. The detected current signal after the PD can be expressed as:

$$\begin{aligned} i_D(t) &= R \cdot \left| A_{LO} e^{j\omega_{RF} t} + I(t) \right|^2 \\ &= R \cdot \left[A_{LO}^2 + I(t)^2 + 2A_{LO} \left(I(t) cos(\omega_{RF} t) \right) \right] \end{aligned} \tag{2.41}$$

where R is the responsivity, A_{LO} is the amplitude of the local oscillator, ω_{RF} the frequency where the auxiliary source is allocated and $I(t)$ the in-phase part of the RX signal. After the RF down-conversion and the LPF, the signal at the input of the electrical decoder is given by:

$$i_r(t) = \Re \left[i_D(t) \right] cos(\omega_{RF} t) = R \cdot \left[2A_{LO} I(t) \right] \tag{2.42}$$

A downside of the direct-AM/DD system with RF down-conversion presented above (figure 2.20) is that since only one signal can be TX, the HS is still required. That is especially sad if one considers that the remote heterodyne RX with its corresponding RF down-conversion could very easily be adapted to detect both phase and quadrature components by just adding an electrical phase shifter and another RF mixer, thus doubling the capacity of the system.

It is also worth saying in this sense that SC fading can appear due to the CD, although it cannot be considered CS since are originated at BB after down-conversion as the result of that *electrical image* SC arrive at the RX with a different phase shift. Thus, for some SC distances and fiber length may be as

large as 180º giving rise to the fading. Thereby, as it is studied in-depth in section 4.4.1, in these cases is also necessary the contribution of the imaginary part.

A more efficient alternative would be to use two MZM biased in NP with a $\pi/2$ phase difference. This modulator is known as optical In-Phase/Quadrature (oIQ). Figure 2.21 illustrates the basic scheme of this kind of AM/DD system.

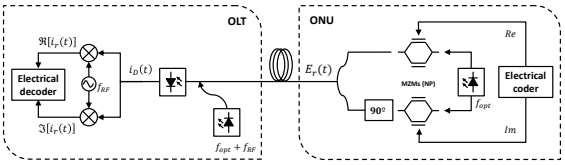

Figure 2.21: Basic scheme of a direct-AM/DD optical system with an oIQ modulator and remote heterodyne optical carrier (ADR05).

Mathematically, the expression at the output of the nested MZM is $E_r(t) = I(t) + jQ(t)$. The detected current can be expressed as:

$$i_D(t) = R \cdot \left[A_{LO}^2 + I(t)^2 + Q(t)^2 + 2A_{LO}\left(I(t)cos(\omega_{RF}t) + Q(t)sin(\omega_{RF}t)\right)\right] \quad (2.43)$$

And after the RF down-conversion and the LPF, the signals at the input of the electrical decoder are given by:

$$\Re[i_r(t)] = R \cdot [2A_{LO}I(t)] \quad \& \quad \Im[i_r(t)] = R \cdot [2A_{LO}Q(t)] \quad (2.44)$$

An interesting alternative system exploits the availability of an oIQ modulator at the TX to SSB modulate an RF tone that could act as carrier for detection. Such a system was proposed and analyzed by Peng [73]. As steaming from the previous analysis, for the signal to be detected IMD free the RF tone frequency has to be allocated at a $f_{RF} = 3B/2$ from the TX optical carrier, being B the signal BW. Figure 2.22 illustrates the basic scheme of this kind of direct-AM/DD system.

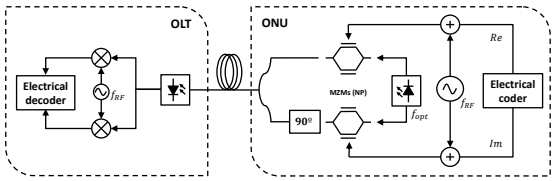

Figure 2.22: Basic scheme of a direct-AM/DD optical system with oIQ TX and remote heterodyne electrical carrier (ADR06).

The downside lies in the reduced power levels that may be allocated to the auxiliary carrier due to the limited dynamic range of the MZMs.

2.3.3 Amplitude modulation with coherent detection systems (AM/CO)

The discussion of optical OFDM TX systems has started from the most simple and straight-forward optical TX systems, the conventional IM/DD. As foreseen and discussed in the introduction, due to the fundamental characteristics of IM/DD systems and those of OFDM modulation, in order to adapt the first to the latter, several considerations had to be made and different alternatives of TX and RX designs were proposed and discussed in the previous sections. A common goal, met in different degrees by each proposal, was to try to keep the optical system as simple and cost-effective as possible, sometimes at the expense of TX efficiency and/or complexity at the OFDM system level.

On the contrary, this section tries to come up with an oOFDM system design which is optimized from the viewpoint of the OFDM system requirements, even if it entails great complexity and cost from the optical system point of view. That means to try to reproduce at the optical level the structure of a typical electrical OFDM system which in state-of-the-art optics implies to use an oIQ TX and a CO RX as seen in the generic scheme in figure 2.23.

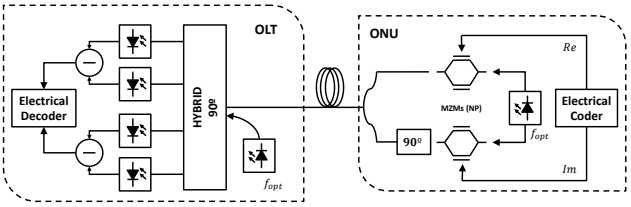

Figure 2.23: Basic scheme of a direct-AM/CO optical system with oIQ modulator and 90º hybrid (AC01).

Comparing with the IM/DD systems, the CO RX is the analogous to the eIQ down-converter just as the oIQ based on nested MZMs with additional $\pi/2$ phase delay is the analogous of the eIQ up-converter into the optical domain. Therefore, this scheme can be considered the exact translation into the optical domain of the typical OFDM TX system structure and it enjoys all the good features of a pure OFDM system such as efficient linear equalization, and it also is spectrally efficient because no GB is required.

Because the detected signal is amplified through the power in the local carrier, CO detection based systems also have better sensitivity. On the downside, because there is usually no correlation between the RX optical signal and the carrier used for the detection, the direct-AM/CO systems are very sensitive to PN. Otherwise, they also require very precise adjustment of all the parameters

and also polarization control which not only increases the complexity of the system, but also the overall cost.

The CO demodulation of optical signals requires the use of a 90º optical hybrid [74]. Figure 2.24 illustrates the CO demodulation process through the use of an optical 90º hybrid.

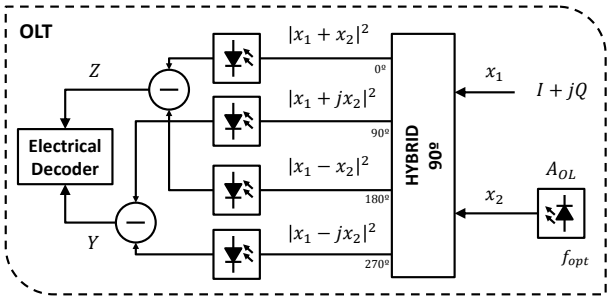

Figure 2.24: Hybrid 90º scheme with four outputs.

As seen in the figure 2.24, there are four outputs that are fed to two pairs of balanced PD. These PD transform the optical input into the electrical domain and then by subtracting in pairs the output signals, they are able to amplify, recover and separate the in-phase (I) and quadrature (Q) components of the input signal as explained next.

Consider the RX signal is fed to port 1 of the hybrid $x_1 = I(t) + jQ(t)$ while the local oscillator is injected through port 2, being $x_2 = A_{LO}$. Each one of the outputs of the balanced PDs at the outputs of the hybrid is obtained as:

$$\begin{aligned} x_{(0^\circ)}(t) &= |x_1(t) + x_2(t)|^2 = |I(t) + jQ(t) + A_{LO}|^2 \\ &= A_{LO}^2 + I(t)^2 + Q(t)^2 + 2I(t)A_{LO} \end{aligned} \tag{2.45}$$

$$\begin{aligned} x_{(90^\circ)}(t) &= |x_1(t) + jx_2(t)|^2 = |I(t) + jQ(t) + jA_{LO}|^2 \\ &= A_{LO}^2 + I(t)^2 + Q(t)^2 + 2Q(t)A_{LO} \end{aligned} \tag{2.46}$$

$$\begin{aligned} x_{(180^\circ)}(t) &= |x_1(t) - x_2(t)|^2 = |I(t) + jQ(t) - A_{LO}|^2 \\ &= A_{LO}^2 + I(t)^2 + Q(t)^2 - 2I(t)A_{LO} \end{aligned} \tag{2.47}$$

$$\begin{aligned} x_{(270^\circ)}(t) &= |x_1(t) - jx_2(t)|^2 = |I(t) + jQ(t) - jA_{LO}|^2 \\ &= A_{LO}^2 + I(t)^2 + Q(t)^2 - 2Q(t)A_{LO} \end{aligned} \tag{2.48}$$

In figure 2.24, Z and Y express the amplification and recovery of the fundamental signal components I and Q respectively, so making use of (2.45), (2.46),

(2.47) and (2.48), they result in:

$$\begin{aligned} Z(t) &= x_{(0^\circ)}(t) - x_{(180^\circ)}(t) = |x_1(t) + x_2(t)|^2 - |x_1(t) - x_2(t)|^2 \\ &= 4I(t)A_{LO} \end{aligned} \tag{2.49}$$

$$\begin{aligned} Y(t) &= x_{(90^\circ)}(t) - x_{(270^\circ)}(t) = |x_1(t) + jx_2(t)|^2 - |x_1(t) - jx_2(t)|^2 \\ &= 4Q(t)A_{LO} \end{aligned} \tag{2.50}$$

Each one of these signals may now be directly fed to the real and imaginary inputs of the OFDM decoder as seen in figure 2.24.

An alternative implementation of the CO decoder shown in figure 2.25 requires only 3 signals from the optical hybrid.

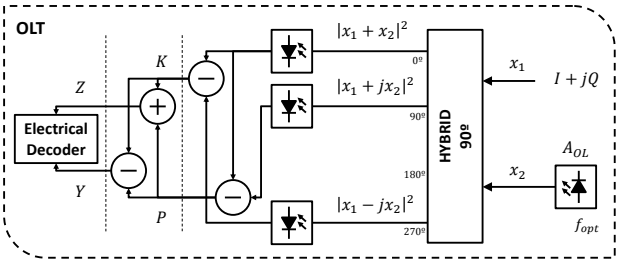

Figure 2.25: Hybrid 90º scheme with three outputs.

Following the scheme in figure 2.25, the real and imaginary parts of the OFDM signal are obtained as:

$$\begin{aligned} Z(t) &= K(t) + P(t) = \left|x_{(0^\circ)}(t) + x_{(270^\circ)}(t)\right|^2 + \left|x_{(0^\circ)}(t) - x_{(90^\circ)}(t)\right|^2 \\ &= 4I(t)A_{LO} \end{aligned} \tag{2.51}$$

$$\begin{aligned} Y(t) &= K(t) - P(t) = \left|x_{(0^\circ)}(t) - x_{(270^\circ)}(t)\right|^2 - \left|x_{(0^\circ)}(t) - x_{(90^\circ)}(t)\right|^2 \\ &= 4Q(t)A_{LO} \end{aligned} \tag{2.52}$$

Finally, for applications that may switch complexity to the RX such as the US in PONs, a CO RX may be employed in conjunction with a cost-effective effective-AM TX with analog or digital GB addition and IM, such as in the US of the ACCORDANCE paradigm. See figure 2.26.

In this section, the different combinations of optical modulation and detection in a P2P link have been reviewed. Nevertheless, it is worth recalling here that an optical network consists of both, DS and US, each one with its challenges and requirements. In chapter 5, two network architectures proposed by

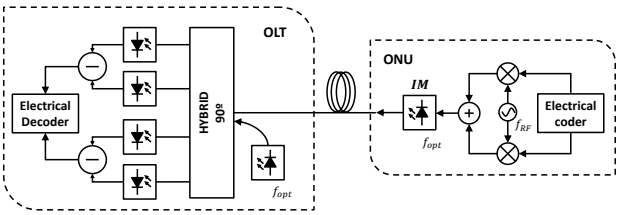

Figure 2.26: Basic scheme of an effective-AM/CO optical system with analog GB addition (IGC01).

the EU ACCORDANCE project [4] are presented.

The main ACCORDANCE proposal is called R-OFDMA-PON and consists on a high performance network architecture based on a direct-AM/DD with an oIQ TX for the DS (ADR05) and an effective-AM/CO with analog GB addition (IGC01) remodulating an optical carrier sent from the OLT by means an RSOA for the US. On the other hand, the cost-effective proposal is called S-OFDMA-PON and is based on and effective-AM/DD with digital or analog GB insertion (IGD01, IGD02) in both directions.

Each of these strategies have their advantages and drawbacks which are analyzed in-depth in chapter 5, nevertheless, considering the cost-efficiency as a key topic of this Thesis, different techniques such as EBA, PAPR mitigation algorithms or multiband ONUs approach are used over the S-OFDMA-PON in order to further reduce the overall costs and improve its performance.

Scenario		Transmitter										Receiver					
Type	Acronym in the Thesis	Main features		HS	RF up stage	GB	Data bandwidth	ℜ/ℑ	Modulator	MZM Bias	Carrier TX	SSB/DSB	RX	RF down stage	Hybrid 90°	Auxiliar carrier	Spectral location	Physical location
IM/DD + BB	**IDD1**	**IM**	✗	**DMT**	✓	✗	✗	50%	ℜ	**DML/MZM/EAM**	**QP**	✓	**DSB**	**DD**	✗	✗	✗	✗	✗
effective-AM/DD + digital GB	**IGD01**	**AM**	**effective**	**DMT**	✓	✗	✓	**25%**	ℜ	**DML/MZM/EAM**	**QP**	✓	**DSB**	**DD**	✗	✗	✗	✗	✗
effective-AM/DD + digital GB + remote heterodyne	IGDR01	AM	effective	DMT	✓	✗	✓	50%	ℜ	DML/MZM/EAM	QP	✓	SSB	DD	✓	✗	Laser	Heterodyne	TX/RX
effective-AM/DD + digital GB + remote heterodyne	IGDR02	AM	effective	DMT	✓	✗	✓	50%	ℜ	DML/MZM/EAM	QP	✓	SSB	DD	✓	✗	RF-Tone	Heterodyne	TX
effective-AM/DD + analog GB	**IGD02**	**AM**	**effective**	**eIQ**	✗	✓	✓	**100%**	ℜ+ℑ	**DML/MZM/EAM**	**QP**	✓	**DSB**	**DD**	✓	✗	✗	✗	✗
effective-AM/DD + analog GB + remote heterodyne	IGDR03	AM	effective	eIQ	✗	✓	✓	100%	ℜ+ℑ	DML/MZM/EAM	QP	✓	SSB	DD	✓	✗	Laser	Heterodyne	TX/RX
effective-AM/CO + analog GB + remote heterodyne	**IGC01**	**AM**	**effective**	**eIQ**	✗	✓	✓	**100%**	ℜ+ℑ	**DML/MZM/EAM**	**QP**	✓	**SSB**	**CO**	✗	✓	**Laser**	**Heterodyne**	**RX**
direct-AM/DD + BB + SL-OFDM	AD01	AM	direct	DMT	✓	✗	✗	25%	ℜ	1 MZM	NP	✗	DSB	DD	✗	✗	✗	✗	✗
direct-AM/DD + digital GB + SL-OFDM	AGD01	AM	direct	DMT	✓	✗	✓	12.5%	ℜ	1 MZM	NP	✗	DSB	DD	✗	✗	✗	✗	✗
direct-AM/DD + remote heterodyne	**ADR01**	**AM**	**direct**	**DMT**	✓	✗	✓	**50%**	ℜ	**1 MZM**	**NP**	✗	**SSB**	**DD**	✓	✗	**Laser**	**Heterodyne**	**TX/RX**
direct-AM/DD + remote heterodyne	ADR02	AM	direct	DMT	✓	✗	✓	50%	ℜ	1 MZM	NP	✗	SSB	DD	✓	✗	RF-Tone	Heterodyne	TX
direct-AM/DD + analog GB + SL-OFDM	AGD02	AM	direct	eIQ	✗	✓	✓	50%	ℜ+ℑ	1 MZM	NP	✗	DSB	DD	✗	✗	✗	✗	✗
direct-AM/DD + remote heterodyne	ADR03	AM	direct	eIQ	✗	✓	✓	100%	ℜ+ℑ	1 MZM	NP	✗	SSB	DD	✓	✗	Laser	Heterodyne	TX/RX
direct-AM/DD + remote heterodyne	ADR04	AM	direct	eIQ	✗	✓	✓	100%	ℜ+ℑ	1 MZM	NP	✗	DSB	DD	✓	✗	Laser	Homodyne	TX/RX
direct-AM/DD + analog GB + remote heterodyne	AGC01	AM	direct	eIQ	✗	✓	✓	100%	ℜ+ℑ	1 MZM	NP	✗	SSB	CO	✗	✓	Laser	Heterodyne	RX
direct-AM/DD + oIQ + remote heterodyne	**ADR05**	**AM**	**direct**	**oIQ**	✗	✗	✓	**100%**	ℜ+ℑ	**2 MZM**	**NP**	✗	**SSB**	**DD**	✓	✗	**Laser**	**Heterodyne**	**TX/RX**
direct-AM/DD + oIQ + remote heterodyne	**ADR06**	**AM**	**direct**	**oIQ**	✗	✗	✓	**100%**	ℜ+ℑ	**2 MZM**	**NP**	✗	**SSB**	**DD**	✓	✗	**RF-Tone**	**Heterodyne**	**TX**
direct-AM/DD + oIQ + homfodyne	**AC01**	**AM**	**direct**	**oIQ**	✗	✗	✗	**100%**	ℜ+ℑ	**2 MZM**	**NP**	✗	**SSB**	**CO**	✗	✓	**Laser**	**Homodyne**	**RX**
direct-AM/DD + oIQ + heterodyne	AC02	AM	direct	oIQ	✗	✗	✗	100%	ℜ+ℑ	2 MZM	NP	✗	SSB	CO	✓	✓	Laser	Heterodyne	RX

Table 2.1: Classification of oOFDM systems.

Chapter 3

Chromatic Dispersion and its effects in OFDM optical systems

In the previous chapter, the most fundamental principles of optical signal propagation focusing on conventional IM/DD systems on the one hand, and the basis of conventional OFDM modulation techniques on the other, were reviewed in order to analyze the options to combine both technologies towards the definition of oOFDM systems of practical interest. Several alternatives were analyzed discussing advantages and drawbacks, and potential application scenarios.

This chapter aims at taking a closer look to the CD effect which is the main limiting impairment in the optical fiber transmission systems of interest in this Thesis work. It starts by reviewing its most basic principles and laying the foundations for a mathematical analysis. Afterwards, a special attention is devoted to the reference frequency concept. As it will be seen a proper understanding of its role in simulations is key in order to properly decode the RX signal. It is seen that the reference frequency choice has an impact on the position of the temporal window for CP extraction. The analysis has helped to properly choose the reference frequency values for simulations depending on the kind of signal sent, whether it is SSB or DSB, as well as the minimum required length and position of the temporal window for CP extraction.

The chapter follows with an in-depth analysis of the DINLD and the CS effects due to the CD as well as the methods to mitigate them by means of simulations of a conventional IM/DD oOFDM system (ID01). The constellations obtained when each of the compensation techniques is applied are shown and analyzed.

3.1 Chromatic dispersion principles

CD is a deterministic distortion characteristic of the optical fiber causing differential delays among the different spectral components of a transmitted signal. It leads to a frequency dependence of the rate at which the phase of the wave propagates (optical phase velocity) and its effect on the TX optical signal basically scales linearly with propagation distance and quadratically with data rate [54]. In order to understand the effect of CD the fiber is characterized through its transfer function, $H(\omega)$ as:

$$H(\omega) = e^{-j\beta(\omega)L} \tag{3.1}$$

where $\beta(\omega)$ represents the frequency dependence of the propagation constant of the fundamental mode propagating in the fiber and L is the fiber propagation distance. Propagation loss is neglected in this analysis, and can be added afterwards.

In an ideal case, the phase constant $\beta(\omega)$ has a linear dependence with frequency, meaning that the spectral components undergo the same time delay, which is the same as saying that they travel at the same velocity. At RX the same signal will be obtained without any distortion but with a delay.

On the contrary, in a dispersive channel, the phase constant has a nonlinear dependence with frequency and as a consequence of the different arrival times of the frequency components, the recovered signal at the RX side will differ from the transmitted one.

In order to see this mathematically, a Taylor expansion of the phase constant against frequency is considered around an arbitrary chosen reference frequency as:

$$\beta(\omega) = \beta_0 + \beta_1(\omega - \omega_{ref}) + \frac{\beta_2}{2}(\omega - \omega_{ref})^2 + \dots \tag{3.2}$$

where,

$$\beta_0 = \beta(\omega_{ref}) \qquad \beta_1 = \left.\frac{\partial\beta}{\partial\omega}\right|_{\omega=\omega_{ref}} \qquad \beta_2 = \left.\frac{\partial^2\beta}{\partial\omega^2}\right|_{\omega=\omega_{ref}} \tag{3.3}$$

The number of relevant terms in the above expansion will depend on the rate of change of the phase constant against frequency. Since usually $\triangle\omega \leq \omega - \omega_{ref} \ll \omega_{ref}$, terms up to second-order may properly describe the phase constant variation over the signal BW in most of the cases.

The first term (β_0) in (3.3) represents a constant optical phase shift which will affect all spectral components of the RX optical signals and may thus be arbitrarily set to zero.

The second term (β_1) is associated to the group delay at the reference frequency which is the inverse of the group velocity (v_g) times the fiber length, i.e.

$$\beta_1 = \left.\frac{\partial\beta}{\partial\omega}\right|_{\omega=\omega_{ref}} = \frac{1}{v_g} = \frac{\tau_g}{L} \tag{3.4}$$

and so, v_g is the velocity with which a narrow band envelope signal over a carrier frequency ω_{ref} will propagate through the fiber. Considering a frame of reference moving with the group velocity $t' = t - \tau_g = t - L/v_g$ [75], this term can also be taken to be zero.

The third term (β_2) in (3.3) represents the group delay variation experienced by the different spectral components around the central frequency ω_{ref} and therefore is responsible for the widening of the pulses. Mathematically, the group velocity dispersion β_2 can be expressed as the derivative of the group delay, i.e. β_1 as follows:

$$\beta_2 = \left.\frac{\partial^2\beta}{\partial\omega^2}\right|_{\omega=\omega_{ref}} = \frac{\partial}{\partial\omega}\left(\frac{1}{v_g}\right) = \frac{\partial}{\partial\omega}\left(\frac{\tau_g}{L}\right) \tag{3.5}$$

Under the above assumptions, the transfer function (3.1) can be expressed as:

$$H(\omega) = e^{-j\frac{\beta_2}{2}(\omega-\omega_{ref})^2 L} \tag{3.6}$$

In practice, the CD parameter is characterized by the dispersion coefficient D defined as

$$D = \frac{\partial\beta_1}{\partial\lambda} = \frac{1}{L}\cdot\frac{\partial\tau_g}{\partial\lambda} \tag{3.7}$$

and whose units are (s/m^2). On its side, the term $\partial\tau_g/\partial\lambda$ can be substituted by:

$$\frac{\partial\tau_g}{\partial\lambda} = \frac{\partial\tau_g}{\partial\omega}\cdot\frac{\partial\omega}{\partial\lambda} = \frac{\partial\tau_g}{\partial\omega}\cdot\frac{\partial}{\partial\lambda}\left(\frac{2\pi c}{\lambda}\right) = \frac{\partial\tau_g}{\partial\omega}\cdot\left(-\frac{2\pi c}{\lambda^2}\right) = \frac{\partial\tau_g}{\partial\omega}\cdot\left(-\frac{\omega^2}{2\pi c}\right) \tag{3.8}$$

where c is the light speed in vacuum and $\lambda = 2\pi c/\omega$. Finally, considering (3.5), applying (3.8) into (3.7) evaluated at ω_{ref}, the CD is given by:

$$D = -\frac{\omega_{ref}^2}{2\pi c}\cdot\beta_2\ \left[\frac{ps}{nm\cdot km}\right] \tag{3.9}$$

The CD coefficient value depends on the carrier wavelength. There is a null

dispersion wavelength ($1.33\mu m$, 2^{rd} window) where $D = 0$. Above this wavelength ($D > 0$, $\beta_2 < 0$) is the anomalous dispersion regime, whereas below this wavelength ($D < 0$, $\beta_2 > 0$) propagation is said to be in the normal dispersion regime [75]. The 3^{rd} window of optical communications which is assumed in this work belongs to the anomalous dispersion regime with $D = 17ps/(nm \cdot km)$.

Finally, by using (3.9) in equation (3.6), a transfer function of the transmission medium is obtained as:

$$H(\omega) = e^{j\pi cD\left(\frac{\omega-\omega_{ref}}{\omega_{ref}}\right)^2 L} \tag{3.10}$$

3.2 Optical fiber reference frequency

Connecting with the previous analysis, this section is focused on the reference frequency parameter in the Virtual Photonics Interface (VPI) [76] fiber simulation module. This parameter is directly associated to the dispersive characteristics of the fiber but it is not a physical characteristic of the fiber; it rather has to be understood as the reference for arrival times at the fiber output, and in that sense, it is related to the synchronization at the RX side.

For the specific case of an OFDM signal it is worth having a closer look to the delays suffered by each SC when travelling through the fiber for properly setting the reference frequency values and taking the CP preambles out.

Even when the specifics of the following mathematical analysis consider an effective-AM/DD with analog GB addition (IGD02), as illustrated in figure 3.1, the results are seen to apply also to effective-AM/DD with digital GB addition (IGD01) or to direct-AM/DD with oIQ TX and auxiliary carrier (ADR05, ADR06).

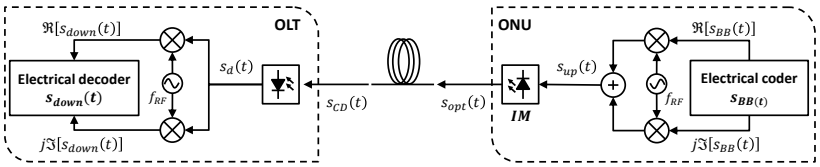

Figure 3.1: Basic scheme of an effective-AM/DD optical system with analog GB addition (IGD02).

Following the scheme in figure 3.1, at the output of the electrical coder, one has the BB OFDM signal, which from (2.23) can be written as:

$$s_{BB}(t) = \sum_{i=-\infty}^{\infty} p(t - iT_{OFDM}) \cdot \sum_{n=-\frac{N}{2}}^{\frac{N}{2}-1} a_{ni} \cdot e^{j\phi_{ni}} \cdot e^{jn\triangle\omega(t-iT_{OFDM})} \tag{3.11}$$

where $c_{ki} = a_{ni} \cdot e^{j\phi_{ni}}$ are the complex symbols to be sent and N is the number of SCs. For simplicity and without loss of generality we may consider a single OFDM frame and set $i = 0$ in (3.11) to get:

$$s_{BB}(t) = p(t) \cdot \sum_{n=-\frac{N}{2}}^{\frac{N}{2}-1} a_n \cdot e^{j\phi_n} \cdot e^{jn\triangle\omega t} \tag{3.12}$$

The signal is then up-converted to an RF frequency (ω_{RF}). Mathematically:

$$s_{up}(t) = \Re\left[s_{BB}(t) \cdot e^{j\omega_{RF}t}\right] = \Re\left[\Re\left[s_{BB}(t)\right] + j\Im\left[s_{BB}(t)\right] \cdot e^{j\omega_{RF}t}\right] \tag{3.13}$$

$$s_{up}(t) = p(t) \cdot \sum_{n=-\frac{N}{2}}^{\frac{N}{2}-1} a_n \cdot cos\left(\omega_{RF}t + n\triangle\omega t + \phi_n\right) \tag{3.14}$$

We may at this point drop the pulse frame function, which is in practice restricting the non-zero time interval to the frame time length and recover it afterwards. An optical modulation stage then takes the signal to the optical domain. Even when the optical modulation signal spectrum may slightly differ for each of the various scenarios under consideration, the assumption of an optical carrier and two OFDM signal sidebands at each side, appropriately retains all of the basic features and greatly simplifies the analysis. That is equivalent to consider an AM plus carrier modulation as follows:

$$s_{opt}(t) = E_0 cos(\omega_0 t) \cdot [A_0 + s_{up}(t)] \xrightarrow{if normalized} \rightarrow s_{opt}(t) = cos(\omega_0 t) \cdot [1 + s_{up}(t)] \tag{3.15}$$

$$s_{opt}(t) = cos(\omega_0 t) + \left[\sum_{n=-\frac{N}{2}}^{\frac{N}{2}-1} a_n \cdot cos\left(\omega_{RF}t + n\triangle\omega t + \phi_n\right)\right] \cdot cos(\omega_0 t) \tag{3.16}$$

$$s_{opt}(t) = cos\left(\omega_0 t\right) + \sum_{n=-\frac{N}{2}}^{\frac{N}{2}-1} a_n \cdot \frac{1}{2}[cos\left(\left[\omega_0 + \omega_{RF}\right]t + n\Delta\omega t + \phi_n\right) + cos\left(\left[\omega_0 - \omega_{RF}\right]t - n\Delta\omega t - \phi_n\right)] \tag{3.17}$$

Indeed, this expression corresponds to a DSB signal, shown graphically in figure 3.2 (left).

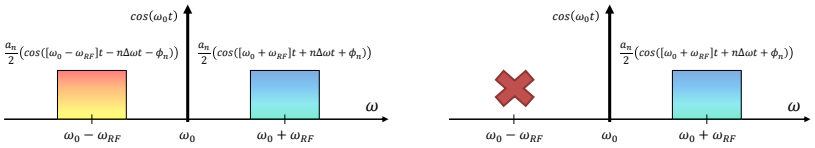

Figure 3.2: Graphical interpretation of the optical spectra of a DSB (left) and SSB (right) transmissions considering (3.17).

Firstly, the case when one of the sidebands is removed to obtain a SSB signal such as in [77, 78] will be considered. The optical modulated signal in its LPE form is:

$$s_{opt}^{SSB}(t) = 1 + \sum_{n=-\frac{N}{2}}^{\frac{N}{2}-1} \frac{a_n}{2} \cdot e^{j((\omega_{RF}+n\triangle\omega)t+\phi_n)} \tag{3.18}$$

Using the fiber transfer function in (3.6), one gets:

$$s_{CD}^{SSB}(t) = \left[1 + \sum_{n=-\frac{N}{2}}^{\frac{N}{2}-1} \frac{a_n}{2} \cdot e^{j((\omega_{RF}+n\triangle\omega)t+\phi_n)}\right] * \mathcal{F}^{-1}\left(e^{-j\frac{\beta_2}{2}(\omega-\omega_{ref})^2 L}\right) \tag{3.19}$$

Since each SC may be considered as a frequency delta, the above operation is equivalent to particularizing the exponential in the fiber transfer function to every SC, i.e.

$$s_{CD}^{SSB}(t) = e^{-j\frac{\beta_2}{2}(\omega_0-\omega_{ref})^2 L} + \sum_{n=-\frac{N}{2}}^{\frac{N}{2}-1} \frac{a_n}{2} \cdot \left[e^{j([\omega_{RF}+n\Delta\omega]t+\phi_n)} \cdot e^{-j\frac{\beta_2}{2}(\omega_0+\omega_{RF}+n\Delta\omega-\omega_{ref})^2 L}\right] \tag{3.20}$$

Taking out common phase constants:

$$s_{CD}^{SSB}(t) = 1 + \sum_{n=-\frac{N}{2}}^{\frac{N}{2}-1} \frac{a_n}{2} \cdot \left[e^{-j\frac{\beta_2}{2}(\omega_{RF}+n\Delta\omega)^2 L} \cdot e^{j([\omega_{RF}+n\Delta\omega]t+\phi_n)} \cdot e^{-j\beta_2(\omega_0-\omega_{ref})(\omega_{RF}+n\Delta\omega)L}\right] \tag{3.21}$$

and rearranging, the following expression is obtained:

$$s_{CD}^{SSB}(t) = 1 + \sum_{n=-\frac{N}{2}}^{\frac{N}{2}-1} \frac{a_n}{2} \cdot \Big[e^{-j\frac{\beta_2}{2}(\omega_{RF}+n\Delta\omega)^2 L} \cdot e^{j[(\omega_{RF}+n\Delta\omega)(t-\beta_2(\omega_0-\omega_{ref})L)]} \cdot e^{j\phi_n} \Big] \quad (3.22)$$

The normalized signal after the PD ($R = 1$) is obtained by taking the squared-modulus operation, if IMD terms are either considered negligible or assumed to fall in non-overlapping frequency bands owing to GB and filtered out, only terms at the RF frequency are relevant, and are given by:

$$s_d^{SSB}(t) = \sum_{n=-\frac{N}{2}}^{\frac{N}{2}-1} a_n \cdot cos\left(\left[(\omega_{RF} + n\Delta\omega)\left(t - \beta_2\left(\omega_0 - \omega_{ref}\right) L\right) \right] - \frac{\beta_2}{2}\left(\omega_{RF} + n\Delta\omega\right)^2 L + \phi_n \right) \quad (3.23)$$

The detected signal is then RF down-converted and LPF resulting in:

$$s_{down}^{SSB}(t) = \Re\left[s_d(t) \cdot e^{-j\omega_{RF}t} \right] \quad (3.24)$$

Grouping together all terms containing the SC frequencies $n\triangle\omega$, the signal is conveniently written as:

$$s_{down}^{SSB}(t) = \sum_{n=-\frac{N}{2}}^{\frac{N}{2}-1} a_n \cdot cos\left(n\Delta\omega \left(t - \beta_2 L\left(\omega_0 - \omega_{ref}\right) - \beta_2 L\omega_{RF} - \frac{\beta_2}{2} Ln\Delta\omega \right) - \beta_2 L\omega_{RF}\left(\omega_0 - \omega_{ref}\right) - \frac{\beta_2}{2} L\omega_{RF}^2 + \phi_n \right) \quad (3.25)$$

Let the signal entering the OFDM decoder in compact form be :

$$s_{down}^{SSB}(t) = \sum_{n=-\frac{N}{2}}^{\frac{N}{2}-1} a_n \cdot cos\left(n\triangle\omega\left(t - t_s - t_n\right) + \phi_n - \phi_0 \right) \quad (3.26)$$

Now, recovering the pulse frame window in (3.11), the OFDM decoder singal

is:

$$s_{down}^{SSB}(t) = \sum_{n=-\frac{N}{2}}^{\frac{N}{2}-1} a_n \cdot p(t - t_s - t_n) \cdot cos\left(n\triangle\omega\left(t - t_s - t_n\right) + \phi_n - \phi_0\right) \quad (3.27)$$

where,

$$t_s = \beta_2 L\left(\omega_0 + \omega_{RF} - \omega_{ref}\right) \quad (3.28)$$

$$t_n = L\frac{\beta_2}{2} n\triangle\omega \text{ where } -\frac{N}{2} \leq n \leq \frac{N}{2} \quad (3.29)$$

$$\phi_0 = \beta_2 L\omega_{RF}\left(\omega_0 + \frac{\omega_{RF}}{2} - \omega_{ref}\right) \quad (3.30)$$

By comparing the RX signal (3.27) to the TX OFDM signal in (3.14), it can be seen that there is an overall delay common to all SCs t_s (3.28) which depends on the choice of ω_{ref} and also a differential delay which is different to every SC and proportional to the frequency spacing, t_n in (3.29). In addition, there is a common added phase shift which is the same for all SCs (3.30) and that can be compensated through equalization.

Figure 3.3 provides a graphical representation of the signal at the RX side specifying the arrival times of all frequencies involved. Whatever the ω_{ref} choice, it is seen that the arrival times of the SC are symmetrically arranged along the sides of the common delay t_s. In order to remove ISI, the CP extraction window must therefore be centered around the t_s time instant, relative to the start of a TW, i.e. the rectangular pulse $p(t)$.

It is seen that a convenient choice of ω_{ref} is $\omega_0 + \omega_{RF}$, in the middle of the data band, so that $t_s = 0$, at the start of the TW. The higher frequency SC will arrive after $\omega_0 + \omega_{RF}$ and will therefore be present at the beginning of the TW, while the lower frequency SC would have to have arrived before $\omega_0 + \omega_{RF}$ and, due to the periodicity of the FFT algorithms in which VPI simulations are based, will be found at the end of the TW . This reference frequency choice is also convenient since when no CP is added the OFDM sequence starts right at the beginning of a TW. As observed in section 2.2.6, if CP is not allocated when ISI affects the symbols, it will be not avoided.

Figure 3.3 is a time-frequency diagram of the OFDM signal at the RX side featuring three OFDM symbol frames. The y-axis represents the SCs from the closest to the farthest with respect to the optical carrier. The time length of the OFDM symbol is defined as T_{OFDM} and the data BW as $n\triangle\omega$ with $-N/2 \leq n \leq N/2$. The change of OFDM frame is indicated with a line which as steaming from the previous analysis, is tilted as a consequence of the differential delay among

SCs due to the effect of the CD. Taking into account our RX synchronization strategy, as seen in figure 3.3, the OFDM symbol starts when the SC allocated at ω_{ref} is RX. Thus, the lowest frequency SC will arrive to the RX $\left|t_{-N/2}\right|$ seconds before and the highest frequency SC will arrive $\left|t_{N/2}\right|$ seconds after it.

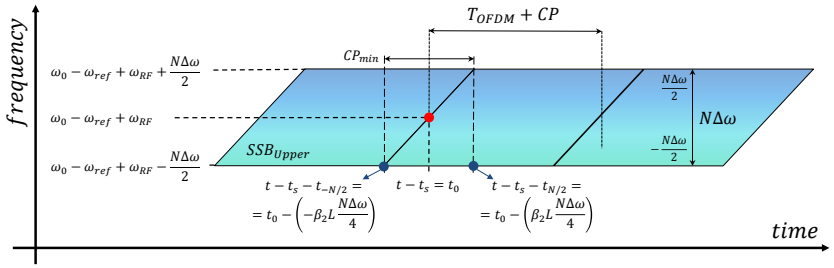

Figure 3.3: Illustration of the CD effect over an OFDM symbol in a SSB transmission.

It is then seen that the difference in arrival time between the lowest and highest frequency SC is two times $t_{N/2}$ and as seen it gives the ISI contaminated part of the RX signal and therefore the one that has to be taken away by CP extraction. It then follows that for an SSB TX signal the minimum CP length is:

$$CP_{min}(SSB) = 2\left|t_{N/2}\right| = 2 \cdot \left| L\frac{\beta_2}{2} \cdot \frac{N\triangle\omega}{2} \right| = \beta_2 L \frac{BW}{2} \tag{3.31}$$

As it is illustrated in figure 3.4, the steps to extract the CP from the RX OFDM frames are: remove the symbols that could not be allocated to a complete OFDM frame from the Rx sequence; separate the resulting TW into OFDM symbols (T_{OFDM}) considering reference frequency chosen and reorganize them into the $T_{OFDM} \times N_{FFT}$ matrix illustrated in figure 2.9 and finally extract the CP from all OFDM frames. Notice that, even when it is appended at the start of TX OFDM frame, for the first and last OFDM symbols half of it needs to be extracted at the beginning of the first frame and the other half needs to be extracted at the end of the last OFDM frame. Otherwise, some ISI will be included in each OFDM frame.

Isolating β_2 from 3.9, the CP length for the SSB case can be obtained by:

$$CP_{SSB} \geq \pi c \left|D\right| L \cdot \frac{BW}{\omega_{ref^2}} = \pi c \left|D\right| L \cdot \frac{BW}{(\omega_0 + \omega_{RF})^2} \tag{3.32}$$

In the case of DSB the information of an SC travels in two different optical frequencies. Due to CD one sideband will lag the other, so that in reception two superposed replicas of the OFDM sequence will be present, as seen in the figure 3.5. Mirroring the analysis for SSB, for the DSB case one may readily write,

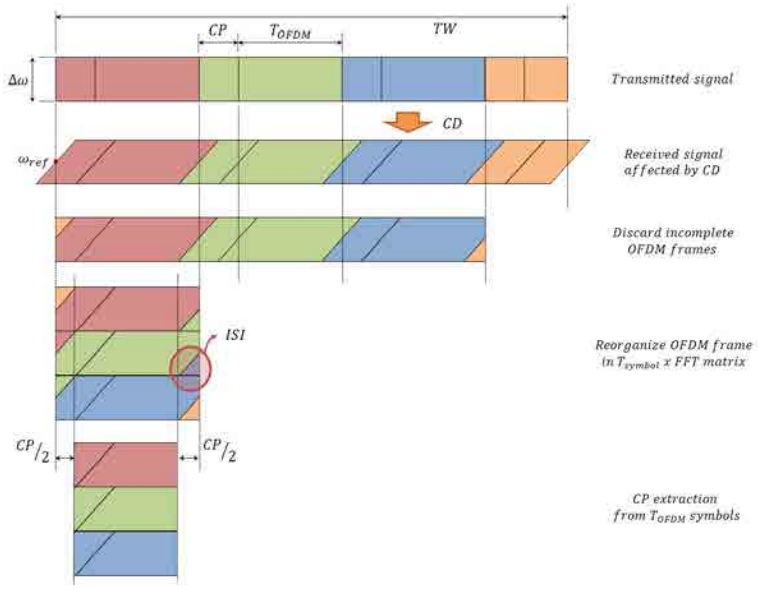

Figure 3.4: CP extraction at the receiver.

$$
\begin{aligned}
& s_{down}^{DSB}(t) = \\
& = \sum_{n=-\frac{N}{2}}^{\frac{N}{2}-1} a_n \cdot p(t - t_s^- - t_n^- - iT_{OFDM}) \cdot cos\left(n\Delta\omega\left(t - t_s^- - t_n^-\right) + \phi_n - \phi_0^-\right) \\
& + \sum_{n=-\frac{N}{2}}^{\frac{N}{2}-1} a_n \cdot p(t - t_s^+ - t_n^+ - iT_{OFDM}) \cdot cos\left(n\Delta\omega\left(t - t_s^+ - t_n^+\right) + \phi_n - \phi_0^+\right)
\end{aligned}
\tag{3.33}
$$

where, analogously to the SSB case:

$$t_s^{\pm} = \beta_2 L\left(\omega_0 - \omega_{ref}\right) \pm \beta_2 L\omega_{RF} \tag{3.34}$$

$$t_n^{\pm} = \frac{\beta_2}{2} Ln\triangle\omega \text{ where } -\frac{N}{2} \leq n \leq \frac{N}{2} \tag{3.35}$$

$$\phi_0^{\pm} = \beta_2 L\omega_{RF}\left(\omega_0 - \omega_{ref}\right) \pm \frac{\beta_2}{2} L\omega_{RF}^2 \tag{3.36}$$

One may now understand the RX signal as composed of two SSB signals (one upper sideband and one lower sideband) which are arriving at the RX with a differential time delay. Figure 3.5 follows the same scheme than in figure 3.3, but with the addition of the lower sideband and GBs. Specifically, the blue frames correspond with the upper sideband, the yellow frames with the lower sidebands, and finally the white part corresponds with GBs at each side. As in figure 3.3, $N\triangle\omega$ is associated with the BW of one sideband and the time length of the OFDM symbol frame is defined as T_{OFDM}.

As seen in the figure, whatever the choice of ω_{ref}, the CP window needs to be centered at $t_s = (t_s^+ + t_s^-)/2 = \beta_2 L(\omega_0 - \omega_{ref})/2$. The convenient choice here is therefore $\omega_{ref} = \omega_0$, in order to have $t_s = 0$. With that choice, the CP window position in the RX TW will be the same than for the SSB case, but a longer CP will be required, such as

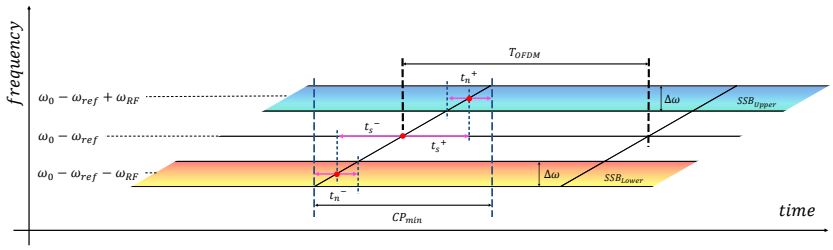

Figure 3.5: Illustration of the CD over an OFDM symbol in a DSB transmission.

As in the previous case, the minimum CP time length in order to avoid the CD effects can be obtained by:

$$\begin{aligned} CP_{min}(DSB) &= \left(t_{-N/2}^- + t_s^-\right)\left(t_s^+ + t_{N/2}^+\right) = 2 \cdot \left|t_{N/2} + t_s\right| \\ &= \beta_2 L \frac{BW}{2} + 2\beta_2 L \omega_{RF} \end{aligned} \tag{3.37}$$

Finally, comparing the required CP length for both SSB (3.31) and DSB (3.37) , one gets:

$$CP_{DSB} = CP_{SSB} + 2\beta_2 L \omega_{RF} \tag{3.38}$$

and, as in 3.32, isolating β_2 from 3.9, the CP length for the DSB case can be obtained by:

$$CP_{DSB} \geq \pi c \left|D\right| L \cdot \left(\frac{BW + 4\omega_{RF}}{\omega_{ref}^2}\right) = \pi c \left|D\right| L \cdot \left(\frac{BW + 4\omega_{RF}}{\omega_0^2}\right) \tag{3.39}$$

A part from the CP required to avoid ISI, a DSB signal is also affected by

the CS effect. As seen above, as a consequence of TX two sidebands, the same SC is arriving twice at the RX with a differential delay which also implies a change in phase which may result in a destructive sum leading to the loss of the information brought by this SC. See Figure 3.6 (left). At the right hand side of figure 3.6 the optical DSB signal spectra (top) and the electrical signal spectra after detection (bottom) obtained through VPI simulations of a 10GHz DSB with GB OFDM 45km fiber transmission are shown. A sufficiently long CP of 1.54ns obtained from (3.39) has been added to avoid ISI and then taken out according to the ω_{ref} choice. The amplitude fading effect is clearly seen in the electrical spectrum.

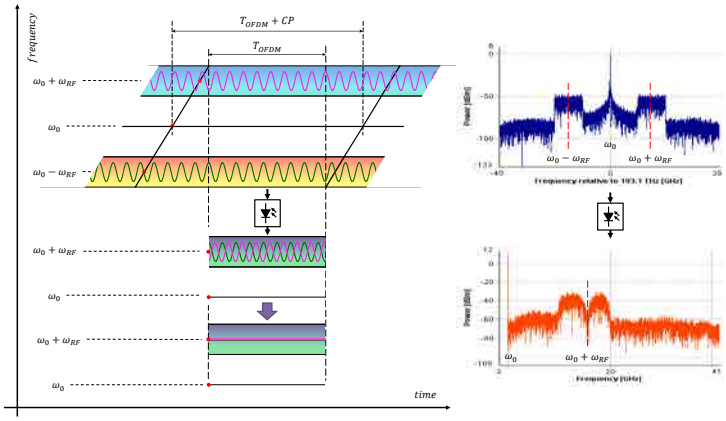

Figure 3.6: Amplitude fading (CS) through destructive interference between the SC brought by different sidebands. Optical (top) and electrical (bottom) signals and their corresponding spectra as obtained from a VPI simulation of an IGD01 OFDM system with a signal BW of 10GHz and for 45km of fiber.

3.3 Effects of chromatic dispersion in IM/DD oOFDM systems

As already mentioned, the main effects of CD over the data band in the conventional IM/DD optical system (ID01) are the DINLD, the CS effect, the differential SC delay spread and the PN decorrelation. This section is focused on the DINLD and CS effects presenting their mitigation strategies in an ID01 VPI simulation.

3.3.1 Dispersion-Induced Nonlinear Distortion

As discussed, the minimum GB necessary so that the IMD band does not overlap the data signal band after detection is as wide as the data band [57, 62],

nevertheless for some applications, some overlap may be tolerated with an acceptable signal quality. In order to separate the concept of **core network** and **access network**, the simulations of the same IM/DD systems were divided into two groups depending on the optical fiber length. Thus, lengths below 500km were considered access while from 1000km onwards they were considered core. This division is necessary in order to justify why it is not imperative to use a GB in access communications.

The simulations consider IGD01 with QPSK modulation 256-FFT size and 0dBm. For core-network fiber lengths, from 1000km to 8000km, a fixed electrical BW of 10GHz was considered, while for access-network fiber lengths, from 100km to 500km, the electrical BW were changed from 5GHz to 20GHz. That is because the optical fiber lengths relevance was considered for core-networks while the BW flexibility was considered for access-networks.

Figure 3.7 and 3.8 show constellations and BER results for the core and access cases respectively. In the graphs, 50% of GB means the theoretical minimum to avoid DINLD, i.e., the same as the data band. The GB was increased by padding with zeros the SCs closest to the optical carrier following a digital GB addition strategy (IGD01). In order to focus on the DINLD effect, a 3rd order band-pass gaussian optical filter centered at $\omega_0 + \omega_{RF}$ was added in order to filter the optical carrier and one of the sidebands to send just a SSB signal and therefore avoid the CS. Furthermore, the corresponding CP in each case was mathematically obtained to avoid ISI contributions. The simulations of figure 3.7 were made up to 5000km since for an electrical BW of 10GHz, the CP needed for higher lengths are higher than an OFDM symbol.

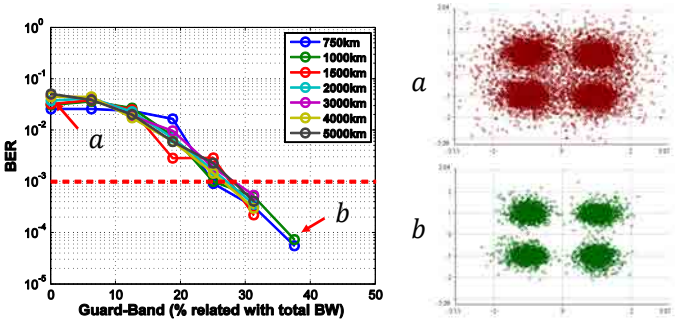

Figure 3.7: BER against the percentage of GB added with respect to a fixed electrical BW of 10GHz for core-network lengths (left) and representative constellations (right).
.

As it can be seen in figure 3.7, the GB needed for core-network lengths to avoid the IMD effect is around 25%-30% whatever the optical fiber length. Nevertheless, when access-network lengths, in figure 3.8, are evaluated it is seen the lower the optical fiber length, the lower the minimum GB needed. Specifically, a GB of around 18% is needed for 500km and an electrical BW of 5GHz; conversely, no GB is required when such length is reduced to 250km. Furthermore,

as expected, the lower the BW, the lower the minimum GB required. For instance, a GB of around 25-30% is needed for 500km and an electrical BW of 10GHz, and a GB of 18% when BW is reduced to 5GHz. Still inside figure 3.8, it is seen that in many of the cases tested, a GB is not strictly necessary to ensure the signal is detected at a FEC limit BER of 10^{-3}. In fact, just the cases with 500km and electrical BWs of 10GHz and 5GHz need GB to reach the quality threshold.

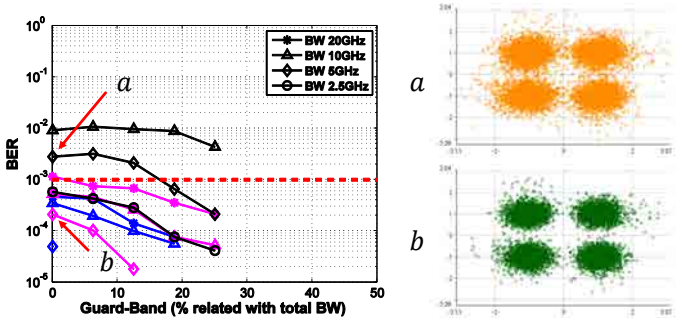

Figure 3.8: BER against the percentage of GB added with respect a variable electrical BW for optical fiber lengths based on access cases (left) and representative constellations (right). Blue, pink and black colors correspond with 100km, 250km and 500km fiber lengths.

Figure 3.7(a) show the resulting constellation when fiber length was set to 1000km and the BW was set to 10GHz without GB. As expected from the results shown in the graph, the symbols are not totally well-detected due to the effect of the IMD over the data band. On contrary, in figure 3.7(b), 37% of the BW was used to allocate a GB and consequently, the IMD effects were avoided resulting in a clearer constellation. On its side, figure 3.8(a) and (b) show the cases without GB, with an electrical BW of 5GHz and 500km (black) and 250km (pink) fiber lengths, respectively. According to the results plotted in the graph, the data of the first constellation are not properly detected at all and, on contrary, in the second case the results are below the FEC limit and therefore, it is seen a clearly constellation.

3.3.2 Carrier Suppression

The simulations contained in this section were performed with the same IM/DD oOFDM system than in previous section and aim at illustrating the phenomena of CS. In order to focus on the CS effect, the electrical BW was set to 10GHz and a fiber length of 100km was used so that IMD effects are negligible, even in absence of a GB as concluded in the previous section. Furthermore, the minimum theoretical CP length of 0.43ns which corresponds with 1.7% of the T_{OFDM} is added in order to avoid ISI contributions and the optical filter mentioned in the previous section was removed to firstly send a DSB signal.

In this section, three different methods to avoid the effect of the CS over a signal in an ID01 optical system were tested: ZP the affected SC, filtering out one sideband, and using an auxiliary carrier with a frequency offset for detection.

Results for the ZP method are presented in figure 3.9. It is seen how the BER improves as the gap is made wider at the location of the fading. Gap limit is obtained beyond which there are no further BER improvements. The downside of this method is that it requires the prediction of the SC where fadings will occur and that it depends on the fiber length.

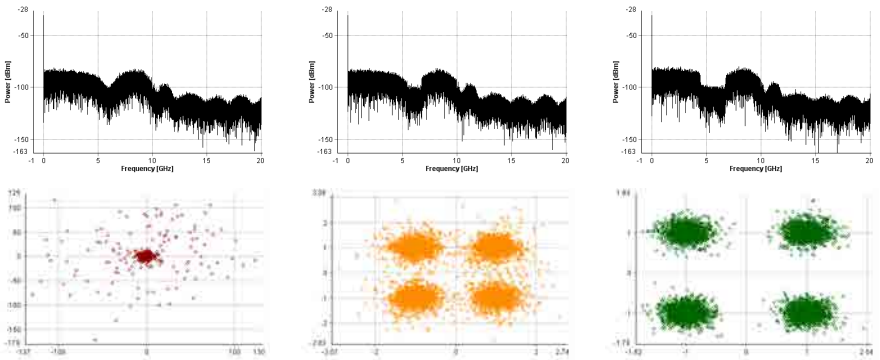

$BER = 0.0276$ $BER = 0.00181$ $BER = 0$

Figure 3.9: Electrical spectra (top) and constellations (bottom) of a conventional IM/DD oOFDM system (ID01) which 0 (left), 16 (center) and 29 SCs(right) removed at the position of carrier fading. The simulations were made with 256-FFT and 100km of optical fiber. The CP added is the 1.7% of an OFDM symbol of 25.6ns.

Taking into account that the CS is analogous to the image frequency effect, another solution to avoid the interference between both sides of the TX is to remove one of the sidebands by means an optical filter. The optical spectrum in figure 3.10 (top) shows that the left sideband is not filtered. Therefore, the CS affects the detected signal and the constellation shown is wrong. In the electrical spectrum is shown how the detected data signal is affected by CS with several faded SCs. Conversely, figure 3.10 (bottom) shows that the abovementioned optical filter was added to the scenario completely removing the left sideband and therefore avoiding the effect of CS over the data band. A clear data band spectrum and a correct constellation are obtained.

Finally, as an alternative to sideband filtering, an auxiliary carrier at a proper distance from the data band may be added to the receiver signal before the DD. In practice, it is difficult to ensure stability of the spectral distance between the data band and the auxiliary carrier unless they have been generated from the same laser source by using for example a MZM in the NP, as it is proposed in [4]. Even in that case, when the signal band and the auxiliary carrier follow different optical paths, the PN correlation may be lost and PN effects will impair the detected signal. As told, PN is analyzed in chapter 5 and compensation techniques based on pilot tones are discussed in chapter 8.

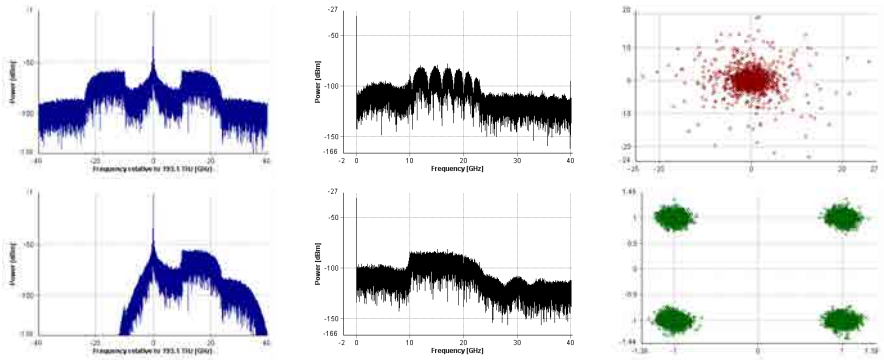

Figure 3.10: Optical spectra (left), electrical spectra (center) and constellations (right) of a transmission affected by CS without (top) and with (bottom) optical filter of 32GHz. The simulations were made with 256FT and 100km of optical fiber.

The simulations presented below were performed with the effective-AM (IGD-01) instead of a direct-AM such ADR05 since in order to detect with an auxiliary carrier is required a kind of AM modulation and in order to follow the same setup than the previous CS compensation methods. Figure 3.11 shows two examples of detection with an auxiliary carrier with different spectral distances relative to the data band. In order to leave out the PN effect, which in any case could be compensated by post-processing based on pilot tones, correlated laser sources were considered in the simulations.

Notice that the spectral separation between optical sources is critical to well detect the data band. In figure 3.11 (top) the optical spacing is 35GHz and it is not enough high because it can be seen in the electrical spectrum an overlapping between the beating of the TX optical source with the data band and the beating of the auxiliary optical source with the same data band. In the orange constellation can be seen that an overlapping between both data bands results in a wrong detection. Conversely, the optical spacing in figure 3.11 (bottom) was increased until 50GHz, and as shown, the green constellation is clear because there is no overlapping between the abovementioned data bands and the spurious beating neither affects the data band detected by the auxiliary carrier.

Thereby, the method of padding the SCs affected by CS is the simplest one due to the alterations and changes has to be applied within the pre and post-processed stages leading to present a low complexity cost. Nevertheless, this method implies to characterized the effect of CS for each case and therefore it has to predict which SCs will be affected by CS. Furthermore, the cost of this method is also the lowest, since no additional filters and optical sources are needed.

On the other hand, the optical filter method avoids completely the CS leaving a constellation with low EVM, as it can be seen in the corresponding constel-

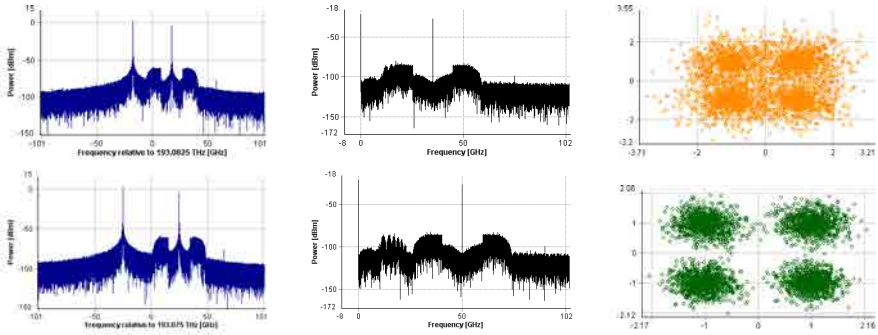

Figure 3.11: Optical spectra (left), electrical spectra (center) and constellations (right) of a transmission affected by CS with a spectral spacing between optical carriers of 35GHz (top) and 50GHz (bottom). The simulations were made with 256-iFFT and 100km of optical fiber.

lation. In turn, this may lead to a sensitivity improving. Furthermore, a SSB signal always will present a higher spectral efficiency than a DSB signal such in the other cases. However, the optical filter addition implies a cost increasing and the detection with an auxiliary carrier usually provokes the PN effect over the signal RX due to the decorrelation between both optical sources, already mentioned in section 2.1.5.4. In most of cases and depending on the correlation between both optical carriers, this kind of PN can be avoided by phase compensation algorithm based on pilot tones [41].

Finally, as a good feature of the auxiliary carrier insertion, it allows to independently set the power into the optical carrier and into the data band. A well-known result indicates that the Signal-to-Noise Ratio (SNR) is maximized for an optimum unity Carrier-to-Signal Power Ratio (CSPR) [67]. It has also been shown that in presence of fiber nonlinearities, this optimum CSPR value is changed and thus it allows to increase the total TX power into the fiber with a beneficial effect over the PONs power budget [68].

3.4 Chromatic dispersion compensation

In order to show how the constellation is compensated with the solutions against CD proposed in the sections above, a conventional IM/DD oOFDM system (ID01) with an electrical BW of 20GHz and QPSK providing a total BR of 80Gbps, with a fiber length of 500km was simulated.

Figure 3.12 shows the resulting optical and electrical spectra and the constellation without application of any kind of dispersion compensation strategy. As it can be seen in the optical spectrum as well as in the electrical one, the signal band is allocated in BB. The result is that due to the accumulated dispersion over 500km of fiber over such a wideband signal leads to catastrophic destruc-

tion of the constellation and an unacceptable BER. The reference frequency of the optical fiber in this case is set to $\omega_0 + \omega_{RF}$ in order to make the decoder starting at wrong time instant (t_s).

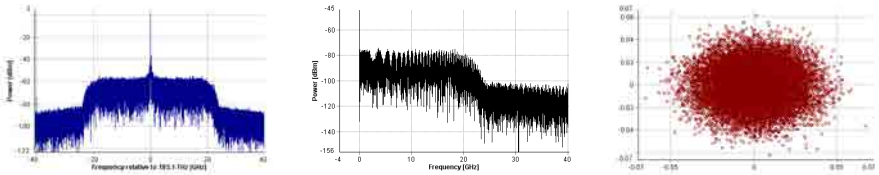

Figure 3.12: Optical (left) and electrical (center) spectrum, and the resulting constellation of an optical system without any CD compensation and incorrect synchronization $\omega_{ref} = \omega_0 + \omega_{RF}$ (BER = 0.53741).

The next step is to ensure the correct synchronization by changing the reference frequency of the optical fiber depending on the TX. In this first case, as the TX signal is a DSB, the reference frequency has to be equal to the frequency which the optical carrier is allocated $\omega_{ref} = \omega_0$. Even when a failed RX is obtained, one may begin to sense a cross-shaped constellation.

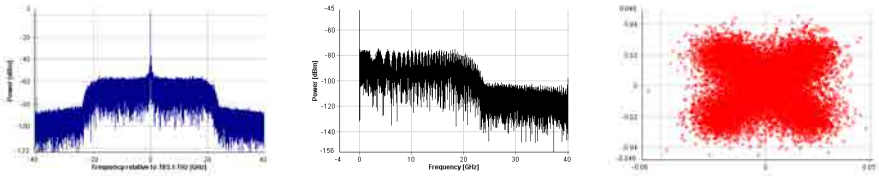

Figure 3.13: Optical (left) and electrical (center) spectrum, and the resulting constellation of an optical system with the correct synchronization $\omega_{ref} = \omega_0$ (BER = 0.49416).

In order to remove the CS effect, an optical filter was added to eliminate one of the signal side bands as it is shown in the optical spectrum of figure 3.14. The center frequency and BW of this filter need to be chosen for efficient suppression of one of the sidebands while ensuring enough power in both the optical carrier and the other sideband, thus a 3rd gaussian optical filter centered at 15GHz with a BW of 32GHz was used to transmit a SSB signal. It can be seen that a circumference-shaped constellation was obtained. As seen in previous sections, to maintain a correct synchronization in this SSB case, the reference frequency needs to be changed to $\omega_{ref} = \omega_0 + \omega_{RF}$.

Afterwards, a spectral GB is inserted in order to avoid the DINLD. In figure 3.15, the gap between optical carrier and data band can be observed in the optical spectrum as well as in the electrical one. The price of adding the GB has been to reduce the width of data signal band. This also involves changing the center frequency of the band and changing thus, the reference frequency of the optical fiber in accordance besides readjusting the optical filter parameters.

Although a failed RX with only a slightly lower BER of 0.45838 is obtained,

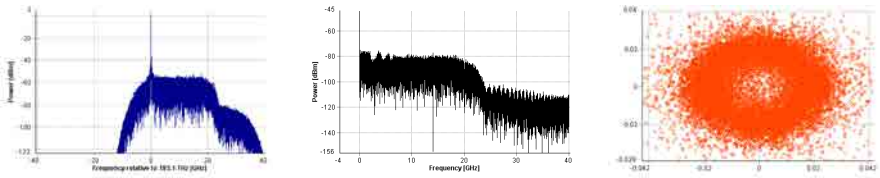

Figure 3.14: Optical (left) and electrical (center) spectrum, and the resulting constellation of an optical system with a SSB optical filter (BER = 0.4813).

it is observed that the ring-shaped constellation is much more defined. This indicates that DINLD effects have been avoided from the signal and but the differential shift among SCs produced by the differential phase shift among SC due to the CD remains.

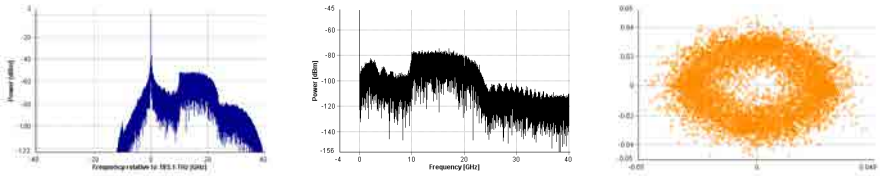

Figure 3.15: Optical (left) and electrical (center) spectrum, and the resulting constellation of an optical system with a GB between optical carrier and signal band (BER = 0.45838).

Thus, 1-tap equalization computed through training symbols is added at the post-processing stage of the conventional OFDM decoder to alleviate the effect of the aforementioned subcarrier delays. The constellation finally resembles that of the QPSK modulation format used, and a BER of 0.01525 is obtained (figure 3.16 left).

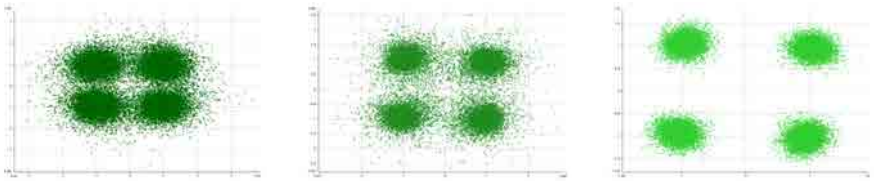

$BER = 0.01525$ $BER = 0.006825$ $BER = 0$

Figure 3.16: Constellation shapes when 1-tap equalization (left), first CP extraction method (center) and second CP extraction method from previous section (right) is added.

Still some improvement is possible by removing ISI through CP insertion. This CP is mathematically obtained applying 3.32 and corresponds to the 33.56% of a frame. Figure 3.16 (center) shows the constellation resulting to extract the CP without considering the ω_{ref} and therefore, some ISI appears

within the frame decoded leading to a non-zero BER. Instead, in figure 3.16 (right), the CP was extracted in a correct way, considering the ω_{ref} as a beginning of the TW and as expected, the resulting BER is 0.

Chapter 4

Optical OFDM systems for access

Once the principles of optical modulation and detection systems have been established, and the main characteristics and advantages of OFDM signal modulation techniques have been reviewed, it is time for a quantitative performance analysis of the most interesting scenarios over access distances. Thus, this chapter presents the study and performance comparison considering up to 100km fiber propagation distances among eight oOFDM systems, selected from those discussed in section 2.3 as the more relevant for OFDM PONs.

As explained in chapter 2, the more conventional optical TX system characteristics are not directly compatible with an OFDM modulation of data. Mainly two strategies may be followed to define a system that may take advantage of both the good features of optical TX and OFDM modulation, either to work on an electrical level and try to adapt the OFDM techniques for conventional IM/DD optical TX, or else to change the optical domain so that the optical TX system more closely follows the characteristics of OFDM modulation. Also hybrid solutions may be contemplated.

Thus, in this chapter, the eight oOFDM systems are classified considering the abovementioned strategies used being an **electrical oOFDM** (ID01, IGD01 and IGD02) or and **optical oOFDM** solution (AC01) if the electrical or the optical domain is modified, respectively; and a **hybrid oOFDM** solution if both domains are modified (ADR01, ADR05, ADR06 and IGC01).

In each section, a minimum sensitivity analysis through VPI simulations as a function of the propagated fiber length is performed for each oOFDM system, and at the end of the chapter, a ranking between the scenarios in terms of maximum reach and power budget is stablished.

The electrical oOFDM solutions are analyzed in section 4.2. Basically, these solutions rely on HS to remove the imaginary electrical component allowing

thus, an IM and DD. Also in this section, the strategies to avoid the DINLD based on the GB insertion are included. Right after, in section 4.3, , the direct-AM/CO optical system based on an oIQ TX and CO RX is analyzed. As it will be seen, this kind of system allows to send both real and imaginary parts and avoids the effect of DINLD without any kind of GB. Finally, hybrid optical OFDM systems are analyzed in section 4.4. This section studies the conditions under which solutions of this kind can be compatible and interesting in some scenarios.

Figure 4.1 features a tree classification of oOFDM systems according to the strategy followed for TX and RX. From table 4.1, it was concluded that a variety of combinations between TX and RX can be compatible. This chapter aims to evaluate those which could make more sense from a network perspective in order to compare them and stablish the abovementioned power budget ranking.

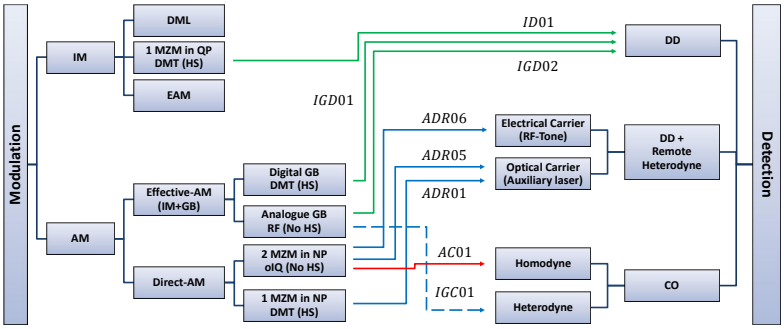

Figure 4.1: Classification of oOFDM transmission systems.

Each tree branch in figure 4.1 corresponds with a combination between a TX and RX. Specifically, the green braches correspond with combinations based on electrical oOFDM solution (section 4.2), the red one is the optical system based on the optical oOFDM solutions (section 4.3) and finally the blue ones are the hybrid oOFDM solutions (section 4.4). Notice that the colors and the acronyms are associated with table 2.1 in chapter 2. In addition, this chapter continually refers to figure 4.1 to be aware of the location of the currently optical system analyzed.

Table 4.1 contains a list of references classified by the oOFDM setup analyzed linked to the acronyms in chapter 2, table 2.1 and figure 4.1.

Some oOFDM techniques were left out of the scope of this Thesis, as they can be considered as particular cases or only slight modifications of the techniques described. Among them, it can be found the DC-biased-oOFDM (DCO-OFDM) [87, 103], the Asymmetrically Clipped-oOFDM (ACO-OFDM) [104], the Adaptive Modulation-OFDM (AM-OFDM) [105], the All-oOFDM (AO-OFDM) [106], the Orthogonal Band Multiplexed-OFDM (OBM-OFDM) [107], the Multiple-Input Multiple-Output-OFDM (MIMO-OFDM) [108] and the power efficient OFDM [109].

Acronym	TX		RX	References
ID01	IM (BB)	DMT	DD	[55, 79–85]
IGD01	Effective-AM	DMT	DD	[43, 56, 86–88]
IGD02	Effective-AM	RF	DD	[43, 57, 62, 78, 86, 89–92]
AC01	Direct-AM	oIQ	Homodyne CO	[44, 58, 74, 93–96]
ADR01	Direct-AM (BB)	DMT	Aux. Laser + DD	[97]
ADR05	Direct-AM	oIQ	Aux. Laser + DD	[68, 98, 99]
ADR06	Direct-AM	oIQ	RF-Tone + DD	[67, 73, 100–102]
IGC01	Effective-AM	RF	Heterodyne CO	[44]

Table 4.1: Researches references classified per optical systems.

The aim of this chapter is to elaborate a ranking list which classifies the eight oOFDM systems in terms of power budget. It is important to bear in mind that due to the very different characteristics of all the systems, it is difficult to find a common set of parameters that would allow for comparisons of universal validity. In the analysis that follows, the common parameters framework has been carefully chosen so that it is representative of relevant network conditions, but the resulting ranking must be understood in the context from which it has been derived.

4.1 Simulation strategies

The simulations consider Montecarlo BER computation in order to determine the RX sensitivity values for a FEC threshold of 10^{-3} as a function of the propagated fiber length. For quick reference, table 4.5, at the end of this chapter, provides a summary list of the main characteristics of the simulations, classified for all the different oOFDM systems texted, with reference to the acronyms in chapter 2. The schemes of the corresponding VPI simulation setups may be found in appendix B.

As a rule of thumb around 100 errors are needed to be counted for estimating a BER value, therefore, 2^{17} bits were randomly generated and mapped into Binary Phase-Shift Keying (BPSK), QPSK and 16QAM modulation format for a fixed power launched into the fiber of 3dBm in order to avoid fiber nonlinearity effects. An EDFA at the TX side is used to ensure this power level is kept fixed in all scenarios.

Since the interest relies in cost-effectiveness we have taken the maximum electrical BW as a key parameter because it largely determines the cost of transceivers. Notice that the electrical BW may differ from the data BW due to, for example, the presence of GB. Also, in some cases the required electrical BW may be different in TX and in RX. In all cases the electrical BW is taken as the maximum required. Using that criterion, the electrical BWs analyzed were 1.25GHz, 2.5GHz, 5GHz, 10GHz, 20GHz and 40GHz. The total BR needed as

well as the effective data rate in each case was set according to these parameters and the characteristics of the oOFDM system.

Loss and dispersion in the fiber were set to 0.2dB/Km and 17ps/(nm · km), typical values in the 3rd transmission window without taking into account losses due to connectors and splices. Furthermore, an ideal synchronization of RX was always assumed by proper choice of the fiber reference frequency according to the analysis in section 3.2. Since the study focuses in access-networks maximum fiber lengths up to 100km are considered.

Distributed Feedback (DFB) light sources are assumed with an emission power of 7dBm (5mW) and a PN BW of 0.5MHz. Compensation of PN is left out of the analysis by considering correlated PN properties among all sources involved. PN compensation techniques are discussed in chapter 8.

External optical modulation is always assumed. As specified in table 4.5 the MZM is considered biased at $V_{\pi/4}$ (QP) with an ER of 30dB [71] for both IM and effective-AM TXs, and biased at $V_{\pi/2}$ (NP) with an ER of 70dB for the direct-AM TXs. These values of ER have been chosen so that the finite ER is not a limiting factor in the system's performance. The fact that this value is significantly higher for the cases of NP indicates that a proper extinction of the carrier is critical. In practice optical filters for carrier rejection could be required when employing lower ER MZMs.

When it comes to practical realization of the oOFDM systems simulated, it is worth noting that the results obtained when the MZM is biased at QP may be extrapolated to optical modulation through DML, by following the equivalences derived in chapter 2.

The electrical signal injected to MZM is firstly multiplied by a MI factor of 0.2 in order to avoid PAPR problems by limiting the signal amplitude to lie within the linear zone of the MZM transfer. High values of PAPR have been identified as one of the challenges related to OFDM systems. High PAPR effects and compensation techniques are covered in chapter 6.

As about the carrier wavelength issued by the ONU, two cases may be distinguished: colored and colorless ONU. Broadly speaking, colored ONUs emit in a specific wavelength, different from other ONUs to avoid interferences in the US, and therefore specific equipment must be installed at each user-premises. This is an option which operators do not like due to stock and inventory problems, especially for massive deployments. On its side, colorless ONUs may be adjusted to transmit in any wavelength, which usually entails installation of the same equipment at each user-premise, easing installation and maintenance. In order to contribute to colorless operation, and therefore a cost reduction of the supposed deployment, no optical filters that may restrict the operation wavelength in transceivers have been employed in the simulations presented in this chapter.

On the RX side, PDs with a constant thermal noise density 2.1e^{-11}A/H$^{1/2}$ [110] were used in all scenarios to detect the signal sent.

As about the OFDM system characteristics, we consider 256 SCs and an ideal DAC/ADC conversion with the same sampling rate as the symbol rate. An analysis of the impact of finite quantization bit (QB) DAC/ADC conversion is carried out in chapter 8.

The pulse shaping characteristic of the anti-aliasing filters in both TX and RX were assumed to follow a square-root raised-cosine function with a roll-off factor of 0.18. We have confirmed that this value well-match the results obtained in the laboratory, and it is also the reference value used for example in [78].

The symbols time spreads generated for the fiber propagation lengths and BW in the simulation are negligible for most of the optical systems tested; nevertheless in order to set the same features for all of them, the CP was set to 12.5% of the OFDM frame. Finally, the first three OFDM symbols were used for training a 1-tap equalizer to compensate for the channel transfer function.

4.2 Electrical oOFDM systems

In this section, the optical systems based on modifying the electrical domain are analyzed. The classification starts with the conventional IM/DD (ID01) oOFDM system, and continues with the digital (IGD01) and analog (IGD02) GB additions.

4.2.1 Conventional IM/DD (ID01)

Figure 4.2 illustrates the architecture of a conventional IM/DD oOFDM TX system corresponding to the (ID01) green branch in figure 4.1. Example spectra obtained at different points in the setup for an electrical BW of 1.25GHz are given as insets. Since only one signal component is modulated, the HS is imposed among the SCs so that the OFDM signal is purely real. That entails a data redundancy that translates into an effective data TX capacity that is half the maximum that could be reached given the DSP capabilities of the system. Thus, for the electrical BWs considered, the total BR goes from 2.5Gbps for the BPSK and 1.25GHz case up to 320Gbps for the 16QAM and 40GHz case, nevertheless, as just the real part is sent, the effective data rates is only half.

Following figure 4.2, the output real signal in BB (blue) is introduced into the MZM biased at QP. The spectrum of the resulting DSB signal is shown in green. After being sent through the optical fiber, it is detected with a PD which converts it back to the electrical domain as it is illustrated in the inset in red. This signal is finally delivered to the BB decoder where the HS property is applied in order to decode the incoming symbols.

It is seen that no spectral GB is left between the carrier and the data band and therefore as explained in section 2.3.1, DINLD is expected to contaminate the signal for the longer fiber reaches and the wider BWs. On the other hand,

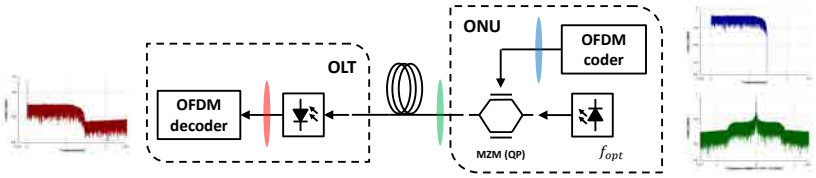

Figure 4.2: Conventional IM/DD oOFDM system scheme (ID01). Insets show the signal spectra at different points in the setup for an electrical BW of 1.25GHz and 100km fiber length.

since the two sidebands resulting from the modulation are jointly detected, also CS will be a factor for those cases.

Figure 4.3 shows the sensitivity results for OFDM signals modulated into BPSK (left), QPSK (center) and 16QAM (right). At first glance, as expected, it is seen how the signal BW is a critical factor due to the effect of the CS and the DINLD.

The B2B sensitivities are seen to lie in the range of -19dBm and -11.5dBm for BPSK, -17.5dBm and -10dBm for QPSK and -13dBm and -5dBm for 16QAM. This means a 1.5dB penalty to double the data rate from BPSK up to QPSK and a penalty of 6dB to quadruple it from BPSK up to a 16QAM. Furthermore, a penalty of 1.5dB is also observed to double the BW.

Only the two lowest BW tested, 1.25GHz and 2.5GHz are seen to maintain the B2B values up to the 100Km of fiber propagation, while for 5GHz there is a 4.5dB penalty for both BPSK and QPSK and more than 10dB for 16QAM. For the higher BWs tested the sensitivity increases dramatically from 0km to 35km. Considering a 1dB sensitivity penalty the maximum reaches are 17km, 5km and 1km for 10GHz, 20GHz and 40GHz respectively.

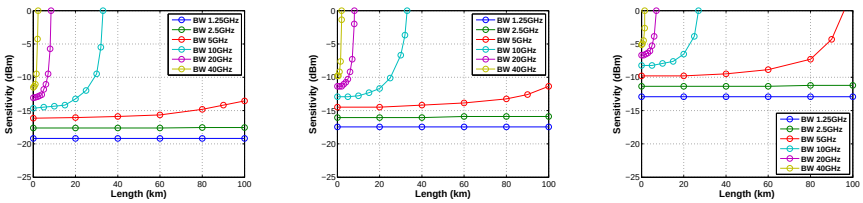

Figure 4.3: Sensitivity against fiber length of the RX signal modulated into BPSK (left), QPSK (center) and 16QAM (right) of the ID01 scenario.

4.2.2 Effective-AM/DD with digital GB (IGD01)

Figure 4.4 shows the basic architecture of an effective-AM/DD oOFDM system with digital GB addition (IGD01) corresponding to the green branch in figure

4.1. The setup is the same than in the previous section, but as seen in the inset now a spectral GB of the same width than the data BW is digitally added by ZP half of the SC.

The spectrum of the BB coded signal (blue) shows how a digital ZP features a noise floor with a -50dB difference with the active SC with a power closer to 0dBm. Notice that neither the DINLD nor the CS effects appear in the received (red) electrical spectrum because the electrical BWs and the optical fiber lengths used for the simulations of the insets are too low, as already observed in the study of figure 3.7.

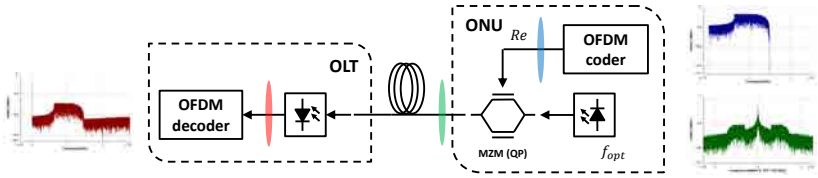

Figure 4.4: Effective-AM/DD oOFDM with digital GB scheme (IGD01). Insets show the signal spectra at different points in the setup for an electrical BW of 1.25GHz and 100km fiber length.

As expected, the results of this system in figure 4.5 closely follow those presented in figure 4.3 except for a sensitivity improvement in B2B of about 1.5dB for all electrical BW analyzed. The improvement is mainly due to the reduction of the useful SC within the electrical BW with a fixed total transmitted power entailing an increase of the effective power sent per SC.

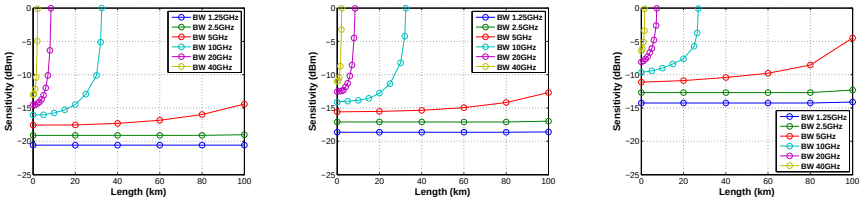

Figure 4.5: Sensitivity against fiber length of the RX signal modulated into BPSK (left), QPSK (center) and 16QAM (right) of the IGD01 scenario.

We may also highlight the case of 5GHz with 16QAM and 100km where the sensibility is -4.5dBm. For this sensitivity value in ID01 only 90km of fiber are allowed. This can be associated to reduction of the effects of DINLD owing to the GB.

All in all, even when the effective data sent is halved only a moderate increase in performance is achieved because CS due to DSB transmission seems to be the limiting effect. Several strategies to avoid CS were studied in section 3.3.2. From these, addition of an optical filter in the ONU could be advantageous for increasing reaches, but in this work we have discarded that option in order to

preserve the colorless operation.

Total data rates range from 2.5Gbps to 320Gbps, respectively for BPSK and 1.25GHz, and 16QAM with 40GHz. Due to the redundancy of the digital ZP, and the need for HS, effective data rates are divided by four (0.625Gbps to 80Gbps)

The sensitivities obtained for B2B lie in the range of -20.5dBm and -13dBm for BPSK, -18.5dBm and -11dBm for QPSK and -14.5dBm and -6.5dBm for 16QAM; and the 1dB penalty distance for BWs of 10GHz, 20GHz and 40GHz are around 16km, 4km and 1km respectively, independent of the modulation format.

4.2.3 Effective-AM/DD with analog GB (IGD02)

Figure 4.6 illustrates the architecture of an effective-AM/DD oOFDM system with analog GB addition corresponding to the (IGD02) green branch in the scheme of figure 4.1. As shown, an RF up/down-conversion stage is included at the TX and RX respectively, which can handle both the real and the imaginary parts of the OFDM signal as I/Q components at the RF frequency. The HS is thus not required here, and also no redundancies thus the DSP power may be exploited in full and reduced to half with respect IGD01.

This in turn leads to a reduction of the data rates (both total and effective). Specifically, the total BR goes from 0.625Gbps for the BPSK and the 1.25GHz case up to 80Gbps for the 16QAM case with 40GHz. In this case, no HS redundancy is required because the IQ setup allows to send both the real and imaginary parts, and also no ZP because the GB is obtained analogically, and therefore the total and effective data rates are the same, also coincident with the effective data rate of IGD01 which however needs a total data rate four times larger, increasing the DSP requirements. This DSP efficiency in IGD02 is at the expense of more complex transceivers at the electrical level which should include the RF stages.

Figure 4.6 also includes as insets the spectra found at different points for an electrical BW of 1.25GHz and 100km optical fiber. In order to avoid IMD, a GB as wide as the data signal has been included into the electrical BW, meaning an RF frequency in the up/down conversion stages of $3/4 \cdot \mathrm{BW}$, 0.9375GHz for this specific case. The blue spectrum of figure 4.6 shows the up-converted signal shifted to 0.9375GHz. It is seen that as compared with the digital GB addition, the RF up-conversion provides a lower noise floor in the GB. The signal is then applied to an MZM biased at QP to yield the optically modulated signal spectrum plotted in green. After fiber propagation and DD, the electrical spectrum shown in red is obtained. Afterwards, the resulting electrical signal is down-converted to BB by means of a RF down-conversion stage resulting in the spectra in purple, which neatly shows the effect of down-conversion resulting in detected DC power being converted to 0.9375GHz, and a replica of the data BW centered at 1.875GHz.

Notice that while the total electrical BW in the optical transceivers continues to be 1.25GHz, the low pass pulse-shaping stage with BW of 0.625GHz included in the OFDM decoding module will get rid of these high frequency components and retain only the low-pass signal band.

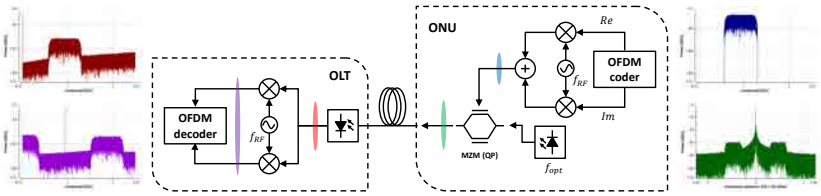

Figure 4.6: Effective-AM/DD oOFDM system with analog GB scheme (IGD02). Insets show the signal spectra at different points in the setup for an electrical BW of 1.25GHz and 100km fiber length.

Figure 4.7 shows the sensitivity results for fiber propagated distances up to 100km. As in previous setups, the most salient conclusion is that for the higher BW simulated the DSB signal is severely affected by the CS effect limiting the maximum optical fiber reach. As expected, the sensitivities for the cases with lowest BW are good because the CS effect does not affect the signal sent. In addition, they are about the same than for IGD01 and only slightly better than for ID01, showing reduced impact of DINLD. Actually the electrical spectrum in figure 4.6 does not show significant IMD power into the GB for this distances and BWs.

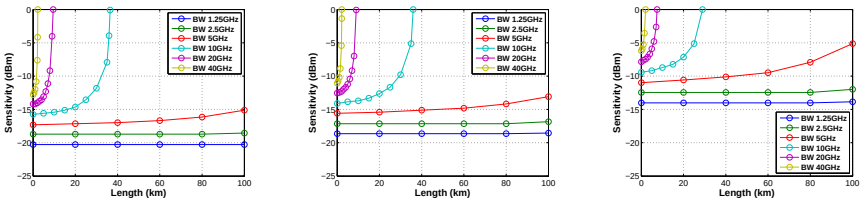

Figure 4.7: Sensitivity against fiber length of the RX signal modulated into BPSK (left), QPSK (center) and 16QAM (right) of the IGD02 scenario.

Furthermore, the optical fiber reaches for a 1dB sensitivity penalty with respect to B2B are very close to those in IGD01. From section 4.2.2 and 4.2.3 it can be concluded that the IGD01 and IGD02 have almost the same performance, with the latter at the expense of more complex and costly implementation at the hardware level, but also relaxing the requirements of the DSP as only one fourth of the data handling capacity is required for the same effective data rates and electrical BWs.

4.3 Optical oOFDM systems

Optical OFDM systems that make use of oIQ modulators and CO detectors are included in the optical oOFDM category. They may be thought of as an optical domain replica of a conventional electrical OFDM system. At present, this kind of optical equipment is costly and difficult to install and maintain and thus it is not suitable for massive network deployment. Even when in chapter 2 we distinguished between the homodyne and heterodyne cases as possible oOFDM implementations, for access networks, the heterodyne strategy does not make much sense because AM/CO systems are not affected by DINLD or CS. Therefore, just the homodyne strategy is analyzed in this section.

4.3.1 Homodyne Direct-AM/CO with oIQ TX (AC01)

Figure 4.8 illustrates the basic architecture of an homodyne direct-AM/DD oOFDM system with an oIQ TX corresponding to the (AC01) red branch in the scheme of figure 4.1. The optical local oscillator is centered at the middle of the OFDM data band so that directly the real and imaginary components of the OFDM signals are obtained in BB. Since the system is based on AM and CO detection, linear channel distortions remain linear after detection and linear equalizers have good performances without the need of any kind of spectral GB.

Simulated total and effective data rates for this system go from 2.5Gbps for the BPSK and 1.25GHz case up to 320Gbps for 16QAM and 40GHz case.

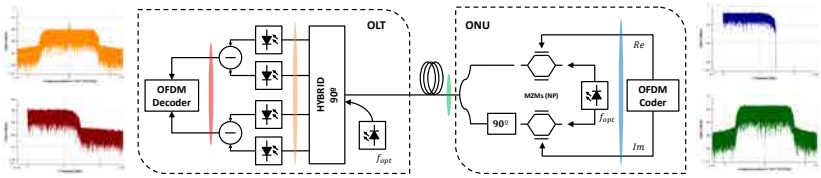

Figure 4.8: Homodyne direct-AM/CO with oIQ TX scheme (AC01). Insets show the signal spectra at different points in the setup for an electrical BW of 1.25GHz and 100km fiber length.

Following the schematic of figure 4.8, the electrical output of the coder in BB (spectrum in blue) is optically modulated by the oIQ TX. The green spectrum shows that the optical carrier has been removed. After the fiber propagation the optical signal is introduced into the optical hybrid in the RX together with the local oscillator resulting in the spectrum in orange, and finally detected by the two pairs of balanced PDs in order to get the electrical photocurrents for the real and imaginary parts of the BB OFDM signal (spectrum in red) to be directly fed to the OFDM decoder.

The sensitivity results of figure 4.9 corroborate that neither DINLD nor CS effects affect the CO detection. Thus no significant penalties are incurred up to

100km propagation. It is observed an around 3dB increase in sensitivity every time the BW is doubled starting at -55.5dBm, -52dBm and -44dBm for BPSK, QPSK and 16QAM, respectively. Also a 3dB penalty is seen for doubling the data rate by upgrading from BPSK to QPSK and around 9dB from QPSK to 16QAM.

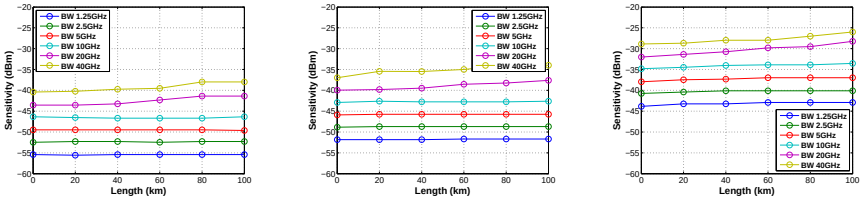

Figure 4.9: Sensitivity against fiber length of the RX signal modulated into BPSK (left), QPSK (center) and 16QAM (right) of the AC01 scenario.

These results allow us to conclude that under realistic access PON conditions optical oOFDM systems may reach superior performance levels than electrical oOFDM approaches. In the specific scenario simulated, the penalties for using an electrical instead of an optical lie around 35dB, while for the higher range BW, i.e. from 10GHz to 40GHz electrical OFDM systems are seen to be limited to distances shorter than 100km mainly because of DINLD and CS effects in the DSB signal considered.

4.4 Hybrid oOFDM systems

The systems in this section result from a combination between TX and RX in the two previous sections and correspond with the blue branches in figure 4.1. As seen in table 4.1, two kinds of combinations are analyzed here: a direct-AM TX combined with a DD RX (ADR01, ADR05 and ADR06), and an effective-AM with an analog GB combined with a heterodyne CO RX (IGC01).

4.4.1 Direct-AM/DD and remote heterodyne (ADR01)

Figure 4.10 illustrates the architecture of a conventional AM/DD oOFDM system corresponding to the ADR01 blue branch in the scheme of figure 4.1. Following the scheme of figure 4.10, the electrical OFDM BB signal (blue) is optically modulated by means of one MZM in NP, to obtain the signal in the green spectrum. In this case, as seen in the red spectrum corresponding with the signal after the DD, the electrical BW in RX is four times higher than that required in TX. As said, the simulations are labeled according to the maximum electrical BW required by the system, which in this case is that in RX.

Since only one MZM is used in TX, only one of the OFDM signal components can be modulated and HS is required. Therefore, the effective data rate is half

the total BR which in the case of figure 4.10 is 0.625Gbps. In order to DD the signal sent through the optical fiber, an auxiliary carrier is added at the RX side with a 0.9375GHz separation from the data band to consider a spectral GB to avoid IMD products to fall into the detection data BW. Since the transmitted signal does not include an optical carrier, all the TX power corresponds to data and therefore when mixed with the carrier in RX a high CSPR (see spectrum in yellow) gives rise to powerful IMD products apparent in the detections GB. This in contrast to IGD01 and IGD02 where a carrier was included in TX and a lower CSPR produced negligible IMD. Another interesting feature of this scheme is related to the electrical BW in the TX which is restricted to that required for the signal data, i.e. 0.3125GHz. Furthermore, the received signal is SSB and the CS is avoided. The signal after detection (red) is down-converted to BB (purple) through an RF stage with an electrical oscillator at 0.9375 GHz and input to the OFDM decoder where the HS condition is applied in order to recover the data sequence sent. This scheme constitutes a low-cost TX option which could be suited to the US of a PON.

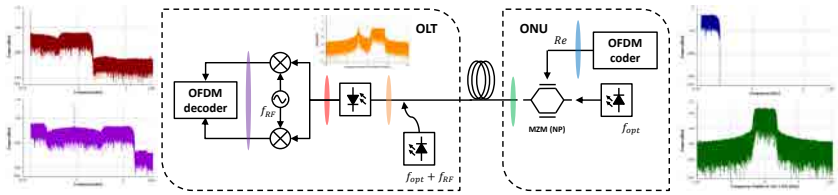

Figure 4.10: Direct-AM/DD oOFDM system and remote heterodyne auxiliary laser scheme (ADR01). Insets show the signal spectra at different points in the setup for an electrical BW of 1.25 GHz and 100km fiber length.

Notice that although the sent signal is purely real, in RX, instead of applying the HS with just one down-conversion mixer, an IQ down-conversion stage is used. As revealed by the results in figure 4.11 the IQ down-conversion stage is required for proper signal decoding when the channel distortion is high, i.e. for the higher BW and length cases. The dramatic sensitivity increase observed for the 40GHz case cannot be attributed to CS at the optical level, because we only have one sideband in detection, neither to IMD because we left a spectral GB, and as seen is not there if both real and imaginary parts are detected.

In order to understand what is happening, it is instructive to have a look at the spectra at different points in the setup for the electrical BW of 40GHz in figure 4.12. It is verified that indeed, no optical CS is present in the detected signal and that IMD products are relegated to the GB. Yet, SC fadings are observed in the down-converted BB signal. The reason for these fadings is that SC at the same distance from the auxiliary carrier will be finally down-converted to the same electrical frequency in the BB signal, and the contributions will add up. Because they have actually travelled over different optical frequencies, due to CD these *electrical image* SC will arrive at the RX with a different phase shift, which for some SC distances and fiber lengths may be as large as 180º

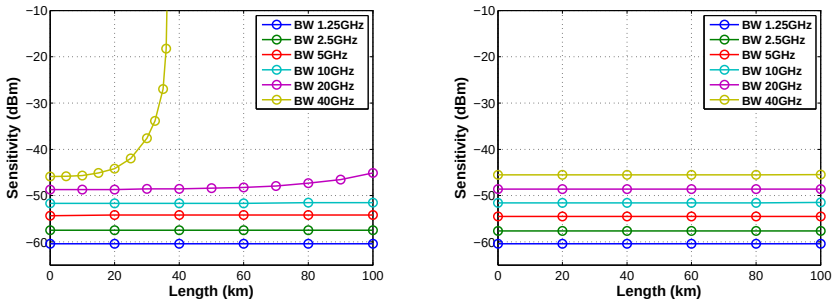

Figure 4.11: Sensitivity against fiber length for ADR01 with BPSK and HS RX (left) and IQ RX (right).

giving rise to the fading. Thus, in these situations is necessary the contribution of the imaginary part in order to reconstruct the original signal sent.

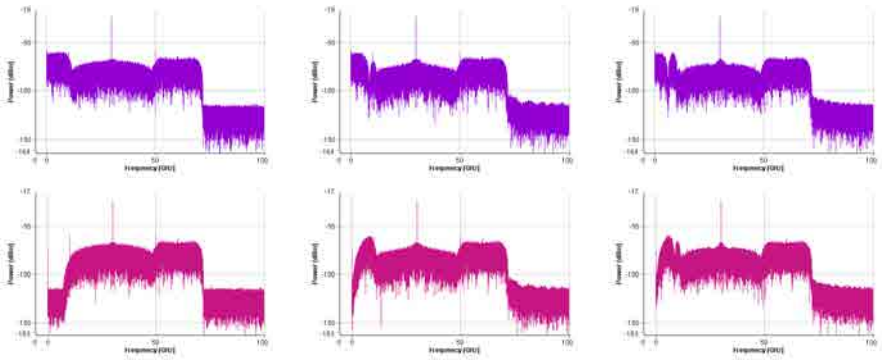

Figure 4.12: Electrical spectra of the real (top) and imaginary (bottom) part of a signal with 40GHz electrical BW and BPSK detected after the down-conversion stage transmitted through 0km (left), 50km (center) and 100km (right) optical fiber length.

Figure 4.13 shows the sensitivity results for QPSK and 16QAM using the IQ RX. In general, the sensitivities are better than the AC01 mainly due to two reasons. On the one hand, since a GB between the optical carrier and the data band is necessary, the power per SC is higher because the TX output power is uniformly distributed among less SCs; on the other hand, just one component is sent so again, the total power is higher because it does not have to be divided into real and imaginary components. Of course the penalty is a reduction by four of the effective data rate for the same electrical BW consumed. Specifically, the total BR range in this case goes from 0.625Gbps for the BPSK and 1.25GHz case up to 80Gbps for the 16QAM with 40GHz meanwhile the effective data rate are the halved of the total BR.

In this case, the sensitivities for B2B lie in the range of -60.5dBm and -46dBm for BPSK, -56.5dBm and -41.5dBm for QPSK and -48dBm and -33dBm

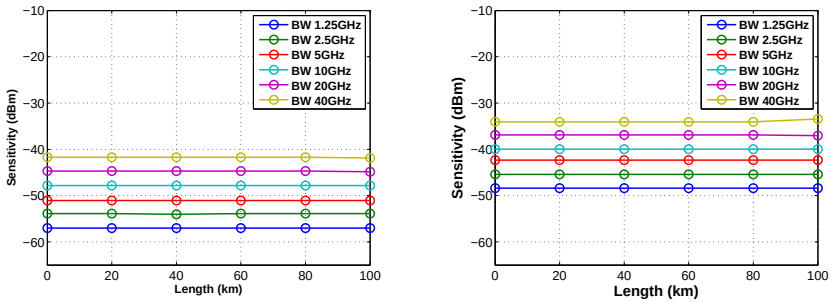

Figure 4.13: Sensitivity against fiber length of the RX signal modulated into QPSK (left) and 16QAM (right) of the ADR01 scenario.

for 16QAM. Furthermore, as in previous strategies, a penalty of 3dB is observed when doubling the BW and also when upgrading from BPSK to QPSK. On its side, the penalty is 12.5dB when upgrading from BPSK to 16QAM. Furthermore, independent of the modulation format, we found no significant sensitivity penalty up to 100km whatever the electrical BW.

4.4.2 Direct-AM/DD with oIQ and remote heterodyne (ADR05/ADR06)

Figures 4.14 and 4.15 illustrate two options for a direct-AM/DD oOFDM system with oIQ TX and heterodyne detection, characterized by the fact that DD in the RX is performed with the aid of an optical tone at a different frequency than that used for modulation. Both systems differ in the way the optical tone for DD is added and correspond to the blue branch of the oOFDM systems tree in figure 4.1. Specifically, figure 4.14 shows an ADR05 scheme with optical carrier addition, which as seen, consists on using another laser source which can be located either at TX or RX, while in figure 4.15 the setup of the ADR06 scheme with electrical carrier addition is found. In this case, an RF tone with an appropriate frequency is added to both oIQ branches with the same amplitude and a 90^{o} relative phase shift, such that it is modulated in SSB **[111].** Advantages and drawbacks of both approaches were discussed in section 2.3.2.In short, the use of independent laser sources as in the 'optical' carrier addition produces PN but provides the advantage of locating the auxiliary carrier at the RX side, which is convenient for the US, while the electrical carrier addition is power-constrained due to the reduced dynamic range of MZM.

Independent of the carrier addition method, the spectra shown in figures 4.14 and 4.15 allow to see that IMD and CS free detection will take place because of SSB+GB detection. Here the electrical BW is 1.25GHz, because it is the maximum BW required in RX, even when in TX the electrical BW required is lower. Furthermore, in both, ADR05 and ADR06 systems the total BR and the effective data rate are the same, so from 0.625Gbps for BPSK and 1.25GHz to

80Gbps for 16QAM and 40GHz.

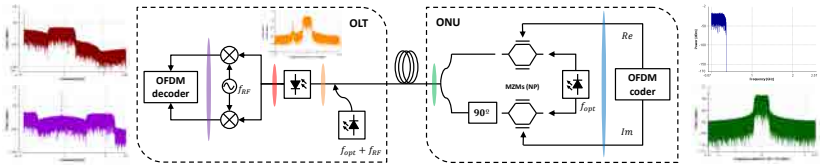

Figure 4.14: Direct-AM/DD oOFDM system with oIQ modulator and remote heterodyne optical carrier addition (laser) scheme (ADR05). Insets show the signal spectra at different points in the setup for an electrical BW of 1.25GHz and 100km fiber length.

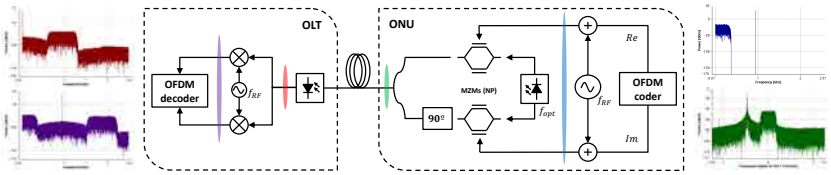

Figure 4.15: Direct-AM/DD oOFDM system with oIQ modulator and heterodyne electrical carrier addition (RF-Tone) scheme (ADR06). Insets show the signal spectra at different points in the setup for an electrical BW of 1.25GHz and 100km fiber length.

Figure 4.16 shows the sensitivity results of the ADR05 system for fiber propagated distances of up to 100km. In this case, the sensitivities are constant up to 100km and within the range from -57dBm to -42dBm for BPSK, from -54dBm to -38.5dBm for QPSK from -45.5dBm to -30.5dBm for 16QAM. As in previous sections, the penalty for doubling the BW and the modulation format from BPSK to QPSK is 3dB, and 12dB to from the BPSK to 16QAM.

When compared to ADR01 the sensitivity in this case is almost 2.5dB worst since, although the data BW is the same, both real and imaginary components of the OFDM signal are sent halving the power for each component.

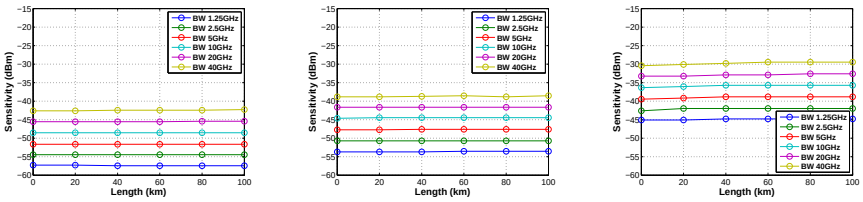

Figure 4.16: Sensitivity against fiber length or the RX signal modulated into BPSK (left), QPSK (center) and 16QAM (right) for ADR05 scenario (laser).

On its side, figure 4.17 shows the sensitivity for the ADR06 system. As for ADR05, IMD products and CS are avoided due to the GB between the optical carrier and the data BW and the SSB TX respectively, and consequently

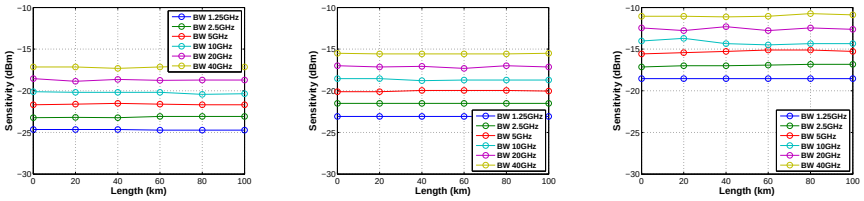

Figure 4.17: Sensitivity against fiber length of the RX signal modulated into BPSK (left), QPSK (center) and 16QAM (right) for ADR06 scenario (RF-Tone).

a constant sensitivity against fiber length up to 100km is obtained. Nevertheless, in this case, the sensitivity values obtained are significantly higher than for ADR05, with ranges from -24.5dBm to -17.5dBm for BPSK, from -23dBm to -15.5dBm for QPSK and from -18.5dBm to -11dBm for 16QAM. This corresponds with a penalty of around 32.5dB with respect to ADR05. Reasons can be found in the lower power allocated to data in ADR06 because the transmitted power is shared with the optical carrier and in the distortion introduced by the MZM when modulating the RF-tone. Therefore, the behavior of the ADR06 is closer to that of the ID01, IGD01 and IGD02 than it is to the best performing scenarios such as AC01, ADR05 or ADR01.

4.4.3 Effective-AM/CO with analog GB (IGC01)

Figure 4.18 illustrates the basic architecture of an effective-AM/CO oOFDM system with analog GB addition corresponding to IGC01 blue discontinuous branch in figure 4.1. As seen, the TX is the same than in the IGD02 option, with an analog GB addition through electrical up-conversion. The up-converted signal, in blue, shows the 1.25GHz of electrical BW are equally shared by data and GB. This up-converted signal is optically modulated by means of an MZM biased in QP to obtain the optical signal whose spectrum is shown in green. After fiber propagation, at the RX, the optical signal is introduced into the optical 90º hybrid together with the auxiliary optical source allocated at the center of the data band.

In figure 4.18 the spectrum resulting from addition of the received optical signal and the optical local source is shown in orange. Finally the optical signal is converted back to the electrical domain by means of two pairs of balanced PDs to obtain the real and imaginary parts of the OFDM signal. The spectrum of these signals looks as that shown in red. Besides the low-pass OFDM signal with a BW of 0.3125GHz, one obtains a tone at 0.9375GHz, coming from the beating of the 2 optical carriers, and a replica of the OFDM signal centered at 1.875GHz, due to beating of the 2 signal bands with the carrier sent from TX. Even when the optical sources have a finite BW of 1MHz, the tone resulting from the optical carriers beating has negligible BW because correlation properties have been assumed in simulations.

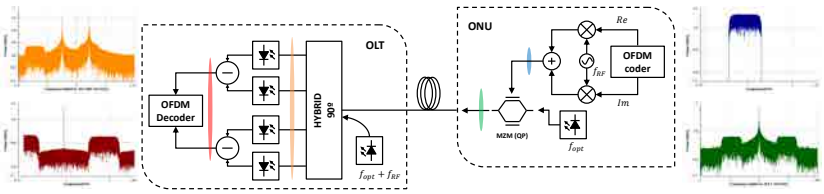

Figure 4.18: Scheme of an effective-AM/CO oOFDM system with analog GB (IGC01). Insets show the signal spectra at different points in the setup for an electrical BW of 1.25 GHz and 100km fiber length.

Figure 4.19 shows the sensitivity results. As it is firstly seen, although the modulation is an effective-AM like that in IDG01 and IDG02, this system presents an improvement of about 15dB. This improvement is mainly due to the coherent detection, with an auxiliary carrier addition that boosts the detected power. In fact, the more relevant difference of this system against the IGD02 system (which has the closest architecture) is the avoidance of the CS due to the CO detection.

Specifically, the sensitivity ranges obtained are -35dBm to -20dBm for BPSK, -32dBm to -17dBm for QPSK and -23dBm to -8dBm for 16QAM. In addition, one has a 3dB penalty for doubling the data rate by upgrading from BPSK to QPSK and 9dB from QPSK to 16QAM and 3dB for doubling the BW.

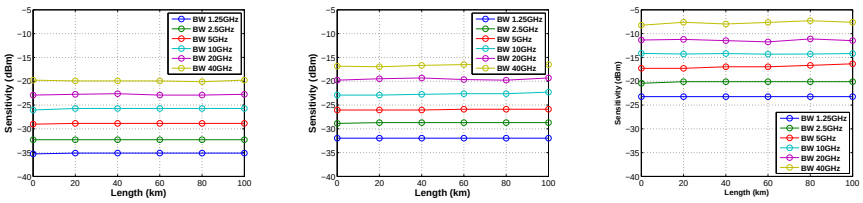

Figure 4.19: Sensitivity against fiber length of the RX signal modulated into BPSK (left), QPSK (center) and 16QAM (right) for IGC01 scenario.

4.5 Overall optical system comparison

After the detailed description of each of the systems simulated and the discussion of the sensitivity values obtained, in this section we aim at summarizing the main results and conclusions and at stablishing comparisons among them, mainly in the form of ranking classifications.

In table 4.2, the eight oOFDM systems have been listed taking the sensitivity value at 100km for the BPSK and 1.25GHz electrical BW sensitivity value as reference. Also, the main characteristics and impairments that may affect the quality of the received signal are given in order to assess the sensitivity penalties

found. Specifically, these impairments are divided into two groups depending on whether they reduce the power per SC or else they distort the signal. It is interesting to note that for the system features taken as reference, the former group has more weight for the resulting sensitivity ranking than the latter, mainly because it directly depends on the optical fiber length and the electrical BW, which in the case shown in table 4.2 is the lowest one. Results for larger electrical BWs shown in appendix C, reveal a greater impact of signal distortion on the obtained sensitivity values.

In table 4.2 a check mark means that such feature may have a negative effect on the sensitivity value found. As mentioned, the way in which the total power is distributed among the SC is critical and makes a difference in the resulting ranking. The systems analyzed, then can be divided in three groups depending on the sensitivity: the first group is composed by the ID01, IGD02, IGD01 and ADR06, and show sensitivities around -20dBm, the second groups is just composed by IGC01 in the middle table with a sensitivity of -35dBm, and finally the third group is composed by the AC01, the ADR05 and the ADR01 systems which show sensitivities from -55dBm to -60dBm.

Focusing on the first group, it is clearly seen in the table that the main reason of the low sensitivity is that the power of 3dBm with which the signal is launched has to be shared between the TX optical carrier and the data band. Also, no auxiliary carrier is added and specifically, the ID01 has the worst sensitivity because no GB is included either, so the same power than IGD01 has to be uniformly distributed among the double of SCs. On the other hand, the power of IGD02 is reduced because both components of the OFDM signal, real and imaginary are sent. Thus, IGD01 presents a slightly better sensitivity because it just sends the real part of the OFDM signal using the HS. On its side, the last system of this group, the ADR06 presents a sensitivity of almost 3dB better than the others showing the same power impairments than IGD02. This means that in this case, the absence of distortion impairments makes the difference in sensitivity.

Acronym	Carrier in TX	No Auxiliar Carrier	No GB	$\Re$ & $\Im$ parts	IMD	CS	Sensitivity with BPSK and 1.25GHz at 100km (dBm)
ID01	✓	✓	✓		✓	Optical	**-19.18**
IGD02	✓	✓		✓		Optical	**-20.27**
IGD01	✓	✓				Optical	**-20.58**
ADR06	✓	✓		✓			**-24.65**
IGC01	✓			✓			**-35.27**
AC01			✓	✓			**-55.43**
ADR05				✓			**-57.30**
ADR01						Electrical	**-60.43**

Table 4.2: Sensitivity values for BPSK and 1.25GHz electrical BW at 100km, and main impairments affecting the oOFDM systems evaluated.

The second group composed by IGC01 is situated in the middle table mainly

because on the one hand, it transmits an optical carrier from the TX which takes a part of the 3dBm of transmitted power but on the other hand, the auxiliary carrier of 7dBm used for the CO detection brings a power boost to the signal prior to detection.

Finally the third group shows the best performances since, they do not transmit any optical carrier and therefore the total power in the signal is 3dBm and in addition, they use an auxiliary carrier to CO or DD the signal. Specifically, it is seen that the AC01 shows the worst sensitivity because it sends both components and no GB is included in the electrical BW. The next one is the ADR05 because it includes a GB but also sends both components and finally the best system of the ranking is the ADR01 because it is only affected by electrical CS, which as detailed in section 4.4.1, this is not a problem for an electrical BW as low as 1.25GHz and in any case this impairment can always be avoided by adding an IQ RX instead of a HS RX.

It is also worth noting that the sensitivity improvements are mostly accompanied by an increase on the systems cost and complexity, and since received power has been seen to constitute a critical factor, a way for closing the sensitivity gap would be to include a pre-amplification stage before the PD, in DD RX approaches as it has been proposed in solutions such as Accordance [4]. On the other hand, since the above ranking considers the same electrical BW some of the systems, even if worst in terms of sensitivity, allow for greater effective data rates, or better exploit the DSP power and are therefore less costly and power-efficient, and in those senses it could be considered a better option in some cases.

Table 4.3 attention is focused on total BR required which directly provides the DSP power needed, the effective data rate and the effective BW occupied. Notice that the total BR of the systems which requires two DACs/ADCs in order to process both, real and imaginary components are expressed as two times the total BR required by one DAC/ADC. It is seen that the best system both from the point of view of DSP usage and highest data rate is the AC01. Some systems are seen to provide a 100% DSP usage as well and are therefore cost and energy efficient from this point of view, but their use of the electrical BW is not so efficient providing total data rates which are 50% of the maximum achievable with a BPSK modulation format. In most of the cases, this is a consequence of the need of a GB either in TX or RX since the electrical BW is always taken as the maximum required in the system.

On the other side, we find the IGD01 system which provides the maximum total data rate possible with this maximum electrical BW and modulation format, but makes very inefficient use of it, with only 25% resulting in an effective data rate of 0,625Gbps, the same data rate than IGD02, but with a four times higher DSP power.

Finally, also with a maximum electrical BW usage there is ID01 with a 50% efficiency in DSP power due to the need of HS and providing 1.25Gbps.

Acronym	Analog GB	Digital GB	$\Re$ part	Effective Data BW (GHz)	Total BR (Gbps)	Total BR / Effective BR (%)	Effective Data Rate (Gbps)
IGD01		✓	✓	0.625	2.5	25	0.625
ID01			✓	1.25	2.5	50	1.25
AC01				1.25	2.5	100	2.5
ADR01	✓		✓	0.3125	1.25	50	0.625
IGD02	✓			0.3125	0.625 × 2	100	1.25
ADR06	✓			0.3125	0.625 × 2	100	1.25
IGC01	✓			0.3125	0.625 × 2	100	1.25
ADR05	✓			0.3125	0.625 × 2	100	1.25

Table 4.3: Total and effective rates and bandwidths for BPSK and 1.25GHz electrical BW at 100km and main impairments affecting the features evaluated.

Finally, in order to assess the potential of any of the oOFDM options discussed in this chapter to be used in access PONs, table 4.4 summarizes the power budget and splitting ratios that any of them may provide for the BPSK and 1.25GHz case with 100km fiber length.

Acronym	Power Budget (dB)	Splitting Budget (dB) at 100km	Splitting Ratio at 100km	Effective data rate per user (xbps)	Effective data rate per user (xbps) with 64 ONUs
ID01	22.18	2.18	1	1.25Gbps	✗
IGD02	23.27	3.27	2	312.5Mbps	✗
IGD01	23.58	3,58	2	312.5Mbps	✗
ADR06	27.65	7.65	4	156.2Mbps	✗
IGC01	38.27	18.27	64	9.76Mbps	9.76Mbps
AC01	58.43	38.43	4096	610.3Kbps	39.06Mbps
ADR05	60.3	40.3	8192	76.29Kbps	9.76Mbps
ADR01	63.43	43.43	16384	19.97Kbps	4.84Mbps

Table 4.4: Power budget in B2B, splitting budget and splitting ratio at 100km, effective data rate per user with the maximum splitting ratio at 100km and effective data rate per user with 64 users for the oOFDM systems evaluated for the case of BPSK modulation and an electrical BW of 1.25GHz.

Considering table 1.1 and [18], the typical power budget of an OFDM-PON is in the range of 30-36.5dB, i.e. a network capacity of 64 ONUs at 100km taking into account a fiber attenuation of 0.2dB/km. Thus, table 4.4 shows that for the specific case of a BPSK modulation and a BW of 1.25GHz, the oOFDM systems which fulfill the power budget requirements with more than 64 users served are those with auxiliary carrier: IGC01, AC01, ADR05 and ADR01. From those, as seen, in terms of effective data rate, the best solution is AC01.

Among the systems and cases evaluated, for a target of 40Gbps per user with 64 users at 100km only AC01 presents the required performance for a fixed 10GHz, 20GHz and 40GHz maximum electrical BW with BPSK; 10GHz and 20GHz with QPSK and just 5GHz with 16QAM. Also the specific case of ADR05 for a fixed 40GHz electrical BW and QPSK fulfills the requirements. The data

rate that could be offered per user would be 625MHz. More comparative tables showing the obtained values for other electrical BW can be found in appendix C.

		Electrical oOFDM			Optical oOFDM	Hybrid oOFDM			
		IM/DD	Effective-AM/DD		Direct-AM/CO	Direct-AM/DD			Effective-AM/CO
		DMT (HS + BB) (ID01)	Digital GB (IGD01)	Analog GB (IGD02)	oIQ + Homodyne (AC01)	DMT (Hs + BB) + Aux. Carrier (ADR01)	oIQ + Aux. Laser (ADR05)	oIQ + RF-Tone (ADR06)	Analog GB + Heterodyne (IGC01)
Global Parameters	Bits	2^{17}	2^{17}	2^{17}	2^{17}	2^{17}	2^{17}	2^{17}	2^{17}
	Modulation Index	0.2	0.2	0.2	0.2	0.2	0.2	0.2	0.2
	Roll-Off	0.18	0.18	0.18	0.18	0.18	0.18	0.18	0.18
	N_{FFT}	256	256	256	256	256	256	256	256
	Digital GB	✗	128	✗	✗	✗	✗	✗	✗
	RF frequency	✗	✗	$1.5BW_{data}$	✗	$1.5BW_{data}$	$1.5BW_{data}$	$1.5BW_{data}$	$1.5BW_{data}$
	CP	12.5%	12.5%	12.5%	12.5%	12.5%	12.5%	12.5%	12.5%
	Equalization symbols	3	3	3	3	3	3	3	3
Laser Tx	Linewidth	$0.5MHz$	$0.5MHz$	$0.5MHz$	$0.5MHz$	$0.5MHz$	$0.5MHz$	$0.5MHz$	$0.5MHz$
	Power	$7dBm$	$7dBm$	$7dBm$	$7dBm$	$7dBm$	$7dBm$	$7dBm$	$7dBm$
	Correlation	✓	✓	✓	✓	✓	✓	✓	✓
	Emission Freq.	ω_0	ω_0	ω_0	ω_0	ω_0	ω_0	ω_0	ω_0
MZM	ER	$30dB$	$30dB$	$30dB$	$70dB$	$70dB$	$70dB$	$70dB$	$30dB$
	Bias	$V_\pi/4$ QP	$V_\pi/4$ QP	$V_\pi/4$ QP	$V_\pi/2$ NP	$V_\pi/2$ NP	$V_\pi/2$ NP	$V_\pi/2$ NP	$V_\pi/4$ QP
Amplifier TX	Output power	$3dBm$	$3dBm$	$3dBm$	$3dBm$	$3dBm$	$3dBm$	$3dBm$	$3dBm$
	Max. Gain	$100dB$	$100dB$	$100dB$	$100dB$	$100dB$	$100dB$	$100dB$	$100dB$
Optical Fiber	Max. Length	$100km$	$100km$	$100km$	$100km$	$100km$	$100km$	$100km$	$100km$
	Attenuation	$0.2dB/km$	$0.2dB/km$	$0.2dB/km$	$0.2dB/km$	$0.2dB/km$	$0.2dB/km$	$0.2dB/km$	$0.2dB/km$
	ω_{ref}	ω_0 17	ω_0 17	ω_0 17	ω_0 17	ω_0 17	ω_0 17	ω_0 17	$\omega_0 + \omega_{RF}$ 17
	Dispersion	$ps/(km \cdot nm)$	$ps/(km \cdot nm)$	$ps/(km \cdot nm)$	$ps/(km \cdot nm)$	$ps/(km \cdot nm)$	$ps/(km \cdot nm)$	$ps/(km \cdot nm)$	$ps/(km \cdot nm)$
Amplifier RX	Gain	20	20	20	✗	✗	✗	20	✗
	Noise figure	$6.5dB$	$6.5dB$	$6.5dB$	✗	✗	✗	$6.5dB$	✗
Auxiliar Laser	Linewidth	✗	✗	✗	$0.5MHz$	$0.5MHz$	$0.5MHz$	✗	$0.5MHz$
	Power	✗	✗	✗	$7dBm$	$7dBm$	$7dBm$	✗	$7dBm$
	Correlation	✗	✗	✗	✓	✓	✓	✗	✓
	Emission freq.	✗	✗	✗	ω_0	$\omega_0 + \omega_{RF}$	$\omega_0 + \omega_{RF}$	✗	$\omega_0 + \omega_{RF}$
Photodetector	Responsitivity	$0.9A/W$	$0.9A/W$	$0.9A/W$	$0.9A/W$	$0.9A/W$	$0.9A/W$	$0.9A/W$	$0.9A/W$
	Thermal noise	$2.1e^{-11}A/Hz^{1/2}$	$2.1e^{-11}A/Hz^{1/2}$	$2.1e^{-11}A/Hz^{1/2}$	$2.1e^{-11}A/Hz^{1/2}$	$2.1e^{-11}A/Hz^{1/2}$	$2.1e^{-11}A/Hz^{1/2}$	$2.1e^{-11}A/Hz^{1/2}$	$2.1e^{-11}A/Hz^{1/2}$
	Short noise	On	On	On	On	On	On	On	On
DSP	Active SC %	50%	25%	100%	100%	50%	100%	100%	100%

Table 4.5: Optical OFDM scenarios characteristics.

Chapter 5

OFDM-PON Architectures

While previous chapters have covered the analysis of P2P oOFDM systems, this chapter is focused on OFDM-PON architectures considering the relevant challenges in both directions, US and DS.

One of the main impairments of the US direction is the OBI effect [113–115], which refers generically to different kinds of interfering mixing products generated by the joint detection of all the ONU US signals. This chapter contains an analysis of this phenomenon in section 5.1, which aims at a better understanding of its main underlying principles and consequences. Depending on its origin, a distinction is made between the OBI due to multiple carrier detection and the OBI due to electrical spectrum overlap. Simple analytical models are presented that help to understand the effects observed in simulations.

Also, a description of two options for the design of an OFDM-PON is included in this chapter. Both options arouse as a consequence of the works within the EU ACCORDANCE project [4, 116]. The main ACCORDANCE proposal is the Remodulation-OFDMA-PON (R-OFDMA-PON) in section 5.2.1, and the second proposal is the ACCORDANCE low-cost proposal called Statistical-OFDMA-PON (S-OFDMA-PON) in section 5.2.2.

A pros and cons analysis of each option is carried out in connection with the oOFDM TX/RX systems basic characteristics as discussed in previous chapters, to move on to a more in-depth analysis of the S-OFDMA network which is the main goal of this chapter.

We begin the examination of the US S-OFDMA-PON by the study of the minimum frequency spacing between two adjacent optical carriers to avoid OBI effects in the detected signal. Right after, the design of two ONU boards and the corresponding OLT for the US direction is presented. Finally, an algorithm to insert and distribute the ONUs into the PON, reducing the rejection probability is described [117–119]. After that, two studies are experimentally performed with the ONU boards designed. On the one hand, EBA strategies are studied

into the US direction to reuse the power difference due to the variation of the BWs to compensate for differential link losses caused by geographically spread users [120–122]. On the other hand, the multiband ONU multiplexing approach in both directions is compared with the digital multiplexing [123, 124] also with the previously designed boards. The multiband approach, also proposed for use in the ACCORDANCE R-OFDM network, reduces the ONU's complexity and lowers down its energy requirements by allowing each ONU to process just its corresponding data BW instead of the complete DS BW.

5.1 Optical Beat Interference

In this section, two types of OBI are considered in connection with OFDMA-PONs. The first type of OBI arises when all ONUs transmit with the same optical carrier in different electrical data bands. Since the optical carrier is the result of the addition of carriers coming from different ONUs, and whose PNs are decorrelated, simultaneous DD of the US signal leads to incorrect decoding, as it will be seen and understood in the following analysis.

5.1.1 OBI due to multiple carrier detection

PN in optical communications may be understood as small random fluctuations of the optical carrier wavelength. The laser linewidth provides the PN BW and specifies the margin in which these wavelength fluctuations typically take place [42]. When an OFDM signal is modulated as an optical data band preserving the original carrier, there is correlation between the optical carrier and the optical data band meaning that these frequency fluctuations are synchronized and therefore when mixed, give rise to a steady electrical frequency free from PN. Conversely, when these are not correlated, the detected electrical frequency fluctuates in a frequency margin which is twice the PN BW. It then seems natural to model the effect of PN as a slight noisy frequency detuning of the RX electrical signal, so that following the conventions in section 2.2.2, the detected signal at the decoder may be written as follows:

$$s_d^{SSB}(t) = \sum_{i=-\infty}^{\infty} \left(p(t - iT_{OFDM}) \cdot \sum_{n=-\frac{N}{2}}^{\frac{N}{2}-1} c_{ki} \cdot e^{j(\omega_d + n\triangle\omega)(t - iT_{OFDM})} \right) \quad (5.1)$$

where ω_d is the frequency detuning which we will assume small as compared with the SC spacing $\triangle\omega \gg \omega_d$ so that orthogonality is not lost, and since $\triangle\omega$

is the inverse of the time frame in radians per second. One has:

$$s_d^{SSB}(t) \approx \sum_{i=-\infty}^{\infty} \left(p(t - iT_{OFDM}) \cdot e^{-j(\omega_d \cdot iT_{OFDM})} \cdot \sum_{n=-\frac{N}{2}}^{\frac{N}{2}-1} c_{ki} \cdot e^{jn\triangle\omega t} \right) \quad (5.2)$$

As seen, when $\omega_d \ll \triangle\omega$, the OFDM signal includes a phase term which is different for every OFDM frame. This is consistent with the constellations observed in the simulations of figure 5.1 where an IGDR01 system (see table 2.1) has been considered. In particular, a signal modulated into QPSK with an electrical BW of 10GHz was optically modulated with a 1MHz laser, sent through 100km of optical fiber and DD with an auxiliary carrier decorrelated (top) and correlated (bottom) with the TX optical carrier. Notice that in order to observe the effect of PN, the DINLD and the CS were avoided by means the minimum theoretical GB and an optical filter for SSB. Furthermore, a separation of 25GHz has been considered between optical sources in order to avoid overlapping between data bands.

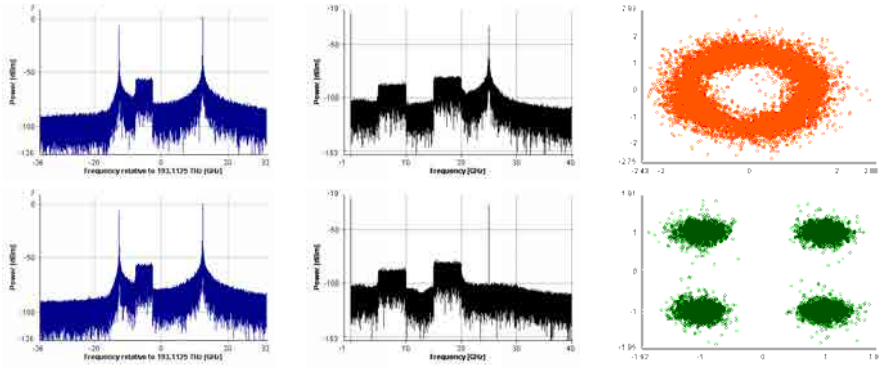

Figure 5.1: Optical (left), electrical (center) spectra and constellation (right) of an IGDR01 system with auxiliary carrier decorrelated (top) and correlated (bottom) with the TX optical source.

The ring-shaped constellation indicates that as predicted by (5.2), there is a different starting phase shift for every OFDM symbol frame due to the effect of the PN. When there is correlation between the optical carrier and the data band, the constellation is seen to acquire the correct shape.

Notice, that the effect of the PN is also apparent in the electrical spectra of the signal after the PD where the mixing product from both optical carriers at 25GHz is broader in the decorrelated case. It more or less has double the optical signals BW. Conversely, in the correlated case a very thin line is observed despite the fact that the optical signals show a broad optical BW, because the fluctuations of the optical wavelength for both carriers are synchronized.

Thus, considering the PN effect defined in (5.2), the OBI effect from multiple

detections can be understood as the addition of the signal coming from the beating of the data signal with its original carrier yielding the correct RX plus the beating of the same data band with a decorrelated carrier affected by PN (5.3).

$$s_d^{SSB}(t) \approx \sum_{i=-\infty}^{\infty} \left(p(t - iT_{OFDM}) \cdot \sum_{n=-\frac{N}{2}}^{\frac{N}{2}-1} c_{ki} \cdot e^{jn\triangle\omega t} \right) \cdot \left(1 + \cdot e^{-j(\omega_d \cdot iT_{OFDM})}\right) \tag{5.3}$$

That explains the constellations shown in figure 5.2 where on the one hand, there is the correct-detected QAM symbol and on the other there is the effect of PN drawing a ring-shape around each QAM symbol.

In order to illustrate and understand the nature and effects of the multi-carrier OBI, we conducted and compared two different simulation experiments both based on an IGDR01 system and using 1MHz linewidth lasers. One simulation considers detection of an OFDM signal with correlated optical carrier in presence of a decorrelated OFDM signal whose data occupies a non-overlapping optical band but with an optical carrier at the same wavelength as the first optical carrier. As it will later be seen this simulation recreates the US direction of the Accordance R-OFDMA-PON. In order to check the validity of the model represented by expression (5.2), the second simulation considers the detection of the same OFDM signal in presence of a correlated optical carrier with a 500kHz detuning with respect to the transmission optical carrier. The results in figure 5.2 reveal constellations with similar shapes, thus confirming the validity of the detuned carrier model to simulate the effect of PN.

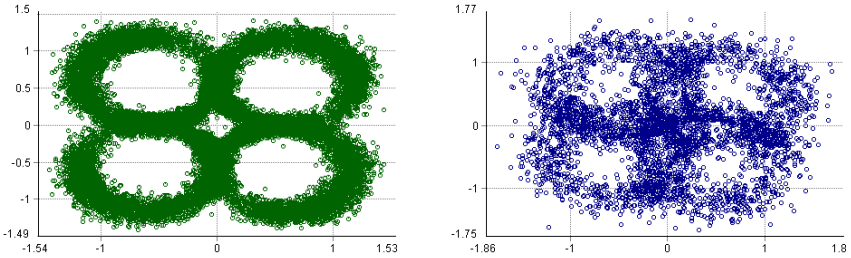

Figure 5.2: Constellations for an IGDR01 B2B system with interfering correlated carrier with a 500kHz detuning (left) and with interfering decorrelated carrier at the same wavelength (right). In both cases, the linewidth of lasers was 1MHz.

The same simulations were used to obtain the constellation of a DSB signal. From a mathematical point of view, the DSB signal in this case has to be understood as the sum of two signals such as those defined in (5.3) with same amplitude and opposing phases with respect to the QAM symbol position. As it is illustrated in figure 5.3, this translates into a cross-shaped constellation. As in the previous case, the constellation from the decorrelated carrier simulation

presents more dispersed points than the detuned one.

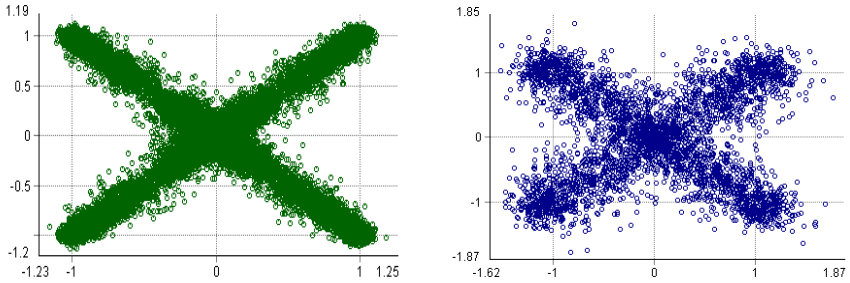

Figure 5.3: Same as in figure 5.2 but for DSB signals.

5.1.2 OBI due to electrical spectrum overlap

In addition to the multiple carrier detection effect above discussed, OBI may also emerge by the overlap of a spurious beat between two optical carriers, between two sub-bands, or between an optical carrier and a data band. One way to avoid these interference beats is to allocate a wide enough spectral gap between the carrier wavelengths of ONUs sharing an US medium.

As an example of this effect, in figure 5.4 several optical spectra and their corresponding constellations are presented showing the results of a simulation test with two ONUs transmitting with optical carriers at specific spectral distances and occupying different electrical sub-bands. To simplify the setup the multiplexing of users was made in the digital domain by assigning to each ONU half of the available 256 SC and setting to zero the other half to be occupied by the other ONU.

It is seen how the decoded constellations improve when the two optical carriers move away from each other. Blue spectra and constellations correspond to the ONU in BB and therefore as the carriers move away from each other, this ONU is first free from OBI. The theoretical minimum gap between two optical carriers within ideal conditions is twice the overall BW. In this case, for correct simultaneous DD of the two 3.125GHz OFDM QPSK signals with GB it is 12.5GHz corresponding with 0.1nm.

Among the OBI reduction techniques in OFDMA-PONs we may list CO detection, combination with TDMA, spectral broadening, and also centralized ONU wavelength monitoring and detuning [118]. The latter technique, based on wavelength control of non-preselected random wavelength lasers is analyzed in more detail in section 5.3.

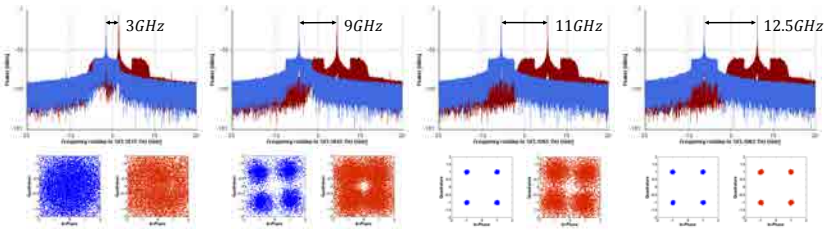

Figure 5.4: Spectra and decoded constellations for simultaneous detection of two ONU with an electrical BW of 6.25GHz with an IGD01 B2B system for differential ONU wavelength spacing.

5.2 Network architectures

Once the origin and the consequences of OBI in the US have been analyzed, in this section we discuss the potential of different network design strategies to deal with OBI-related problems.

Since users in an OFDMA-PON, are multiplexed into different electrical frequency bands, with optical spectrum efficiency in mind, one would like to use the same optical band. On the other hand, for cost reasons, the ONUs are likely to use any of the modulation techniques which include a carrier. Due to wavelength fluctuations with temperature and other environmental factors, if users are to share the same optical band, the only practical way for them to keep the orthogonality of the complete US is to share the same optical source, which could be sent from the OLT and remodulated at the ONUs. That however, does not avoid the multicarrier OBI problem explained in the previous section because after traveling different paths to every user, the optical carriers will have lost correlation, and therefore the remodulated optical carrier which arrives to the OLT is the result of the addition of many decorrelated carriers coming from each ONU which as seen, cannot be used for DD. Instead, an auxiliary carrier detection scheme should be in place at the cost of adding PN which can be compensated through pilot tones.

That is the strategy behind the ACCORDANCE main proposal, under the name Remodulated-OFDMA-PON since in the US the same optical carrier from the OLT is remodulated by a Reflective Semiconductor Optical Amplifier (RSOA) in each reflective ONUs. This network architecture is explained in more detail in 5.2.1.

On the other hand, in the ACCORDANCE project an alternative low-cost option was also studied. This option considers the placement of each user into a different optical band, with enough spectral distance so that through DD independent user detection takes place at the OLT. The advantage is that every user is detected with its own correlated carrier, thus avoiding PN and multicarrier OBI related effects. In this case the ONUs should include an optical light source which in order to avoid OBI should be maintained at a wide enough spectral

distance from the rest of user wavelengths. That entails the requirement of a wide optical spectral band if a large number of users is to be served.

This strategy is called Statistical-OFDMA-PON since direct-modulated non-preselected wavelength local DFB sources in the ONUs are used, i.e. the ONU lasers are all identical but when installed, their emission wavelength takes a random value within a wide spectral optical band. This aims to reduce expenditures for operators by eliminating the need of large inventories and complex provisioning. In order to maximize the number of users that can be allocated in a given spectral band, the tuning properties of the non-preselected wavelength DFBs may be exploited.

In relation with the oOFDM systems listed in chapter 4, the R-OFDMA-PON consists on an IGC01 for the US and ADR05 for the DS. This distribution clearly follows the cost requirement in PONs by allocating low-cost emitters and receivers at the ONUs (effective-AM and DD) and the most costly transceivers at the OLT (oIQ and CO). The S-OFDMA-PON on its side, may consist on an IGD01 or an IGD02 in both directions.

5.2.1 Remodulated OFDMA-PON

In figure 5.5, the basic scheme of the R-OFDMA-PON is illustrated and the most relevant electrical and optical spectra are shown. Specifically, the bottom spectra, i.e. from (b) to (d), and top spectra, i.e. from (e) to (h) correspond with the DS and US, respectively.

As seen, the OLT incorporates two optical sources for the US and the DS at different wavelength bands. In order to maintain the frequency difference between the optical carrier used to modulate the signal and the one used to detect it in both directions, the optical sources feed the same MZM biased in NP and driven by a 18.75GHz signal. The optical spectrum of figure 5.5(a) is obtained at the output of the MZM, i.e. four optical carriers, two for US and two for DS with a frequency spacing of 37.5GHz.

For the DS, one of the optical carriers is used to optically modulate the signal by means of an oIQ modulator and the other is sent as an auxiliary carrier for DD at the ONU side. The DS is thus an SSB signal as seen in the spectrum in figure 5.5(b). Both the carrier and the modulated data band follow the same path down to the ONU and therefore they are likely to keep correlation properties. The SSB signal scheme is also free from CS in the DD process. In order to prevent IMD products to overlap with the signal through DD, the minimum GB may be allocated which in this scheme implies a total usable BW of 25GHz, as seen in figure 5.5(b). After detection at the ONU (c), the signal is down-converted to BB (d) by means of an RF stage with a local oscillator within the frequency band assigned to the ONU. Notice that the use of a tunable RF stage enables EBA schemes.

For the US, one of the two optical carriers remains in the OLT to CO detect

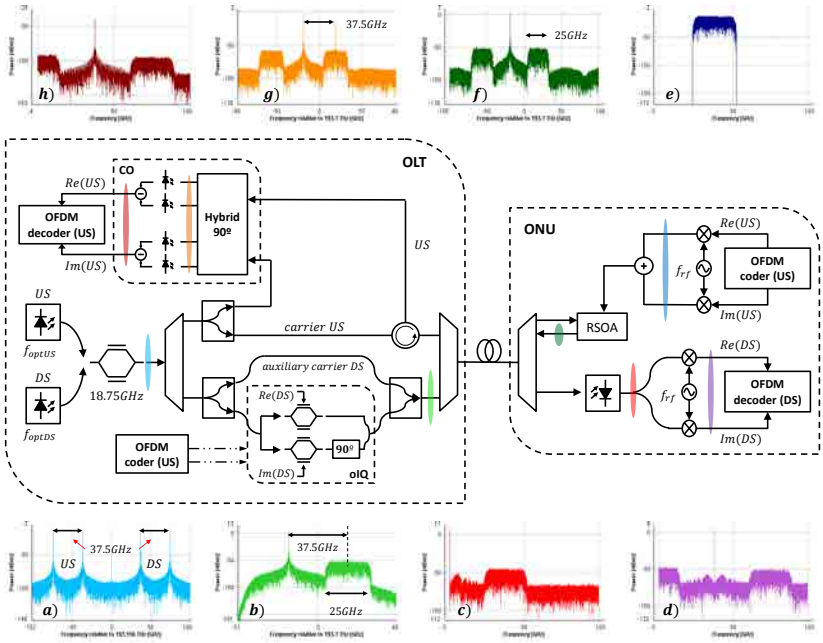

Figure 5.5: Scheme of high performance ACCORDANCE solution: R-OFDMA-PON.

the signal and the other is sent towards the ONU to be intensity remodulated. Thereby, a 25GHz GB is added for effective-AM through low-cost IM modulation at the ONU, compatible with CO detection at the OLT illustrated in figure 5.5(e). After remodulation the (f) spectra is obtained. Even when due to the use of RSOAs or EAMs the US signal contains an optical carrier which could be used for DD at the OLT, the addition of carriers at the same wavelength coming from the different ONUs leads to multiple detection OBI as discussed in previous sections and therefore a CO RX is a better option, also considering that such a costly RX is shared among all the users in the PON. On the other hand, even when in this case the US is a DSB signal, CS is avoided due to the homodyne CO detection with an auxiliary carrier located right in the center of the bands in figure 5.5(g). Also no IMD products are generated by the CO detection.

The GB in this case serves the purpose of guaranteeing the compatibility between low-cost IM modulation at the ONU and CO amplitude detection at the OLT because it allows to obtain an effective-AM modulation through IM modulators such as EAM at the ONU. An alternative that would avoid the allocation of the GB and thus halve the electrical BW requirements of modulators and up-conversion stages would be to use pure-AM modulation with a MZM biased into the NP, but at present, MZMs are considered not a very good option for ONUs due to cost and complexity.

Contrary to the DS, in this case, the data band and the carrier used for

detection will most probably have lost correlation due to the difference of optical paths followed, but as aforesaid this kind of PN can be corrected by several algorithms. Notice the importance of maintaining the same frequency spacing in both directions to modulate and detect the OFDM signal correctly. That is guaranteed by the MZM NP biasing scheme of replicating the carriers at the OLT as seen in the (a) spectra.

Through the works carried out in the context of the EU project ACCORDANCE, it has been seen that this scheme may be up to the requirements of future PON networks. Challenges still remain though because implementation is still beyond cost requirements for commercial PON deployments. In addition, the remodulation scheme suffers from Rayleigh Backscattering (RB) problems and the network reach is restricted by the fact that the optical carrier needs to travel twice the distance OLT-ONU.

5.2.2 Statistical OFDMA-PON

Figure 5.6 illustrates the ACCORDANCE low-cost S-OFDMA-PON architecture. As a fundamental difference with the previous approach, each ONUs must host an optical light source tuned to a different optical data band, and the minimum distance between the ONUs wavelengths to avoid OBI must be ensured at all times. Even when the increase in cost may not be so relevant, because directly modulated DFB sources exist at competitive prices, at least comparable to that of RSOAs or EAMs as required by the previous remodulated architecture, installation, provisioning, stock and inventory problems derived from the fact that each ONU requires a different transceiver are a huge concern for operators. In order to overcome this, non-preselected light sources have emerged whose emission wavelength takes a random value within a large optical band. When installed, there is a probability that the unit causes OBI problems in the US with an existing unit in the PON, which basically depends on the number of multiplexed units and the characteristics of the random function followed by the emission wavelength. If that is the case, the unit will be discarded and another unit should be tried until OBI-free detection is obtained at the OLT. The use of direct-modulated non-preselected wavelength local DFB laser sources in the ONU makes this approach very cost-effective while reducing expenditures for operators by eliminating the need of large inventories and complex provisioning.

Furthermore, it has been seen that temperature tuning of the DFB in a limited spectral range may dramatically decrease the laser's rejection probability down to values of practical interest for massive PON deployment [118]. Following the scheme of figure 5.6, the ONU TX consists of a DFB laser with non-preselected wavelength in the C-band. The emission frequency of the ONU laser is regulated through temperature and current control circuits to avoid interference.

The OLT includes an intelligent activation and operation algorithm like those proposed in [125, 126] to initialize and track the λ of the ONUs lasers by cen-

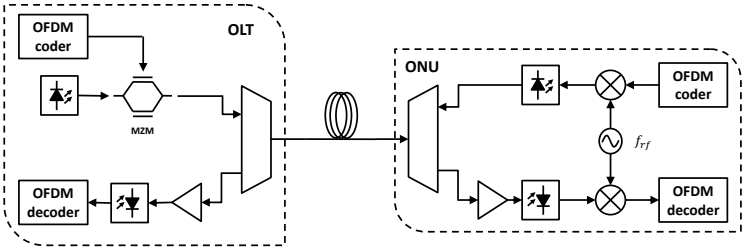

Figure 5.6: Scheme of low-cost ACCORDANCE solution: S-OFDMA-PON.

trally measuring and sending instructions to the control circuits. As a result, the ONU rejection probability can be minimized [118]. Thus, with centralized feedback wavelength control, it can be ensured the ONUs λ is kept at enough spectral distance to reduce the OBI at the OLT below a quality threshold. As said, since the ONU lasers emit at random wavelengths and are centrally managed to maintain the overall performance, this PON architecture is referred as Statistical-PON. Just like in R-OFDMA-PON, the RF up/down conversion stages allow to reduce the required DSP power requirements in the ONU.

5.3 Upstream S-OFDMA-PON design and characterization

Building on the previous description of the S-OFDM, this section presents the design and implementation of the experimental setup to test the US direction by means two low-cost ONU transmitters.

As said, centralized control of the emission frequency of the random non-preselected independent laser sources at the ONUs allows to significantly reduce the ONUs rejection probability and to maximize the number of users served by the PON. The ONUs boards must then be capable of automatic tuning of their emission frequency. This is achieved by specific temperature and current control circuits which have been designed and built with such a purpose. In order to specify the set of requirements to be met by those circuits, a first experiment meant to determine the wavelength tuning margins and selectivity required for OBI-free operation was carried out and its results are presented in section 5.3.1. Afterwards, section 5.3.2 contains a description of the boards.

5.3.1 Minimum spectral gap to avoid OBI

In order to determine the minimum frequency gap needed between two adjacent ONU wavelengths to avoid OBI, a first experiment was carried out based on the future characteristics of the ONU board design.

Figure 5.7 illustrates a scenario with two users with different wavelengths transmitting an OFDM signal consisting of 256 SC with QPSK coded data at 12.5Gbps. ONU_1 uses the first 128 SCs, while ONU_2 uses the last ones. Data was generated randomly for a total length of 2^{18} bits. The HS property was employed in order to get a real OFDM signal. The data was loaded to an AWG for converting it to analog at 6.25GSa/s. The electrical signal modulates the light source by means of a MZM biased at QP. The effective data BW for both ONUs is 3.125GHz. The light sources at both ONUs were DFBs with total unmodulated laser linewidth of 30MHz. The optical OFDM signal then travelled through 6km fiber; it was detected with an Avalanche Photodiode (APD) and captured with 50GSa/s Real-Time Oscilloscope (RTO). The signal was then post-processed in Matlab® performing the FFT and QPSK decoding for measuring the BER of ONU_1 data. The wavelength of ONU_1 was left static at 1550.83nm, while the ONU_2 wavelength was swept.

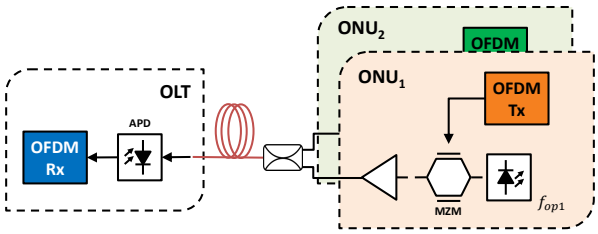

Figure 5.7: System schematics to find the minimum frequency spacing between the ONUs carrier wavelengths in the US S-OFDM experimental setup.

Figure 5.8 shows the BER results obtained as a function of the wavelength gap between the carriers. As seen, the BER for ONU_1 is kept constant and below the FEC margin of 10^{-3} for optical gaps larger than 0.075nm (9.375GHz in C-band). It is a consistent result since it nearly corresponds to the sum of the modulated BWs of each ONU. Therefore, the ONU tuning circuits must allow for spectral gaps on the order of 0.1nm.

5.3.2 Design and characterization of ONU boards with wavelength control

This section presents the basic structure and the characterization of the ONU boards designed to test the US of the S-OFDM-PON. Figure 5.9 (left) shows it is composed of 3 stages: the data-processing section, the electrical section, and the optical section.

The data-processing section is where mapping to modulation format, OFDM modulation, and data conditioning take place. In practice, it is composed of a Field-Programmable Gate Array (FPGA) followed by a DAC, which works as an interface with the electrical modules. In our case, the operations were performed off-line in a PC with Matlab® and then an AWG did the conversion to the analog

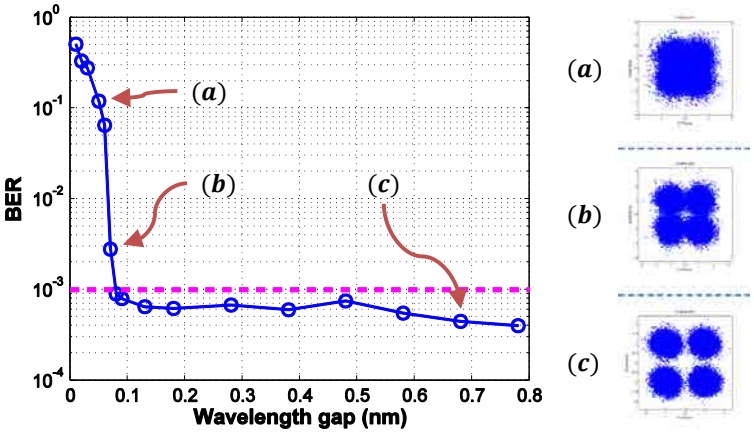

Figure 5.8: BER against spectral spacing between optical carrier wavelengths of consecutive ONUs, the insets show the constellation of ONU_1 in each case.

domain with 8-bits resolution.

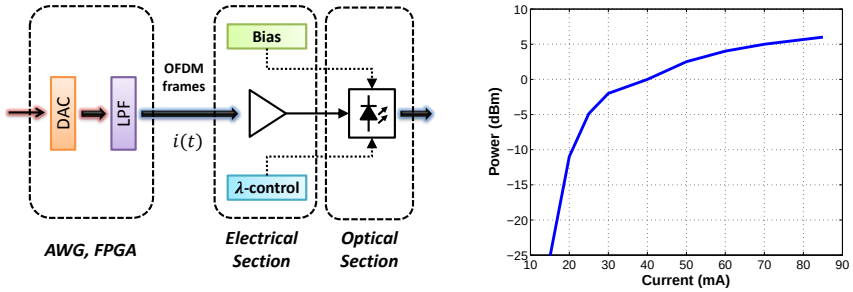

Figure 5.9: ONU board stages (left) and optical power against injection current for the ONU laser (FLD150F2BP) (right).

Right after the data processing section, the electrical section is mainly a signal conditioning stage for optimum transmission. The signal obtained from the DAC can be amplified to take advantage of the laser response. There is also a biasing circuit that ensures work in the linear part of the laser transfer characteristic. As shown in figure5.9 (right), the bias for 0dBm power launch into the fiber has been measured at 40mA.

In our experiments the biasing current at the ONUs boards is fixed to 40 mA to set the optical carrier power at 0dBm, and the temperature is controlled by a Peltier device in order to implement the automatic wavelength adjustment functionality. The temperature is changed in 1 degree steps by means of an 8 positions switch that acts over the Peltier device through a control circuit. Thus for each position of the switch the wavelength is changed by 0.1nm

Finally, the optical section is composed by a low-cost DFB laser (FLD150F2BP), whose frequency response in figure 5.10 (right) shows a modulation BW of up to 6 GHz. The DFB laser biasing current was fixed at 40mA through a current control circuit to set the optical carrier power at 0dBm, and was directly modulated to produce the optical transmitted signal. The fiber connectorized laser output is then connected to the ONU output optical fiber.

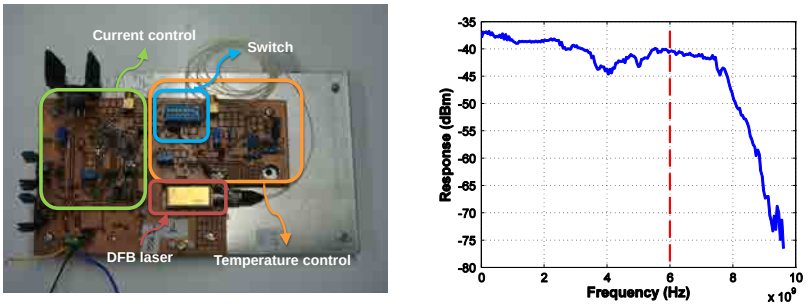

Figure 5.10: ONU circuit layout with temperature and current control circuits for wavelength tuning (left) and frequency response of the ONU laser (FLD150F2BP) (right).

The ONU electrical and optical sections are integrated in a board whose input is connected to the off-line processing AWG. Figure 5.10 (left) depicts the setup of the designed ONU with temperature and current wavelength control circuits. A compact unit containing a pair of ONUs boards was assembled in a case occupying a standard rack unit and it was used for the experiments of the following sections. Figure 5.11 shows a picture taken at the UPC labs.

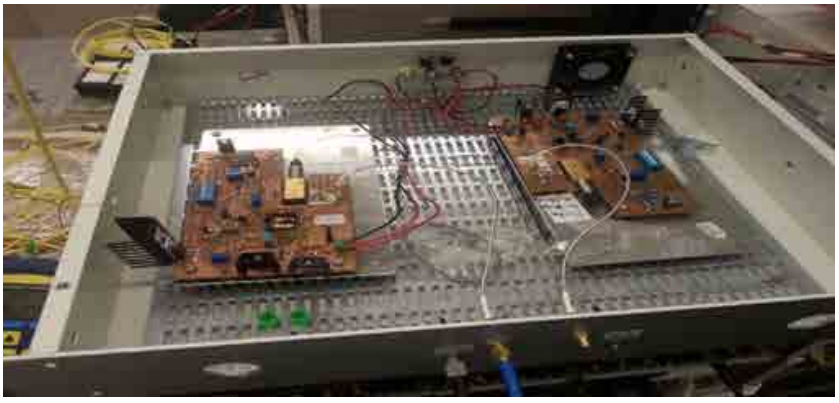

Figure 5.11: Rack-unit containing the ONUs.

In order to test the λ-tuning ability of the temperature control circuit we measured the optical spectra at the output of the ONU for different positions of the temperature control switch. Figure 5.12 illustrates the process of bringing together the ONUs carrier wavelengths up to the point where OBI starts

to degrade the detection for the 6.25GHz US signal. See the next section for a detailed description of the experiment. As seen, initially, ONU_1 and ONU_2 emitted at 1554.7nm and 1554.2nm respectively. In order to improve the optical spectrum efficiency, ONU_2 was tuned to displace its emission λ rapidly by 0.4nm with 0.1nm steps to 1554.6nm where the RX quality was maintained [118].

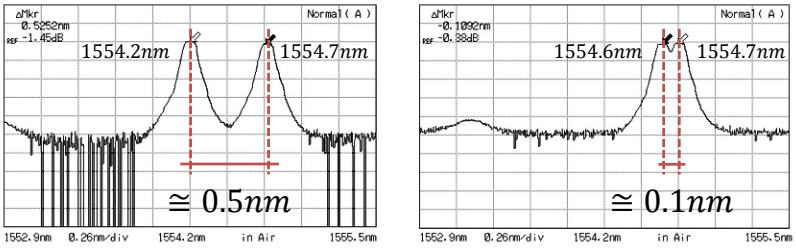

Figure 5.12: Optical spectra of the US signal initially (left) and after moving the lambda-tuning switch of the temperature controller circuit of ONU_2 board by 4 positions (right).

5.4 Differential link-loss compensation

A system requirement demanded by operators for future PONs is the ability to reuse the existing fiber architectures [127]. One way is to ensure the OLT RX has sufficient dynamic range to handle the differential losses caused by users spread around the central office. Thus, in this section, the US S-OFDMA-PON architecture previously proposed and implemented, and shown in figure 5.6 is studied to investigate the potential of EBA and bit-loading strategies in order to increase the differential loss margin for acceptable BER in the OLT RX.

As it is well-known, in an OFDM-PON, the launched power of a TX is uniformly distributed among the SCs assigned to each user. Thus, considering the same power launched, the lower the number of active SCs, the higher the power into each one and the distance between the ONU and the ODN or OLT can be higher. This is the basic idea behind differential link-loss compensation through EBA schemes. Considering a couple of ONUs with a different distance to the ODN, a higher number of SCs may be addressed to the closer ONU and the rest to the farthest one in order to compensate the losses due to the difference in fiber length. The same happens with modulation format since the lower the modulation format the lower the required sensitivity for a given quality threshold at the RX, so the higher the optical fiber length between the ONU and the ODN.

The experiments of this section were carried out with two identical ONUs boards as described in5.3.2, transmitting data simultaneously towards the OLT.

Figure 5.13 shows the basic setup. In order to emulate the activation process in the Statistical-PON with efficient optical BW occupation, the wavelength of ONU_1 was fixed at 1554.7nm while that of ONU_2 was tuned with the aid of the manual temperature controlling switch down to 1554.6nm. As concluded through the experiments of section 5.3.1 a frequency spacing of 0.1nm is enough to avoid OBI.

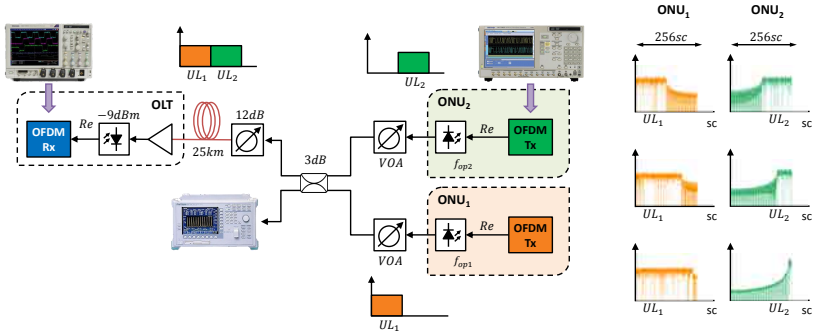

Figure 5.13: System setup schematics (left) and SCs allocation for each ONU (right).

For each ONU, 2^{18} bits were generated randomly and mapped into QPSK modulation. In order to get a real signal the QPSK symbols were accommodated to have HS. From the total 256 SCs ONU_1 placed its data into the first 128 and set to zero the rest for them to be occupied by the data of ONU_2 whose first 128 SCs were set to zero, see the insets of figure5.13. The OFDM signals were loaded into an AWG which produced samples at 5GSa/s with 8 bits resolution into two separate channels. No CP was added since for the fiber lengths considered no significant CD was generated. Each output signal was then injected into each of the ONU boards to directly modulate their DFB laser, whose carrier power was fixed to 0dBm with the aid of the current control circuit. A Variable Optical Attenuator (VOA) is connected at the output of each ONU board. Both optical signals were then joined by a 50/50 coupler (3dB) and the complete OFDM US signal passed through a 12dB optical attenuation stage for emulating a total PON splitting ratio of 16. The signal then travelled through a 25km of SMF with an attenuation of 0.2dB/km. Right after, it was detected by a single 10GHz PIN preceded by an EDFA which kept the input optical power to the PD at -9dBm. The signal was then sampled with a 50GHz RTO which also processed the data immediately after sampling. Data from both ONUs were carefully synchronized by means of a variable electrical delay line at the output of ONU_2 to allow simultaneous processing at the OLT with a 256-FFT. Finally the BER for each ONU was computed.

As a previous step, the P2P scenario was explored. Figure 5.14 shows results of BER against sensitivity.

Figure 5.14 gives insight into the decrease in sensitivity expected from increasing the active SCs when the total launched power is kept fixed. As seen,

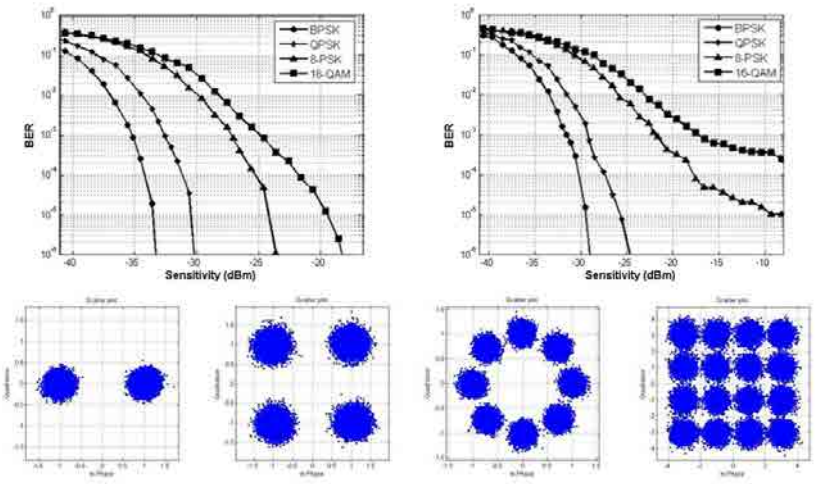

Figure 5.14: BER against RX optical power for a P2P scenario and BPSK, QPSK, 8-PSK and 16-QAM with 128 (left) and 256 (right) SCs. The constellations are given for 128 SCs and BER of 10^{-5}.

whatever the number of SCs, the penalty for upgrading from BPSK is 3dB for QPSK, 5dB for 8PSK and 7dB for 16QAM. This power difference can be employed to allow users which are closer to the OLT to TX with higher level modulation formats than farther ONUs.

In a first experiment, each ONU had half of the total SCs. The TX optical power was measured just after the VOAs and was adjusted to be equal for both ONUs. Then, the TX optical power of ONU_2 was lowered in 0.5dB steps while keeping constant the ONU_1 power at 0dBm and the same procedure was carried out with ONU_1 keeping ONU_2 optical power fixed. Notice that since a 3dB coupler is used to optical joint both ONUs after the VOAs, the overall OSNR is reduced by 3dB. Figure5.15, plots the average BER of ONU_1 and ONU_2 obtained against the difference in power measured as $\triangle P = P_{ONU_2} - P_{ONU_1}$ when SCs are symmetrically allocated in both, the VPI simulation (left) and the experimental (right).

Good agreement is observed between the simulated and the experimental results with about 1.5dB dynamic range between ONUs for a threshold BER of 10^{-3} and QPSK. According to simulations, higher order modulations cannot reach the 10^{-3} BER threshold for both ONUs simultaneously while a broader dynamic margin (DM) of about 8dB is achieved for BPSK. Furthermore, since the SCs are symmetrically allocated the behavior of both ONUs is almost the same, symmetrically and mirrored from a point which is a little bit higher than $\Delta P = 0dB$, meaning that ONU_2 requires a little more power than ONU_1 to show the same behavior because of distortions affecting the higher frequency part of the spectrum where ONU_2 is located.

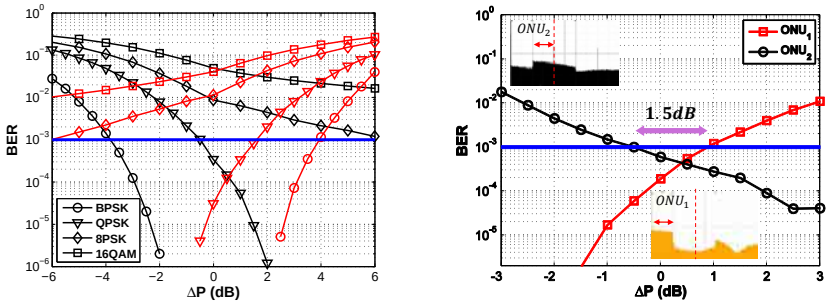

Figure 5.15: BER against differential RX power between ONUs for 50%-50% BW allocation. Left: VPI simulation with BPSK, QPSK, 8PSK and 16QAM; Right: laboratory with QPSK. The orange and black insets correspond with the received electrical spectrum at the oscilloscope of ONU_1 and ONU_2 respectively [121].

To extend the dynamic margin ensuring the proper detection of both ONUs, EBA techniques were considered to asymmetrically allocate the SCs to the ONUs. Specifically, SCs of ONU_2 were added to ONU_1 in order to decrease the effective BW of the higher frequency ONU and thereby increase its OSNR. Figure 5.16 shows the experimental results obtained when ONU_2 has 25%, 12.5%, 6.25% and 3.125% of the total BW

As the SCs sharing of ONU_2 is reduced (from a) to d)), for the same fixed total power, the power per SC increases and the BER is reduced. In the graphs it is shown that as the ONU_2 SC sharing goes from 25%, to 12.5%, to 6.25% and to 3.125% the 10^{-3} BER threshold is achieved respectively with 3, 6, 8 and 12 dB less total power in ONU_2 as compared to the total power in ONU_1 which is kept fixed at 0dBm. As for the curves of ONU_1, since the power per SC is reduced as its SC sharing increases (from a) to b)) it is seen that it becomes more vulnerable to the interference of the tails of ONU_2 so that in order to reach the 10^{-3} BER threshold, a lower power in ONU_2 is tolerated going from $\Delta P = 0dB$, to almost $\Delta P = -3dB$. The impact of the power reduction over the BER in ONU_1 is not very pronounced because the percentage of SC affected by the tails of ONU_2 over the total is reduced as the ONU_1 SC sharing increases.

Figure 5.17 is summary graphic with the RX dynamic range (ΔP) against the percentage BW occupied by each ONU. The tolerable differential link-loss between the ONUs raises from 1.5dB to 11.4dB when the relative BW of the highest frequency ONU (ONU_2 in this case) varies from 50% to 1.6%. This allows to properly detecting ONUs within differential distances of 7.5km up to 57km or considering ONUs at the same distance with an additional splitting ratio of 1:8.

Figure 5.17 shows the possibility to use EBA to manage different link-loss present in a PON for a QPSK modulation format in both ONUs. Recalling the simulation results showing a critical dependence of the power margin on the modulation format (figure 5.15 and 5.16) in the next experiment we considered

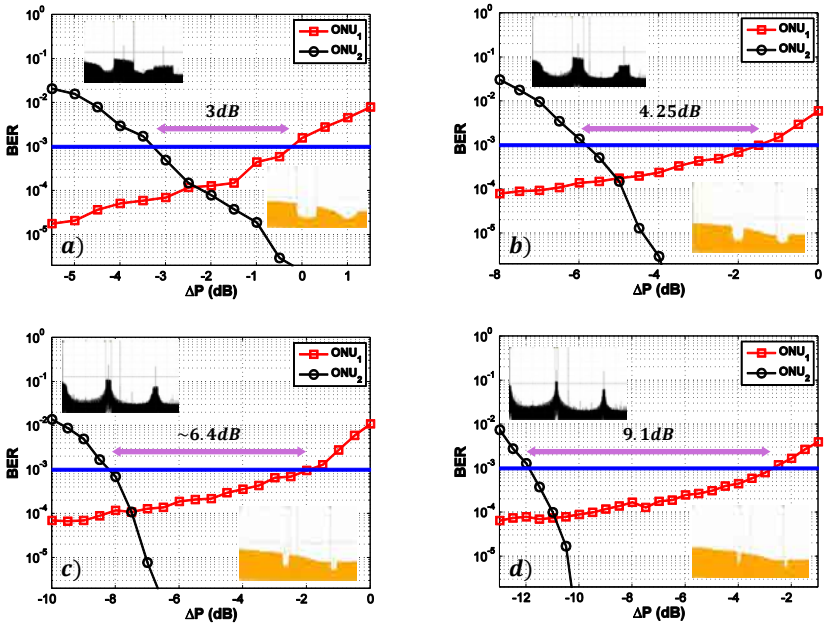

Figure 5.16: BER against differential RX power between ONUs for 75%-25% (a), 85.5%-12.5% (b), 93.75%-6.25% (c) and 96.875%-3.125% (d) BW allocation. The orange and black insets correspond with the electrical spectra at the RX oscilloscope of ONU_1 and ONU_2 respectively [122].

different combinations of modulation formats into each ONU. In figure 5.18 (left), the ONU_2 modulation format was changed from BPSK to 16QAM while the ONU_1 format was kept fixed at BPSK (left) and at QPSK (right).

As expected, the dynamic range obtained is higher for lower modulation levels in ONU^2 at the expense of a lower effective BR with around 1-2 dB penalty for each modulation level increase in any of the ONUs.

Finally, figure 5.19 aims to evaluate and summarize the RX sensitivities results obtained in the experiments carried out in this section ensuring the FEC limit BER of 10^{-3} (level lines) as a function of both parameters studied, the modulation format and the BW of each ONU.

The lines in figure 5.19 can be used to allocate the active SCs and modulation format for each ONU according to the users' BW need and available power budget. As an example, fora 0dBm ONU power, 20dB ODN and two users at a differential distance of 30km translating into a differential link loss of 6dB, following the -26dBm curve in figure 5.19 it can be seen that a BW share of 80% and 20% for ONU_1 and ONU_2, correspondingly, modulated into QPSK may fulfill the requirements.

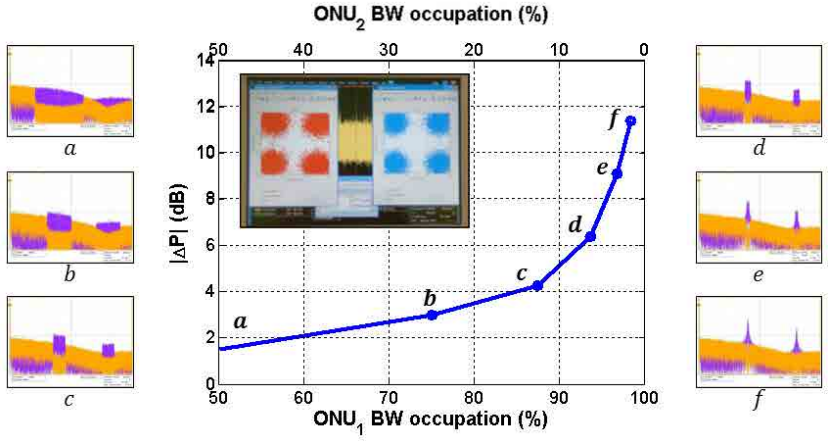

Figure 5.17: Differential power allowed between ONUs against the BW allocation for each ONU and their corresponding electrical spectra. The orange and purple insets correspond with the electrical spectra at the RX oscilloscope of ONU_1 and ONU_2 respectively [121, 122]. The inset corresponds with the resulting constellation of a QPSK transmission with 50%-50% for ONU_1 (blue) and ONU_2 (red).

5.5 Multiband S-OFDMA-PON

As mentioned in the introduction of the chapter, in current PON deployments, each ONU processes the complete signal BW even if the user employs only a small portion of it. Instead, the multiband OFDM approach proposed in this section reduces the energy requirements and the total cost of the network by allowing each ONU to process only the data assigned to it. Thus, in this section both directions of the S-OFDMA-PON are experimentally analyzed for both, digital and multiband multiplexing approaches in order to compare their performances.

5.5.1 Experimental setups

Two experimental setups are described in this section: the S-OFDMA-PON with multiband multiplexing, in figure 5.20, and with digital multiplexing, in figure 5.21. For the US direction, both of them employ the wavelength unable ONU transmitter boards described in section 5.3.

As seen, the main difference between both schemes is the inclusion of a RF stage in the PONs for the up/down-conversion of the BB US/DS data in the multiband multiplexing approach. The added hardware complexity is compensated by a reduction of the required DSP power since in multiband multiplexing each ONU just processes its own SC.

The multiband multiplexed US can be considered as an IM/DD (ID01) sce-

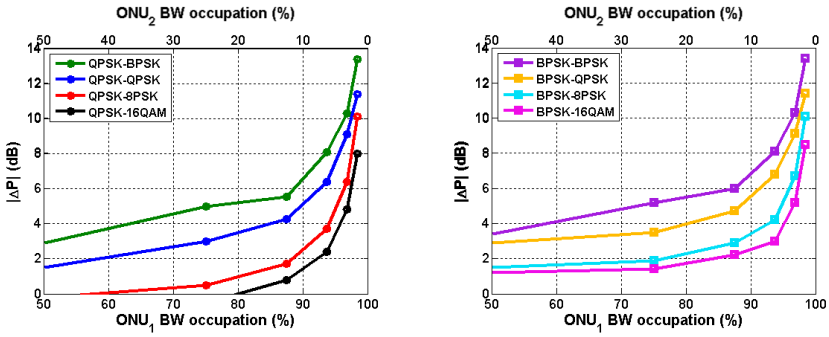

Figure 5.18: Differential power between ONUs at BER 10^{-3} against the BW allocation for ONU_1 modulation format of QPSK (left) and BPSK (right) for different ONU_2 modulation formats (first and second legend columns correspond with ONU_1 and ONU_2 modulation formats, correspondingly).

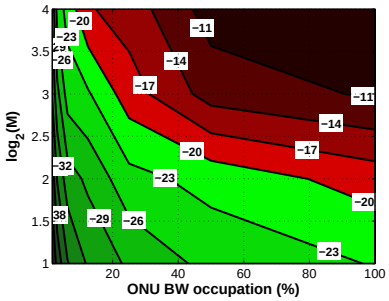

Figure 5.19: RX sensitivity at f 10^{-3} BER level lines (in dBm) as a function of modulation format and ONU BW occupation percentage (M: modulation bits). As a guideline, forbidden and allowed areas for a 0dBm ONU power and 20dB ODN are identified in red and green color respectively.

nario with RF-stages before directly modulating the signal by means a DFB laser in order to locate the ONUs band in their corresponding frequency slot. The HS constraint could be avoided if the up-conversion stage had included an additional mixing stage at 90^o to accommodate the imaginary part of the OFDM signal. In our case, the added hardware complexity was not justified for the intended tests. On its side, the digital multiplexing US can be considered as the same IM/DD (ID01) scenario without the abovementioned RF-stages, so the HS constraint cannot be avoided.

In the DS direction, the OLT TX randomly generates a total of 2^{19} bits. In order to get a real signal, the OFDM symbols were accommodated to have HS in a 256-iFFT. This FFT size was chosen because it is currently achievable in FPGA real-time processing [129]. No CP was added since for the fiber lengths considered no significant CD was generated. The first half of the SCs carried the information of ONU_1, whereas the second half of SCs was filled with the ONU_2

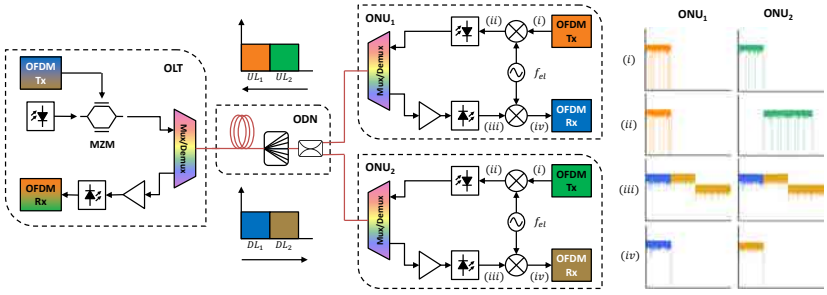

Figure 5.20: Experimental setup block diagram of the multiband S-OFDMA-PON with RF stages at ONUs(left) and representation of the data spectra in ONU_1 and ONU_2 (right).

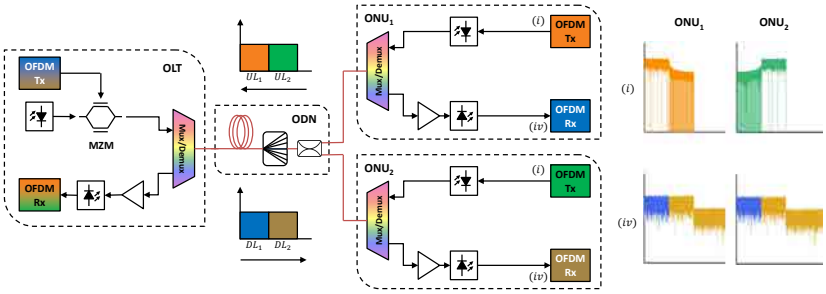

Figure 5.21: Experimental setup block diagram of the digital S-OFDMA-PON without RF stages at ONUs (left) and representation of the data spectra in ONU_1 and ONU_2 (right).

data. The OFDM signal was loaded into an AWG which produced samples at 5GSa/s with 8-bits resolution DAC in two separated channels. This entailed a maximum effective capacity of 1.25Gbps for each user with BPSK modulation and 2.5Gbps with QPSK, so that each user signal always had a data BW of 1.25GHz. The electrical output was amplified and modulated a DFB laser emitting at 1600.85nm through a MZM biased at QP with an insertion loss of almost 6dB. The resulting optical signal with a total power of 0dBm was sent to the ODN after a red/blue filter.

The ODN was the same than in the previous section, i.e. 25km of SMF adding a 5dB of attenuation at the TX, an optical attenuator of 12dB which simulated a splitter of 1:16 and a 50/50 optical coupler which added an extra attenuation of 3dB. Thus, the total loss of the ODN was 20dB.

At the ONU RX, after the red/blue filter, the isolated DS component was pre-amplified by a semiconductor optical amplifier (SOA) with 18dB gain and NF of 6.5dB and then detected by a PIN PD. An alternative to simplify the RX design with an APD without the SOA was also evaluated. Digital-to-analog conversion and demodulation were carried out by a 50GSa RTO. In the multi-

band case, owing to the RF down-conversion, demodulation with a 128-FFT size is used, while in the digital multiplexing case a 256-FFT is required.

In the US direction, each ONU randomly generated a total of 2^{18} bits in order to send the same total amount of data than in the DS. The data were mapped into either a BPSK or a QPSK modulation and the resulting symbols converted from serial to parallel in order to be modulated. In the multiband case, the modulation considered the relevant symbols only with a 128-FFT size, while in the digital case a 256-FFT size was used by padding with zeros the SC assigned to the other user. Comparing the spectra in figures 5.20(i) and 5.21(i), a higher noise level in the BW assigned to the other user is observed in the digital multiplexing case. The resulting symbols were accommodated to HS to get a real OFDM signal.

The optical output into each ONU was obtained by direct modulation of a 6GHz DFB laser with 1554.7nm and 1554.2nm wavelength respectively for ONU_1 and ONU_2. In the multiband multiplexing case, prior to optical modulation the BB signals were shifted to their corresponding frequency slot taking advantage of the aforementioned RF stages. The optical output was then adjusted to 0dBm, passed through a red/blue filter and joined a 3dB optical coupler with the contribution coming from the other ONU.

The OLT RX involved a single 10GHz PIN PD preceded by an EDFA which kept the input optical power to the PD at -9dBm. The signal was then sampled with a 50GSa/s RTO. Finally, the digital samples were demodulated with a 256-FFT, followed by a 1-tap equalizer whose coefficients were set by a known training sequence in the initial four OFDM symbols and the BER for each ONU US signal was computed.

Finally, in order to emulate the activation process in the S-OFDMA-PON limiting the OBI below a tolerable value, initially ONU_1 emitting at 1554.7nm was connected to the PON and afterwards ONU_2 emitting at 1554.2nm was turned on and was rapidly tuned through the manual switch to the closest wavelength to ONU_1 allowing correct detection, i.e. 1554.6nm. See figure 5.12.

5.5.2 Results

5.5.2.1 Downstream

We present here the results for DS of the multiband setup (figure 5.20). As a first test, both ONUs equally shared the available SCs. The electrical oscillator frequency of the RF mixer in ONU_2 (f_{IF2}) was set to 1.25GHz in order to displace the signal to BB; instead ONU_1 did not need any RF stage as it was assigned the lowest spectral band in the OFDM signal, which started at BB. Then each ONU only processed its own half of the SCs. Figure 5.22 plots the BER against the sensitivity for both ONUs with BPSK and QPSK modulation. As shown, at a FEC limit target BER of 10^{-3}, both ONUs detect the BPSK and QPSK signal at -25dBm and -20dBm respectively. The difference in the RX power between

both modulation formats could give the possibility to switch it according to the power budget available and BW demand of each user as discussed in previous sections. A small difference of about 0.5dB among the ONUs is observed mainly caused by small drifts in ONU_2 RF oscillator frequency. Also, the limited BW of the PD, the electrical components in RX and mainly the non-ideal filters could cause some distortion in the higher part of the spectrum.

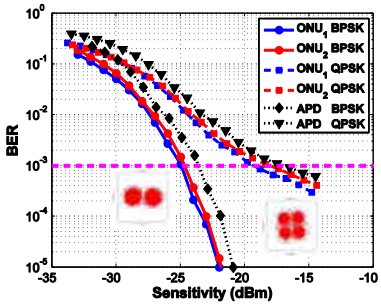

Figure 5.22: BER against sensitivity for the two ONUs equally sharing the total BW with BPSK and QPSK modulation in DS. The black lines correspond to the averaged curves of both ONUs with APD-based RX. The constellations are for BER of 10^{-3} in ONU_1 [123].

Since the ONU is a cost-sensitive element in the PON, the SOA and the PIN PD were replaced by a single APD (FRM5N143DS). Figure 5.22 includes the averaged performance graphs over both ONUs when employing the APD with BPSK and QPSK. There is a penalty of about 1.5dB for the APD RX for both modulation formats.

Given the penalty due to RF frequency drifts shown in figure 5.22, in a second set of experiments, a spectral Guard Interval (GI) with empty SCs was considered between the data spectrum of ONU_1 and ONU_2. Notice that both ONUs have the same amount of active SCs. We left f_{IF2} unchanged and discarded the unused SCs in each ONU after demodulation. The data BW percentage per ONU measured as the operative SCs divided by the total available, was thus, reduced. The BER results in figure 5.23 show sensitivity improvements at 10^{-3} BER of 1.7dB for BPSK and 4.6dB for QPSK with the SC reduction of 1.56%, and an improvement of 5.3dB and 9.7dB with a reduction of 25%.

Figure 5.24 plots the RX sensitivity at BER of 10^{-3} against data BW percentage for both ONUs modulated into BPSK and QPSK of the S-OFDMA-PON multiband multiplexing (left) and digital multiplexing (right) approaches.

The graph with the results of the multiband multiplexing approach, at the left side, shows how as the data BW percentage per ONU is decreased, the sensitivity improves about 3-4 dB for any 10% reduction in used BW. Consistent with previous observations yielding significant increases of performance by ZP only a small percentage of the SC closer to the other user BW, a sharp sensitivity increase is obtained for BW percentages higher than 45%.

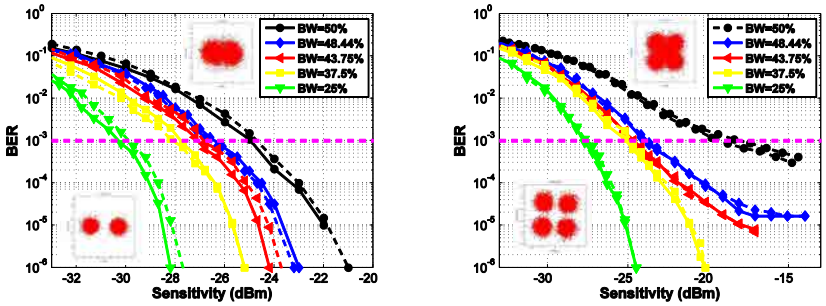

Figure 5.23: BER against sensitivity for multiband OFDM DS with BPSK (left) and QPSK (right) modulation formats for different data BW percentages. The solid and dotted lines correspond to ONU_1 and ONU_2 respectively. The insets show the constellations at a RX power of -27dBm for $BW = 50\%$ and $BW = 25\%$.

The results for the digital multiplexing approach plotted in figure 5.21show almost the same behavior of the sensitivity against the BW variation. Only a more pronounced effect of the non-ideal LPF giving rise to a sharp increase of sensitivity is observed $BW_{ONU} > 45\%$, with multiband multiplexing approach. Also noticed from figure 5.24, is the fact that ONU_2 had almost 1dB sensitivity penalty with respect to ONU_2 which can be attributed to small drifts in the electrical oscillator frequency.

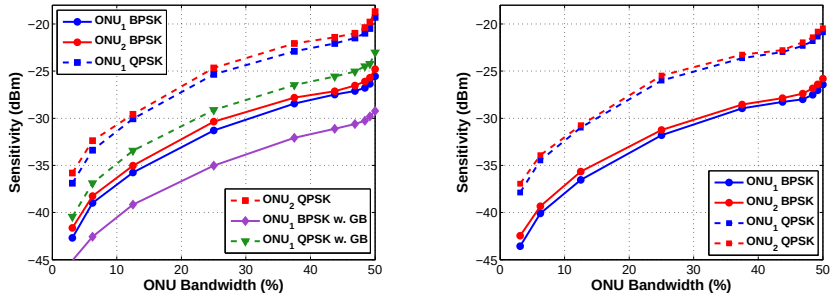

Figure 5.24: RX sensitivity at BER of 10^{-3}against effective data BW with BPSK and QPSK modulation formats with multiband multiplexing (left) and with digital multiplexing (right). The purple and green lines in the left graph correspond to ONU_1curves with GB [123].

For simplicity, the previous setups have not considered a spectral GB between the data band and the carrier. From our previous theoretical analysis we know that a GB of at least the same BW as the signal is required for either obtain an effective-AM modulation with an IM modulator or for avoiding IMD in IM/DD systems. In order to assess the improvement in performance that may be derived from use of a GB in figure5.24 (left) we have included results which consider a GB for ONU_1.

In our setup, the maximum oscillator frequency of the RF stages is 6GHz. For our 5GHz signal, this entails a maximum GB of 3.5GHz in the DS signal which is not enough to avoid IMD to spectrally overlap with the signal when it is DD. Thus, the GB test was carried out in P2P configuration with ONU_1 only. As seen, there is an improvement of nearly 4.5dB for both modulation formats. However, this enhancement comes at the expense of a wider BW requirement in the electrical hardware.

In order to determine the tolerance against small frequency drifts, in the next experiment the RF oscillator frequency was varied and the corresponding BER was processed. In addition, a time delay was also added at the ONUs output to measure its tolerance to synchronization drifts between the optical signals from each ONU. Figure5.25 shows the BER results for different frequency drifts and different time delays. It is seen that the drift and delay tolerances are limited to ±5kHz and around ±2ns.

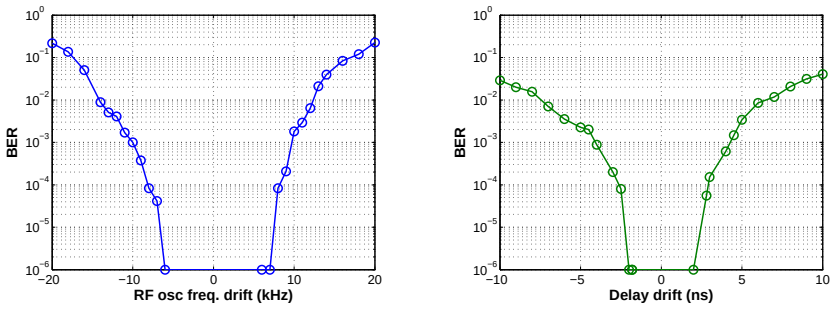

Figure 5.25: BER against RF oscillator drift (left) and time delay synchronization drift (right).

5.5.2.2 Upstream

We present now results for the US in the multiband multiplexing setup. As said, the emission wavelengths of DFBs laser were first adjusted to the minimum OBI-free distance of 0.1nm. Thus, ONU_1 and ONU_2 are located at 1554.7 and 1554.6 correspondingly, after tuning the ONU_2 optical source laser.

Since the ONUs' US spectra have to be accurately synchronized, identical electrical and optical paths between the 3dB optical coupler and the ONUs electrical TX generator need to be carefully adjusted. In a commercial network, the ONUs could be coordinated with the ranging protocol during the activation process. Figure 5.26 (left) plots the BER against the RX sensitivity computed at the OLT for both ONUs with both, BPSK and QPSK modulation.

Both ONUs were detected properly below the target BER of 10^{-3} at -24dBm and -18dBm for BPSK and QPSK respectively. However, there was a BER floor appearing in the QPSK signal close to BER of 10^{-3}. The same was observed for

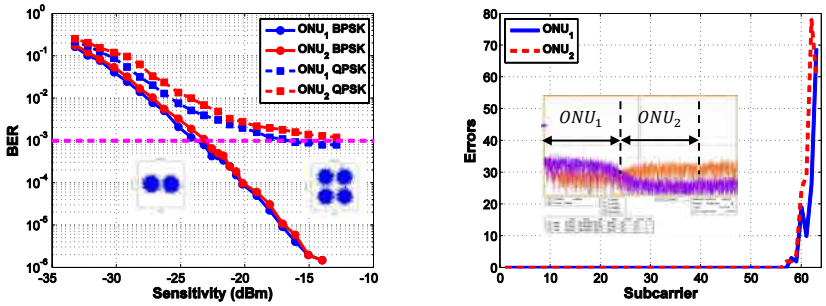

Figure 5.26: BER against sensitivity for both ONUs with BPSK and QPSK modulation. The constellations are for ONU_1 at BER of 10^{-3} (left) and total errors against SC number (right) [123].

the BPSK signal but the floor was below BER of 10^{-5}. This motivated to look for the errors in each SC. Figure 5.26 (right) shows the number of errors found into every SC for both ONUs. Interestingly, the errors occurred in the SCs closest to the other ONU part caused by a slight overlapping due to the spectrum tails (non-ideal filter response), as seen in the inset of figure 5.26 (right).

In order to improve the performance, a spectral GI was set between the ONU signals by tuning the electrical oscillator frequencies. Each ONU occupied 25% of the BW and both were spectrally together firstly. Then the ONU_2 spectrum was separated from that of ONU_1 by tuning the RF oscillator frequency (f_{IF2}). The OLT processed both the ONUs data spectra and the GI. The RX sensitivity for detecting both ONUs with a BER of 10^{-3} is plotted against the spectral GI in figure 5.27. As it can be checked, for a 3dB penalty, a 6.25% frequency GI is needed for QPSK and a moderate 1.56% for BPSK because of its lower SNR requirement. Therefore, in order to increase the modulation there is a penalty of a 4.7% GI. Specifically for the scenario proposed, 312.5MHz and 78MHz are needed for QPSK and BPSK respectively.

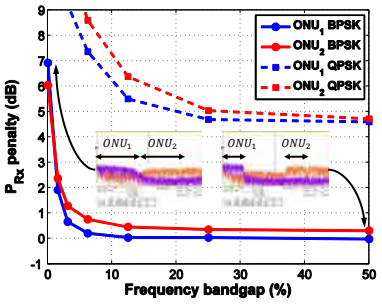

Figure 5.27: RX power for BER of 10^{-3} against frequency GI. The insets illustrate the increase of the frequency GI between the ONU contributions [123].

Right after checking that a GI between both ONUs improves the system

performance, EBA techniques were also evaluated in US. Thus, the BW occupied by each of the ONUs was lowered by ZP some of the SCs and the RF oscillator frequency for ONU_2 was kept fixed at 5GHz. As a result the spectral separation between the users was also increased improving the RX sensitivity at the cost of a less efficient use of the available DSP power. Figure5.28 shows the BER against the sensitivity for different data BW percentages per ONU for both BPSK and QPSK modulation formats. As in the DS scenario, significant improvements in sensitivity are obtained for a very small GI. The outcome can also be observed in clearer blue constellations. In this case, taking a BER of 10^{-3}, the improvement achieved between the BW of 50% and 48.44% is around 1.6dB and 5.5dB for BPSK and QPSK respectively, and up to 7.29dB and 11.05dB are obtained by reducing the SC down to 25%.

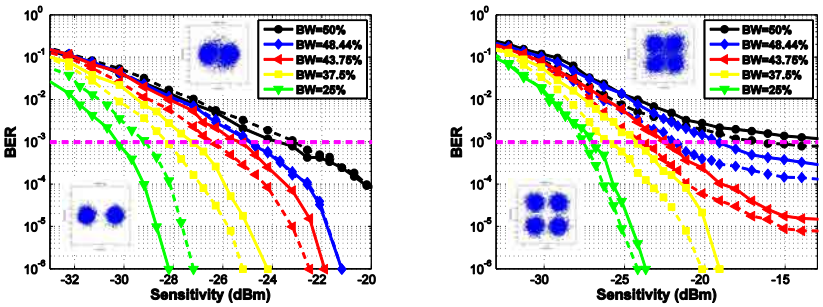

Figure 5.28: BER against sensitivity for multiband OFDM US with BPSK (left) and QPSK (right) modulation formats. The solid and dotted lines correspond to ONU_1 and ONU_2 respectively and the insets are the constellations obtained at a RX power of -27dBm for $BW = 50\%$ and $BW = 25\%$ [124].

Otherwise, as expected from figure 5.27 results, there were penalties for $BW_{ONU} > 45\%$ due to spectral overlapping in the neighboring user SCs (insets of figure 5.29 (left)). Due to the limited BW of the DFB lasers, a spectral GB was not tested in the US. However, a performance improvement is expected if a GB is left between the OFDM signals and the optical carriers provided that the frequency separation between the users is correspondingly increased to prevent OBI.

When increasing the ZP, besides enlarging the spectral GI, the total power is distributed into fewer SCs, increasing their SNR. Hence, clearer constellations and improved RX sensitivity were obtained yet at the price of a lower effective BR. The RX sensitivity when reducing the data BW percentage from 50% to 25% improves by 6dB for BPSK. Similar values were obtained for DS (figure 5.24 (left)). For QPSK, the RX sensitivity is as low as -24.5dBm with data BW percentage of 25%, almost 8dB better than with 50%. The performance was again slightly better for ONU_1 which operated in BB than for ONU_2 because of small drifts in f_{IF2} and the non-ideal filter response which caused some distortion in the higher part of the spectrum.

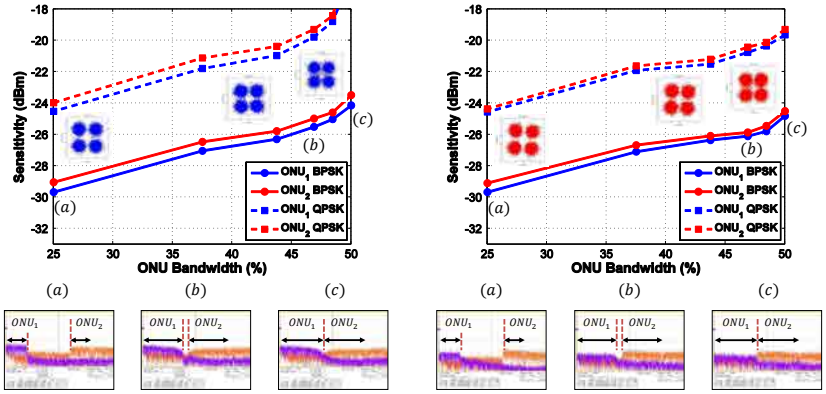

Figure 5.29: RX sensitivity at BER of 10^{-3} against effective data BW for both ONUs with BPSK and QPSK modulation formats with multiband multiplexing (left) and with digital multiplexing (right) [123].

For comparison, the same experiments were carried out with the digital multiplexing of users with BPSK, QPSK, and several ZP percentages. The RX sensitivity against data BW percentage measured at the OLT for each ONU is plotted in figure 5.29 (right). The results are almost 1dB better than the multiband OFDM due to the small drifts in the frequency oscillator. For $BW_{ONU} > 45\%$ the non-ideal electrical filters used in multiband OFDM to confine and limit the BW of each ONU did not remove the spectral tails completely producing overlapping between the US contributions. Thus in these cases the RX sensitivity of the digitally multiplexed ONUs is better by 2dB. However the multiband OFDM has the relevant advantage of lowering the ONU DSP complexity by reducing the FFT size through the help of an RF mixer. This translates directly into the power consumption, which is also lowered.

Chapter 6

Signal folding and auxiliary label techniques for PAPR reduction in oOFDM systems

As seen in previous chapters, OFDM systems are robust against linear channel distortions and channel selective frequency fadings, and have been the technology of choice in many communication standards. Challenges remain though, for example in relation to very large PAPR values which increase as the number of SCs does. High PAPR requires transceiver units with greater linearity, larger dynamic range, and high peak power management capabilities, thus increasing costs and power consumption [130]. In addition, in the optical case, a DC-bias offset needs to be added to the bipolar OFDM signal in order to make it unipolar.

In this chapter, two techniques are proposed in order to on the one hand, mitigate the impact of high PAPR on the signals with multiple carriers such as OFDM, and on the other improve the sensitivity of PONs based on conventional IM/DD (ID01) with bipolar signals by recovering the sample signs. Respectively, Data-Labeled OFDM (DL-OFDM) technique is based on folding the original OFDM signal to compress it between the values where the amplifiers and optical modulators are linear; while the Sign-Labeled OFDM (SL-OFDM) technique consists on sending the absolute value of the OFDM signal and a label that contains information about the sign of each sample.

The chapter begins by explaining the nature of the PAPR problem in MC optical systems, then the techniques and alternatives to mitigate it are discussed, and finally both algorithms, the DL-OFDM and the SL-OFDM are evaluated and experimentally tested into a PON.

6.1 Peak-to-Average Power Ratio basics

The PAPR of an OFDM signal is mathematically defined as:

$$PAPR = \frac{max\left[s(t) \cdot s^*(t)\right]}{E\left[s(t) \cdot s^*(t)\right]},\ t \in [0,\, T_s] \tag{6.1}$$

where $s(t)$ is the OFDM complex symbol signal. Assuming a worst case scenario with all the SCs adding in phase and a modulus 1 such as for instance for QPSK a maximum PAPR value is obtained as:

$$PAPR = \frac{max\left[\left|\sum_{k=1}^{N} 1\right|\right]}{E\left[\left|\sum_{k=1}^{N} 1\right|\right]} = \frac{N^2}{\frac{1}{2}N} = 2N \tag{6.2}$$

where N is the number of SCs. It can be seen that the PAPR value will depend on the number of SCs and the level of SNR that must be maintained [131]. In earlier investigations [132, 133] with OFDM modulation, it was shown that for N carriers the worst-case PAPR could be as large as N times the mean power of the signal. Furthermore, from (6.2) it can be deduced that the theoretical maximum of PAPR is $10log_{10}(2N)$ in dB.

However, taking into account that a very large PAPR value is a rare event, its behavior is characterized probabilistically through the complementary cumulative distribution function (CCDF) P_C, which is expressed as:

$$P_C = Pr\left\{PAPR > \vartheta_P\right\} \tag{6.3}$$

Namely, P_C is the probability that the PAPR value exceeds a particular value ϑ_P. Figure 6.1 shows the probability of a given PAPR value calculated by the above expression for different number of SCs.

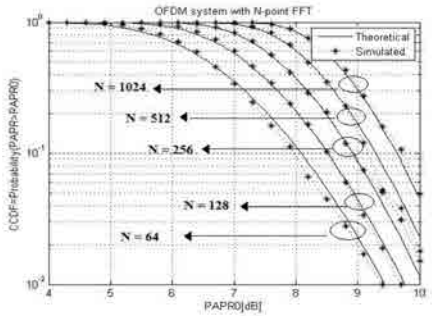

Figure 6.1: CCDF (P_C) for the PAPR of OFDM signals for different numbers of SCs [134].

6.2 PAPR reduction algorithms

The PAPR reduction algorithms proposed so far allow for trade-offs among basically three figures of merit of the OFDM signal: PAPR, BW efficiency, and computational complexity.

Techniques based on *clipping* [134–137] consist on saturating the digital signal before the optical amplifier in order to accommodate it at its dynamic range and avoid the effects of the saturation due to the amplifier. A filter is often used in order to reduce the Out-of-Band (OOB) components introduced by clipping. This filter causes peak-regrowth usually not that harmful that it counteracts the benefits. Basically for this kind of technique, a trade-off must be met between the signal distortion introduced by clipping and the advantages derived from a reduced PAPR value. Its main advantage is low complexity which in addition, does not grow with the number of carriers.

Techniques involving coding consist in modifying the coded signal so that high PAPR samples are avoided. Some level of redundancy is often required in order to communicate the signal modifications to the receiver end, with the side advantage of not introducing distortion to the signal. Nevertheless, the complexity then grows exponentially with the number of SCs and therefore, these kind of techniques are only suited for small number of SCs.

The *redundant coding* method classifies the overall possible symbols depending on the resulting PAPR and just the messages whose peak power are below a certain maximum allowed value will be valid. The rest of the messages are sent as equivalent low PAPR messages. Some redundancy bits indicate which symbols have been sent as equivalent low PAPR symbols. Many different strategies may be followed in order to select the correspondence with equivalent low PAPR symbols, and also the redundant bits coding [132, 138, 139]. In fact, the SL-OFDM and DL-OFDM methods proposed below can be casted within this category.

Another PAPR reduction technique based in coding is the *Selected Mapping* technique (SLM) [140–143] whose block diagram is depicted in figure 6.14 (left). A set of different phase sequences are generated and each one is multiplied by the data sequence prior to Inverse Discrete Fourier Transform (IDFT). The resulting frame with the lowest PAPR is sent through the channel and therefore, the amount of PAPR reduction depends on the number of phase sequences and their design. The phase sequence used is sent as side information.

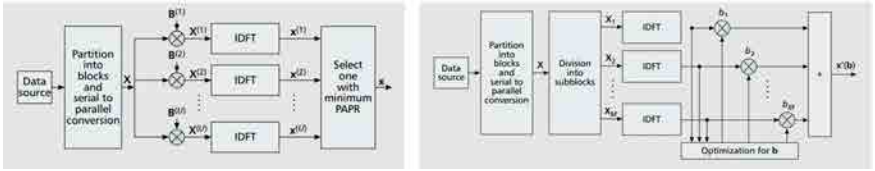

Figure 6.2: Block diagram of the SLM (left) and PTS [144] (right) techniques.

In the *Partial Transmit Sequence* (PTS) technique, depicted in figure 6.14 (right), an input data block of N symbols is partitioned into disjoint sub-blocks. Contrary of SLM, after the IDFT, each sub-block is combined with a set of phase factors in order to minimize the PAPR in the time domain [145]. The selection of the phase factors is limited to a set with a finite number of elements to reduce the complexity. The combination of phase factors which minimizes the PAPR has to be sent to the RX as side information in order to recover the original signal.

The *Interleaving* algorithm is also a coding-based technique where a set of interleavers is used to reduce the PAPR of the MC signal. An interleaver is a device that operates on a block of N symbols and reorders or permutes them. Both, TX and RX store the permutation indices in memory and the aim is to compare these permuted data blocks and choose the ones which have the lowest PAPR. The amount of PAPR reduction depends on the design and the number of interleavers used [146].

On its side, tone techniques are based on adding a data-block signal to the original MC signal to reduce its peaks. In the *Tone Reservation* (TR) method [147], the TX selects a subset of SCs which are not used to carry data, but serve as a means for PAPR reduction. The idea is that the data in these SCs is used to reduce the PAPR since, at the receiver, the data allocated in such SCs will be discarded and the rest of the signal decoded. On the other hand, the basic idea of *Tone Injection* (TI) techniques is to increase the constellation size so that each of the points in the original basic constellation can be mapped into several equivalent points in the expanded constellation [147,148]. Therefore, the extra degrees of freedom can be used for PAPR reduction. In figure 6.3, a constellation for 16QAM modulation with the equivalent representation of one original symbol is illustrated.

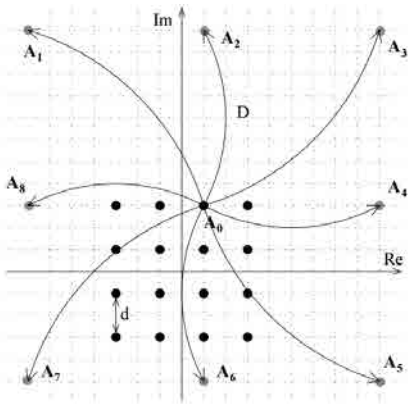

Figure 6.3: Generalized constellation for 16-QAM mapping. Each symbol has 9 equivalent representations [148].

Finally, *Adaptive Modulation* (AMOOFDM) of SCs (bit-loading) techniques may also be exploited for reducing the PAPR. These techniques are based on

manipulating the modulation format of individual SCs according to the frequency response of a given TX link. Furthermore, AMOOFDM decreases the probability of independently modulated SCs being added up coherently by the iFFT in a WDM-OFDM system [149].

Following, a table summarizes the properties of each of the PAPR reduction schemes discussed.

PAPR reduction techniques	Distortion	Power increase	Redundancy	Complexity
Clipping & filtering	✓			Low
Redundant coding			✓	Medium Increase with SCs
SLM			✓	High Increase with sub-block
PTS			✓	High Increase with sub-block
Interleaving			✓	Medium Increase with SCs
TR		✓	✓	Low
TI		✓		High complexity TX
AMOOFDM			✓	Medium
DL-OFDM			✓	Low

Table 6.1: Comparison of PAPR reduction techniques [144].

As aforementioned, this chapter proposes two algorithms: a generic one in order to reduce the penalty caused by large PAPR, the DL-OFDM; and a particularization used to eliminate the need of DC-bias and extending the dynamic range using the NP of MZM [150, 151]. Taking into account the section, these methods can be included into the techniques involving coding.

6.3 Data-Labeled OFDM algorithm

In connection with high PAPR effects, the basic idea of the DL-OFDM algorithm is to set a range in which the modulators and amplifiers are sufficiently linear in order to avoid signal distortion. Thus, the upper and lower limits are used as symmetry axes about which the signal is folded as many times as necessary in order to obtain a waveform whose values lie within such limits. In this algorithm, the signal is sent together with side information called Data Label (DL) in order to indicate the number of times the signal has been folded and the sign of the original TX sample.

6.3.1 Signal folding

6.3.1.1 Basic concept

The concept of folding can be defined as the substitution of the original signal in the points where the symmetry axes are exceeded by a symmetric replica with reference to the axes which is comprised between the limits. This concept can be understood from the MZM transfer function effect over the signal samples that exceed the limits.

Figure 6.4 shows the signal at the output of a MZM biased at QP and considering the overall DM of an input signal constrained within such DM at the left side, and an input signal exceeding those limits at the right side. The points where the input signal exceeds the limits have been highlighted by a red dashed circumference. Focusing on figure 6.4 (right), notice that the sample indicated in brown $(a - a')$ is not folded because it is allocated within the MZM DM; conversely, the input sample indicated in pink $(b - b')$ exceeds such DM and at the output it is folded against the upper DM limit.

The idea is to perform such folds in the pre-processing stage constraining the original signal within the MZM DM and send auxiliary information about how the original signal has been modified in order to reconstruct it at the RX. The difference when using this algorithm is that, the signal will be still distorted but we know how and thereby, this distortion can be compensated.

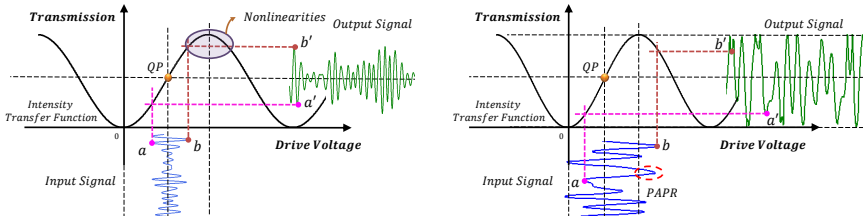

Figure 6.4: MZM output optical signal with low PAPR (right) and with high PAPR (left).

Notice that, for a DML, considering its transfer function depicted in figure 2.1 (left) the samples exceeding the lower DM limit are naturally trimmed or clipped. Nevertheless, this algorithm would be also available in such scenarios.

6.3.1.2 Coder and decoder

In the TX, a coder determines a set of limits which are used as axes (black, pink and green lines in figure 6.5(i)) around which the signal components are folded to keep the amplitude values within the linear region of the first period of the MZM transfer function (black lines (i)).

After folding the signal in (ii), the algorithm generates a DL with the in-

formation about the number of folds obtained through a reference table. The number of folds is an integer whose sign indicates if the fold is positive or negative, that is, if the original sample is either above or else below the 0 threshold. Figure 6.5(iii) shows a DL with five possible levels which mean two positive level folds, two negative level folds and a zero level to indicate that there is no folds. Finally the DL signal is allocated as side information as shown in figure 6.5(iv) to finally send to the RX. Notice that a zoom has been applied to (ii), (iii) and (iv) plots for a better comprehension. Meanwhile, in the RX there is a decoder where the full frame is detected and the DL separated from the data signal. Then, the signal and the DL are combined in order to recover the original signal.

In the next section several simulations will be presented in order to optimize the amplitude and the location of the DL within the signal, as well as the maximum number of folds and the MZM dynamic range.

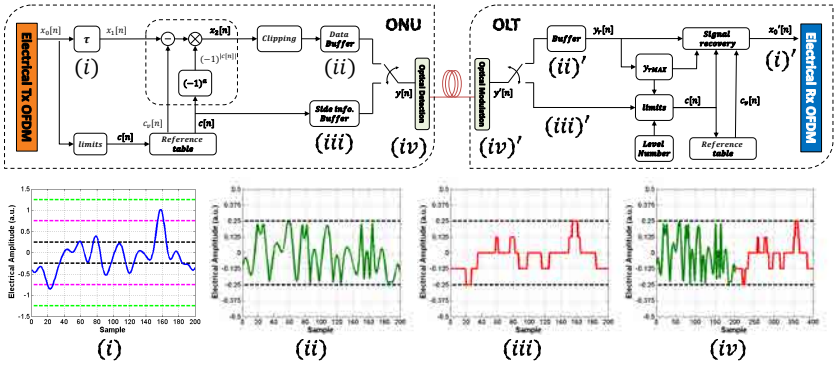

Figure 6.5: DL-OFDM algorithm block diagram with insets indicating the original OFDM signal (i), the signal folded (ii), the data-label signal (iii), and the DL-OFDM signal (iv).

Before going deep into the functions of the TX and RX, it is interesting to mathematically understand the concept of folding. Figure 6.6 graphically illustrates the folding of a signal exceeding below and above the limits of the DM (black dotted lines), which as seen, comprises amplitude values going from zero to $\Delta = 0.5$. The images are divided in several regions by dotted lines (blue and purple) which represent the number of folds needed by the samples within those margins in order to allocate them into the DM. Therefore, the maximum amplitude of the signal (in absolute value), will indicate the maximum number of folds that will be required to allocate the entire signal within the limits of the MZM, 3 folds in the case shown in figure 6.5. Let us first consider a negative (downwards) signal fold (from figure 6.6 (a) to (b)). As seen, all samples exceeding the DM upper limit are folded considering the upper DM limit as a mirror axis. Mathematically, in order to perform this fold, a change of sign is required firstly and $2\triangle$ offset needs to be added afterwards. The folded signal version with a negative fold (red) is then found as $y_1[n] = -x[n] + 2\Delta$, with $x[n]$

the original signal (blue). As seen in the figure, this folding operation allows the samples within the +1 folding level (between 1 and 1.5) to be re-allocated within the DM, whereas the rest of samples still lie outside the DM and therefore more folding operations are required for reallocating the whole within the DM limits. A second signal fold then needs to be applied, this time around the lower DM axis. Since this axis is precisely located at the zero amplitude value, the positive (upwards) folding operation just consists on a change of sign, and so, the folded signal version with two folds $y_2[n] = -y_1[n]$. seenIt is important to note that the folding operation only affects the samples outside the DM whereas the samples within the DM remain unchanged. After the 2nd fold operation now the samples within the +1 and the -1 levels of folding are properly re-allocated within the DM. Following the methodology, the subsequent negative folding operations will follow the same negative fold rule, i.e. $y_i[n] = -y_{i-1}[n] + 2\Delta$, while the positive folds will follow the sign change rule, i.e. $y_i[n] = -y_{i-1}[n]$ until the entire original signal is properly allocated within the limits stablished by the MZM DM.

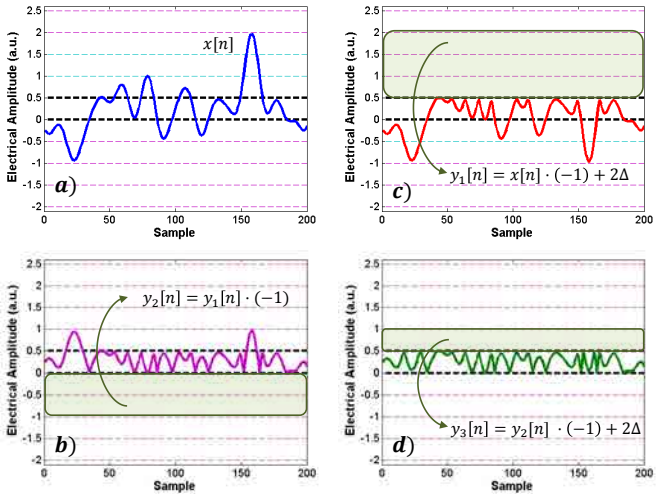

Figure 6.6: Graphical steps for the signal folding of a signal which requires 3 folds.

The process for obtaining the folded signal in figure 6.6 is then:

$$y_0[n] = x[n] \tag{6.4}$$

$$y_1[n] = -y_0[n] + 2\Delta = -x[n] + 2\Delta \tag{6.5}$$

$$y_2[n] = -y_1[n] = -\left(-x[n] + 2\Delta\right) = x[n] - 2\Delta \tag{6.6}$$

$$y_3[n] = -y_2[n] + 2\Delta = -\left(x[n] - 2\Delta\right) + 2\Delta = -x[n] + 4\Delta \tag{6.7}$$

This expressions and the explained process can be extrapolated for further number of folds as:

$$y_4[n] = -y_3[n] = -\left(-x[n] + 4\Delta\right) = x[n] - 4\Delta \tag{6.8}$$

$$y_5[n] = -y_4[n] + 2\Delta = -\left(x[n] - 4\Delta\right) + 2\Delta = -x[n] + 6\Delta \tag{6.9}$$

$$y_6[n] = -y_5[n] = -\left(-x[n] + 6\Delta\right) = x[n] - 6\Delta \tag{6.10}$$

$$\vdots$$

If now, we want to apply the folding operation on a sample-by-sample basis, we need to know how many folding operations need to be undergone by each sample. As seen, this is a function of the folding level on which every sample is originally located. Let $y[n, c]$ be the folded signal after the whole folding process with c the folding level in which the sample n is originally located. Taking into account the $c[n]$ value corresponding to each signal sample, and following the above reasoning, for even and odd folding levels respectively, one has:

$$y[n, c_{even}[n]] = (-1)^{|c[n]|} \cdot \left(x[n] - c[n] \cdot \Delta\right) \tag{6.11}$$

$$y[n, c_{odd}[n]] = (-1)^{|c[n]|} \cdot \left(x[n] - (c[n] + 1) \cdot \Delta\right) \tag{6.12}$$

These expressions can be combined in a single general equation depending on the evaluated sample n and its original folding level $c[n]$ as:

$$y[n, c[n]] = (-1)^{|c[n]|} \cdot \left(x[n] - \left(c[n] + sin^2\left(c[n] \cdot \frac{\pi}{2}\right)\right) \cdot \Delta\right) \tag{6.13}$$

For our algorithm and considering the number of folds which will be used (detailed in section 6.4.3.1), it is easier to use a reference table associating the DL values with the folding levels, as it will be explained below.

More in-depth, figure 6.7 shows the block diagram of the DL-OFDM coder at the TX. The original signal $x[n]$ is divided into two equal signals. The first signal suffers a delay generating the signal $x_1[n] = x_0[n - \tau]$ in order to synchronize it with the DL.

The second signal passes through the '*limits*' block where the DM of the

signal is stablished and taken as reference in order to divide the overall signal in levels/folds (pink dashed lines in figure 6.6). As observed such levels are multiples of the DM and $c[n]$ associates each sample with its corresponding folding level index. The level within the DM limits is associated with the index 0, therefore the upper levels are numerated from 1 upwards and the lower levels are numerated from -1 downwards.

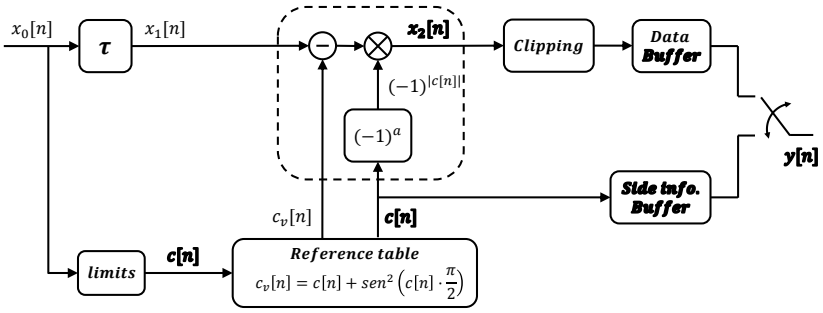

Figure 6.7: Block diagram of DL-OFDM coder. Dotted box corresponds with (6.15) expression.

The DL signal containing the folding level indices corresponding to each sample $c[n]$ is used to find the offset signal $c_v[n]$ as:

$$c_v[n] = c[n] + sin^2\left(c[n] \cdot \frac{\pi}{2}\right) \tag{6.14}$$

Analogous to expression (6.13), the folded signal $x_2[n]$ is obtained as:

$$x_2[n] = (-1)^{|c[n]|} \cdot (x_1[n] - c_v[n] \cdot \Delta) \tag{6.15}$$

Finally, considering that in this algorithm, the number of folds can be fixed, the signal $x_2[n]$ is sent to the clipping block where the samples exceeding such number of maxim folds allowed, are saturated or clipped, distorting then the signal. Right after, this signal is sent to a buffer. Signal $c[n]$, with number of folds, is also sent to another buffer in order to generate the side information DL signal and a switch toggles the folded data signal and the DL as illustrated in figure 6.5(iv).

Figure 6.8 illustrates a block diagram of the decoder at the RX. The RX signal $y'[n]$ is divided by a switch in two parts, one with the folded data signal and the other with the DL. The data signal is sent to the buffer $y_r[n]$, while the DL is sent to the '*limits*' block where together with the information about the maximum number of levels/folds allowed and the maximum value of the RX signal y_{rMAX}, determines the level where each sample was allocated at the TX original signal before applying the DL-OFDM algorithm.

The resulting $c[n]$ signal is sent to the '*signal recovery*' block and used to

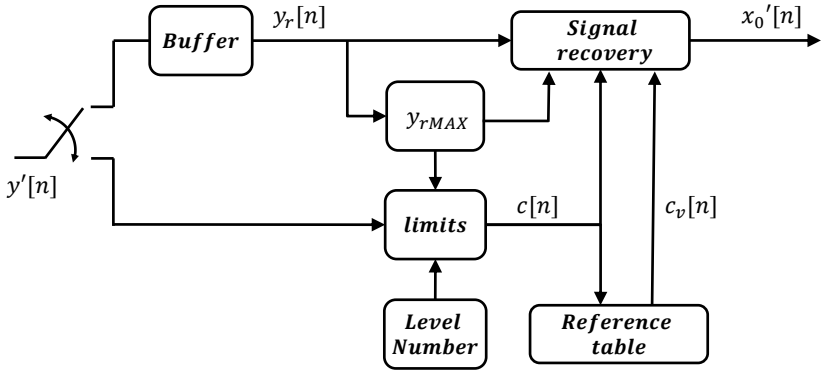

Figure 6.8: Block diagram of DL-OFDM decoder.

check the corresponding offset $c_v[n]$ in the same reference table used in the TX. Therefore, together with $c[n]$ and the received signal $y_r[n]$, they are used as the inputs of the signal recovery block where (6.16) is performed in order to acquire the original data TX ($x_0'[n]$). Notice that, in this case, the expression follows the inverse order than in the TX meaning that the signal is being unfolded.

$$x_0'[n] = (-1)^{|c[n]|} \cdot y_r[n] + c_v[n] \cdot \Delta \tag{6.16}$$

In the following sections, the main features of the side information are studied and optimized. Next, the DL-OFDM algorithm performance is analyzed and compared with conventional OFDM (C-OFDM) systems experimentally and by VPI simulations of a P2P conventional IM/DD (ID01) scenario; and finally, both algorithms are applied in the S-OFDM-PON described in chapter 5 in order to evaluate the improvements provided by this novel algorithm into a PON.

6.3.2 Side information coding

As said, the basic idea of this proposal is to send side information together with the data in order to reconstruct the received folded signal. Nevertheless, considering that the SL is added after the iFFT, if each sample has its equivalent SL, it is clearly concluded that its BW efficiency will be halved, i.e. the BR has to be doubled to maintain it, whatever the modulation format.

Two important choices to make for the side information design are: the amplitude of the side information and where to allocate it within the TX data signal. As about the first matter, it is instructive to have a look into a typical sample value distribution.

Figure 6.9 shows the folded data distribution for a 128-iFFT signal modulated into QPSK for MI of 1.2, 2 and 3 corresponding with PAPRs of 8.1dB, 10.2dB and 11.4dB. In order to balance the amplitude of DL with the ampli-

tudes of the signal, we consider the maximum amplitude in which 90% of the signal samples were concentrated. From figure 6.9, it is clearly seen that, the higher the PAPR, the higher the probability of the maximum amplitude values because of the signal folding. It is then practical to set the DL amplitude equal to the maximum amplitude of the signal after folded (100%).

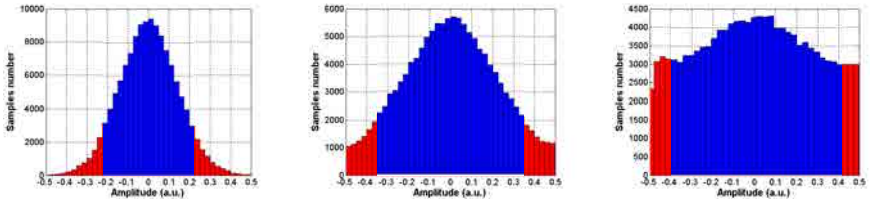

Figure 6.9: Samples values densities as a function of the electrical amplitude of the folded OFDM signal with 2 folds allowed for QPSK with 128-FFT and PAPRs of 8.1dB, 10.2dB and 11.4dB from left to right. The blue zone corresponds to the 90% of the samples.

About the second matter, we considered four different strategies: allocating the whole DL sequence at the beginning (a) or at the end (b) of the OFDM time domain signal, allocating the DL sequence interleaved within the same OFDM frame (c), and time-interleaved (d). In order to better understand this proposals, figure 6.10 shows where is allocated the DL sequence within the matrix $FFT \times T_{OFDM}$ from figure 2.9 (latex). Thus, firstly the FFT is applied over the overall data signal and therefore as it needs the same amount of DL than the data, the red slots in figure 6.10 are leaved empty to allocate the DL sequence afterwards.

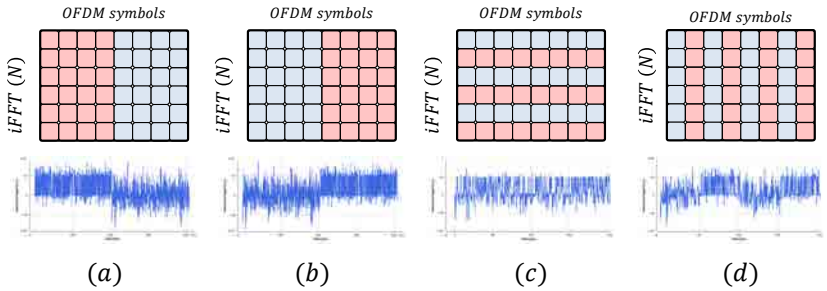

Figure 6.10: $FFT \times T_{OFDM}$ symbols matrix with the four DL sequence allocation strategies proposed for the DL-OFDM algorithm design: DL set at the beginning (a) and at the ending (b) of the TX data signal and DL set interleaved within the same OFDM frame (c) and time-interleaved (d).

6.3.3 DL-OFDM applications to P2P

6.3.3.1 Simulation setup and results

A VPI simulation of an ID01 scenario was performed with a total of 2^{17} bits randomly generated and mapped with both, BPSK and QPSK. The symbols were converted from serial to parallel and were then modulated with 128-iFFT. In order to get a real-valued signal necessary for IM, the iFFT input data was arranged with HS. The electrical BW was set to 2.5GHz. The generated electrical OFDM signal was amplified to obtain different values of MI to intentionally produce high values of PAPR, which in turn were compensated with the DL-OFDM algorithm. Specifically, a MI of 1 is associated with the 100% of the MZM dynamic range usage considering its field response. Afterwards, it was modulated with a laser linewidth of 1MHz by means of a MZM biased at $V_{\pi/4}$ (QP).. The launched power was 0dBm to avoid nonlinearities.

The ODN entailed 25km of optical fiber. The optical signal RX is DD with a single PD, LPF to avoid the alias at high frequencies, decoded with a decoder based on DL-OFDM, equalized with 1-tap equalizer and finally the BER is computed.

In a first experiment, we tested the best option for allocation of the side information. For this experiment, a maxim of 2 folds was allowed (one positive and one negative) and a MZM dynamic margin of 100% was used.

Figure 6.11 plots the sensitivity penalty results for BER of 10^{-3} against the PAPR level for the four proposals. The sensitivity penalty is seen to decrease as the PAPR increases up to a maximum PAPR value which as shown is 13dB. Very small differences in sensitivity are observed between the fourth methods, with time-interleaved DL presenting slightly better results, and constituting the choice in future DL-OFDM studies.

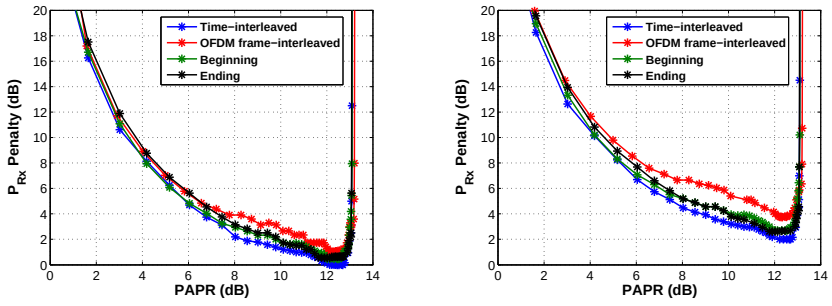

Figure 6.11: Sensitivity penalty at a BER of 10^{-3} against PAPR for four DL sequence distribution proposals on a BPSK (left) and QPSK (right) signal with an electrical BW of 2.5GHz and 128-iFFT. The MZM dynamic range is 100% and the 2 folds were allowed. The sensitivity reference is -38dBm.

For the second experiment, the same scenario was used in order to optimize

the MZM dynamic margin as well as the number of folds. Furthermore, the C-OFDM where DL-algorithm is not applied is plotted to compare it with the results obtained with the DL-OFDM cases.

Figure 6.12 shows the sensitivity penalty results for a BER of 10^{-3} against the PAPR level for different percentage of DM of the MZM with 2 folds, and different number of folds with a DM of 100%. The results follow the same behavior than figure 6.11. In the case of C-OFDM, it is also seen that the sensitivity penalty decreases as the PAPR increases, but just up to a maximum PAPR value of 7dB, 6dB below that for the DL-OFDM case. Thus, a first conclusion is the DL-OFDM is robust against higher PAPR values than C-OFDM. In fact, in all of the cases simulated, better sensitivity results are obtained for the DL-OFDM algorithm for similar PAPR values. The improvement is very small when PAPR is low, because the signal amplitude is still in the range of the MZM so there is no need to further process the data.

From figure 6.12 (left) it is seen that the higher the MZM dynamic margin percentage, the higher the sensitivity with around 1dB penalty between 100% and 80%, and 3dB penalty between 100% and 50%. This is because, considering the same number of 2 folds, a higher amount of data signal is clipped.

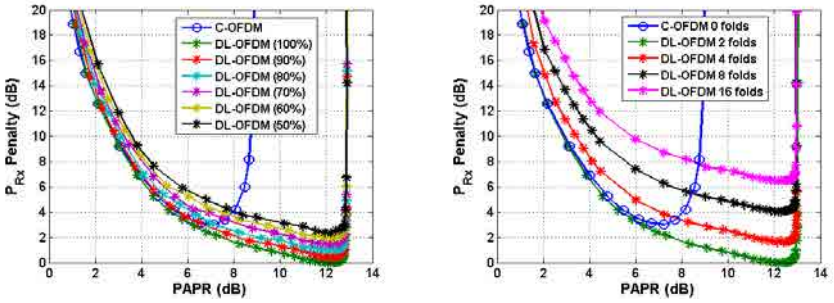

Figure 6.12: Sensitivity penalties against PAPR for C-OFDM (circles) and DL-OFDM (asterisks) with QPSK and 128-iFFT and an electrical BW of 2.5GHz for different MZM dynamic ranges and 2 folds (left) and for different number of folds and 100% DM. The sensitivity reference is -38dBm.

It is interesting to notice in figure 6.12 (right), that the penalty increases with the number of folds because a higher number of folds for a same DM means a higher complexity to detect each level at the RX for a proper signal unfolding.

It can be concluded that the best DL-OFDM performance is achieved with a MZM dynamic range of 100% and a maximum of 2 folds. These are the values which will be considered from now onwards. In addition, the sensitivity value improvement (achieved for PAPR of 12dB) over C-OFDM (achieved for PAPR of 6.5dB) is around 3dB.

Finally, a third experiment with VPI simulations was performed in order to compare both algorithms, C-OFDM and DL-OFDM considering different

electrical BW, modulation formats and PAPR values. Figure 6.13 plots the sensitivity penalty against the PAPR of a C-OFDM signal (circle) and DL-OFDM signal (asterisk) modulated into BPSK at the left side and QPSK at the right side with electrical BWs of 1.25GHz, 2.5GHz and 5GHz.

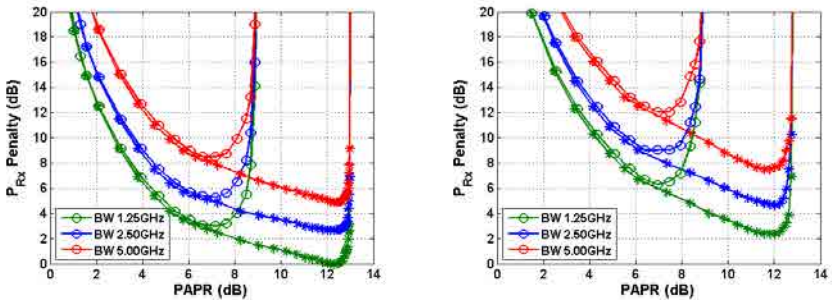

Figure 6.13: Sensitivity penalties against PAPR for C-OFDM (circle) and DL-OFDM (triangle) algorithms with BPSK (left) and QPSK (right), and 128-iFFT for electrical BWs of 1.25GHz, 2.5GHz and 5GHz. The DM was set to 100% and 2 folds were allowed. The circles and asterisks correspond with C-OFDM and DL-OFDM algorithms, respectively. The sensitivity reference is -38dBm..

As seen, the penalty for doubling the electrical BW or upgrading the modulation format is around 3dB for both algorithms. Furthermore, comparing a line with circles and a line with asterisks with the same color and graph, meaning the same electrical BW, the sensitivity penalty of C-OFDM as compared to DL-OFDM is 3dB for BPSK and around 4dB for QPSK. Thus the higher the modulation format, the higher the penalty. On the other hand, comparing the line with asterisks from figure 6.13 (right) with the line with circles from figure 6.13 (left) with the same color, meaning the same effective data BW, the penalty is 1dB or less. Notice that these comparisons take into account the corresponding optimal PAPR ranges because as seen, the C-OFDM algorithm cannot support signals with a PAPR beyond 8dB whereas the DL-OFDM system tolerates PAPRs as high as 13dB.

6.3.4 DL-OFDM applications to PON

In this section, we explore the potential applications of the DL-OFDM algorithm to access PONs. As it will be shown, the scenario and its features are based on the P2P scenario from section 6.3.3.

One of the characteristic features of the DL-OFDM algorithm is that it causes a widening of the electrical signal spectrum. This effect is not critical in DS, because once the DL information is stripped off the signal, the orthogonality is recovered, but when it is applied to the US, it produces a BW overlap between users that prevents correct joint OFDM detection of the complete US signal. In the following section, both directions are analyzed and it is demonstrated DL-

OFDM presents an improvement over the C-OFDM scenario for DS, whereas challenges still remain for a practical

6.3.4.1 Downstream S-OFDMA-PON scenario with DL-OFDM algorithm

In this section, a DS S-OFDMA-PON scenario with both, the DL-OFDM and C-OFDM algorithms is simulated and both systems compared. A block diagram of the S-OFDMA-PON with DL-OFDM algorithm is depicted in figure 6.14. In the OLT, the signal is mapped with BPSK and QPSK and modulated with 256-iFFT. Next, the DL is added to the signal following the time-interleaved scheme and input to the MZM biased in QP and fed with a laser of 1MHz linewidth. The optical signal is then sent through 25km of optical fiber. The signal in each ONU is down-converted to BB and recovered by means of the DL-OFDM algorithm to be finally decoded by the OFDM RX. Notice that the multiband multiplexing approach was used, so each ONU just processes a 128-iFFT. The rest of features and scenario characteristics are the same than in the P2P scenario.

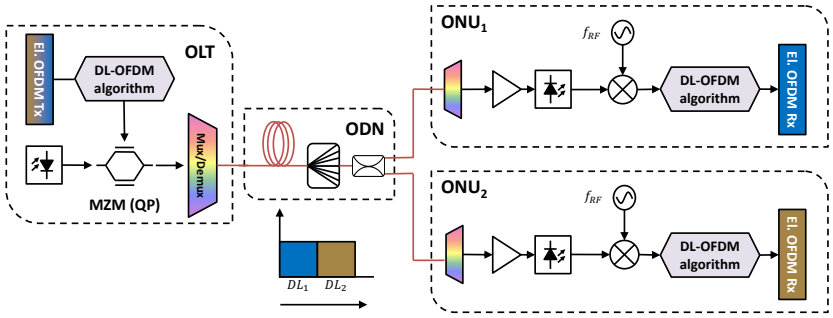

Figure 6.14: Block diagram of a downstream S-OFDMA-PON with DL-OFDM algorithm.

The curves in figure 6.15 confirm the same behavior than in the P2P scenario in figure 6.13. Again, the ability of the DL-OFDM algorithm to deal with higher PAPR values is demonstrated, 13dB vs 7.8dB with C-OFDM. For the respective maximum PAPR values, both systems feature a minimum sensitivity value whose value is 3 dB higher for C-OFDM in BPSK and up to 4 dB higher with QPSK. A penalty of 2-3dB is observed when increasing the modulation format from BPSK to QPSK with both algorithms, as well as when doubling the electrical BW. For a better view of figure 6.15, ONU_2 curves are not plotted, nevertheless the performance is slightly better for ONU_1 operating in BB than for ONU_2 because of the non-ideal filter response in the OLT RX which caused some distortion in the higher part of the spectrum.

Afterwards, in order to see the impact of spectral overlaps between the information of each user, the useful data BW of both ONUs was reduced by means

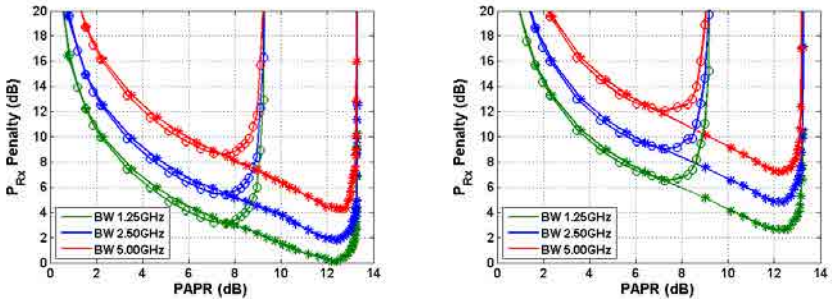

Figure 6.15: Sensitivity penalties against PAPR for ONUI comparing a C-OFDM (circle) and DL-OFDM (asterisk) with BPSK (left) and with QPSK (right). The sensitivity reference is -45.3dBm.

of ZP and the sensitivity was obtained for different PAPR values with a total electrical BW of 2.5GHz for BPSK and QPSK (figure 6.16).

Specifically, two PAPR values were chosen from figure 6.15, a PAPR of 1.40dB for both algorithms and the respective optimum PAPR values, 7.75dB and 12.2dB for C-OFDM and DL-OFDM. As expected, the lower the ONU BW, the higher the sensitivity with about 18dB penalty from the maximum 50% BW occupied down to only 5% for a PAPR of 1.40dB, and 12dB for both the PAPRs of 7.75dB and 12.5dB.

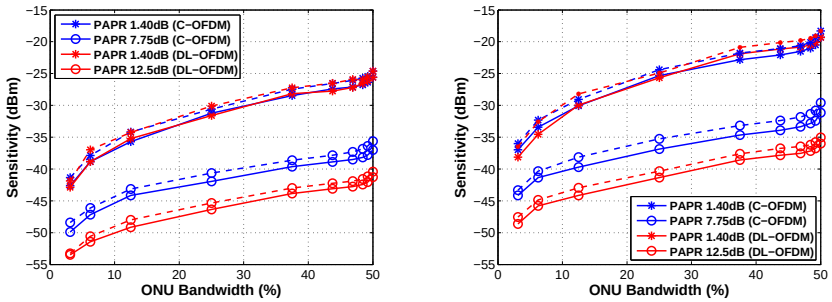

Figure 6.16: Sensitivity penalty against ONU BW for C-OFDM (blue) and SL-OFDM (red) with BPSK (left) and with QPSK (right). Continuous and dotted lines correspond to ONU_1 and ONU_2, respectively.

Furthermore, it is also noticed that the improvement between the best sensitivity value of SL-OFDM over C-OFDM is around 3dB and 4dB respectively for BPSK and QPSK, independent of the useful BW size.

6.3.4.2 Upstream S-OFDMA-PON scenario with DL-OFDM algorithm

This section aims to applying the DL-OFDM algorithm on the US direction of the S-OFDMA-PON through VPI simulations, and determining whether the increase in computational complexity and the reduction in effective data rate inherent to the DL-OFDM algorithm may be outweighed by the improvement on the sensitivity values and the increase in the tolerable PAPR.

As previously discussed, the addition of a DL into the signal after the iFFT causes the loss of orthogonality of the TX signal. In a P2P link or in a DS direction this is not critical since the orthogonality is recovered once the labels are discarded and the original signal reconstructed. However, this is not possible for the US signal due to spectral overlap between the multiplexed ONUs contributions. Figure 6.17 shows the spectra of both the C-OFDM signal with the ONUs signals perfectly orthogonal and kept within their respective BWs, and that of the DL-signal where the ONUs signals have lost orthogonality and are spread out of their assigned BW. In both, the roll-off factor for the square root raised cosine characteristic of antialiasing filters is set to 0.2.

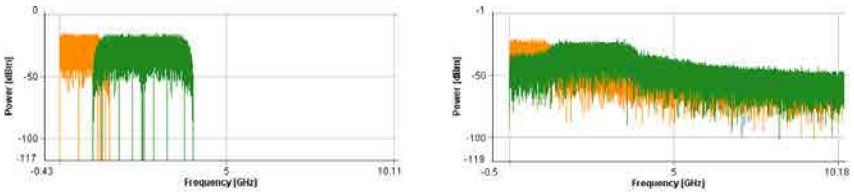

Figure 6.17: Electrical spectrum of both ONUs of a C-OFDM (left) and a DL-OFDM (right). Orange and green spectra correspond with ONU_1 and ONU_2, respectively.

Here we consider two ways of reducing the impact of this spectral overlap over the US signal: the analog and the digital ONUs spectral separation options. The former consists in increasing the local oscillator frequency of ONU_2, while the latter is to reduce the data BW by ZP some of the SC of both ONUs. As it will be seen, both strategies are applied in a US S-OFDMA-PON multiband approach. The downside of the first method is the decrease of the spectral efficiency and the requirement of higher frequency hardware (both local oscillator and OLT detector) although the data BW is kept whereas the downside of the second is the lower data BW although the spectral efficiency and the maximum operation frequency of hardware are maintained.

Figure 6.18 depicts the diagram block of the US S-OFDMA-PON multiband approach with a DL-OFDM algorithm, fixed RF up-conversion frequency in ONU_2 and digital spectral separation of ONUs. As seen in the insets, the overlapping between both ONUs due to the spectral widening is avoided by ZP the SCs closer to the adjacent ONU until both ONUs are properly detected.

Figure 6.19 depicts the diagram block of the same PON strategy but avoiding

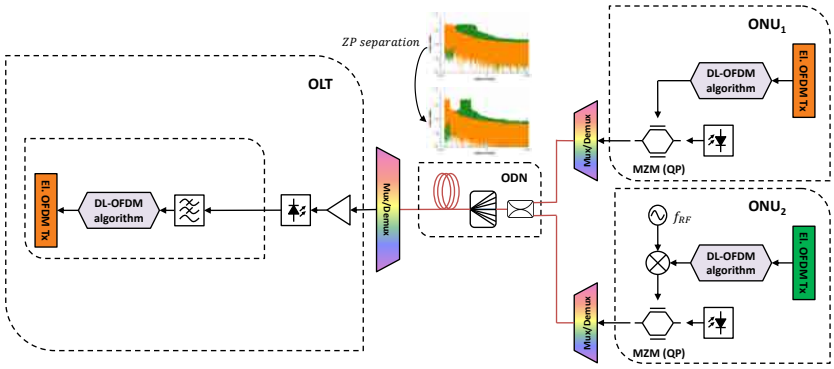

Figure 6.18: Block diagram of an US S-OFDMA-PON multiband approach with DL-OFDM algorithm with digital spectral separation of ONUs. Orange and green spectrum corresponds with ONU_1 and ONU_2, respectively.

the overlapping between both ONUs by a RF analog separation accomplished through the tuning of the frequency of the up-conversion stage in ONU_2. In this case, , two independent OFDM demodulation stages are needed at the OLT in order to down-convert both ONUs to BB, leading to a significant increase in the OLT complexity. The spectral efficiency is also reduced but the data transmission efficiency is higher as the DSPs power is fully exploited. In addition, notice an RF-stage is not needed for the ONU_1 modulation/demodulation since it is in BB.

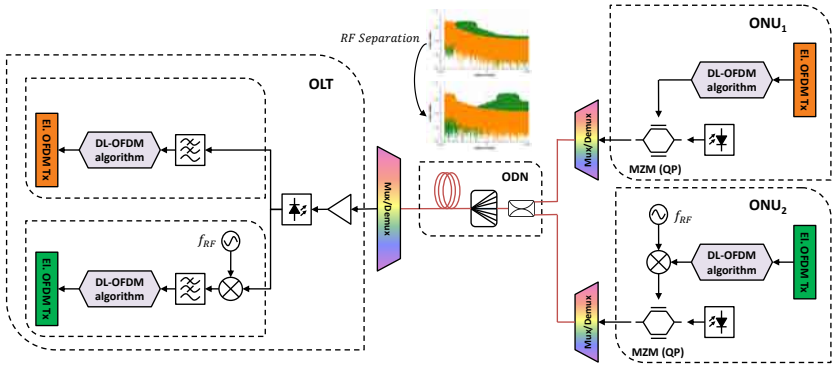

Figure 6.19: Block diagram of an US S-OFDMA-PON multiband approach with DL-OFDM algorithm with analog spectral separation of ONUs. Orange and green spectrum corresponds with ONU_1 and ONU_2, respectively.

Following, both strategies are analyzed and compared against C-OFDM. The tests were carried out with BPSK and QPSK modulation formats and total electrical BWs of 2.5GHz, i.e. 1.25GHz per ONU. As well as in the DS, the total FFT size was 256-point equally shared by both ONU. The rest of features are the same than in the DS scenario.

Firstly, following the digital separation of users approach corresponding to the diagram block of figure 6.19, the RF oscillator of ONU_2 was fixed to 2.5GHz while ONU_1 was left to BB and the effective data BW of each ONU was reduced by increasing the ZP for the DL-OFDM. The BER results of the B2B case in figure 6.20 (left) show that, the BER improves when lowering the percentage of used BW since the spectral separation between both ONUs is increased and the overlap reduced. Specifically, a percentage of unused spectrum of 12% and 20% is enough for BPSK and QPSK, respectively, in order to obtain a BER of 10^{-3}. In turn, these values are translated into a minimum gap between ONUs of 24% (15 SCs) and 40% (25 SCs) respectively for BPSK and QPSK.

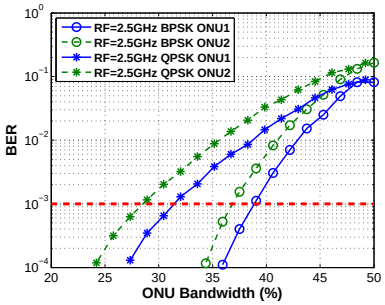

Figure 6.20: BER against effective data BW with DL-OFDM algorithm of each ONU for BPSK and QPSK with BW of 1.25GHz per ONU, RF LO of 2.5GHz in B2B for a PAPR of 12dB.

After that, these minimum percentage of padded SCs (12% for BPSK and 20% for QPSK) for RF frequency of 2.5GHz are used on the transmitted signals in US S-OFDMA-PON with digital separation of users to evaluate the sensitivity against the PAPR and compare it with results obtained with C-OFDM with no ZP. Figure6.21 plots the results obtained with BPSK at the left side and QPSK at the right side. Thus, the penalty between both algorithms and BPSK are 2dB and 3dB for ONU_1 and ONU_2 respectively, and with QPSK are around 3dB and 4dB also for ONU_1 and ONU_2, respectively

It is interesting to notice that the impact of the ONU's cues which overlap with the adjacent ONU increases with the PAPR level, as shown in figure 6.22. That leads to the conclusion that the ZP size depends on PAPR value and must be made wide enough in order to ensure the FEC limit BER of 10^{-3} in both ONUs is achieved for all PAPR values, or at least the most probable ones.

In the next round of tests we consider the setup in figure 6.18 with the analog separation of users. As abovementioned, the idea is to avoid the ZP by increasing the LO frequency of ONU_2. Notice that, the LO frequency in the OLT also has to increase for the ONU_2 down-conversion to BB. Figure 6.23 plots the results of BER against the RF frequency shift for different PAPR values. In figure 6.23 (left) it can be checked that while for BPSK the BER is reduced as the spectral distance is increased with a minimum of 6GHz to ensures below

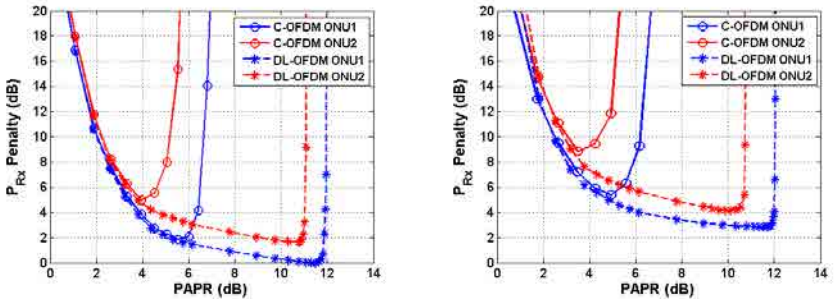

Figure 6.21: Sensitivity penalties against PAPR of C-OFDM and DL-OFDM with digital user separation for BPSK (left) and QPSK (right) with an ONU_2 local oscillator frequency of 2.5GHz and a total effective BW of 76% and 60% respectively. Continuous and dotted lines correspond to C-OFDM and DL-OFDM, respectively.

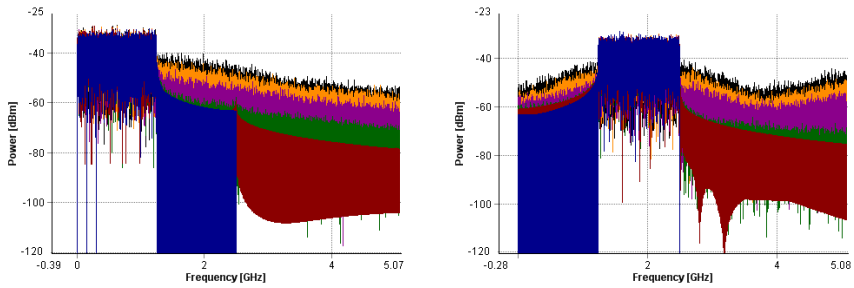

Figure 6.22: Electrical spectrum of ONU_1 (left) and ONU_2 (right) for different PAPR levels up to 12dB. The blue spectrum corresponds with the C-OFDM signal.

FEC BER for all PAPR used. For QPSK a BER floor is observed that increases with the PAPR, with a maximum tolerable PAPR of 9.54dB and a required spectral distance of 4GHz for a BER of 10^{-3}.

In view of the above results, considering a 6GHz spectral separation obtained with BPSK case with PAPR of 10.27dB plus a 25% safety margin, for the next experiment we fixed the RF frequency in ONU_2 to 7.5GHz. In addition, in order to obtain a proper detection, the minimum ZP required considering a LO of 7.5GHz and a PAPR of 12dB was obtained as in figure 6.20. In figure 6.24, it is seen a ZP gap of 30% of the electrical BW (19 SC) is required for a BER above 10^{-3} in the B2B case.

Figure 6.25 plots the results obtained for both ONUs with C-OFDM and DL-OFDM algorithms modulated with BPSK at the left side and QPSK at the right side. For the BPSK case only an analog spectral separation of 7.5GHz is applied (since it is enough as observed in figure 6.23) while for the QPSK both the 7.5GHz analog and a 19 SC digital spectral separation were used.

The results at the left-hand side of figure 6.25 show that the lowest sensitivity

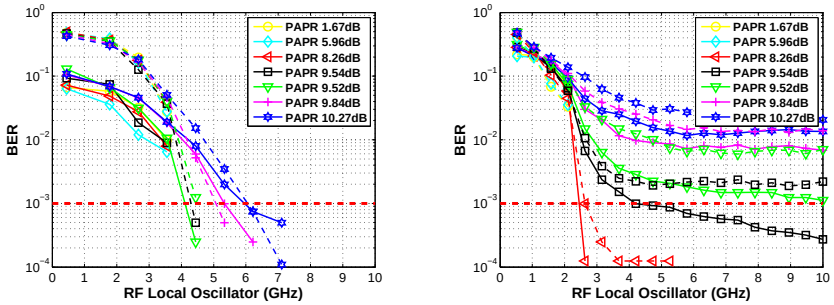

Figure 6.23: BER against local oscillator frequency of ONU_2 for DL-OFDM system with analog user separation modulated into BPSK (left) and QPSK (right) in B2B for different PAPR levels and both ONUs. Continuous and dotted lines correspond to ONU_1 and ONU_2, respectively.

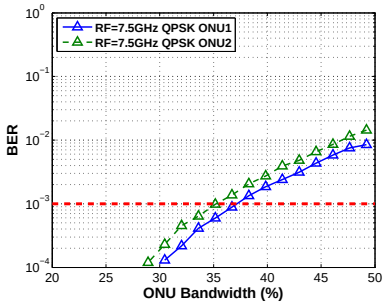

Figure 6.24: BER against effective data BW with DL-OFDM algorithm of each ONU for QPSK with RF local oscillator of 7.5GHz (right) in B2B for a PAPR of 12dB.

values for both DL-OFDM and C-OFDM are very close with DL-OFDM 1dB worse for ONU_1 and 1dB better for ONU_2. As in previous results, these lowest sensitivity values are reached with higher PAPR values when using DL-OFDM, with differences of 6dB for ONU_1 and 7dB for ONU_2.

Conversely, at the right-hand side when also ZP is added apart from the analog separation, the results are quite similar than in figure 6.21 showing a penalty of around 5dB for both ONUs between both C-OFDM and DL-OFDM algorithms, and again for higher PAPR values in DL-OFDM with differences on the order of 7dB.

Again, the conclusion is that the minimum spacing is a function of the PAPR because so is the height of the spectral tail causing the overlap between the ONUs data BW. In addition, this results show that, the digital separation by means of ZP is more efficient than the analog separation, but in any case, very wide spectral gaps would be required rendering the method inefficient and unpractical for a massive deployment.

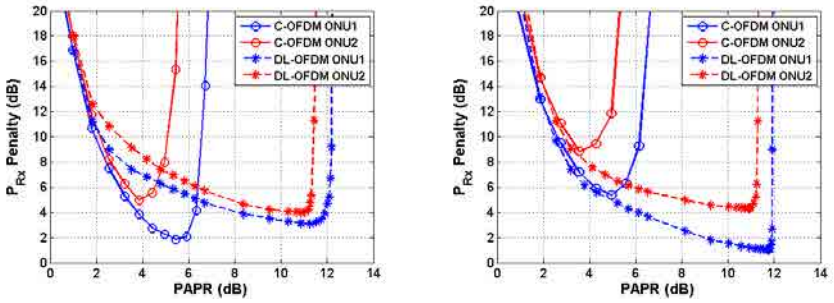

Figure 6.25: Penalty sensitivities against PAPR of C-OFDM and DL-OFDM for BPSK (left) and QPSK (right) with an ONU_2 local oscillator at 7.5GHz and with an effective data BW of 100% and 70% respectively. Continuous and dotted lines correspond to C-OFDM and DL-OFDM, respectively.

6.4 Sign-Labeled OFDM algorithm

This algorithm can be considered as a particularization of DL-OFDM and it focuses on extending the dynamic range of the optical system by eliminating the need of a carrier to detect the signal.

6.4.1 Absolute value signal with sign

6.4.1.1 Basic concept

In figure 6.26, compares the modulation process undergone when biasing the MZM either in QP or else NP. Since the focus is on the electrical signal after DD, the power transfer functions have been used. As seen, if the NP is used the signal sign is lost after DD. Therefore, the basic idea of this algorithm is to send an auxiliary information together with the data signal with information about the sign of each sample in order to DD the signal sent without the needed of an auxiliary optical source.

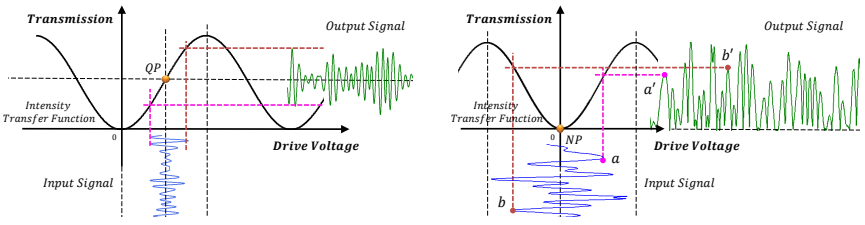

Figure 6.26: Output signal of a MZM biased at QP (left) and NP (right).

The aim of this section is to present an efficient algorithm allowing to restore the original bipolar signal with sign out from the positive only signal after

DD. Appendix D includes some proposals which aimed at restoring the signal without any kind of side information. The analysis of those proposals allowed to conclude that a Sign Label (SL) with side information was needed. Hence, after the following SL-OFDM block diagram description in section 6.4.1.2, the characterization of the side information such as in section 6.3.2 will be presented.

6.4.1.2 SL-OFDM algorithm block diagram

Figure 6.27 illustrates the block diagram of the SL-OFDM algorithm. The OFDM bipolar signal in (i) is converted into absolute values in (ii) and the sample's signs are extracted, the optimal coding values are found in (iii) and saved in the SL vector. Finally both, the electrical positive signal and the SL are joined in the same signal in (iv) to be optically modulated and sent through the channel.

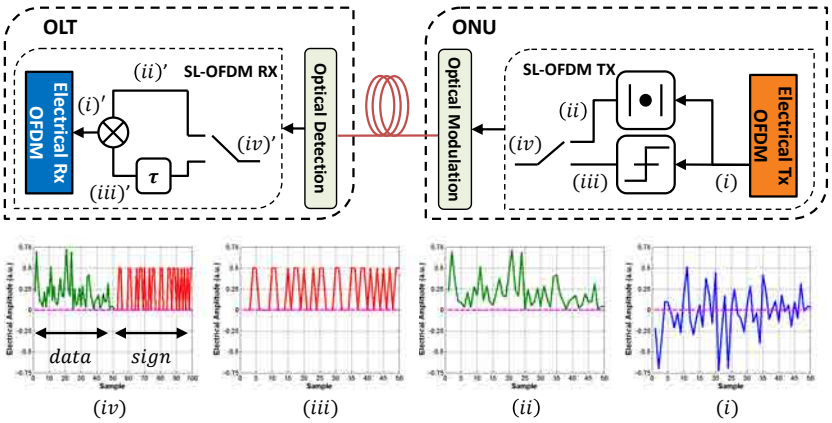

Figure 6.27: SL-OFDM block diagram with insets showing the original OFDM signal (i), the absolute signal (ii), the sign-label (iii), and the SL-OFDM signal (iv).

At RX, the complete signal is detected, separating the side information from the absolute value OFDM signal. The side information is coded as 1 if the samples are positive and -1 if they are negative. Afterwards, the translated information is multiplied by the absolute value OFDM signal finally recovering the original signs of each sample and thus, the original signal sent. All the operations can be done in the digital domain, allowing to better exploit the resolution of the ADC/DAC by avoiding the need of a bit to represent the sign . Since the SL has only two possible values it is easily transformed into the analog domain with the same DAC used for the OFDM magnitude signal.

6.4.2 Side information-based proposals

The basic idea of this proposal is to send side information together with the data in order to determine whether a specific RX sample is originally positive or negative. As in DL-OFDM, sending this kind of side information, the BW efficiency will be halved and the BR has to be doubled to maintain the same BW required.

As in the DL-OFDM algorithm, there are two important characteristics to specify: the SL distribution within the TX data signal and its amplitude. The procedure for choosing both features is similar to that followed in section 6.3.2, and also the results obtained are. Thus, the histograms and analysis in order to finally conclude that the amplitude of the SL will be normalized to 0.5 and the SLs time-interleaved can be found in the appendix E.

6.4.3 SL-OFDM applications to a P2P scenario

6.4.3.1 Simulation setup and results

In this section, both algorithms, C-OFDM and SL-OFDM are simulated with a P2P scenario with the same features than in the P2P simulations of DL-OFDM in section 6.3.3. Figure 6.28 plots the sensitivity penalty against the MI for both the C-OFDM and SL-OFDM algorithms with both BPSK and QPSK for electrical BWs of 1.25GHz, 2.5GHz and 5GHz. In this case, the SL-OFDM curves decrease sharply until a MI of around 0.25 is reached then they experience a smooth increase up to MI of 2.5 when there is a dramatic increase of the sensitivity. It is worth highlighting that while the MI value is indicating the maximum DM in practice the majority of samples would be comprised within 80% of this maximum value and thus the sensitivities for BER 10^{-3} are kept within reasonable values even for MI as high as 2 meaning that the signal DM is twice the MZM DM.

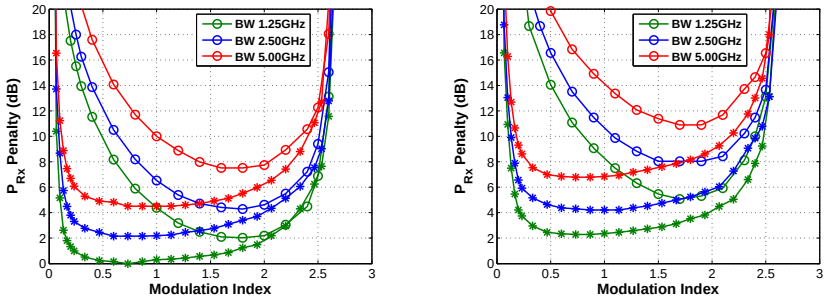

Figure 6.28: Sensitivity penalty against MI comparing a C-OFDM (circle) and SL-OFDM (triangle) with BPSK (left) and with QPSK (right). The sensitivity reference is -37dBm. The strategy used is the time-interleaved SL.

Conversely, the C-OFDM curves present a more gradual reduction of sensitivity when the MI is increased and reach sensitivity minima which are on the order of 2dB higher than the minima reached by the corresponding SL-OFDM system. Those sensitivity minima are reached with MI values between 0.5 and 1 for SL-OFDM while the optimal margin for C-OFDM is located between MIs of 1.5 and 2. On the other hand, the penalty for the same MI can be as high as 10dB, as the case of MI 0.5 in BPSK. The penalty to double the BW and the modulation format is 2dB in both cases.

6.4.3.2 Experimental setup and results

Figure 6.29 depicts a scheme of the setup used to experimentally test the SL-OFDM algorithm. A total 218 bits were randomly generated and modulated into QPSK and 8QAM formats. The complex valued symbols were then sent in parallel to a 64/256-point iFFT with HS in order to obtain a real valued OFDM signal. No CP was added since for the fiber lengths and BR involved no significant amount of CD was generated. The SL-OFDM algorithm as explained in the previous section was applied in the required case. The OFDM sequence was uploaded to an AWG for conversion to the analog domain at a sample rate of 1.25GSa/s with a resolution of 8 bits. The analog electrical signal was then modulated into an optical carrier at 1549.9nm fed by an external cavity laser to a MZM with a half-wave voltage of 3V biased at the NP. Electrical amplification was used to exhaust the MZM dynamic range, which means a MI of 1 corresponding to a peak to peak voltage of 3dB as shown in figure 6.29 (left). The modulated optical signal was then amplified to a power of -3dBm and launched into B2B and 25km SMF.

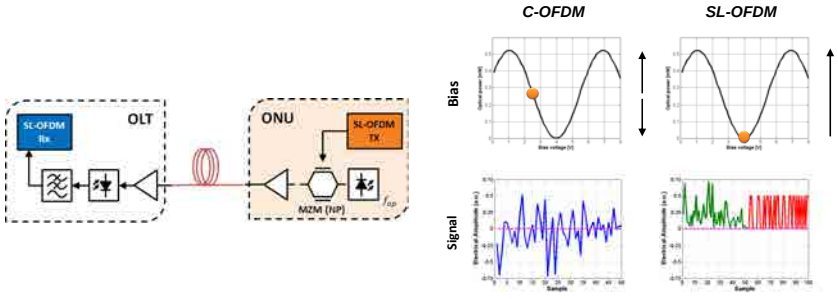

Figure 6.29: Experimental setup (left); bias, signal in time and electrical spectrum for C-OFDM and SL-OFDM (right).

The RX consisted of a 50GHz band-pass optical filter centered at the TX wavelength and in the detection stage either an 8GHz APD or else 1.5GHz PIN PD preceded by an EDFA, were used in different tests. The EDFA set an input power of -16dBm to the PIN. The RX electrical signal was then captured with a 50GHz RTO. The samples were processed offline recovering the signal using the SL auxiliary information to performing the FFT and modulation format

decoding. Finally the BER was computed.

Both C-OFDM and SL-OFDM in an IM/DD system (ID01) were measured for comparison. In the first one, the MZM was biased at its QP with a DC bias of 1.5V and in the second, the amplitude of the SL was optimized and fit into the MZM biased at its NP with a DC bias of 3V.

The system was first tested with a QPSK modulation format, 64-FFT size and the PIN based RX. The performance of the system was measured in terms of the optical RX power and the corresponding BER. Then, the SL-OFDM signal was uploaded and sent through the same system. The performance of both techniques in B2B is plotted in figure6.30 (left). It is observed that for a target FEC limit BER of 10^{-3}, the SL-OFDM outperforms C-OFDM and improves the RX sensitivity by almost 3dB. A similar enhancement is noticed in figure 6.30 (right) in which the signal traveled through fiber distances of 25km.

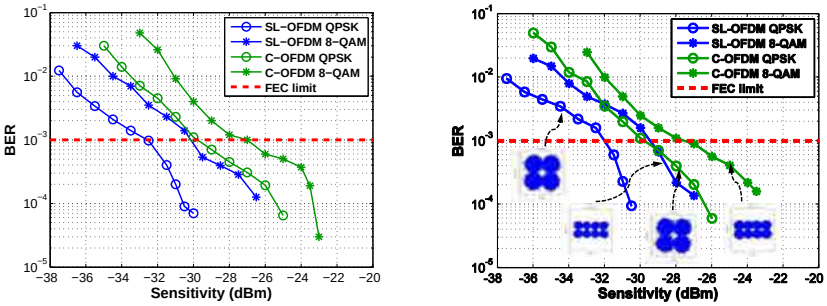

Figure 6.30: BER plots against RX optical power with C-OFDM and SL-OFDM for fiber lengths of 0km (right) and 25km (left) and 64-point FFT.

Both techniques were also evaluated with 8QAM modulation. Since the distance between the neighboring states is reduced, the 8QAM is expected to present a penalty with respect to QPSK [152]. Indeed, the sensitivity values at FEC BER dropped by 2dBs for both systems, but still the penalty for using C-OFDM is maintained around 2dB for both QPSK and 8QAM. This suggests that the performance improvement of SL-OFDM over C-OFDM is able to potentially scale to higher modulation formats.

In the next experiment, the FFT size was increased to 256. The performance results are plotted in figure 6.31 (left) for a fiber length of 25km and QPSK. In this situation, SL-OFDM boosts the RX sensitivity by a little more than 3dB at the FEC limit. These results indicate that SL-OFDM is effective for different FFT sizes .

An additional test consisted in exchanging the optical RX PD with an APD. Data was modulated into QPSK and the FFT had 256-points. Figure 6.31 (right) plots the performance results showing the same 3dB improvements at FEC limit when using SL-OFDM. The sensitivity values are lower than in the APD case which is mainly explained by the absence of an optical amplifier and the higher

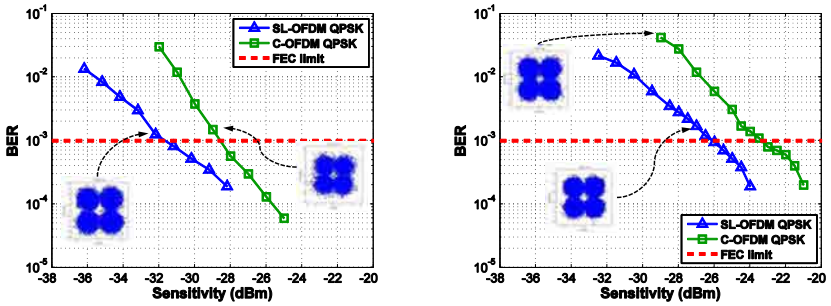

Figure 6.31: BER plot against RX optical power with PIN (right) and APD (left) in RX and 256-FFT.

electrical noise.

These results confirm that by better exploiting the linear DM of the MZM SL-OFDM allows around 2-3 dB sensitivity improvements for a 10^{-3} FEC limit BER.

6.4.4 SL-OFDM applications to PON

In this section we explore the potential applications of the SL-OFDM algorithm to access PONs by means of a VPI simulation environment based on the P2P scenario from section 6.4.3.1.

In section 6.3.4.2 it was observed that for DL-OFDM, the loss of orthogonality causes a widening of the electrical signal spectrum which is critical for the US direction to the point of making it a bad choice for PON. The same phenomenon of electrical BW widening has been observed in SL-OFDM and therefore it suffers from the same problems in the US. This is why in this section just the DS results are presented.

6.4.4.1 Downstream S-OFDMA-PON sceanrio with SL-OFDM algorithm

In this section, a DS S-OFDMA-PON scenario with both, the SL-OFDM and C-OFDM algorithms is simulated. Notice that, when C-OFDM is applied, the MZM is biased in QP, whereas when SL-OFDM is applied, the MZM is biased in NP.

The same block diagram of figure 6.14 can be considered by changing the algorithm section by the SL-OFDM and the MZM bias point to NP. In the OLT, the signal is mapped with BPSK and QPSK and modulated with a 256-iFFT. Next, the SL is appended at the end of each OFDM frame and input to the MZM biased in NP and fed with a laser of 1MHz linewidth. The optical

signal is then sent through 25km of optical fiber. The signal RX in each ONU is recovered by means of the SL-OFDM algorithm and down-converted to BB to be finally decoded by the OFDM RX. Notice that the multiband multiplexing approach was used, so each ONU just processes a 128-iFFT. The rest of features and scenario characteristics are the same than for the P2P scenario.

Figure 6.32 shows the penalty against MI for BPSK and QPSK modulation formats with different electrical BWs for both scenarios. The curves confirm the same behavior than in the P2P scenario in figure 6.28 with slightly lower improvements in sensitivity of the SL-OFDM as compared to the C-OFDM.

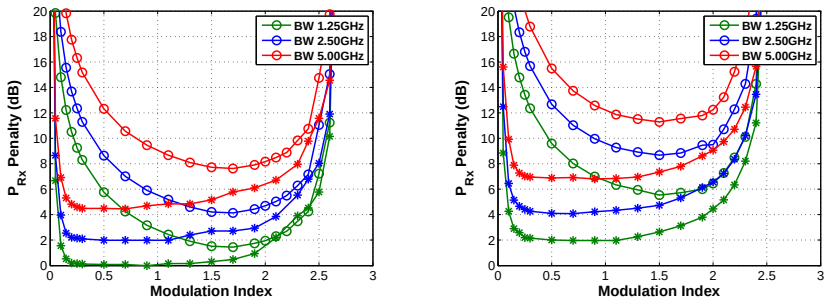

Figure 6.32: Sensitivity penalty against MI comparing a C-OFDM (circle) and SL-OFDM (triangle) with BPSK (left) and with QPSK (right). Continuous and dotted lines correspond to ONU1 and ONU2, respectively. The sensitivity reference is -39.8dBm.

As in DL-OFDM, the performance is slightly better for ONU_1 which operated in BB than for ONU_2 because of the non-ideal filter response in the OLT RX which in simulation is a square-root raised-cosine with a 0.2 roll-off, so they are not plotted. These results confirm the performance improvement of the SL-OFDM algorithm over C-OFDM systems in the DS of the simulated PON.

Finally, in order to see the impact of the spectral overlap between ONUs in the DS signal, the useful data BW percentage of both ONUs was reduced by increasing the ZP and the sensitivity was obtained for different MIs and a total electrical BW of 2.5GHz for both BPSK and QPSK. Figure 6.33 compares the sensitivity results of both algorithms and shows that the behavior related with the useful data BW percentage is similar in both cases.

It is also seen that the different MI values analyzed barely have impact on the sensitivity value in the SL-OFDM whereas it may give rise to up to 10dB differences in C-OFDM for MI going from 0.17 to 1, as also steams from the results in figure 6.32. For SL-OFDM a value of -39dBm in the RX sensitivity was reached when each SL-OFDM ONU employed the total BW with BPSK and around -45dBm when each one employed only 25% of the BW with a MI of 0.17 to 1. For QPSK, these values are -34dBm and -40dBm, respectively.

Nevertheless, the improvement of SL-OFDM as compared to C-OFDM is

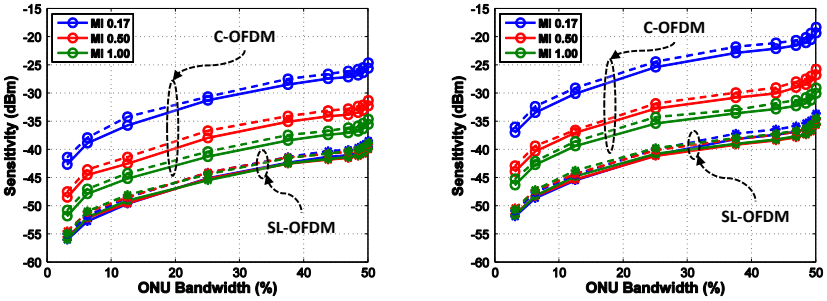

Figure 6.33: Sensitivity penalty against ONU BW percentage comparing a C-OFDM (circle) and SL-OFDM (asterisk) with BPSK (left) and with QPSK (right) for both ONUs.

the same whatever the BW per ONU, going in QPSK from 4dB up to 13dB and in BPSK from 5.3dB up to 15dB, respectively for MI of 1 and MI of 0.17.

In practice, in order to optimize the value of sensitivity one would prefer to use an MI value as high as possible (even when that would increase costs as a larger DM would be required in devices) and in that case the expected sensitivity improvements are around 3-4dBs.

As a conclusion, as compared to conventional IM/DD C-OFDM systems the novel SL-OFDM requires few additional digital operations keeping the implementation simple and presents better sensitivity values,. In addition, SL-OFDM is potentially more energy-efficient than C-OFDM since the MZM operates in its NP enhancing the sensitivity of PON systems based on IM/DD. Finally, it was checked that the sensitivity gains derived from using SL-OFDM are high for a low MI range going from 0.5 to 1 which translates into cost reductions as high linearity devices are not strongly needed.

Chapter 7

ADC/DAC quantization in an OFDMA-PON

Due to the cost of implementing oOFDM, the design of the DSPs required for the digital operations, the optimization of optical components such as amplifiers and the DAC/ADC's at the TX and RX have become one of the hot topics in this area.

The DSPs design optimization is basically a two-sided problem, which implies studies at two different levels: on the one hand, the number of arithmetic operations per bit needed to convert the original message to an OFDM signal in the TX and the complementary functions for decoding it in the RX; and on the other, the number of bits required to represent the signal at various points within the TX and RX [15]. A reduced group of researches consider the latter, and about the first matter, different papers compare the number of arithmetic operations of the DSP on oOFDM systems and single carrier optical systems [153] and determine that the computational requirements are almost the same [154–156].

The design of the DAC/ADC's is one of the most critical factors in high capacity optical communications systems such as those based on OFDM since several operations need to be carried out in the digital domain, requiring heavy data processing and making it expensive and power consuming. In [157] a study of the effect of clipping and quantization noise due to limited resolution of ADC/DAC on the performance of an oOFDM system is presented coming to the conclusion that the error introduced by limited DAC/ADC resolution is equally distributed among all SCs and can be used to reasonably predict BER performance treating the clipping and rounding error as an Additive White Gaussian Noise (AWGN) process. In [158], a study on the minimization of the required DAC resolution concluded that the signal degradation caused by quantization is independent of the SC modulation format and that the performance improvement by using higher resolution is saturated. Thus, a working point in

which the penalty is minimal with a limited number of bits could benefit the overall cost without affecting the performance.

Considering that the higher the number of QBs required by the DAC/ADC's, the higher the complexity and the cost of the devices, this chapter aims at studying the DAC/ADC's performance over different scenarios and optimize their resolution [159].

Firstly, two representative scenarios of DD, the IM/DD oOFDM system (ID01) and the direct-AM/DD oOFDM system with oIQ modulator and remote heterodyne auxiliary optical source (ADR05) are simulated with VPI in P2P in order to study their performance by varying the DAC/ADC's resolutions. Considering the ranking stablished in table 4.2, these two systems have been chosen because they are respectively the lowest and highest performance oOFDM system based on DD.

A comparison between the results of both scenarios is presented by means of the sensitivity penalty at FEC limit BER to be paid for reducing the QB. Afterwards, the ID01 system was experimentally reproduced and analyzed, and the constant BER curves shown against FFT size, modulation format and resolution. Finally, as a last section, the US direction of both types of S-OFDMA-PON presented in chapter 5, analog and digital users multiplexing were simulated by fixing the ADC at OLT and varying the resolution of the DACs at both ONUs. The main objective is to reduce the TX DAC allocated at the ONU at the expense of a high ADC resolution at the OLT in order to reduce the overall network costs.

7.1 P2P scenarios: simulation and experimental results

7.1.1 Simulation setups and results

Two P2P scenarios were simulated with VPI, based on the ID01 and ADR05 OFDM systems whose schemes are illustrated in figures 7.1 and 7.2 respectively. The context of these P2P is the US of OFDMA-PONs low-cost TX and that is the reason behind the interest of study the behavior of both, ADC and DAC, in order to reduce the DAC's resolution.

In both cases the simulations considered a total of 2^{17} bits at a BR of 10Gbps randomly generated and mapped into BPSK, QPSK and 16QAM. The symbols were converted from serial to parallel and modulated with a 256-iFFT. In the ID01, the iFFT input data was arranged with HS in order to get a real-valued signal necessary for IM, while since the system allows for simultaneous modulation of both the real and the imaginary components of the OFDM signal, this was not necessary for the ADR05. Taking into account the aforementioned modulation formats, the effective BW were 5GHz, 2.5GHz and 1.25GHz although

due to the requirement of a GB for DD the AM signal, the electrical BW for the ADR05 is twice as big. The iFFT samples were transformed back to serial and quantized with a DAC followed by an anti-alias filter. No CP was added since for the fiber lengths considered no significant CD was generated. The linewidth of the optical sources was 1MHz. The optical power of the launched signal was fixed to 0dBm and then sent through 100km of fiber.

The RX is composed of an optical amplifier that compensates the fiber losses, a single PD to detect the optical signal and the ADC followed by the OFDM decoder. The electrical signal after the PD is filtered to avoid aliasing effects at high frequencies and an ADC converts it to a digital signal. Afterwards data samples are converted into parallel and sent to a 256-FFT to demodulate the SCs. The first two OFDM symbols were used for training a 1-tap equalizer to compensate for the channel. Data is then sliced for symbol decision, demapped and the BER is computed. The QB of the DAC at TX and the ADC at RX were varied.

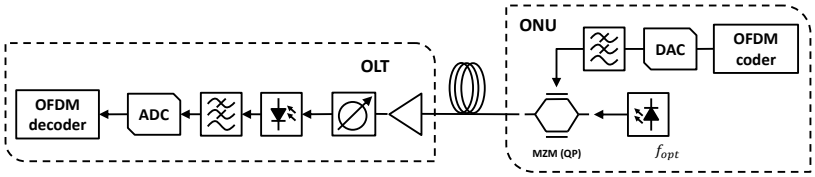

Figure 7.1: Conventional IM/DD oOFDM system scheme (ID01).

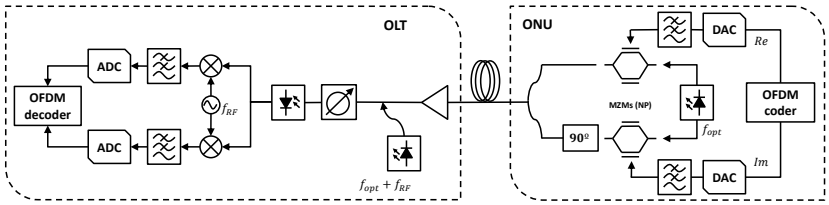

Figure 7.2: Direct-AM/DD oOFDM system scheme (ADR05).

For the ADR05 system in figure 7.2. the auxiliary optical carrier injected at the OLT was allocated at, 7.5GHz and 3.75GHz and 1.875 GHz frequency distance with respect to the TX carrier [160], for BPSK, QPSK and 16QAM, respectively. These spectral separations allow to avoid DINLD contributions as studied in section 3.3.1. In the simulation the optical sources are correlated in order to avoid PN which in any case may be reduced through pilot tones such as in chapter 8. As a result, two DACs at TX were needed instead of one as in ID01 scenario. The RX consists of an optical amplifier and a single PD followed by an RF down-conversion stage to bring back both the in-phase and in-quadrature components to BB, thus obtaining respectively the real and imaginary parts of the OFDM signal which were then sampled, processed and the BER was computed.

These first tests are focused on determining the minimum QB required in TX DAC at ONU and RX ADC at OLT. The QB of the DAC/ADC was varied from 3 to 10. The sensitivity results are plotted in figure 7.3, 7.4 and 7.5, as constant penalty curves for both the ID01 and the ADR05 scenarios. The RX sensitivity for infinite resolution DAC and ADC was considered as reference being -20dBm for ID01 and -35dBm for ADR05. In order to firstly show the most restrictive case, figures 7.3, 7.4 and 7.5 plot the results with 16QAM, QPSK and BPSK modulations and table 7.1 is a summary of the observed penalties. Insets show the constellations barely seem to change from the best to the worst cases at 3dB penalty

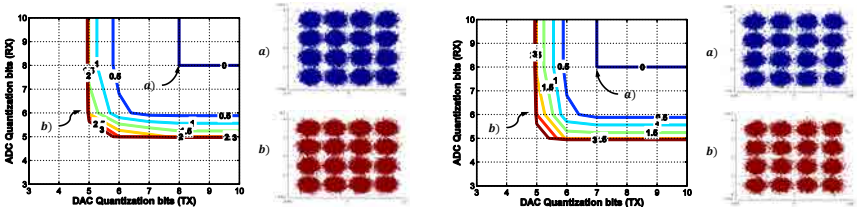

Figure 7.3: Sensitivity penalties against DAC/ADC resolutions for a P2P ID01 (left) and ADR05 (right) oOFDM systems with 16-QAM. The reference sensitivities are -20dBm for the ID01 and -35dBm for the ADR05 scenarios.

Interestingly, the sensitivity penalties observed have a similar behavior for both systems. At a penalty of 0.5dB, both systems require around 6 bit DAC and 6 bit ADC. At a 3dB penalty, both TX systems require 5 bits for the ADC and 5 bits for the DAC. For lower QB the penalty is higher than 3dB and increases quickly, even making the signal impossible to be detected when the QB are less than 5 QBs in both, DAC and ADC.

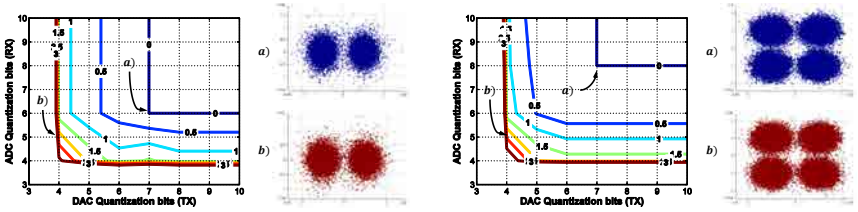

Figure 7.4: Sensitivity penalties against DAC/ADC resolutions for a P2P ID01 oOFDM system modulated into BPSK (left) and QPSK (right).

The main difference which can be found between the results obtained from BPSK and QPSK cases of both scenarios is the case of 0dB penalty. Specifically, the ID01 requires 1 bit and 2 bits more for DAC and ADC, respectively if both scenarios are performed with QPSK. The other penalties plotted in the graphs present similar values of DAC/ADC QBs for both systems being the ADR05 slightly better in some cases such the ADC for QPSK with 1dB penalty since ID01 needs 1QB more than ADR05. Finally, as expected, the modulation format

increasing also affects the minimum QB required for the converters, increasing on the order of 1-2QBs.

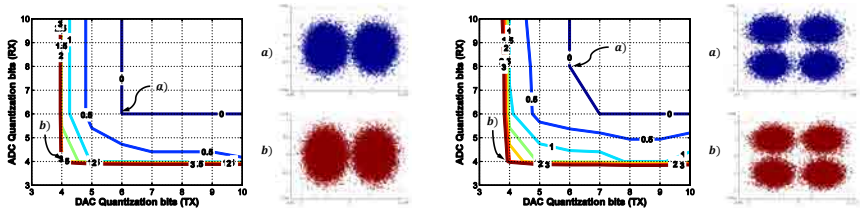

Figure 7.5: Sensitivity penalties against DAC/ADC resolutions for a P2P ADR05 oOFDM system modulated into BPSK (left) and QPSK (right).

In table 7.1, the QB requirements found are summarized:

	Penalty	0dB	0.5dB	3dB
BPSK	DAC	7	5	4
	ADC	6	6	4
QPSK	DAC	7	5	4
	ADC	8	6	4
16QAM	DAC	8	6	5
	ADC	8	6	5

	Penalty	0dB	0.5dB	3dB
BPSK	DAC	6	5	4
	ADC	6	5	4
QPSK	DAC	7	5	4
	ADC	7	5	4
16QAM	DAC	7	6	5
	ADC	8	6	5

Table 7.1: Minimum QBs required for different penalties for ID01 (left) and ADR05 (right) scenarios.

7.1.2 Experimental setup and results

In order to experimentally test the performance of the ID01 scenario for different DAC/ADC resolutions, a total 218 bits were randomly generated and modulated into BPSK and QPSK formats. Again, the focus is on the US direction because it is usually the most challenging. The complex valued symbols were then sent in parallel to a 16, 64 and 256-point iFFT with HS in order to obtain a real valued OFDM signal. No CP was added since for the fiber length and BR involved no significant amount of CD was generated. The OFDM sequence was uploaded to an AWG which produced samples at 10GSa/s with different DAC resolutions. The output signal was then directly modulated with a DFB laser launching a power of 0dBm and sent through 100km SMF.

The OLT RX consisted of a 10GHz PIN PD preceded by and EDFA to compensate for the link losses and a 50GHz band-pass optical filter centered at the TX wavelength in order to avoid the alias at high frequencies due to IM modulation. The RX electrical signal was then captured with a 50GHz RTO. The QB options in the RTO are reduced to 10 and 8 QB, so at the OFDM decoder, the samples were processed offline with Matlab@ converting the signal from analog to digital by means an ADC with different QB and performing the FFT and modulation format decoding. Finally the BER was computed.

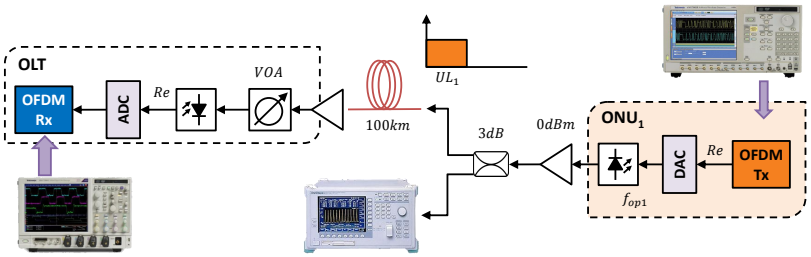

Figure 7.6: Experimental setup block diagram.

The procedure followed to obtain the graphs presented below consisted on varying, the attenuation by means of a VOA located before the PIN until a BER close to the FEC limit of 10^{-3} was achieved with 8 bits resolution DAC/ADC. Afterwards, this attenuation was fixed and the QB of both converters was varied to obtain the constant BER curves as a function of DAC/ADC resolutions. Notice that the values of the curves are labeled according to the corresponding $-log_{10}(BER)$.

In figure 7.7, 7.8 and 7.9 the BER curves are evaluated for a FFT size of 16, 64 and 256, respectively, for both modulation formats, BPSK (left) and QPSK (right). The sensitivity with which the BER was close to the FEC limit and quantized with 8 bits in both DAC and ADC were -19dBm and -16dBm with 16-FFT, -15dBm and -12dBm with 64-FFT and -11dBm and -8dBm with 256-FFT for BPSK and QPSK, respectively.

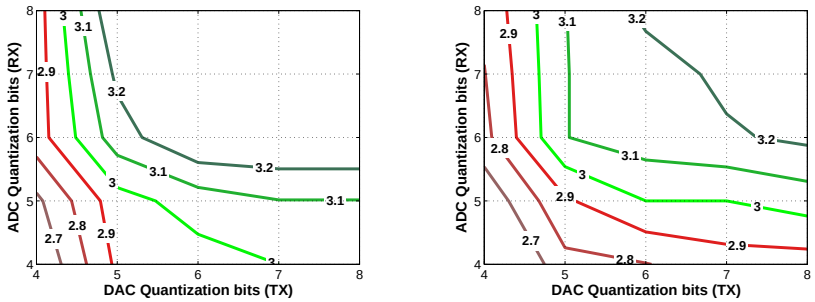

Figure 7.7: Constant BER curves against DAC/ADC resolutions for a P2P ID01 oOFDM system modulated with 16-iFFT into BPSK (left) and QPSK (right). Labels over the curves indicate the $-log_{10}(BER)$ value. The sensitivity reference with 8 bits resolution for both DAC and ADC is -19dBm and -16dBm for BPSK and QPSK, respectively.

As shown in figure 7.7, in order to ensure the BER of 10^{-3}, just 4 bits ADC if DAC had 7 bit resolution are required for BPSK. Taking into account the focus on US, the ONU has to be as cheap as possible to reduce the overall cost of the US TX, the best case was a system with 5 bit DAC and around 5 bit ADC. On

its side, for the QPSK case in figure 7.7 (right), using a DAC of 5 bit and an ADC of 6 bit was the best combination to ensure the FEC limit reducing the cost of the system.

The cases of 64-FFT and 256-FFT with BPSK, at the left side of figures 7.8 and 7.9, need 5 QB ADC or a 6 bit resolution DAC to reach the FEC limit BER, i.e. one ADC bit more than when a 16 FFT size was used. Furthermore, although the behavior when the signal is modulated into QPSK and 64-FFT (figure 7.8 left) is a bit worse than BPSK with the same FFT size (figure 7.8 right), since the resolution bits have to be integers, same QBs in ADC (6) and DAC (5) are required to ensure the FEC limit for BPSK and QPSK and 64 FFT size.

Finally, for the QPSK case with 256-FFT in figure 7.9 (right), the converters have to be better since the BER of 10^{-3} was achieved with 7 bit ADC and 5 bit DAC or vice versa.

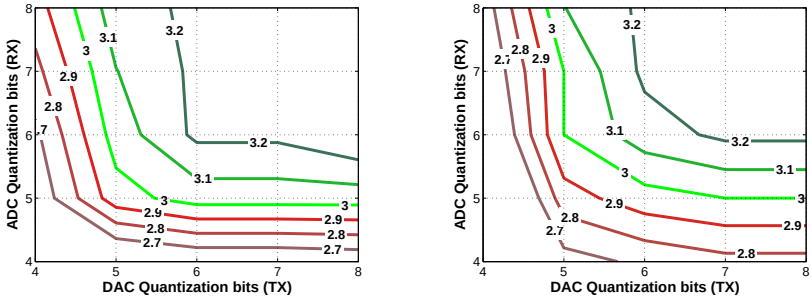

Figure 7.8: Same as figure 7.7 but with 64-iFFT. The sensitivity reference with 8 bits resolution for both DAC and ADC is -15dBm and -12dBm for BPSK and QPSK, respectively.

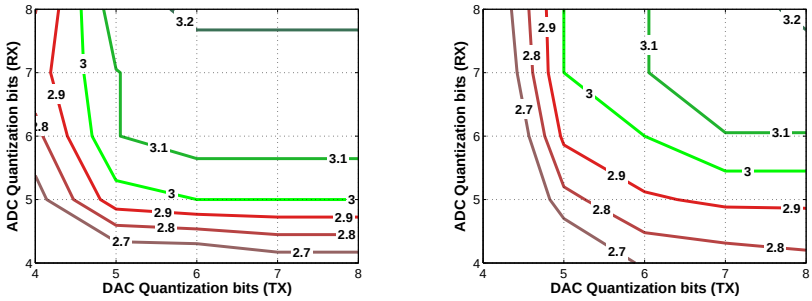

Figure 7.9: Same as figure 7.7 but with 256-iFFT. The sensitivity reference with 8 bits resolution for both DAC and ADC is -11dBm and -8dBm for BPSK and QPSK, respectively.

In essence, the required QBs for FEC BER in all the cases analyzed acquired

very close values of about 5 or 6. That's a direct consequence of the fact that the reference sensitivity was chosen close to the value that provided the FEC BER with 8 QB in both ADC and DAC. That shows also the trade-off between required sensitivity and QBs. In any case, the result of being able to maintain the quality of the transmission with QBs reductions of 2 or 3 bits is very significant.

7.2 M2P scenarios: simulation results

This section aims at studying the effect on the sensitivity of the QB of one ONU to its adjacent and vice versa in the US. Both networks analyzed in chapter 5, the S-OFDMA-PON with digital and multiband multiplexing approaches are tested.

In both scenarios, two ONUs were simulated with QPSK modulation fixing an ADC resolution allocated at the OLT to 6 bits and varying the DAC's of both ONUs. As seen in previous results the 6 bits ADC presents only 0.5dB penalty with DACs of 5 bits or less.

Considering a data BW per ONU of 2.5GHz and a roll-off of 0.2, in order to avoid the OBI due to the detection of both signals by a single PD, a frequency spacing of 7.5GHz was left between optical carriers. Notice that as steaming from the analysis in section 5.1, due to the electrical spectral overlap, it is worth including additional spectral gaps between the electrical spectra of adjacent ONUs. However, for the purposes of simulations no additional electrical spectral gaps have been considered.

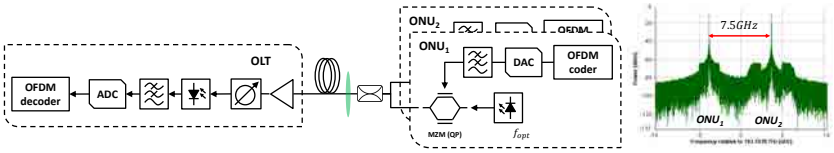

Figure 7.10: S-OFDMA-PON with digital multiplexing approach.

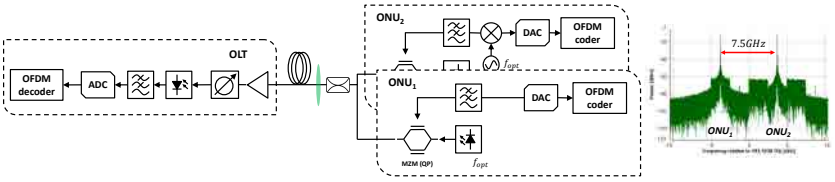

Figure 7.11: S-OFDMA-PON with multiband multiplexing approach.

Figure 7.12 plots the BER against the RX sensitivity for both ONUs with identical (left) and different (right) DAC resolution for the S-OFDMA-PON with digital multiplexing in figure 7.10. Since ONU_1 is located in BB, slightly better performance results were obtained than for ONU_2. For the identical QB

case, it is seen that with 6 bits, no quantization penalty is observed, 2dB penalty is obtained when reducing the QB to 4 bits and the curve corresponding with 5 bits is in the middle of the previous two.

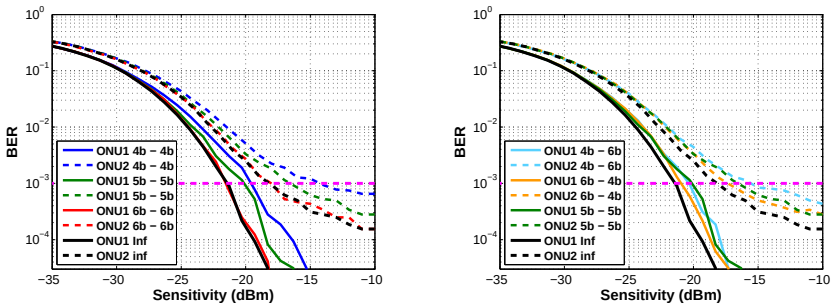

Figure 7.12: BER against sensitivity varying the ADC quantization of both ONUs in a S-OFDMA-PON without multiband approach. The DAC quantization is fixed to 6 bits.

On the other hand, when the QB of both ONUs is different as in figure 7.12 (right), sensitivities worsen a little due to the low DAC resolution ONU. Interestingly, both ONUs are affected similarly regardless of their resolution. This happens because the SCs were divided equally amongst both ONUs. Hence, the effective quantization in the RX signal can be approximated as an average of both the QB in ONU_1 and that in ONU_2. Thus, care should be taken in the PON design if an ONU has lower DAC resolution because it could worsen the other users. However, this also implies that the penalty of a reduced QB ONU will decrease provided that the remaining ONUs contain higher resolution DACs. The concept of the effect of the DAC's QB between ONUs is illustrated in figure 7.13, for both the digital and the multiband multiplexing cases.

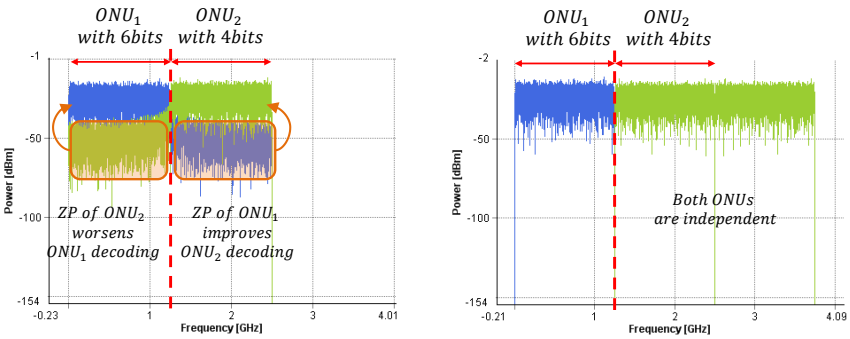

Figure 7.13: Electrical spectra of ONU_1 and ONU_2 at TX of an S-OFDMA-PON for uneven DAC QB in the multiplexed ONUs with both digital (left) and with multiband (right) approach.

It is also interesting to notice that the curve of 5 QBs in both DAC is

allocated around the same sensitivity values than the other two cases with same total QBs unevenly distributed between ONUs (6b-4b and 4b-6b). This implies that in practice, the sum of the QB in all the ONU's DAC's should be taken as reference for sensitivity.

Figure 7.14 shows the results with the multiband approach where for equal QB in both ONUs approximately the same results are obtained than in the digital multiplexing case for ONU_1, i.e. no quantization penalty for 6 bits and 2dB penalty for 4 bits, while ONU_2 seems to be more sensitive to the loss of QB with up to 4.5dB penalty.

The results with different QBs show that contrary to the digital multiplexing approach, the performance of each ONU depends on its own DAC resolution, i.e. the neighboring ONUs do not affect on the sensitivity. Thus, the uneven QB cases play complementary roles in the curves of ONU_1 and ONU_2, i.e. comparing the curves for 6b-4b and 4b-6b, we observe a penalty of about 2dB for ONU_1, and an improvement close to 5dB for ONU_2. The reason for a larger dependence on QB may found in the fact that ONU_2 is located in the higher part of the spectrum and thus it is more sensitive to the non-idealities of the anti-alias filters. As expected, the 5 QBs DAC resolution curve are allocated between the curve corresponding with 6 bits resolution and 4 bits resolution such in figure 7.14 (left).

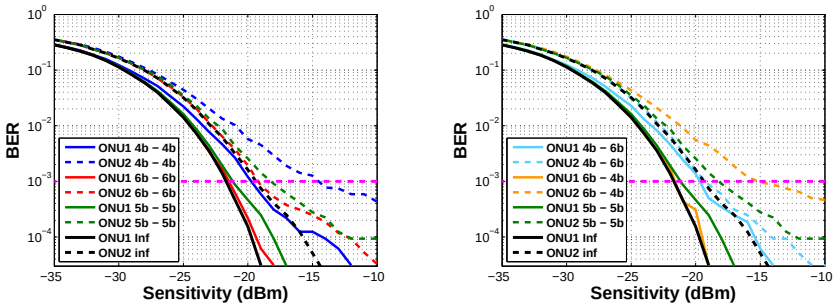

Figure 7.14: BER against sensitivity varying the ADC quantization of both ONUs in a S-OFDMA-PON with multiband approach. The DAC quantization is fixed to 6 bits.

Thereby, the resolution of the DAC/ADC of an OFDM TX/RX was studied in terms of the penalty in the sensitivity with respect to an infinite resolution. On the one hand, in a P2P level, two representative systems of the DD, the IM/DD (ID01) and the direct-AM/DD with remote heterodyne optical source (ADR05) were assessed with similar results for both cases. Specifically, a minimum resolution of 6 bits for both the ADC and DAC was found to achieve penalties lower or equal to 1dB with respect to the ideal case for modulation formats up to 16QAM. Furthermore, for both systems a resolution of 4 bits may be used in systems which support penalties of 3dB. On the other hand, in a M2P level, two scenarios based on the S-OFDMA-PON with and without multiband

approach with two ONUs were also tested, keeping fixed the ADC resolution to 6 bits and the modulation format to QPSK. In both cases, when both ONUs have the same resolution, 6 bits DAC are enough to avoid penalties with respect to infinite quantization at a BER of 10^{-3} while with 4 bits, a penalty of 2dB in both ONUs for the PON digital approach and 2dB and 4dB in ONU_1 and ONU_2 correspondingly for the PON with multiband approach. In addition, if the ONUs have different resolution in the digital case, there is a penalty due to the low resolution ONU, i.e. there is a contribution which can improve or worsen the adjacent ONU, instead in the multiband case, the performance of each ONU only depends on the QB of its own DAC, independent of the DAC's of the rest of ONUs.

Chapter 8

Laser linewidth requirements for remote heterodyne system

As analyzed in previous chapters, optical communication systems which rely in auxiliary carriers for detection are affected by PN [41]. PN is also one of the downsides of the R-OFDMA-PON in its US direction. The basics of PN were studied in section 5.1. Here, we aim at studying through simulations the effect of PN depending basically on the linewidth of the optical sources and the data BW in an oOFDM system based on the ADR01 scenario. In addition, a widely accepted technique based on pilot tones presented in the first section, is used in the simulations to compensate the PN.

8.1 Phase noise compensation: pilot tones

Channel response estimation plays a significant role in communication systems such as OFDM. Training symbols and pilot tones are extensively used in order to improve the performance. While training symbols allow to elucidate the frequency response of the channel at specific instants of time, pilot tones provide an estimation of the channel time response at specific frequencies. Figure 8.1 serves to illustrate the complementary roles played by both channel estimation techniques.

Considering an OFDM coder, the information carried by several SCs is fixed and known by the decoder in order to be used for comparison and time response estimation. In the same way as a reduction on the update interval of equalizer coefficients is required for a rapidly changing frequency response, a reduction on the SC spacing of pilot tones is required if the time response changes significantly

with small frequency intervals.

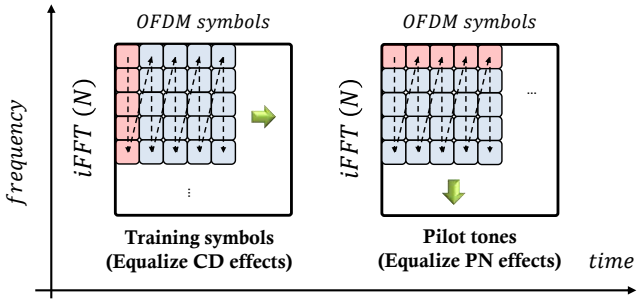

Figure 8.1: OFDM symbols versus iFFT matrix. In pink, training symbols position (left) and pilot tones position (right).

Figure 8.2 shows the optical and electrical spectra and the resulting constellation for a QPSK IGDR01 oOFDM system with an electrical BW of 10GHz, 256-FFT and 1MHz linewidth optical laser. Recalling figure 5.1 for decorrelated carriers a ring-shaped constellation was obtained due to the different starting phase for each OFDM frame, afterwards the signal band was detected by a correlated auxiliary optical source obtaining a proper constellation. In figure 8.2, both optical sources are decorrelated as seen in the optical spectrum and the corresponding electrical spectrum after the DD. In order to properly detect the signal, the PN was eliminated with the aid of pilot tones which are also clearly observed in the first SCs of the data band in both, optical and electrical spectrum. Notice that pilot tones are not equal than the rest of SCs since they are fixed to a unitary value. The pilot tones are used as in 1-tap equalization by means of training symbols but in frequency instead of time (see figure 8.1).

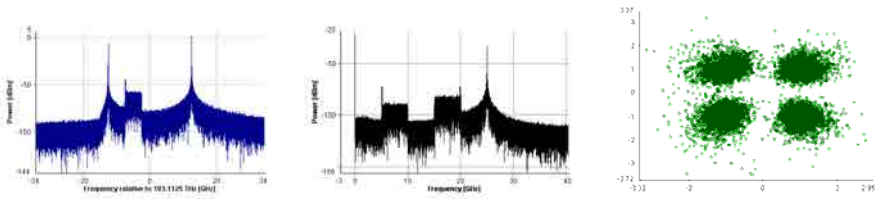

Figure 8.2: Optical (left), electrical (center) spectra and constellation (right) of a TX without (top) and with pilot tones (bottom).

8.2 Simulation setup and results

In this section, the maximum laser linewidth ($\triangle\nu$) allowed under different BR, modulation formats and FFT sizes to ensure the signal is detected at a FEC limit BER of 10^{-3} in a P2P ADR01 oOFDM system with a fiber length of 100km and using the pilot tone compensation algorithm is explored.

The scenario of figure 8.3 was simulated with VPI using a total of 2^{17} bits randomly generated and mapped into an N-QAM format, then converted from serial to parallel to take to the iFFT. The first two SCs in all cases were for pilot tones, since no significant improvement was observed from increasing this number. In order to get a real-valued signal required for ADR01, the HS was imposed to the iFFT input data. No CP was inserted since for the fiber lengths considered no significant CD was generated. The resulting electrical OFDM signal is quantized with 8 bits resolution and filtered with a square-root raised-cosine adjusted to the signal SR and with roll-off factor 0.2 to remove the spectral alias and then modulated into a carrier wavelength λ_{TX} by means of a MZM biased at NP with launched power of 0dBm to avoid fiber nonlinearities.

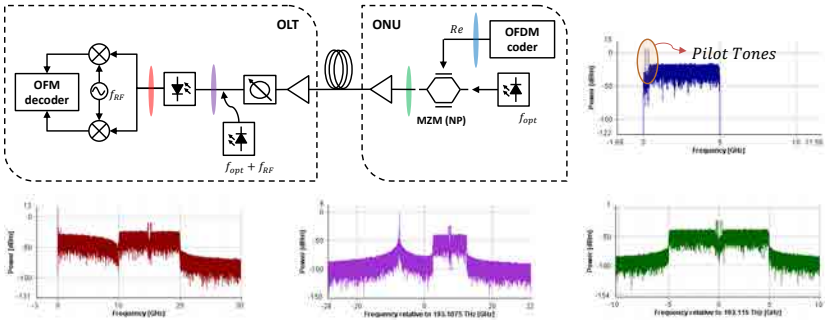

Figure 8.3: Direct-AM/DD oOFDM system (ADR01) with PN compensation.

The OLT RX included an optical amplifier that compensates the fiber loses and a laser injecting an auxiliary optical carrier at $\lambda_{TX} - 1.5BW_{TOT}$ which mixes with the incoming signal. In order to simulate PN effects, in the simulations, the two lasers had decorrelated random PN in a 1MHz linewidth. The emission wavelength of the local laser thus selected guaranteed the minimum optical GB to avoid IMD to spectrally overlap with the signal. Both TX and RX lasers had identical $\Delta\nu$ and emission power of 5mW. Both the received optical signal and the auxiliary carrier were injected to a single PD followed by an electrical filter with square-root raised-cosine characteristic and roll-off factor 0.2 in order to restrict the signal's BW so that aliasing is avoided after ADC. Afterwards the data samples are converted into parallel and sent to an FFT to demodulate the SCs. An algorithm which employs pilot tones was applied to compensate for the PN. Data was then sliced for symbol decision, demapped and the BER was computed. The first two OFDM symbols were used for training a 1-tap equalizer to compensate for the channel frequency response.

Firstly, the bandwidth per subcarrier BW_{sc} was fixed at 156.25MHz. Thus, in the simulations the total BR was adjusted for every value of FFT and QAM format selected following $BW_{sc} = BR/(FFT \cdot BpS)$, where BpS refers to bits per symbol of the N-QAM format selected. Figures 8.4 and 8.5 show the results obtained for different modulation format levels and FFT sizes. The respective tables specify the total signal BW and the total data rate following the color

coding.

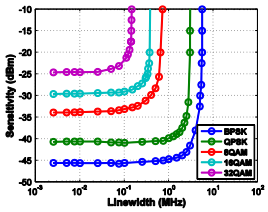

BW_{te} (GHz)	BR (Gbps)
5	40
5	20
5	15
5	10
5	5

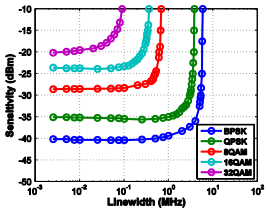

BW_{te} (GHz)	BR (Gbps)
20	100
20	80
20	60
20	40
20	20

Figure 8.4: Sensitivity against laser linewidth with BW_{sc}= 156.25 MHz constant for a FFT size of 32-points (left) and 128-points (right) for different QAM levels. Tables indicate the values of total bandwidth occupied by the OFDM signal and the total data rate for each modulation format following the color coding.

In all cases, a maximum tolerable linewidth is observed, which decreases as the modulation level increases and remains almost unchanged when varying FFT size. On the other hand the sensitivity within the tolerable linewidth value increases by around 5dB when doubling the BpS and by 2-3dB when doubling the FFT size.

As seen in the tables, doubling the FFT size for these constant BW_{sc} tests means doubling the spectral BW occupied by the signal and therefore less power per SC, hence the sensitivity penalty. On the other hand, since the BW_{sc} remains the same, there is no dependence on the maximum tolerable linewidth on the FFT size. On the contrary, when the BpS is increased, even when BW_{sc} is maintained, more decision levels lead to higher sensitivity to PN effects and therefore lower tolerable linewidth.

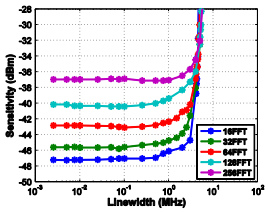

BW_{te} (GHz)	BR (Gbps)
40	40
20	20
10	10
5	5
2.5	2.5

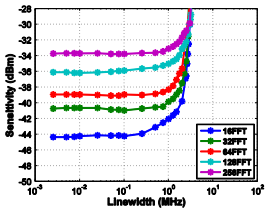

BW_{te} (GHz)	BR (Gbps)
40	80
20	40
10	20
5	10
2.5	5

Figure 8.5: Sensitivity against laser linewidth ensuring a BW_{sc} constant for a signal modulated into BPSK (left) and QPSK (right) for different FFT sizes. Tables indicate the values of total bandwidth occupied by the OFDM signal and the total data rate for each modulation format following the color coding.

As a main conclusion from figures 8.4 and 8.5, for increasing the BR it is better to increase the FFT size than the modulation format since doubling the modulation suffers the same penalty than increasing eight times the FFT size in terms of sensitivity and it does not lead to changes in the linewidth tolerance.

In a second scenario, the data BW (BW_{te}) was fixed at 10GHz, so as it is seen in figure 8.6, the higher the FFT size, the lower the BW_{sc} so that the

OFDM frame length is kept constant. For this case, the combination of BR and modulation format was varied according to $BW_{te} = BR/BpS$ and the BW_{sc} according to $BW_{sc} = BW_{te}/FFT$.

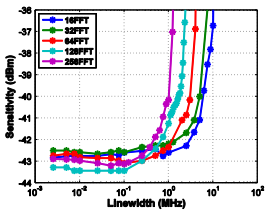

BW_{sc} (MHz)	BR (Gbps)
39	10
78.1	10
156.2	10
312.5	10
625	10

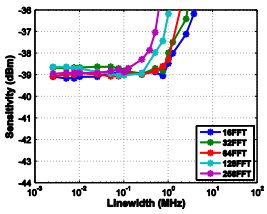

BW_{sc} (MHz)	BR (Gbps)
39	20
78.1	20
156.2	20
312.5	20
625	20

Figure 8.6: Sensitivity against laser linewidth with BW_{te} of 10GHz for a signal modulated into BPSK (left) and QPSK (right) for different FFT sizes. Tables indicate the values of BW_{sc} and the total data rate for each modulation format following the color coding

Figure 8.6 shows the sensitivity against the $\Delta\nu$ tolerance when the FFT size is varied and the modulation format is constant, BPSK and QPSK for the left and the right hand side, respectively. In contrast to the results of figure 8.5, it is noticed that there is no sensitivity penalty for increasing the FFT size, because in this case the total BW is maintained and, so is the power per SC. Nevertheless, the maximum tolerable linewidth is higher when the FFT size is reduced basically because the BW_{sc} is larger and thus the percentage affected by PN is lower. For a 3dB sensitivity penalty, the maximum tolerable linewidth for FFT sizes from 256 to 16 is seen to lie within 1 and 8MHz for the BPSK case, and within 700kHz and 1.5MHz for QPSK. In addition, the graphs reveal around 4dB of sensitivity penalty for upgrading from BPSK to QPSK regardless of FFT size.

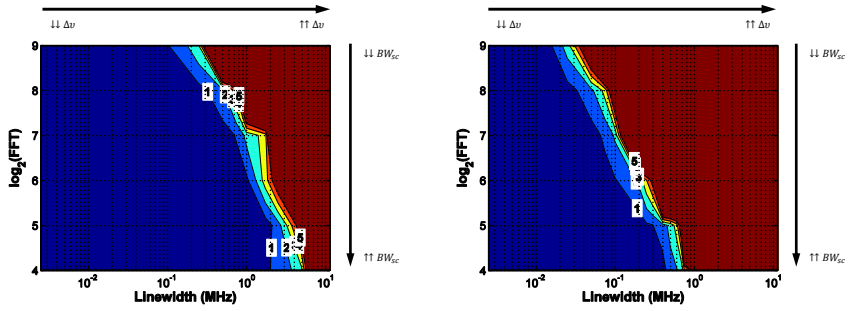

Figure 8.7: RX sensitivity penalty level lines in dB for a fixed BW_{te} of 10GHz against FFT size and laser $\Delta\nu$ with QPSK (left) and 16QAM (right) modulation formats.

Hence, the laser $\Delta\nu$ tolerance directly depends on the BW_{sc}. This relation is appreciated better in figure 8.7 which plots the FFT size $[log_2(iFFTpoints)]$ against the laser $\Delta\nu$ for a fixed total signal BW of 10GHz or in other words, the variation of BW_{sc} against the variation of the laser $\Delta\nu$ tolerance, with level

lines of the RX sensitivity penalty for QPSK (left) and 16QAM (right). The blue area corresponds to the safety zone where there is no PN penalty and the red zone corresponds to the zone with a sensitivity penalty higher than 5dB. It is clearly concluded that the higher the BW_{sc}, the higher the tolerance to the laser $\Delta\nu$, and also that the penalty lines show a lower tolerance to the laser $\Delta\nu$ when increasing the modulation format.

As a last test, both cases, a QPSK transmission with constant BW_{te} of 10GHz and constant BW_{sc} of 156.25MHz (right), were evaluated in terms of the maximum distance reach in a pure dispersive optical fiber with QPSK modulation and a laser $\Delta\nu$ of 100kHz in both TX and RX. The FFT size and the BR were varied to ensure first a constant BW_{te} of 10GHz (figure 8.8 left) and then a constant BW_{sc} of 156.25MHz (figure 8.8 right). Since the laser $\Delta\nu$ was a value inside the null-penalty area (figure 8.7 left), the effects shown in figure 8.8 are due to the fiber CD. It is important to indicate that no CP was employed. The main goal of this analysis is to show the advantage of increase the FFT in terms of maximum reach considering that the lower the FFT size, the higher the $\Delta\nu$.

Considering the case of constant BW_{te} the total time delay caused by dispersion is the same in all cases and since when the FFT size is increased the BW_{sc} is reduced, the OFDM frame time length increases, meaning that fewer bits per frame are affected by ISI and that improves the performance for the higher FFT sizes. Regarding CS effects, a limited number of frequencies can be affected when the fiber length is increased, for higher FFT sizes the percentage of faded SC to the total also improves performance. However, as noticed in figure 8.7, this holds only for this laser $\Delta\nu$ and shorter reaches are expected for higher $\Delta\nu$ values.

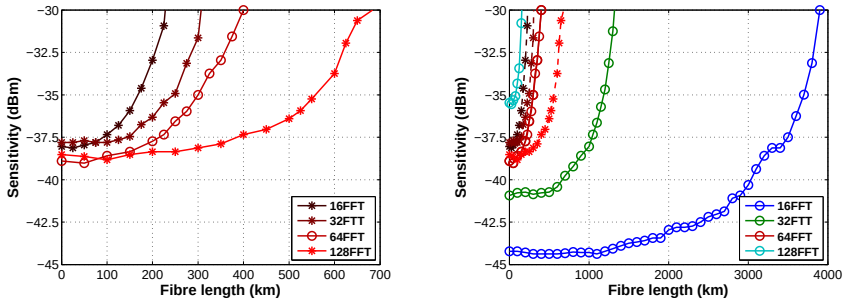

Figure 8.8: RX sensitivity against fiber length of a QPSK transmission with constant BW_{te} of 10GHz (left) and constant BW_{sc} of 156.25MHZ (right).

Conversely, for the constant BW_{sc} assessment, the CD tolerance is higher when reducing the FFT size. This was expected since for this case a lower FFT means lower data BW so there is less delay caused by CD. The best results were obtained with 16-FFT reaching almost 2800km at a 3dB RX sensitivity penalty. The reason for the longer distance achieved in this case is because the BW_{te}

was reduced to 2.5GHz. As observed in figure 8.4 and 8.5 for this scenario there is almost no penalty on the laser $\Delta\nu$ with higher FFT sizes.

Therefore, the laser $\Delta\nu$ tolerance directly depends on the BW_{sc} i.e. on the FFT size considering a constant BW_{te}. As the FFT size is increased with a fixed BR, the BW_{sc} lowers and the effect of CD in the signal is reduced as a consequence of longer frame lengths and lower percentage of faded SC over the total, and so longer fiber distances can be achieved. However, the laser $\Delta\nu$ requirement is more stringent, i.e. the lower the BW_{sc} the less tolerance to laser $\Delta\nu$. On its side, when the modulation format increases, the tolerance to laser $\Delta\nu$ also decreases because PN affects more bits in the same symbol. Hence, the results in this chapter help to elucidate the trade-off between the BR, the FFT size, the modulation format and the laser $\Delta\nu$ which has to be considered when defining the BW allocation for each user.

Chapter 9

Conclusions and future works

9.1 General conclusions

In recent years, the use of OFDM has appeared as an attractive protocol for access PONs in order to provide the exponential demands from both, costumers and operators. The new generation of optical access networks is envisioned targeting longer reach, higher BR, higher user counts and thus more spectral efficiency. Furthermore, the operators are interested in reducing the energy consumption and extending the PONs coverage in order to reduce the required infrastructure. This implies a greater flexibility and more efficient resource management.

Precisely, OFDM has gained interest in research within this field due to its high spectral efficiency, tolerance to CD, BW granularity and elastic BW provisioning. Nevertheless, it also presents critical challenges such as the maximum capacity per user, reach and the overall cost. On this basis, the aim of this Thesis has been to explore the potential of OFDM technologies in PONs.

Firstly, several P2P oOFDM options have been reviewed. Their performance has been assessed with scenarios built in VPI and also classified according to the total BRs used by the DAC/ADCs and the sensitivities achieved. Concerning to the latter, the lowest sensitivities were achieved with scenarios based on transmitting an optical carrier from the TX, since the launched power has to be shared between the band and the carrier, and the highest with scenarios based on use an optical carrier at RX to detect the signal since it brings a power boost to the signal prior to detection. On the one hand, the conventional IM/DD (ID01) has shown the worst sensitivity and the direct-AM/DD with remote heterodyne auxiliary carrier (ADR01), the best, and on the other hand, from the point of view of DSP usage and highest data rate the homodyne direct-AM/CO with oIQ

TX (AC01) and the direct-AM/DD with oIQ TX and remote heterodyne optical carrier addition (ADR05) shows the best and the worst system performance.

Furthermore, as about the simulation scenario a main conclusion is related to the proper choice of the reference frequency parameter of the fiber in connection with CP extraction for both, SSB and DSB OFDM signals. The relation between the CP for a SSB signal and a DSB signal was mathematically obtained and it was also concluded that the CP extraction directly depends on the reference frequency. It has been seen that a proper choice consists for a DSB is set to the same than the emitting laser, and for a SSB signal is set to the RF where the remaining band is centered. Thus, the CP extraction in both cases to totally remove the ISI effect from the neighboring symbols, consisted on extracting the half of the CP length from the beginning of each OFDM symbol and the other half from the end.

The main effects due to the CD dispersion have been also studied by simulations. It has been checked that the GB reduces the DINLD, the optical filtering of one of the bands prevents the CS and the equalization avoid the PN. Nevertheless, these methods also decrease the spectral efficiency or increase the cost and complexity of the network, thus a commitment between mainly the optical fiber length and the signal BW is necessary to avoid these effects without them.

The PN due to the decorrelation between two or more optical carriers has been also analyzed and pilot tone techniques have been implemented in our OFDM coder/decoder to mitigate it. The analysis has shown that just two pilot tones are required to avoid the PN for several BR, BWs, FFTs and modulation formats. The results indicate that the PN are mostly affected by the reduction of the BW per SC, since it diminishes the tolerance to the laser linewidth. Nevertheless, a trade-off between the BR, the FFT size, the modulation format and the laser linewidth is again necessary. The study concludes that a linewidth of 1MHz, which is a cost-effective laser option, is enough for TX until QPSK and 128-FFT. In addition, in order to fix the laser tolerance for higher modulations, the FFT size should to be reduced and vice versa.

In light of the P2P oOFDM systems features identified in the study presented in chapters 2 and 4, an analysis of two oOFDM PON proposals has been made: the Accordance R-OFDMA-PON and the S-OFDMA-PON. The former is based on CO detect the ONUs with an auxiliary carrier presenting a high performance and spectral efficiency but also a high cost and PN problems. On contrary, the latter is based on DD detect the ONUs involving to allocate the ONUs spectrally separated and therefore reduce the spectral efficiency and limit the number of users but also a low-cost solution.

The rest of the Thesis is focused on the S-OFDMA-PON which has been proposed analyzed and designed based on low-cost IM/DD oOFDM system with prototypes for two ONUs and one OLT for experimental testing both, the US and DS. For the design of the ONUs boards, OBI studies have been performed concluding that a separation of 0.1nm between two adjacent users was enough to completely avoid it.

Two multiplexing strategies have been considered within the study of the S-OFDMA-PON: the digital and the multiband multiplexing approaches. While the former allows more flexibility to dynamically assign the network resources, the latter is preferred for cost and energy consumption reasons. The first experiments have been addressed to study the flexibility of the digital multiplexing approach and it has been concluded that the dynamic SC assignment has allowed to see that up to 18dB of differential link-loss, equivalent to an extra length of 90km or a split of 1:64, can be compensated.

Next, both approaches have been compared under the same conditions. The results have shown that 5-6dB are needed to double the modulation format from BPSK to QPSK in the multiband approach and a loss of around 2dB is achieved with respect to digital. Furthermore, in order to improve the performance of the multiband, a spectral GI is set between the ONU signals by tuning the electrical oscillator frequencies. For a 3dB improvement, a 6.25% and a moderate 1.56% frequency GI are needed for QPSK and BPSK, respectively. Therefore, it is concluded that the sensitivity of both approaches can be in the same level at expense of remove few SCs and loss spectral efficiency in the multiband. In addition, the frequency drifts and delay synchronization in the multiband approach have been also considered and it is seen that a BER of 10^{-3} is obtained within a drift of delay tolerance limited to $\pm$10kHz and around $\pm$5ns, respectively.

The results indicate that the improvements resulting from the reduction of energy consumption with the multiband approach offset the penalty in sensitivity. Thus, it can be concluded that the S-OFDMA-PON with multiband approach is an attractive solution for low-cost OFDM-PON.

Two algorithms for improving the performance of the PON, requiring few additional operations and keeping the implementation simple, have also been proposed. On the one hand, the SL-OFDM has been used to extend the dynamic range of the AM/DD oOFDM system (ADR01) as well as to eliminate the needed of DC-bias; on the other hand, the DL-OFDM has been used to mitigate the PAPR effects into a conventional IM/DD oOFDM (ID01) system and into the S-OFDMA-PON.

The DL-OFDM algorithm consists on folding the signal parts allocated out of the dynamic range limits (MZMs, amplifiers and so on) and adds information about the sign and the number of folds performed into the signal. This algorithm is experimentally tested in order to exhaust the MZM dynamic range for a 256-iFFT signal modulated into QPSK and an electrical BW of 5GHz. An improvement of 3dB has been obtained with DL-OFDM against C-OFDM. Afterwards, the algorithm is simulated in a DS/US S-OFDMA-PON scenario with two users for different PAPR values, BWs and modulation formats. When DS was simulated, it is observed that for PAPR higher than 8dB, the higher the PAPR, the higher the improvement of DL-OFDM over C-OFDM until a PAPR of around 13dB. This leads into a cost reduction because it relaxes the linearity requirements of the hardware used.

The SL-OFDM algorithm consists on adding information about the sam-

ple sign into the signal in order to exploit the benefits of using a MZM biased at NP for energy-efficiency. This algorithm has been experimentally tested for several modulation formats, FFT sizes and fiber lengths. The results show improvements of around 3dB with SL-OFDM against C-OFDM. Afterwards, the algorithm is simulated in a DS M2P scenario with two users for different MI values, BWs and modulation formats. It is observed that for MI lower than 2, the lower the MI, the higher the improvement of SL-OFDM over C-OFDM. Such in DL-OFDM this leads into a cost reduction.

The main downside identified in the behavior of both algorithms is the BW widening produced by the addition of the side information, since it results in an overlapping between two adjacent ONUs and therefore an additional distortion. This effect is more sensitive in the US and it has been mitigate by adding ZP or shifting one of the ONU by means the LO. Nevertheless, the improvements are very low at expense of a high ZP or spectral separation required and it also complicates the RX section. These are the main reason because it discarded from both algorithms.

Also, a study of digital-analog converter quantization effects and the minimum resolution required in an OFDMA-PON over 100km fiber length has been carried out. Firstly the tests are performed on P2P networks based on two representative scenarios of DD, the IM/DD (ID01) and the AM/DD oOFDM systems (ADR05). The results are very similar for both cases showing that a minimum resolution of 6 bits for both the ADC and DAC are needed to achieve penalties lower or equal to 1dB with respect to infinite resolution for modulation formats up to 16QAM. In addition, an US M2P scenario based on both S-OFDMA-PON approaches is analyzed fixing the ADC at the RX to 6 QB and varying the DAC QBs in both ONUs. The results show that with digital approach, if QBs of both ONUs are different, the sensitivity of the high DAC resolution ONU worsens due to the contribution of the ZP part of the low DAC resolution ONU and vice versa. Instead, with multiband approach, the sensitivity of both ONUs is totally independent since there is no ZP part because the ONUs are allocated at its respective frequencies by means of a local oscillator. The tests also show that for a BER of 10^{-3}, increasing the DAC resolution from 4 to 6 bits represents a sensitivity improvement of almost 2dB for digital and multiband approaches, correspondingly. This study allows to further reduce the overall cost of the S-OFDMA-PON proposed by optimizing the resolution of DAC/ADC.

Therefore, as a general conclusion, the S-OFDMA proposed is very attractive for low-cost PON deployments due to its flexibility which allows to reuse infrastructures already deployed. Furthermore, between both approaches analyzed, the multiband multiplexing approach presents a good alternative for a PON because on the one hand, it allows to reduce the energy requirement and the total cost of the network at the expense of just a penalty around 2dB without any kind of GI; and on the other hand, the sensitivity of one ONU due to the resolution of the DAC/ADC is not affected by its adjacent ONUs. Finally, it is also demonstrated that the addition of the DL-OFDM algorithm to the

S-OFDMA-PON enhances its sensitivity by 3dB in DS direction adding few additional operations and keeping the implementation simple.

9.2 Future research lines

During this Ph.D. Thesis, research has been developed in access networks towards a low cost solution based on intensity modulation and direct detection proposing and analyzing different alternatives of oOFDM-PON network architectures and techniques such as for example DBA to reallocate the SCs and use the power margin obtained in order to increase the optical fiber length between the ONUs and the OLT or the power split; and also the DL-OFDM algorithm to mitigate the PAPR increasing the sensitivity at the receiver. Furthermore, studies about the compensation of the PN and the reduction of the DAC/ADC resolution have been included with the aim of reducing the overall network cost.

As about DL-OFDM algorithm for PAPR mitigation algorithm performance, considering that some PAPR mitigation methods based on clipping propose the use of an additional filter such as Nyquist or square root rise cosine in order to reduce the spurious tails produced by non-linearities it is interesting to explore the potential improvements that could be derived from inclusion of such filters. Considering that DL-OFDM algorithm also adds non-linearities at the receiver signal, the use of this kind of filters is expected to also allow to reduce the spectrum tails showed in section 6.3.4.2 and thus increase the sensitivity in DS and improve the performance in US. Another interesting proposal consists on applying the DL-OFDM algorithm into methodologies based on bit and power loading and studying the impact on the PAPR reduction and power consumption. We believe that the folding signal concept opens a new avenue for exploration of new algorithms for PAPR mitigation, in which emphasis should be placed on the reduction of the required side information in order to improve the data rate efficiency. Finally, as a general issue, considering that our algorithm has shown good performance in DS transmissions, but has been found unsuitable for US, new algorithms and methodologies should be explored in order to mitigate the PAPR in US.

Also it would be interesting to extend the study about PN compensation by means of pilot tones with an experimental assessment in an US network, considering both the multiband and the digital multiplexing approaches. In this line, a promising line of research is to combine the pilot tones technique to compensate the PN effect and the DL to mitigate the PAPR and to assess their performance into oOFDM-PONs.

Finally, the results of this Thesis should encourage research into the potential contributions of the OFDM technology in commercial PONs by analyzing the connections with actual standardized multiplexing systems such the WDM or UDWDM.

Appendices

Appendix A

Research publications

A.1 Patents

- [**P1**] J. Prat, I. Cano, M. C. Santos and X. Escayola, "Método de codificación-decodificación de la amplitud de la señal mediante plegado y etiquetas de información auxiliares", app. number ES-P2011231426 (PCT/ES2013/0706-34), date 10/11/2012.

A.2 Journal Publications

- [**J1**] I. Cano, X. Escayola, P. C. Schindler, M. C. Santos, V. Polo, J. Leuthold, I. Tomkos, and J. Prat, "Experimental Demonstration of a Statistical OFDM-PON With Multiband ONUs and Elastic Bandwidth Allocation [Invited]," J. Opt. Commun. Netw. 7, A73-A79 (2015).
- [**J2**] I. Cano, M. C. Santos, V. Polo, X. Escayola, and J. Prat, "Dimensioning of OFDMA PON with non-preselected independent ONUs sources and wavelength-control," Opt. Express 20, 607-613 (2012).

A.3 Conference Publications

- [**C1**] I. Cano, X. Escayola, P. C. Schindler, M. C. Santos, V. Polo, J. Leuthold, and J. Prat, "Experimental Demonstration of Multi-band Upstream in Statistical OFDM-PONs and Comparison with Digital Subcarrier Assignment," in Optical Fiber Communication Conference, OSA Technical Digest (online) (Optical Society of America, 2014), paper Th3G.4.
- [**C2**] I. Cano, X. Escayola, A. Peralta, V. Polo, M. C. Santos, and J. Prat, "A Study of Flexible Bandwidth Allocation in Statistical OFDM-based

PON," in. Proc. of 15th ICTON, Cartagena, Spain, 2013, paper Tu.D3.1.

- [**C3**] I. Cano, A. Peralta, V. Polo, X. Escayola, M. C. Santos, and J. Prat, "Differential link-loss compensation through dynamic bandwidth assignment in statistical OFDMA-PON," in Optical Fiber Communication Conference/National Fiber Optic Engineers Conference 2013, OSA Technical Digest (online) (Optical Society of America, 2013), paper OTh3A.5.

- [**C4**] I. Cano, M. C. Santos, X. Escayola, V. Polo, E. Giacoumidis, C. Kachris, I. Tomkos, Member, IEEE, and J. Prat, Member, IEEE, "An OFDMA-PON with Non-Preselected Independent ONU Sources and Centralized Feedback Wavelength Control: Dimensioning and Experimental Results" in. Proc. of 14th ICTON, Coventry, UK, 2012, paper Tu.B3.3

- [**C5**] I. Cano, A. Peralta, X. Escayola, V. Polo, M. C. Santos, and J. Prat, "Experimental assessment of an OFDMA-based statistical PON with flexible bandwidth allocation and sign-labels," in Asia Communications and Photonics Conference, OSA Technical Digest (online) (Optical Society of America, 2012), paper PAF4C.4.

- [**C6**] I. Cano, M. C. Santos, X. Escayola, V. Polo, and J. Prat, "An OFDM-PON with non-preselected ONUs: dimensioning and experimental results," in Advanced Photonics Congress, OSA Technical Digest (online) (Optical Society of America, 2012), paper AW4A.4.

- [**C7**] I. Cano, X. Escayola, V. Polo, M. C. Santos, and J. Prat, "Sign Labeled OFDM with Intensity-Modulation Direct Detection in PON," in European Conference and Exhibition on Optical Communication, OSA Technical Digest (online) (Optical Society of America, 2012), paper P6.04.

- [**C8**] X. Escayola, I. Cano, M. C. Santos, J. Prat, "OFDM-PON performance with limited quantization," in. Proc. of 15th ICTON, Cartagena, Spain, 2013, paper We.A3.2.

- [**C9**] X. Escayola, I. Cano, M. C. Santos and J. Prat, "Laser Linewidth requirements for remote heterodyne OFDM based PON scenario," in Proc. of 16th ICTON, Graz, Austria, 2014, paper Tu.A3.6.

Appendix B

Simulation environment

This Ph.D. Thesis presents several numerical results and graphs based on a simulation environment called Virtual Photonics Interface (VPI) [76] software.

The VPI photonics^{TM} suite gathers a set of software applications designed for running photonic and optical simulations. From this suite, mainly VPItransmissionMaker^{TM} Optical Systems is the application used for the researches about optical OFDM systems in the context of this document. The results of the simulations are shown in the VPI Photonics Analyzer tool.

This tool includes design templates as a base for further developments including the issue of this. Nevertheless, new scenarios have been designed and performed in order to suit with the required characteristics. Furthermore, the OFDM coding and decoding modules offered by this software are not transparent and do not offer the flexibility required by all the tests that it wants to perform. For this reason, we programmed a Matlab$^{@}$ algorithm as a OFDM coding and decoding blocks and interconnect them with the VPI software were their electrical and optical blocks such as filters or lasers were used.

B.1 Graphical user interface, hierarchy and modular design

VPI software has a graphical user interface (GUI), that allows to design TX systems intuitively by using interconnectable blocks which simulate devices (see figure B.1) such as pseudo random bit generators, filters, optical fibers, spectrum analyzers, and so on. Each one of these blocks has settings or parameters that can be adjusted for different behaviors like voltages, frequencies, roll-off factors, etc. The blocks are provided with explanatory documentation sheets which inform of their utility, the function of the related parameters and their range of values and, finally, some of the theory behind to understand how they

were programmed, possibly including some of the equations used.

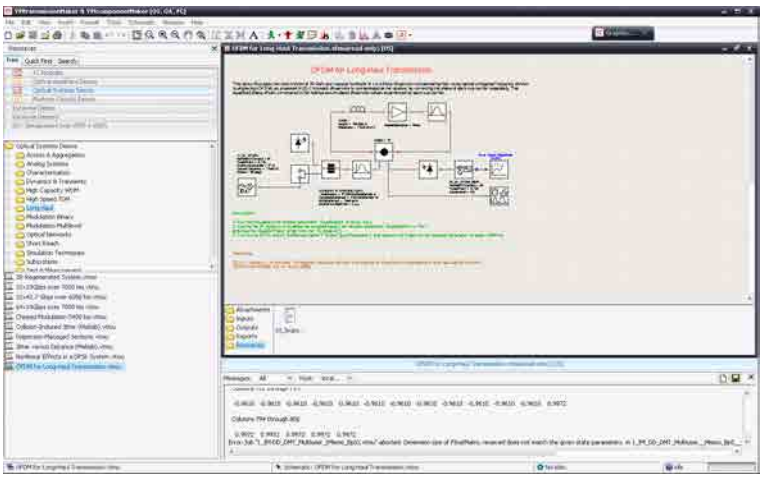

Figure B.1: VPI main window.

For more structured designs, VPI is provided with a hierarchical organization. It has up to three levels of elements or hierarchies: universe, galaxies and stars.

- **Stars**: is a third level and represents a unique module with a specific function which cannot be subdivided into other modules. It has either inputs or outputs, or both.

- **Galaxies**: is a second level and it is composed of several stars and galaxies interconnected. It has either inputs or outputs, or both, that are then used in a higher level galaxy or in the universe.

- **Universes**: is the first and top-most level. It is composed of several starts and galaxies interconnected. The lack of a complete and fully functional universe causes an error from VPI because the whole universe is simulated. It has neither inputs nor output.

With this hierarchy, it is far from difficult to have a well-organized design having in the universe the most representative modules, for example the OFDM coder and the decoder are reduced to a couple of galaxies in the systems created for this Thesis and that is what it is seen from the top level view. If modifications have to be done, just looking inside of them is enough to have access to all of their elements.

A galaxy itself may and usually has parameters. The parameters of the galaxy are added by the user conveniently. Stars and galaxies inside a galaxy are self-contained.

This means that they can only access to the variables generated within the galaxy and the parameters of the galaxy that includes them. Therefore, external data that has to be operated, have to be included in the parameters of the galaxy.

B.2 Global parameters and conditions

Over all the parameters the blocks have, there are some intrinsic to the simulation itself, also known as schematic parameters, which have to be adequately configure for appropriated results. The most relevant are: TimeWindow (TW), SampleRate (SR) and BitRate (BR).

- **TimeWindow**: this parameter sets the period in which a block of data is represented. This time will inevitably fix the spectral resolution of the simulated signals setting, i.e., the resolution of spectral displays. It is linked to the bit rate since an integer number of bits needs to be simulated.
- **SampleRate**: it determines the number of samples taken by second. Therefore if the sampling frequency is higher, the resolution in the time domain is better. This value also determines the maximum simulation frequency limited by the Nyquist rate.
- **BitRate**: it specifies the rate at which bits are TX through the system, so the transmitting BWs depend on this value.

These parameters have to be set properly to fulfill certain conditions so VPI can run the simulations. Otherwise, problems may occur and the simulations cannot be carried out.

First, an integer number of symbols must be generated at the end of the simulation (B.1) because the modulating process fails if that does not happen; for the symbol rate computation it is mandatory to know the number of bits that are used per symbol (B.2), which is accessible through the Bits per Symbols (BpS) variable. An effective solution to make the total number of symbols simulated independent of the bits is the use of the following relationship (B.5).

$$N_{symbols}[symbols] = TW \cdot SR \in \mathbb{N} \tag{B.1}$$

$$SymbolRate[\frac{symbols}{second}] = \frac{BR}{BpS} \tag{B.2}$$

VPI performs the FFT and iFFT, transparently to the user, when simulating systems to make the corresponding calculations for some blocks. By any means it is necessary to have power of two as total amount of simulated samples (B.3). For this reason, SR (B.4) and TW (B.5) must be chosen depending on the number of BpS. This way, resulting number of samples can easily fulfill the

condition since both parameters are already set to a power of 2. Then, in order to avoid problems in the simulations, the following relationships have been used:

$$SR \cdot TW = N_{samples}[samples] = 2^n \quad where \quad n \in \mathbb{N} \tag{B.3}$$

$$SR[Hz] = 2^s \cdot \frac{BR}{BpS} \tag{B.4}$$

$$TW[s] = 2^t \cdot \frac{BpS}{BR} \tag{B.5}$$

where s is 3. TW value is fixed by the total number of bits in the simulation. In our simulation a feasible result meets a BER of 10^{-3}, in order to get a significant number of errors a total of 100000 bits needs to be simulated, then t_{min} is 17 for a BPSK, 16 for a QPSK or 14 for a 16QAM.

On the other hand, the coding parameters are designed to control the common coder and decoder parameters, to avoid inconsistency between two parameters with the same name. The main parameters created in order to perform the simulation shown in this Thesis are:

- **CarrierSeparation**: this value indicates the optical frequency spacing between two optical carriers. Therefore, this value has to be added at the emission frequency of the laser block.
- **CarrierFrequency**: this value indicates the frequency where a band has to be centered in order to avoid IMD. Furthermore, it can be used as a frequency local oscillator value.
- **CP**: gives the possibility of adding a cyclic prefix writing a value between 0 and 1. In the systems studied this value is usually 0 because for fiber length considered no significant CD was generated.
- **N_FFT**: is the number of SCs available to build an OFDM signal. This parameter must be a power of two value, since represents the number of inputs of the iFFT/FFT algorithm. On its side, the Nc parameter indicates the enabled SCs.
- **ZP_Mask**: is an integer array vector which defines the SCs that will be cancelled and is activated if parameter ZP is set to ON position.
- **Vpi**: this parameter is used to indicate the working point of the MZM and it is 2. Thus, if the amplitude of the bias is Vpì/4, MZM works in QP and if it is Vpi/2, MZM works in NP.
- **ModulationIndex**: is the multiplication factor of the signal at the output of the OFDM coder.

- **Number_pilot_tones**: is the number of SCs used as a pilot tones in order to compensate the PN effects if the parameter Phase_Noise is set to ON.
- **Equalization**: if this parameter is set to ON, the number of OFDM symbols indicated by parameter N_training_value are used as a training symbols to equalize the RX signal.
- **DAC_ADC**: if this parameter is set to ON, the signal is quantized with the number of bits indicated by the parameter Nbits_Tx and Nbits_Rx allowing to set different resolutions at the TX and the RX.
- **Modulation**: this parameter indicates the modulation type: PSK or QAM.
- **SignLabeled**: if this parameter is set to ON, the SL-OFDM algorithm is applied to the TX signal and the amplitude of the side information is indicated by the parameter SLamplitude.
- **DataLabeled**: if this parameter is set to ON, the DL-OFDM algorithm is applied to the TX signal. The amplitude of the signal depends on the MZM dynamic range, so it is indicated by the parameter MZMpercent which goes from 0 to 1 being 1 the use of the overall MZM dynamic range.
- **Multilevel**: this parameter indicates the number of folds allowed by the DL-OFDM algorithm. In this Thesis, this value is always 2, but actually it can be increased.
- **Clipping**: if this parameter is set to ON, the parts of the signal after folded the number indicated by multilevel parameter, yet are above or below the dynamic range of the signal, will be clipped.

B.3 OFDM coder and decoder

On the one hand, the OFDM coder is a galaxy with an output for the analog OFDM signal and allows to simulate the digital signal processing of the BB OFDM signal; on the other hand, the OFDM decoder is also a galaxy with an input for the electrical signal after the DD and allows to reconstruct the signal sent for the subsequent calculation of the BER, the Error Vector Magnitude (EVM) and show the corresponding constellation.

Basically, the coders and decoders used in this Thesis can be classified in two types: the DMT-OFDM and the RF-OFDM in figure B.2 and B.3, correspondingly. Commonly, a pseudo random bit sequence is generated as data source and send to the Co-Simulator block which is used to interconnect the VPIphotonics^{TM} software with the Matlab$^{@}$ code. This code allows digitally to modulate the data source into an OFDM signal. At the output of the Co-Simulator block, two digital OFDM sequences are generated: the real and the imaginary parts. Both components are converted to analog signals with the

pulse shaping block that uses a root raised cosine as filter. After that point, the signal from the Co-Simulator in the DMT-OFDM coder is directly sent to the output of the block and the signal from the RF-OFDM coder needs a RF up-conversion stage before send it through the optical modulator. The reasons are deeply described in chapter 2.

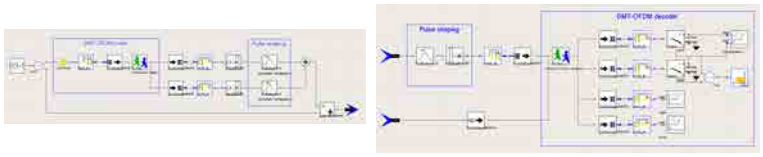

Figure B.2: DMT-OFDM coder (left) and decoder (right) VPI schematics.

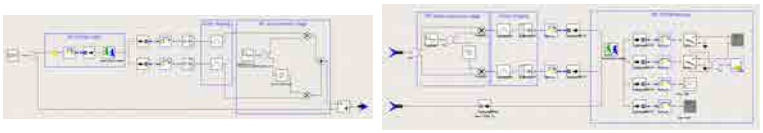

Figure B.3: RF-OFDM coder (left) and decoder (right) VPI schematics.

In the OFDM decoder the electrical signal after the detection in its inputs is amplified and duplicated for the electrical IQ for the RF down-conversion in the case of the RF-OFDM decoder and directly sent to the pulse shaping in the case of the DMT-OFDM decoder. In both cases, the resulting signal/signals goes/go to the Co-Simulator block to reconstruct again the TX bit sequence and therefore show the constellation and obtain the BER and EVM for the following evaluation of the scenario.

B.4 Optical OFDM systems designed

Once the VPI software has been introduced as well as the main parameters and the OFDM coder/decoder blocks described, all P2P oOFDM systems designed for the comparison performed in chapter 4 are illustrated following.

Figure B.4 shows the main scenario used for the IM/DD oOFDM system (ID01) and effective-AM/DD for both, with digital and analog GB (IGD01, IGD02). Obviously, the OFDM coder and decoder blocks are different since ID01 and IGD02 uses a DMT-OFDM coder and decoder, and IGD01 uses a RF-OFDM coder and decoder. As shows, the analog output signal from the OFDM coder is firstly amplified depending on the MI set. Right after, it is optically modulated by means of a MZM, which has another input for the continuous wave laser to modulate its light. At the MZM output, the signal is launched to the optical fiber and detected by a PD. Finally, the electrical signal from the DD is the input for the OFDM decoder to reconstruct the original bit sequence.

Figure B.5 corresponds with the scenario used for simulate the direct-AM/CO

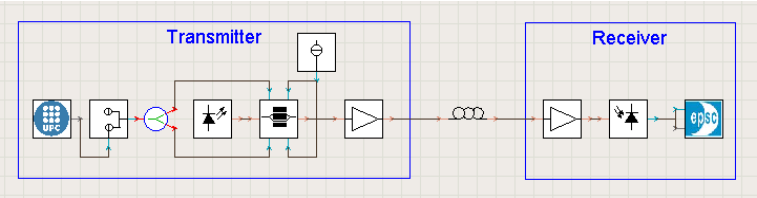

Figure B.4: IM/DD and effective-AM/DD with analog and digital GB VPI schematic (ID01, IGD01 and IGD02).

with oIQ transmitter and homodyne auxiliary carrier (AC01). In this case, both coder and decoder are DMT-OFDM. The electrical OFDM signal from the coder is amplified as in the previous scenario and then optical modulated by the oIQ transmitter composed by two MZMs and a phase shift block. Right after the optical signal is sent through the optical fiber to finally be detected by the 90º hybrid fed by the laser centered at BB. The electrical signal after the PDs is then input to the decoder.

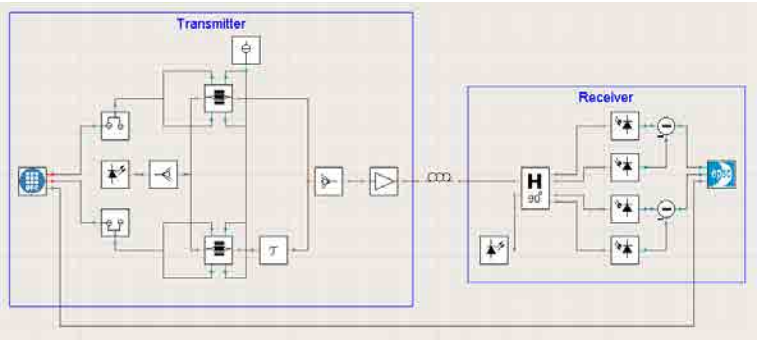

Figure B.5: AM/CO with oIQ transmitter and homodyne auxiliary carrier VPI schematic (AC01).

Figure B.6 illustrates the direct-AM/DD with remote heterodyne auxiliary laser (ADR01) oOFDM system. In this case, particularity respect to figure B.4, there is an auxiliary carrier before the PD in order to add an optical carrier to the signal and can be DD. Hence, coder is a DMT-OFDM, the MZM in biased in NP and the decoder is a RF-OFDM.

Figure B.7 and B.8 shows the VPI scenario used for simulate the direct-AM/DD with oIQ transmitter and remote heterodyne auxiliary carrier with both, and optical and electrical carrier (ADR05, ADR06). In this case, it is illustrated the main scenario and its OFDM coder in order to identify clearly the differences. An auxiliary carrier added before the PD is seen in figure B.7 as well as a coder with the structure of the DMT-OFDM, on contrary an electrical carrier added with a RF-stage at the coder is added at the electrical OFDM signal and the optical modulated so, an auxiliary optical laser is not required.

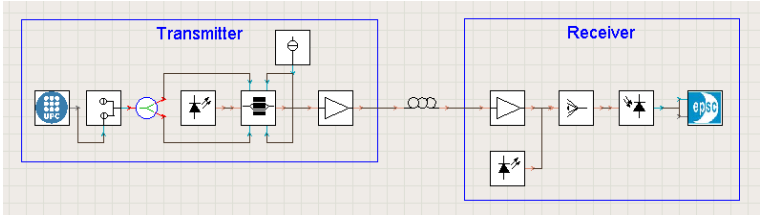

Figure B.6: Direct-AM/DD oOFDM system and remote heterodyne auxiliary laser VPI schematic (ADR01).

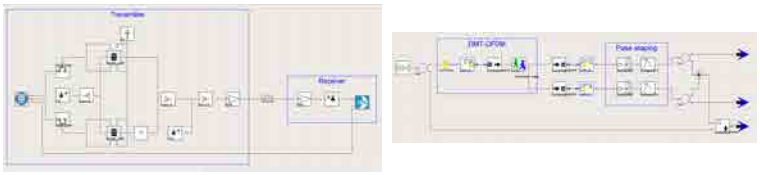

Figure B.7: Direct-AM/DD oOFDM system with oIQ modulator and remote heterodyne optical carrier addition (laser) VPI schematic (ADR05).

Finally, figure B.9 shows the VPI schematic of the effective-AM/CO with analog GB (IGC01). As already known, it is characterized by a RF up-conversion and CO detection, so the coder presents the structure of a RF-OFDM and the decoder is a DMT-OFDM. Otherwise in the image can be clearly seen the IM by means a laser and a MZM, and the CO detection by means the 90º hybrid and the corresponding two pairs of PDs. After that, the RX electrical signal is input to the RF-OFDM decoder.

B.5 Optical OFDM-PONs

Two OFDM-PON architectures were analyzed and studied in chapter 5: the R-OFDMA-PON and the S-OFDMA-PON. Following, the VPI schematics used to simulate the behavior and obtain the spectrums illustrated in such chapter are included.

Figure B.10 shows the US R-OFDMA-PON scenario. As shown, two optical carriers are obtained by means a MZM, and after filtered, one of them is used to IM the signal at the ONUs and the other is used as a remote heterodyne auxiliary carrier to feed the CO RX and thus detect the signal sent. The bit sequence is electrical modulated by a RF-OFDM coder and decoded by a DMT-OFDM decoder.

On its side, figure B.11 shows the DS direction of the R-OFDMA-PON scenario. The schematic shows again two optical carriers filtered and obtained by means a MZM fed by a laser and a sinusoid signal. After that, one optical carrier is used for a direct AM modulation of the signal and the other one

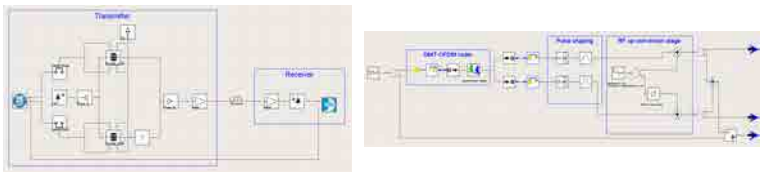

Figure B.8: Direct-AM/DD oOFDM system with oIQ modulator and remote heterodyne electrical carrier addition (RF-Tone) VPI schematic (ADR06).

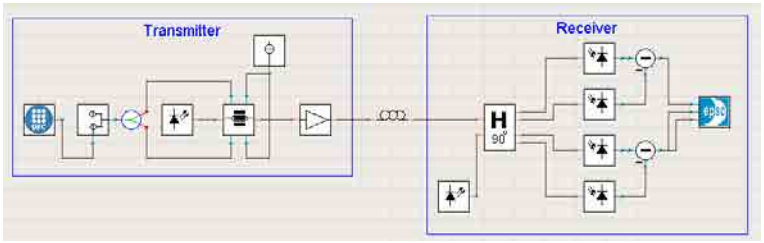

Figure B.9: Scheme of an effective-AM/CO oOFDM system with analog GB VPI schematic (IGC01).

is added after the optical modulation in the OLT to send them through the optical fiber and DD at the ONU RX. Following the same strategy than in the US direction, the OLT TX consists on a DMT-OFDM coder and the ONU RX consists on a RF-OFDM decoder.

Figure B.12 shows the US direction of the S-OFDMA-PON scenario with two ONUs. As clearly shows, both electrical signals are optically modulated by means a MZM fed by a laser. Afterwards, these signals are joined before send them through the optical fiber for finally be DD by a PD. As described in section 5.5, two approaches were used: the multiband and the digital multiplexing. The optical part of both is exactly the same, so figure B.12 are valid for both. The difference relies in the OFDM coder and decoder. As told, for simulate the digital multiplexing approach, both coders have to be DMT-OFDM as well as the decoder, on contrary for simulate the multiband multiplexing, the ONUs which are not centered in BB have to be up-converted by means an RF-stage, so they requires a RF-OFDM. Instead, the decoder is the same than in the digital multiplexing. Finally, the idea for the DS direction of the S-OFDMA-PON in figure B.13 follows the same architecture than the US.

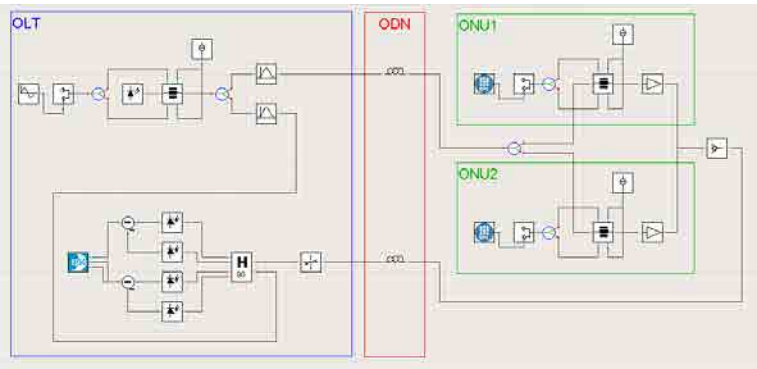

Figure B.10: Upstream R-OFDMA-PON VPI schematic.

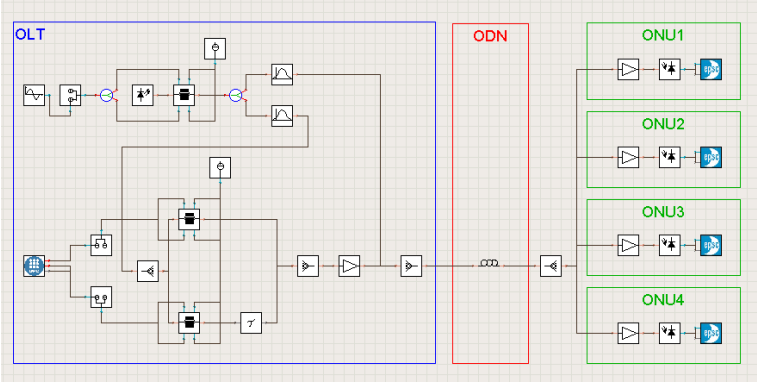

Figure B.11: Downstream R-OFDMA-PON VPI schematic.

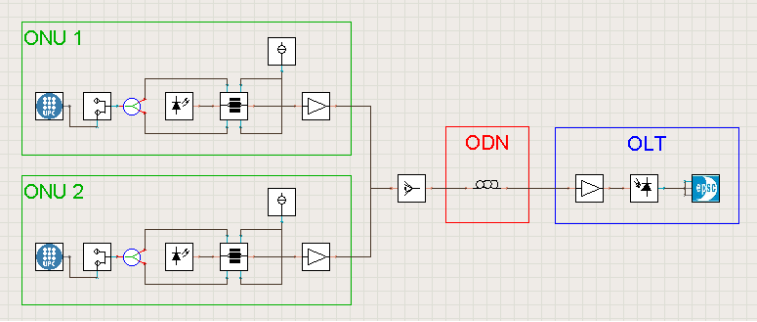

Figure B.12: Upstream S-OFDMA-PON VPI schematic.

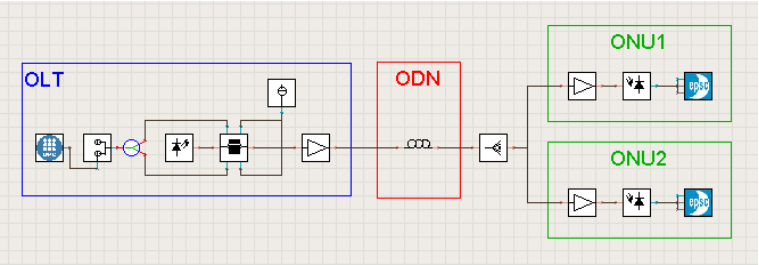

Figure B.13: Downstream S-OFDMA-PON VPI schematic.

Appendix C

Optical OFDM system tables

In this appendix several tables are presented giving information about the total BR, the effective data rate, the sensitivity at 100km, the power budget, the splitting budget and finally the number of ONUs which such system is able to provide. Each table shows the abovementioned information for the eight optical OFDM systems analyzed in chapter 4 with modulation formats of BPSK, QPSK and 16QAM and electrical BWs of 1.25GHz, 2.5GHz, 5GHz, 10GHz, 20GHz and 40GHz. This tables helps to better understand the conclusions in section 4.5 and check which optical OFDM systems fulfills the minimum conditions of an access PON from table 1.1.

Acronym	Total BR (Gbps)	Effective Data Rate (Gbps)	Sensitivity at 100km (dBm)	Power Budget (dB)	Splitting Budget (dB) at 100km	Splitting Ratio at 100km
ID01	2.5	1.25	-19.18	22.18	2.18	1
IGD02	0.625	0.625	-20.27	23.27	3.27	2
IGD01	2.5	0.625	-20.58	23.58	3.58	2
ADR06	0.625	0.625	-24.65	27.65	7.65	4
IGC01	0.625	0.625	-35.27	38.27	18.27	64
AC01	2.5	2.5	-55.43	58.43	38.43	4096
ADR05	0.625	0.625	-57.3	60.3	40.3	8192
ADR01	0.625	0.3125	-60.43	63.43	43.43	16384

Table C.1: Total and effective BR, sensitivity, power budget at B2B, splitting budget and splitting ratio at 100km for the eight optical OFDM systems in chapter 4 evaluated for the case of BPSK modulation and an electrical BW of 1.25GHz.

Acronym	Total BR (Gbps)	Effective Data Rate (Gbps)	Sensitivity at 100km (dBm)	Power Budget (dB)	Splitting Budget (dB) at 100km	Splitting Ratio at 100km
ID01	5	2.5	-17.54	20.54	0.54	1
IGD02	1.25	1.25	-18.55	21.55	1.55	1
IGD01	5	1.25	-19.02	22.02	2.02	1
ADR06	1.25	1.25	-23.08	26.08	6.08	4
IGC01	1.25	1.25	-32.3	35.3	15.3	32
AC01	5	5	-52.3	55.3	35.3	2048
ADR05	1.25	1.25	-54.49	57.49	37.49	4096
ADR01	1.25	0.625	-57.61	60.61	40.61	8192

Table C.2: Total and effective BR, sensitivity, power budget at B2B, splitting budget and splitting ratio at 100km for the eight optical OFDM systems in chapter 4 evaluated for the case of BPSK modulation and an electrical BW of 2.5GHz.

Acronym	Total BR (Gbps)	Effective Data Rate (Gbps)	Sensitivity at 100km (dBm)	Power Budget (dB)	Splitting Budget (dB) at 100km	Splitting Ratio at 100km
ID01	10	5	-13.55	16.55	-3.45	✗
IGD02	2.5	2.5	-15.11	18.11	-1.89	✗
IGD01	10	2.5	-14.41	17.41	-2.59	✗
ADR06	2.5	2.5	-21.68	24.68	4.68	2
IGC01	2.5	2.5	-28.86	31.86	11.86	8
AC01	10	10	-49.65	52.65	32.65	1024
ADR05	2.5	2.5	-51.68	54.68	34.68	2048
ADR01	2.5	1.25	-54.49	57.49	37.49	4096

Table C.3: Total and effective BR, sensitivity, power budget at B2B, splitting budget and splitting ratio at 100km for the eight optical OFDM systems in chapter 4 evaluated for the case of BPSK modulation and an electrical BW of 5GHz.

Acronym	Total BR (Gbps)	Effective Data Rate (Gbps)	Sensitivity at 100km (dBm)	Power Budget (dB)	Splitting Budget (dB) at 100km	Splitting Ratio at 100km
ID01	20	10	✗	✗	✗	✗
IGD02	5	5	✗	✗	✗	✗
IGD01	20	5	✗	✗	✗	✗
ADR06	5	5	-20.35	23.35	3.35	2
IGC01	5	5	-25.74	28.74	8.74	4
AC01	20	20	-46.36	49.36	29.36	512
ADR05	5	5	-48.55	51.55	31.55	1024
ADR01	5	2.5	-51.47	54.47	34.47	2048

Table C.4: Total and effective BR, sensitivity, power budget at B2B, splitting budget and splitting ratio at 100km for the eight optical OFDM systems in chapter 4 evaluated for the case of BPSK modulation and an electrical BW of 10GHz.

Acronym	Total BR (Gbps)	Effective Data Rate (Gbps)	Sensitivity at 100km (dBm)	Power Budget (dB)	Splitting Budget (dB) at 100km	Splitting Ratio at 100km
ID01	40	20	✗	✗	✗	✗
IGD02	10	10	✗	✗	✗	✗
IGD01	40	10	✗	✗	✗	✗
ADR06	10	10	-18.71	21.71	1.71	1
IGC01	10	10	-22.77	25.77	5.77	2
AC01	40	40	-41.36	44.36	24.36	256
ADR05	10	10	-45.43	48.43	28.43	512
ADR01	10	5	-48.58	51.58	31.58	1024

Table C.5: Total and effective BR, sensitivity, power budget at B2B, splitting budget and splitting ratio at 100km for the eight optical OFDM systems in chapter 4 evaluated for the case of BPSK modulation and an electrical BW of 20GHz.

Acronym	Total BR (Gbps)	Effective Data Rate (Gbps)	Sensitivity at 100km (dBm)	Power Budget (dB)	Splitting Budget (dB) at 100km	Splitting Ratio at 100km
ID01	80	40	✗	✗	✗	✗
IGD02	20	20	✗	✗	✗	✗
IGD01	80	20	✗	✗	✗	✗
ADR06	20	20	-17.15	20.15	0.15	1
IGC01	20	20	-19.8	22.8	2.8	1
AC01	80	80	-37.99	40.99	20.99	64
ADR05	20	20	-42.3	45.3	25.3	256
ADR01	20	10	-45.46	48.46	28.46	512

Table C.6: Total and effective BR, sensitivity, power budget at B2B, splitting budget and splitting ratio at 100km for the eight optical OFDM systems in chapter 4 evaluated for the case of BPSK modulation and an electrical BW of 40GHz.

Acronym	Total BR (Gbps)	Effective Data Rate (Gbps)	Sensitivity at 100km (dBm)	Power Budget (dB)	Splitting Budget (dB) at 100km	Splitting Ratio at 100km
ID01	5	2.5	-17.46	20.46	0.46	1
IGD02	1.25	1.25	-18.55	21.55	1.55	1
IGD01	5	1.25	-18.59	21.59	1.59	1
ADR06	1.25	1.25	-23.08	26.08	6.08	4
IGC01	2.5	2.5	-31.99	34.99	14.99	16
AC01	5	5	-51.68	54.68	34.68	2048
ADR05	1.25	1.25	-53.55	56.55	36.55	4096
ADR01	1.25	0.625	-56.99	59.99	39.99	8192

Table C.7: Total and effective BR, sensitivity, power budget at B2B, splitting budget and splitting ratio at 100km for the eight optical OFDM systems in chapter 4 evaluated for the case of QPSK modulation and an electrical BW of 1.25GHz.

Acronym	Total BR (Gbps)	Effective Data Rate (Gbps)	Sensitivity at 100km (dBm)	Power Budget (dB)	Splitting Budget (dB) at 100km	Splitting Ratio at 100km
ID01	10	5	-15.9	18.9	-1.1	✗
IGD02	2.5	2.5	-16.83	19.83	-0.17	✗
IGD01	10	2.5	-16.99	19.99	-0.01	✗
ADR06	2.5	2.5	-21.52	24.52	4.52	2
IGC01	2.5	2.5	-28.71	31.71	11.71	8
AC01	10	10	-48.71	51.71	31.71	1024
ADR05	2.5	2.5	-50.74	53.74	33.74	2048
ADR01	2.5	1.25	-53.86	56.86	36.86	4096

Table C.8: Total and effective BR, sensitivity, power budget at B2B, splitting budget and splitting ratio at 100km for the eight optical OFDM systems in chapter 4 evaluated for the case of QPSK modulation and an electrical BW of 2.5GHz.

Acronym	Total BR (Gbps)	Effective Data Rate (Gbps)	Sensitivity at 100km (dBm)	Power Budget (dB)	Splitting Budget (dB) at 100km	Splitting Ratio at 100km
ID01	20	10	-11.36	14.36	-5.64	✗
IGD02	5	5	-13.08	16.08	-3.92	✗
IGD01	20	5	-12.69	15.69	-4.31	✗
ADR06	5	5	-20.04	23.04	3.04	2
IGC01	5	5	-25.9	28.9	8.9	4
AC01	20	20	-45.74	48.74	28.74	512
ADR05	5	5	-47.61	48.74	28.74	1024
ADR01	5	2.5	-51.05	54.05	34.05	2048

Table C.9: Total and effective BR, sensitivity, power budget at B2B, splitting budget and splitting ratio at 100km for the eight optical OFDM systems in chapter 4 evaluated for the case of QPSK modulation and an electrical BW of 5GHz.

Acronym	Total BR (Gbps)	Effective Data Rate (Gbps)	Sensitivity at 100km (dBm)	Power Budget (dB)	Splitting Budget (dB) at 100km	Splitting Ratio at 100km
ID01	40	20	✗	✗	✗	✗
IGD02	10	10	✗	✗	✗	✗
IGD01	40	10	✗	✗	✗	✗
ADR06	10	10	-18.71	21.71	1.71	1
IGC01	10	10	-22.3	28.9	8.9	4
AC01	40	40	-42.61	45.61	25.61	256
ADR05	10	10	-44.49	47.49	27.49	512
ADR01	10	5	-47.8	50.8	30.8	1024

Table C.10: Total and effective BR, sensitivity, power budget at B2B, splitting budget and splitting ratio at 100km for the eight optical OFDM systems in chapter 4 evaluated for the case of QPSK modulation and an electrical BW of 10GHz.

Acronym	Total BR (Gbps)	Effective Data Rate (Gbps)	Sensitivity at 100km (dBm)	Power Budget (dB)	Splitting Budget (dB) at 100km	Splitting Ratio at 100km
ID01	80	40	✗	✗	✗	✗
IGD02	20	20	✗	✗	✗	✗
IGD01	80	20	✗	✗	✗	✗
ADR06	20	20	-17.15	20.15	0.15	1
IGC01	20	20	-19.3	25.3	5.3	2
AC01	80	80	-37.61	40.61	20.51	64
ADR05	20	20	-41.68	44.68	24.68	256
ADR01	20	10	-44.83	47.83	27.83	512

Table C.11: Total and effective BR, sensitivity, power budget at B2B, splitting budget and splitting ratio at 100km for the eight optical OFDM systems in chapter 4 evaluated for the case of QPSK modulation and an electrical BW of 20GHz.

Acronym	Total BR (Gbps)	Effective Data Rate (Gbps)	Sensitivity at 100km (dBm)	Power Budget (dB)	Splitting Budget (dB) at 100km	Splitting Ratio at 100km
ID01	160	80	✗	✗	✗	✗
IGD02	40	40	✗	✗	✗	✗
IGD01	160	40	✗	✗	✗	✗
ADR06	40	40	-15.51	18.51	-1.49	✗
IGC01	40	40	-16.52	19.52	-0.48	✗
AC01	160	160	-33.99	36.99	16.99	32
ADR05	40	40	-38.55	41.55	21.55	128
ADR01	40	20	-41.86	44.86	24.86	256

Table C.12: Total and effective BR, sensitivity, power budget at B2B, splitting budget and splitting ratio at 100km for the eight optical OFDM systems in chapter 4 evaluated for the case of QPSK modulation and an electrical BW of 40GHz.

Acronym	Total BR (Gbps)	Effective Data Rate (Gbps)	Sensitivity at 100km (dBm)	Power Budget (dB)	Splitting Budget (dB) at 100km	Splitting Ratio at 100km
ID01	10	5	-12.93	15.93	-4.07	✗
IGD02	2.5	2.5	-13.86	16.86	-3.14	✗
IGD01	10	2.5	-14.1	17.1	-2.9	✗
ADR06	2.5	2.5	-18.55	21.55	1.55	1
IGC01	2.5	2.5	-23.24	26.24	6.24	4
AC01	10	10	-42.93	45.93	25.93	256
ADR05	2.5	2.5	-44.8	47.8	27.8	512
ADR01	2.5	1.25	-48.4	51.4	31.4	1024

Table C.13: Total and effective BR, sensitivity, power budget at B2B, splitting budget and splitting ratio at 100km for the eight optical OFDM systems in chapter 4 evaluated for the case of 16QAM modulation and an electrical BW of 1.25GHz.

Acronym	Total BR (Gbps)	Effective Data Rate (Gbps)	Sensitivity at 100km (dBm)	Power Budget (dB)	Splitting Budget (dB) at 100km	Splitting Ratio at 100km
ID01	20	10	-11.21	14.21	-5.79	✗
IGD02	5	5	-11.99	14.99	-5.01	✗
IGD01	20	5	-12.03	15.03	-4.97	✗
ADR06	5	5	-16,83	19.83	-0.17	✗
IGC01	5	5	-20.11	23.11	3.11	2
AC01	20	20	-40.11	43.11	23.11	128
ADR05	5	5	-41.99	44.99	24.99	256
ADR01	5	2.5	-45.43	48.43	28.43	512

Table C.14: Total and effective BR, sensitivity, power budget at B2B, splitting budget and splitting ratio at 100km for the eight optical OFDM systems in chapter 4 evaluated for the case of 16QAM modulation and an electrical BW of 2.5GHz.

Acronym	Total BR (Gbps)	Effective Data Rate (Gbps)	Sensitivity at 100km (dBm)	Power Budget (dB)	Splitting Budget (dB) at 100km	Splitting Ratio at 100km
ID01	40	20	✗	✗	✗	✗
IGD02	10	10	-5.11	8.11	-11.88	✗
IGD01	40	10	-4.49	7.49	-12.51	✗
ADR06	10	10	-15.27	18.27	-1.73	✗
IGC01	10	10	-16.36	19.36	-0.64	✗
AC01	40	40	-36.99	39.99	19.99	64
ADR05	10	10	-38.86	41.86	21.86	128
ADR01	10	5	-42.3	45.3	25.3	256

Table C.15: Total and effective BR, sensitivity, power budget at B2B, splitting budget and splitting ratio at 100km for the eight optical OFDM systems in chapter 4 evaluated for the case of 16QAM modulation and an electrical BW of 5GHz.

Acronym	Total BR (Gbps)	Effective Data Rate (Gbps)	Sensitivity at 100km (dBm)	Power Budget (dB)	Splitting Budget (dB) at 100km	Splitting Ratio at 100km
ID01	80	40	✗	✗	✗	✗
IGD02	20	20	✗	✗	✗	✗
IGD01	80	20	✗	✗	✗	✗
ADR06	20	20	-14.33	17.33	-2.67	✗
IGC01	20	20	-14.2	17.2	-2.8	✗
AC01	80	80	-33.55	36.55	16.55	32
ADR05	20	20	-35.74	38.74	18.74	64
ADR01	20	10	-39.99	42.99	22.99	128

Table C.16: Total and effective BR, sensitivity, power budget at B2B, splitting budget and splitting ratio at 100km for the eight optical OFDM systems in chapter 4 evaluated for the case of 16QAM modulation and an electrical BW of 10GHz.

Acronym	Total BR (Gbps)	Effective Data Rate (Gbps)	Sensitivity at 100km (dBm)	Power Budget (dB)	Splitting Budget (dB) at 100km	Splitting Ratio at 100km
ID01	160	80	✗	✗	✗	✗
IGD02	40	40	✗	✗	✗	✗
IGD01	160	40	✗	✗	✗	✗
ADR06	40	40	-12.61	15.61	-4.39	✗
IGC01	40	40	-11.49	14.49	-5.51	✗
AC01	160	160	-28.24	31.24	11.24	8
ADR05	40	40	-32.61	35.61	15.61	32
ADR01	40	20	-37.02	40.02	20.02	64

Table C.17: Total and effective BR, sensitivity, power budget at B2B, splitting budget and splitting ratio at 100km for the eight optical OFDM systems in chapter 4 evaluated for the case of 16QAM modulation and an electrical BW of 20GHz.

Acronym	Total BR (Gbps)	Effective Data Rate (Gbps)	Sensitivity at 100km (dBm)	Power Budget (dB)	Splitting Budget (dB) at 100km	Splitting Ratio at 100km
ID01	320	160	✗	✗	✗	✗
IGD02	80	80	✗	✗	✗	✗
IGD01	320	80	✗	✗	✗	✗
ADR06	80	80	-10.9	13.9	-6.1	✗
IGC01	80	80	-7.61	10.61	-9.38	✗
AC01	320	320	-25.99	28.99	8.99	4
ADR05	80	80	-29.49	32.49	12.49	16
ADR01	80	40	-33.43	36.43	16.43	32

Table C.18: Total and effective BR, sensitivity, power budget at B2B, splitting budget and splitting ratio at 100km for the eight optical OFDM systems in chapter 4 evaluated for the case of 16QAM modulation and an electrical BW of 40GHz.

Appendix D

Algorithms without side information for SL-OFDM

Firstly, a direct-AM/DD oOFDM system with just one MZM biased at NP and without the auxiliary carrier as in ADR01 is used to detect correctly the signal without any kind of side information. These algorithms aim to increase the spectral efficiency to 100% at expense of increasing the complexity.

In the first algorithm, the signal is oversampled in order to obtain the value allocated between two useful samples to determine whether the sign of the sample has been changed or not. Specifically, if the sample has a value of 0, or close to it, means that the original signal has gone through null axis at that point, and therefore the sign has changed; on contrary, if it is allocated far away of the null axis, the sign has not changed. Thus, theoretically, ensuring the sign of the first sample and following the abovementioned premises, the original signal can be recovered.

As can be observed in figure D.1 (left), most of the oversample values fulfill the condition exposed. Unfortunately, when a sample is detected wrong, the sign decision is also wrong and taking into account that the sign of the next sample depends on the previous, there is a concatenation of errors which makes impossible to recover the correct signal. Specifically, the red zone of the figure corresponds to errors since there are two oversampled values close to null axis but in the original signal the sign has not changed. This means that, the errors in the decision of the sign are concatenated from that zone onward. After an amount of tests, it has been concluded that there is not a threshold which allows to ensure the correct decision of all sign changes without introducing any kind of error. So, this proposal was rejected because of the high number of errors entailed.

In the second algorithm, a straight line joining two consecutive samples with different signs is calculated (green lines in figure D.1 right). If the adjacent

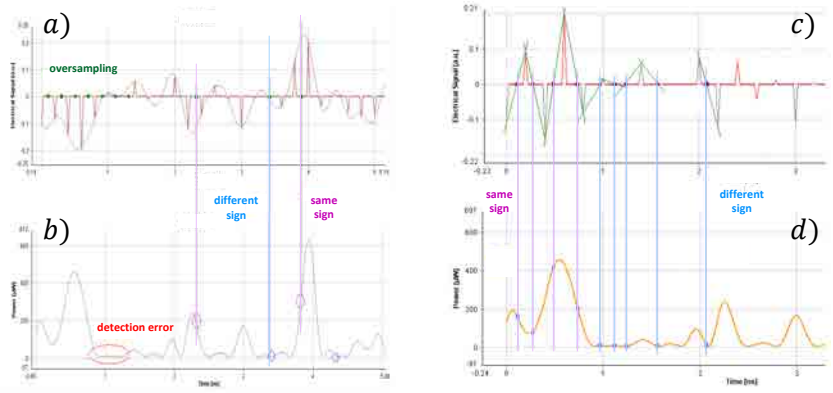

Figure D.1: Electrical signal at the OFDM coder (a), and electrical signal after the DD (b) of the first proposal and, electrical signal at the OFDM coder (c), and electrical signal after the DD (d) of the second proposal.

sample has the same sign, it will be also considered the opposite since the objective is just to obtain the straight line. This line is used to identify the sample for which it crosses the null axis. Afterwards, the location obtained is used in the RX signal to observe whether the corresponding sample is close or far from the null axis as it is illustrated in figure D.1 (d). Finally, as in the previous algorithm, when such sample is close from the null axis is translated into a sign changed; otherwise, the sign remains the same.

Thus, considering that the first sign sample is already known, the first green line is calculated and the decision performed. Once the sign of the second sample has been engaged, the next straight imagine line is calculated and the sign decision performed. This process has to be applied until the last sample. Unfortunately, this algorithm presents the same drawbacks than the previous. There is no a threshold to determine correctly the signs of all samples and one decision error will be concatenated until randomly, the sign is well recover again. Furthermore, calculating each of the imaginary straight critically increases the RX complexity. Therefore, this proposal is also rejected.

The main idea of the third algorithm relies on determine the shape of the signal interval between two useful samples using a specific number of equidistant points. As figure D.2 illustrates, if a specific interval shape is concave means that the sign has changed, on contrary, a convex shape is translated into a sign maintained. The algorithm allows to choose the number of equidistant points used to determine the shape of each interval. Thus, the more points, the more probability to determine the correct shape of the interval and thus, to correct decide if the sign has changed or not.

Nevertheless, this algorithm was also rejected since on the one hand presents the same problems than the previous two and on the other hand the minimum number of points needed to ensure the properly sign decision in all cases would

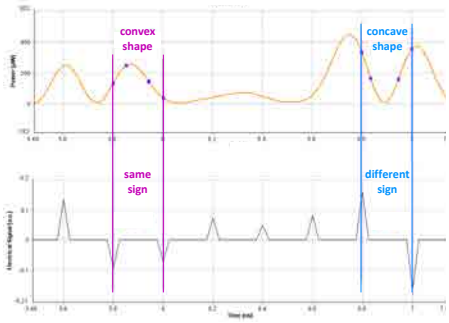

Figure D.2: Electrical signal at the OFDM coder (top) and electrical signal after the DD (bottom) of the third algorithm proposed.

be computationally unfeasible. Furthermore, when the interval shape is just an increasing or a decreasing straight line is also impossible to ensure if the sign was changed or not.

A last attempt to detect the signal without side information was carried on by enhancing the values close to null axis and set a threshold to consider if the values are enough far from null axis to consider if the sign is changed or not. Thus, the RX signal is oversampled to obtain the values situated in the middle of two useful samples and the inverse of that oversampled signal is performed to increase the critical values next to null axis and reduce the rest of the signal.

As it is seen in figure D.3, this proposal is also unfeasible, since as occurs in the previous algorithms, the threshold set will never be too fine to properly identify all sign changes, besides one error will affect the rest of the signal.

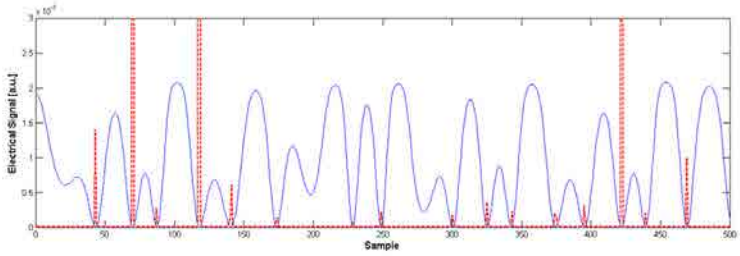

Figure D.3: Electrical signal (blue) after the DD of the fourth algorithm proposed. The red signal corresponds to the inverse of the blue signal.

Therefore, algorithms using side information in order to determine whether a sample is negative or positive have been used in chapter 6, at expense of BW efficiency reduction.

Appendix E

Side information-based proposals for SL-OFDM

As in section 6.3.2, in order to choose the optimal amplitude for the SL, is instructive to have a look into a typical sample value distribution. Figure E.1 (left) shows the original data distribution with an electrical BW of 2.5GHz and a 128-iFFT signal modulated into QPSK. The total amount of samples analyzed was 32000. As seen at the left side, 90% of the data distribution is comprised between 0 and 0.5, being 1 the maximum signal amplitude. It is therefore convenient to choose the 0 and 0.5 values for the SLs corresponding with the negative and positive values, respectivey. Figure E.1 (right) depicts the distribution of the SL vector from which it can be concluded that there are almost the same number of negative and positive values.

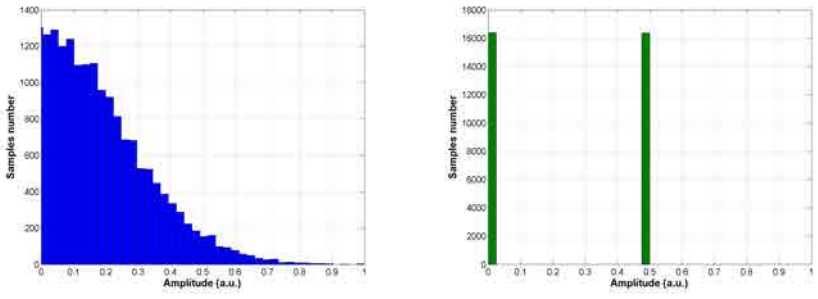

Figure E.1: TX original data distribution (left) and TX sign label distribution (right) for a 128-iFFT signal modulated into QPSK.

Such in section 6.3.2, the same four strategies to distribute the DL within the data signal were proposed and analyzed with a P2P direct-AM/DD without auxiliary carrier at the RX and with a MZM biased at $V_{\pi/2}$ (NP). Furthermore,

the electrical signal is multiplied by the MI in order to regulate its amplitude considering a MI of 1 associated with the 100% of the MZM dynamic range usage. The rest of the features are the same than in SL-OFDM.

Figure E.2 illustrates the power penalty for a BER of 10^{-3} against the MI between the four proposals and modulated into both, BPSK (asterisks) and QPSK (diamonds) with an electrical BW of 2.5GHz. As it can be checked, the best method independent of the modulation format is again allocating the SL interleaved with OFDM data symbols. The best sensitivity results of approach -35dBm are obtained for MIs from 0.5 to 1 with a 1.2 dB penalty difference between the best (interleaved SL) and the worst (SL at the end).

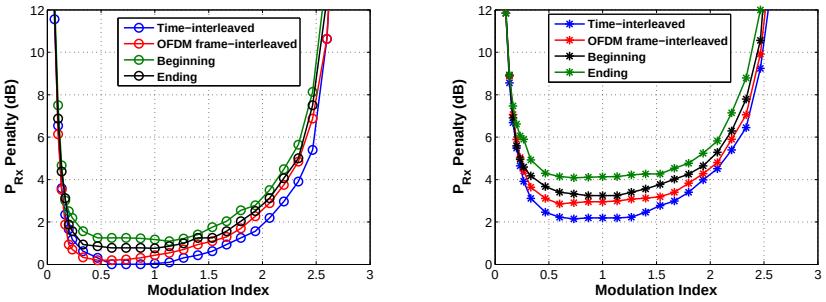

Figure E.2: Sensitivity penalty at a BER of 10^{-3} against MI of all SL distribution proposals of a signal modulated in BPSK (left) and QPSK (right) with an electrical BW of 2.5GHz.

In the following sections, SL-OFDM algorithm is analyzed and compared with a P2P conventional IM/DD oOFDM scenario through both, VPI simulations and laboratory experiments. After that, this algorithm will be also exploited in a PON.

Bibliography

[1] Shaddad, Redhwan Q., et al. "Emerging optical broadband access networks from TDM PON to OFDM PON." RN 3 (2012): 4.

[2] Effenberger, Frank. "Progress in optical access standards." Joint ITU/IEEE Workshop on Ethernet-Emerging Applications and Technologies, Geneva. 2012.

[3] Nate Anderson, "The internet of tomorrow: 100Gbps to your house by 2030," in Arstechnica, March 9, 2010.

[4] Kanonakis, Konstantinos, et al. "ACCORDANCE: A novel OFDMA-PON paradigm for ultra-high capacity converged wireline-wireless access networks."Transparent Optical Networks (ICTON), 2010 12th International Conference on. IEEE, 2010.

[5] Faulkner, David W., et al. "Optical networks for local loop applications."Lightwave Technology, Journal of 7.11 (1989): 1741-1751.

[6] Shumate, P. W. "Optical communications for the public network." 2nd International Conference and Exhibition on Opto-electronics, Kobe, Japan. 1990.

[7] Luo, Yuanqiu, et al. "Resource management for broadband access over time-division multiplexed passive optical networks." Network, IEEE 21.5 (2007): 20-27.

[8] Banerjee, Amitabha, et al. "Wavelength-division-multiplexed passive optical network (WDM-PON) technologies for broadband access: a review [Invited]."Journal of optical networking 4.11 (2005): 737-758.

[9] Park, Soo-Jin, et al. "Fiber-to-the-home services based on wavelength-division-multiplexing passive optical network." Journal of Lightwave Technology 22.11 (2004): 2582.

[10] Spirou, S., et al. "SARDANA: an all-optical access-metro WDM/TDM-PON." (2011).

[11] Prat, Josep, et al. "Results from EU project SARDANA on 10G extended reach WDM PONs." Optical Fiber Communication Conference. Optical Society of America, 2010.

[12] Hui, Rongqing, et al. "Subcarrier multiplexing for high-speed optical transmission." Journal of lightwave technology 20.3 (2002): 417.

[13] Darcie, Thomas E. "Subcarrier multiplexing for multiple-access lightwave networks." Lightwave Technology, Journal of 5.8 (1987): 1103-1110.

[14] Jansen, Sander L. "Short Course OFC, 2010." SC341 OFDM for Optical Communications (Short Course OFC, 2010).

[15] Armstrong, Jean. "OFDM for optical communications." Lightwave Technology, Journal of 27.3 (2009): 189-204.

[16] Cvijetic, Neda. "OFDM for next-generation optical access networks." Lightwave Technology, Journal of 30.4 (2012): 384-398.

[17] Qian, Dayou, et al. "A novel OFDMA-PON architecture with source-free ONUs for next-generation optical access networks." IEEE Photonics Technology Letters 17.21 (2009): 1265-1267.

[18] Vetter, Peter. "Next generation optical access technologies." European Conference and Exhibition on Optical Communication. Optical Society of America, 2012.

[19] Pan, Qi, and Roger J. Green. "Bit-error-rate performance of lightwave hybrid AM/OFDM systems with comparison with AM/QAM systems in the presence of clipping impulse noise." Photonics Technology Letters, IEEE 8.2 (1996): 278-280.

[20] Lowery, Arthur J., Liang Du, and Jean Armstrong. "Orthogonal frequency division multiplexing for adaptive dispersion compensation in long haul WDM systems." Optical Fiber Communication Conference. Optical Society of America, 2006.

[21] Vishwkarma, Lokendra, et al. "Optical Orthogonal Frequency Division Multiplexing: System Concepts and Applications for High Speed Photonic Communication."

[22] Jansen, Sander L., et al. "Optical OFDM–A Candidate for Future Long-Haul Optical Transmission Systems." Optical Fiber Communication Conference. Optical Society of America, 2008.

[23] Cvijetic, Milorad. Optical transmission systems engineering. Artech House, 2004.

[24] Ip, Ezra, and Joseph M. Kahn. "Increasing optical fiber transmission capacity beyond next-generation systems." LEOS 2008-21st Annual Meeting of the IEEE Lasers and Electro-Optics Society. 2008.

[25] Essiambre, René-Jean, et al. "Capacity limits of optical fiber networks."Lightwave Technology, Journal of 28.4 (2010): 662-701.

[26] Jansen, Sander Lars, et al. "121.9-Gb/s PDM-OFDM transmission with 2-b/s/Hz spectral efficiency over 1000 km of SSMF." Journal of Lightwave Technology 27.3 (2009): 177-188.

[27] Sano, Akihide, et al. "No-guard-interval coherent optical OFDM for 100-Gb/s long-haul WDM transmission." Journal of Lightwave Technology 27.16 (2009): 3705-3713.

[28] Shieh, W., Q. Yang, and Y. Ma. "107 Gb/s coherent optical OFDM transmission over 1000-km SSMF fiber using orthogonal band multiplexing."Optics express 16.9 (2008): 6378-6386.

[29] Shieh, W., et al. "Theoretical and experimental study on PMD-supported transmission using polarization diversity in coherent optical OFDM systems."Optics Express 15.16 (2007): 9936-9947.

[30] Sierens, C., et al. "Subcarrier multiple access for passive optical networks and comparison to other multiple access techniques." Global Telecommunications Conference, 1991. GLOBECOM'91.'Countdown to the New Millennium. Featuring a Mini-Theme on: Personal Communications Services. IEEE, 1991.

[31] Luo, Yuanqiu, et al. "Time-and wavelength-division multiplexed passive optical network (TWDM-PON) for next-generation PON stage 2 (NG-PON2)." Lightwave Technology, Journal of 31.4 (2013): 587-593.

[32] Le, Quang Trung, et al. "TDM/DWDM PON extender for 10 Gbit/s downstream transmission." European Conference and Exposition on Optical Communications. Optical Society of America, 2011.

[33] Kang, Jeung-Mo, and Sang-Kook Han. "A novel hybrid WDM/SCM-PON sharing wavelength for up-and down-link using reflective semiconductor optical amplifier." Photonics Technology Letters, IEEE 18.3 (2006): 502-504.

[34] Hsueh, Yu-Ting, et al. "A novel lightwave centralized bidirectional hybrid access network: seamless integration of RoF with WDM-OFDM-PON." Photonics Technology Letters, IEEE 23.15 (2011): 1085-1087.

[35] Qian, Dayou, et al. "41.25 Gb/s real-time OFDM receiver for variable rate WDM-OFDMA-PON transmission." Optical Fiber Communication Conference. Optical Society of America, 2010.

[36] Petermann, Klaus. Laser diode modulation and noise. Vol. 3. Springer Science & Business Media, 2012.

[37] Yariv, Amnon, and Pochi Yeh. "Optical waves in crystal propagation and control of laser radiation." (1983).

[38] Akca, Imran B., et al. "Electro-optic and electro-absorption characterization of InAs quantum dot waveguides." Optics express 16.5 (2008): 3439-3444.

[39] Tang, Chao, et al. "Spectrum efficiency improvement of directly detected OFDM based on balance receiver." Communications and Photonics Conference and Exhibition (ACP), 2009 Asia. Vol. 2009. IEEE, 2009.

[40] Lin, Bangjiang, et al. "Comparison of DSB and SSB transmission for OFDM-PON [Invited]." Journal of Optical Communications and Networking 4.11 (2012): B94-B100.

[41] Peng, Wei-Ren. "Analysis of laser phase noise effect in direct-detection optical OFDM transmission." Journal of Lightwave Technology 28.17 (2010): 2526-2536.

[42] Shieh, William, and Ivan Djordjevic. Orthogonal frequency division multiplexing for optical communications. Vol. 14. Academic press, 2010.

[43] Schmidt, Brendon JC, Arthur James Lowery, and Jean Armstrong. "Experimental demonstrations of electronic dispersion compensation for long-haul transmission using direct-detection optical OFDM." Journal of Lightwave Technology 26.1 (2008): 196-203.

[44] Shieh, W_, Hongchun Bao, and Y. Tang. "Coherent optical OFDM: theory and design." Optics Express 16.2 (2008): 841-859..

[45] Konnerth, K. L., and B. R. Shah. "Optical transmission utilizing injection light sources." Spectrum, IEEE 7.9 (1970): 37-46.

[46] Eliseev, P. G., I. Ismailov, and Yu F. Fedorov. "Injection lasers for multichannel optical communication." Quantum Electronics, IEEE Journal of 6.1 (1970): 38-41.

[47] Rediker, Robert H., and F. J. Leonbercer. "Analysis of integrated-optics near 3 dB coupler and Mach-Zehnder interferometric modulator using four-port scattering matrix." Microwave Theory and Techniques, IEEE Transactions on30.10 (1982): 1801-1804.

[48] Suzuki, M., et al. "Dynamic spectral width of an InGaAsP/InP electroabsorption light modulator under high-frequency large-signal modulation." Electronics Letters 22.6 (1986): 312-313.

[49] Saleh, Bahaa EA, Malvin Carl Teich, and Bahaa E. Saleh. Fundamentals of photonics. Vol. 22. New York: Wiley, 1991.

[50] Peucheret, Christophe. "Direct and external modulation of light." Technical University of Denmark, Denmark (2009).

[51] Pham, Dung Tien, et al. "Laser phase noise and OFDM symbol duration effects on the performance of direct-detection based optical OFDM access network."Optical Fiber Technology 17.3 (2011): 252-257.

[52] Jin, Xianqing, Roger Giddings, and Jianming Tang. "Experimental demonstration of adaptive bit and/or power loading for maximising real-time end-to-end optical OFDM transmission performance." National Fiber Optic Engineers Conference. Optical Society of America, 2011.

[53] Yang, Qi, William Shieh, and Yiran Ma. "Bit and power loading for coherent optical OFDM." IEEE Photonics Technology Letters 15.20 (2008): 1305-1307.

[54] Buchali, Fred, Roman Dischler, and Xiang Liu. "Optical OFDM: A promising high-speed optical transport technology." Bell Labs Technical Journal 14.1 (2009): 125-146.

[55] Giddings, R. P., et al. "First experimental demonstration of real-time optical OFDM transceivers." ECOC 2009 (2009).

[56] Paul, Henning, and Karl-Dirk Kammeyer. "Subcarrier selection for IM/DD OFDM systems." ECOC 2009 (2009).

[57] Dischler, Roman, and Fred Buchali. "Experimental assessment of a direct detection optical OFDM system targeting 10Gb/s and beyond." Optical Fiber Communication Conference. Optical Society of America, 2008.

[58] Takahashi, Hidenori. "Coherent OFDM transmission with high spectral efficiency." ECOC 2009 (2009).

[59] Jansen, Sander L., et al. "Coherent optical 25.8-Gb/s OFDM transmission over 4160-km SSMF." Journal of Lightwave Technology 26.1 (2008): 6-15.

[60] Giacoumidis, E., et al. "Improved transmission performance of adaptively modulated optical OFDM signals over directly modulated DFB laser-based IMDD links using adaptive cyclic prefix." Optics express 16.13 (2008): 9480-9494.

[61] Tang, J. M., and K. Alan Shore. "30-Gb/s signal transmission over 40-km directly modulated DFB-laser-based single-mode-fiber links without optical amplification and dispersion compensation." Journal of Lightwave Technology24.6 (2006): 2318.

[62] Cvijetic, Neda, Dayou Qian, and Ting Wang. "10Gb/s free-space optical transmission using OFDM." Optical Fiber Communication Conference. Optical Society of America, 2008.

[63] Lei, Ming, et al. "Adaptive loading based on frequency-selective fading estimation for ultra high-data-rate OFDM system." Vehicular Technology Conference, 2004. VTC2004-Fall. 2004 IEEE 60th. Vol. 1. IEEE, 2004.

[64] Oh, Ji Sung, Young Mo Chung, and Sang Uk Lee. "A carrier synchronization technique for OFDM on the frequency-selective fading environment." Vehicular Technology Conference, 1996. Mobile Technology for the Human Race., IEEE 46th. Vol. 3. IEEE, 1996.

[65] Tan, Peng, and Norman C. Beaulieu. "Precise BER analysis of π/4-DQPSK OFDM with carrier frequency offset over frequency selective fast fading channels." Wireless Communications, IEEE Transactions on 6.10 (2007): 3770-3780.

[66] Carlson, A. Bruce, Paul B. Crilly, and Janet C. Rutledge. "Communication systems: an introduction to signals and noise in electrical communication."Guía Académica (1986): 129.

[67] Peng, Wei-Ren, et al. "Spectrally efficient direct-detected OFDM transmission incorporating a tunable frequency gap and an iterative detection techniques."Lightwave Technology, Journal of 27.24 (2009): 5723-5735.

[68] Cano, Ivan N., Maria C. Santos, and Josep Prat. "Optimum carrier to signal power ratio for remote heterodyne DD-OFDM in PONs." IEEE Photonics Technology Letters 13.25 (2013): 1242-1245.

[69] Jung, Sang-Min, et al. "Optical beat interference noise reduction by using out-of-band RF clipping tone signal in remotely fed OFDMA-PON link." Optics express 22.15 (2014): 18246-18253.

[70] Kawanishi, Tetsuya, Takahide Sakamoto, and Masayuki Izutsu. "Study of precise optical modulation using Mach-Zehnder interferometers for advanced modulation formats." ECOC 2007 (2007).

[71] Sugihara, Takashi, Tsuyoshi Yoshida, and Kazuyuki Ishida. "Effect of modulator bias control in the presence of a finite extinction ratio in DQPSK pre-equalization systems." Photonics Technology Letters, IEEE 24.5 (2012): 371-373.

[72] Kim, Inwoong, et al. "Mitigation and Monitoring of the Impact of Extinction Ratio of IQ-Modulator on Nyquist M-QAM Signals." Photonics Technology Letters, IEEE 26.2 (2014): 177-179.

[73] Peng, Wei-Ren, et al. "Theoretical and experimental investigations of direct-detected RF-tone-assisted optical OFDM systems." Journal of Lightwave Technology 27.10 (2009): 1332-1339.

[74] Cho, Pak S., et al. "Coherent homodyne detection of BPSK signals using time-gated amplification and LiNbO 3 optical 90° hybrid." Photonics Technology Letters, IEEE 16.7 (2004): 1727-1729.

[75] Agrawal, Govind P. Nonlinear fiber optics. Academic press, 2007.

[76] http://www.vpiphotonics.com

[77] Lowery, Arthur J. "Improving sensitivity and spectral efficiency in direct-detection optical OFDM systems." Optical Fiber Communication Conference. Optical Society of America, 2008.

[78] Lowery, Arthur, and Jean Armstrong. "Orthogonal-frequency-division multiplexing for dispersion compensation of long-haul optical systems." Optics Express 14.6 (2006): 2079-2084.

[79] Lee, Jeffrey, et al. "24-Gb/s transmission over 730 m of multimode fiber by direct modulation of an 850-nm VCSEL using discrete multi-tone modulation."National Fiber Optic Engineers Conference. Optical Society of America, 2007.

[80] Li, Fan, et al. "Real-time demonstration of DMT-based DDO-OFDM transmission and reception at 50Gb/s." (2013): 1155-1157.

[81] Sanya, M. F., et al. "DC-Biased Optical OFDM for IM/DD Passive Optical Network Systems." Journal of Optical Communications and Networking 7.4 (2015): 205-214.

[82] Dissanayake, Sarangi Devasmitha, and Jean Armstrong. "Comparison of ACO-OFDM, DCO-OFDM and ADO-OFDM in IM/DD Systems." Journal of lightwave technology 31.7 (2013): 1063-1072.

[83] Chen, Liang, Brian Krongold, and Jamie Evans. "Performance analysis for optical OFDM transmission in short-range IM/DD systems." Journal of Lightwave Technology 30.7 (2012): 974-983.

[84] Zhou, Ji, et al. "A Cost-Effective and Efficient Scheme for Optical OFDM in Short-Range IM/DD Systems." Photonics Technology Letters, IEEE 26.13 (2014): 1372-1374.

[85] Sanya, Max Fréjus, et al. "Performance analysis of known unipolar optical OFDM techniques in PON IM/DD fiber link." High Capacity Optical Networks and Enabling Technologies (HONET-CNS), 2013 10th International Conference on. IEEE, 2013.

[86] Cao, Z., et al. "Optical OFDM signal generation by optical phase modulator and its application in ROF system." ECOC 2009 (2009).

[87] González, Oswaldo, et al. "OFDM over indoor wireless optical channel."Optoelectronics, IEE Proceedings-. Vol. 152. No. 4. IET, 2005.

[88] Schmidt, Brendon J., Arthur J. Lowery, and Jean Armstrong. "Experimental demonstrations of 20 Gbit/s direct-detection optical OFDM and 12 Gbit/s with a colorless transmitter." National Fiber Optic Engineers Conference. Optical Society of America, 2007.

[89] Qian, Dayou, et al. "100km long reach upstream 36Gb/s-OFDMA-PON over a single wavelength with source-free ONUs." ECOC 2009 (2009).

[90] Amin, Abdullah Al, et al. "Polarization multiplexed 100 Gbps direct-detection OFDM transmission without MIMO processing." ECOC 2009 (2009).

[91] Lowery, Arthur James, Liang Bangyuan Du, and Jean Armstrong. "Performance of optical OFDM in ultralong-haul WDM lightwave systems." Journal of Lightwave Technology 25.1 (2007): 131-138.

[92] Qian, Dayou, et al. "11.5-Gb/s OFDM transmission over 640km SSMF using directly modulated laser." 2008 34th European Conference on Optical Communication. 2008.

[93] Bao, Hongchun, and William Shieh. "Transmission simulation of coherent optical OFDM signals in WDM systems." Optics express 15.8 (2007): 4410-4418.

[94] Ma, Yiran, Yan Tang, and William Shieh. "107 Gb/s transmission over multimode fiber with coherent optical OFDM using center launching technique."ECOC 2009 (2009).

[95] Shieh, William, et al. "Coherent optical OFDM: has its time come?[Invited]."Journal of Optical Networking 7.3 (2008): 234-255.

[96] Sung, Minyong, et al. "DFT-precoded coherent optical OFDM with Hermitian symmetry for fiber nonlinearity mitigation." Lightwave Technology, Journal of30.17 (2012): 2757-2763.

[97] Zhao, Jian. "Intensity-modulation full-field detection optical fast OFDM." Journal of Optical Communications and Networking 5.5 (2013): 465-474.

[98] Qian, Dayou, et al. "64/32/16QAM-OFDM using direct-detection for 40G-OFDMA-PON downstream." Optical Fiber Communication Conference. Optical Society of America, 2011.

[99] Escayola Elias, Francisco Javier, et al. "Laser linewidth requirements for remote heterodyne OFDM based PON scenario." (2004).

[100] Peng, Wei-Ren, et al. "Experimental demonstration of a coherently modulated and directly detected optical OFDM system using an RF-tone insertion."Optical Fiber Communication Conference. Optical Society of America, 2008.

[101] Peng. Wei-Ren, "Experimental demonstration of compensating the I/Q imbalance and bias deviation of the Mach-Zehnder modulator for an RF-tone assisted optical OFDM system". In: 2008 34th European Conference on Optical Communication (ECOC 2008), Brussels, Belgium 21-25 Sept. 2008. Institute of Electrical and Electronics Engineers, 2008.

[102] Peng, Wei-Ren, et al. "Spectrally efficient direct-detected OFDM transmission employing an iterative estimation and cancellation technique." Optics express17.11 (2009): 9099-9111.

[103] Carruthers, Jeffrey B., and Joseph M. Kahn. "Multiple-subcarrier modulation for nondirected wireless infrared communication." Selected Areas in Communications, IEEE Journal on 14.3 (1996): 538-546.

[104] Armstrong, Jean, and Brendon JC Schmidt. "Comparison of asymmetrically clipped optical OFDM and DC-biased optical OFDM in AWGN."Communications Letters, IEEE 12.5 (2008): 343-345.

[105] Duong, Thanh-Nga, et al. "Adaptive loading algorithm implemented in AMOOFDM for NG-PON system integrating cost-effective and low-bandwidth optical devices." Photonics Technology Letters, IEEE 21.12 (2009): 790-792.

[106] Hillerkuss, D., et al. "26 Tbit s-1 line-rate super-channel transmission utilizing all-optical fast Fourier transform processing." Nature Photonics 5.6 (2011): 364-371.

[107] Shieh, W., Q. Yang, and Y. Ma. "107 Gb/s coherent optical OFDM transmission over 1000-km SSMF fiber using orthogonal band multiplexing."Optics express 16.9 (2008): 6378-6386.

[108] Jansen S.L, Morita I., Schenk T.C.W., and Tanaka H., "Long-Haul transmission of 16x52.5-Gb/s polarization division multiplexed OFDM enabled by MIMO processing," OSA Journal of Optical Networking, vol. 7, pp. 172-182, 2008.

[109] Armstrong, Jean, and A. J. Lowery. "Power efficient optical OFDM." Electronics Letters 42.6 (2006): 370-372.

[110] Weiner, Joseph S., et al. "SiGe differential transimpedance amplifier with 50-GHz bandwidth." Solid-State Circuits, IEEE Journal of 38.9 (2003): 1512-1517.

[111] Mottet Alexandre, Bourriot Nicolas and Hauden Jérôme, "Tunable Frequency Shifter Based on $LiNbO_3$-I&Q Modulators," Photline Technologies.

[112] Vettel P., "Next Generation Optical Technologies," 38th ECOC, Amsterdam, Netherlands, paper Tu.3.G.1, September 2012

[113] Soerensen, S. "Optical beat noise suppression and power equalization in subcarrier multiple access passive optical networks by downstream feedback."Journal of lightwave technology 18.10 (2000): 1337.

[114] Won, Y-Y., et al. "OBI noise reduction using gain saturated SOA in reflective SOA based WDM/SCM-PON optical links." Electronics Letters 42.17 (2006): 992-994.

[115] Wood, Thomas H., and N. K. Shankaranarayanan. "Operation of a passive optical network with subcarrier multiplexing in the presence of optical beat interference." Lightwave Technology, Journal of 11.10 (1993): 1632-1640.

[116] Kanonakis, Konstantinos, et al. "An OFDMA-based optical access network architecture exhibiting ultra-high capacity and wireline-wireless convergence."Communications Magazine, IEEE 50.8 (2012): 71-78.

[117] Cano, Iván, et al. "An OFDM-PON with non-preselected ONUs: dimensioning and experimental results." Access Networks and In-house Communications. Optical Society of America, 2012.

[118] Cano, Ivan, et al. "Dimensioning of OFDMA PON with non-preselected independent ONUs sources and wavelength-control." Optics express 20.1 (2012): 607-613.

[119] Cano, I., et al. "An OFDMA-PON with non-preselected independent ONU sources and centralized feedback wavelength control: Dimensioning and experimental results." Transparent Optical Networks (ICTON), 2012 14th International Conference on. IEEE, 2012.

[120] Cano, Iván, et al. "Experimental assessment of an OFDMA-based statistical PON with flexible bandwidth allocation and sign-labels." Asia Communications and Photonics Conference. Optical Society of America, 2012.

[121] Cano, Iván, et al. "Differential link-loss compensation through dynamic bandwidth assignment in statistical OFDMA-PON." Optical Fiber Communication Conference. Optical Society of America, 2013.

[122] Cano, Ivan N., et al. "A study of flexible bandwidth allocation in statistical OFDM-based PON." 2013 15th International Conference on Transparent Optical Networks (ICTON). 2013.

[123] Cano, Iván N., et al. "Experimental Demonstration of a Statistical OFDM-PON With Multiband ONUs and Elastic Bandwidth Allocation [Invited]." Journal of Optical Communications and Networking 7.1 (2015): A73-A79.

[124] Cano, Iván N., et al. "Experimental demonstration of multi-band upstream in statistical OFDM-PONs and comparison with digital subcarrier assignment."Optical Fiber Communications Conference and Exhibition (OFC), 2014. IEEE, 2014.

[125] van Veen, Doutje, et al. "System demonstration of a time and wavelength-set division multiplexing PON." (2013): 564-566.

[126] Kaneko, Shin, et al. "First λ-tunable dynamic load-balancing operation enhanced by 3-msec bidirectional hitless tuning on symmetric 40-Gbit/s WDM/TDM-PON." Optical Fiber Communications Conference and Exhibition (OFC), 2014. IEEE, 2014.

[127] Chanclou, Philippe, et al. "Network operator requirements for the next generation of optical access networks." IEEE Network 2.26 (2012): 8-14.

[128] Desem, Can. "Optical interference in subcarrier multiplexed systems with multiple optical carriers." Selected Areas in Communications, IEEE Journal on8.7 (1990): 1290-1295.

[129] "VIrtex-6 family overview," Xiling Inc. Jan. 2010.

[130] Jones, Douglas L. "Peak power reduction in OFDM and DMT via active channel modification." Signals, Systems, and Computers, 1999. Conference Record of the Thirty-Third Asilomar Conference on. Vol. 2. IEEE, 1999.

[131] Fedra, Zbynek, Roman Marsalek, and Vladimir Sebesta. "Interleaving optimization in OFDM PAPR reduction." Radioelektronika, 2007. 17th International Conference. IEEE, 2007.

[132] Jones, Awinings E., Tim A. Wilkinson, and S. K. Barton. "Block coding scheme for reduction of peak to mean envelope power ratio of multicarrier transmission schemes." Electronics letters 30.25 (1994): 2098-2099.

[133] Shepherd, S. J., et al. "Simple coding scheme to reduce peak factor in QPSK multicarrier modulation." Electronics Letters 31.14 (1995): 1131-1132.

[134] Li, Xiaodong, and Leonard J. Cimini Jr. "Effects of clipping and filtering on the performance of OFDM." Vehicular Technology Conference, 1997, IEEE 47th. Vol. 3. IEEE, 1997.

[135] Ochiai, Hideki, and Hideki Imai. "Performance analysis of deliberately clipped OFDM signals." Communications, IEEE Transactions on 50.1 (2002): 89-101.

[136] Mestdagh, Denis JG, Paul Spruyt, and Bernard Biran. "Analysis of clipping effect in DMT-based ADSL systems." Communications, 1994. ICC'94, SUPERCOMM/ICC'94, Conference Record,'Serving Humanity Through Communications.'IEEE International Conference on. IEEE, 1994.

[137] Bahai, Ahmad RS, et al. "A new approach for evaluating clipping distortion in multicarrier systems." Selected Areas in Communications, IEEE Journal on20.5 (2002): 1037-1046.

[138] Shepherd, Simon, John Orriss, and Stephen Barton. "Asymptotic limits in peak envelope power reduction by redundant coding in orthogonal frequency-division multiplex modulation." Communications, IEEE Transactions on 46.1 (1998): 5-10.

[139] Zhang, Yunjun, et al. "OFDM peak power reduction by sub-block-coding and its extended versions." Vehicular Technology Conference, 1999 IEEE 49th. Vol. 1. IEEE, 1999.

[140] Bäuml, Robert W., Robert FH Fischer, and Johannes B. Huber. "Reducing the peak-to-average power ratio of multicarrier modulation by selected mapping."Electronics Letters 32.22 (1996): 2056-2057.

[141] Breiling, Marco, Stefan H. Müller-Weinfurtner, and Johannes B. Huber. "SLM peak-power reduction without explicit side information." Communications Letters, IEEE 5.6 (2001): 239-241.

[142] Mestdagh, Denis JG, and Paul MP Spruy. "A method to reduce the probability of clipping in DMT-based transceivers." Communications, IEEE Transactions on44.10 (1996): 1234-1238.

[143] Van Eetvelt, P., G. Wade, and M. Tomlinson. "Peak to average power reduction for OFDM schemes by selective scrambling." Electronics letters 32.21 (1996): 1963-1964.

[144] Han, Seung Hee, and Jae Hong Lee. "An overview of peak-to-average power ratio reduction techniques for multicarrier transmission." Wireless Communications, IEEE 12.2 (2005): 56-65.

[145] Müller, Stefan H., and Johannes B. Huber. "OFDM with reduced peak-to-average power ratio by optimum combination of partial transmit sequences."Electronics letters 33.5 (1997): 368-369.

[146] Jayalath, A. D. S., and Chintha Tellambura. "Reducing the peak-to-average power ratio of orthogonal frequency division multiplexing signal through bit or symbol interleaving." Electronics Letters 36.13 (2000): 1161-1163.

[147] Tellado-Mourelo, Jose. Peak to average power reduction for multicarrier modulation. Diss. Stanford University, 1999.

[148] Declercq, David, and Georgios B. Giannakis. "Peak to average ratio reduction for multicarrier transmission: a review." Available from: citeseer. ist. psu. edu/617547. html.

[149] Giacoumidis, E., et al. "Adaptive-modulation-enabled WDM impairment reduction in multichannel optical OFDM transmission systems for next-generation PONs." Photonics Journal, IEEE 2.2 (2010): 130-140.

[150] Cano, Iván N., et al. "Sign Labeled OFDM with Intensity-Modulation Direct Detection in PON." European Conference and Exhibition on Optical Communication. Optical Society of America, 2012.

[151] Prat J., Cano I., Santos M. C. and Escayola X., "Método de codificación-decodificación de la amplitud de la señal mediante plegado y etiquetas de información auxiliares", app. number ES-P2011231426 (PCT/ES2013/070634), date 10/11/2012.

[152] Buchali, F. and Dischler R. "Optimized sensitivity direct detection O-OFDM with multi-level subcarrier modulation." Optical Fiber Communication Conference. Optical Society of America, 2008.

[153] Tubbax, Jan, et al. "OFDM versus Single Carrier with Cyclic Prefix: a system-based comparison." Vehicular Technology Conference, 2001. VTC 2001 Fall. IEEE VTS 54th. Vol. 2. IEEE, 2001.

[154] Bülow, Henning, Fred Buchali, and Axel Klekamp. "Electronic dispersion compensation." Lightwave Technology, Journal of 26.1 (2008): 158-167.

[155] Savory, Seb J. "Digital signal processing options in long haul transmission."Optical Fiber Communication Conference. Optical Society of America, 2008.

[156] Spinnler, B. "Recent advances on polarization multiplexing." 2008 Digest of the IEEE/LEOS Summer Topical Meetings. 2008.

[157] Berger, Christian R., et al. "Theoretical and experimental evaluation of clipping and quantization noise for optical OFDM." Optics express 19.18 (2011): 17713-17728.

[158] Takahashi, Hidenori, et al. "Required resolution of digital-analog-converter for optical OFDM." National Fiber Optic Engineers Conference. Optical Society of America, 2010.

[159] Escayola, Xavier, et al. "OFDM-PON performance with limited quantization."Transparent Optical Networks (ICTON), 2013 15th International Conference on. IEEE, 2013.

[160] Cano Valadéz, Iván Nicolás, et al. "Physical layer evaluation of OFDM-based access networks." (2011).

F. Javier Escayola

F. Javier Escayola Elias was born in Barcelona, Spain, in 1986. He received his B.Sc. and M.Sc. degrees in telecommunication engineering from the Technical University of Catalonia (Universitat Politècnica de Catalunya UPC) in 2010.

The work presented in this Ph.D. Thesis was performed from 2011 to 2015 at the Optical Communications Group of the Signal Theory and Communications department of UPC, under the supervision of prof. Ph.D. Maria Concepción Santos Blanco and Ph.D. Iván Nicolás Cano Valadez. His work is centered on optical access networks and is mainly focused on the next generation OFDM-based Passive Optical Networks.